APRIL 1984
ENVIRONMENTAL SCIENCE & TECHNOLOGY

ES&T

Assessing health effects of air pollution

115A

Environmental Science & Technology ES&T (ISSN 0013-936X) is published monthly by the American Chemical Society at 1155 16th Street, N.W., Washington, D.C. 20036; 202-872-4600, TDD 202-872-8733. Second-class postage paid at Washington, D.C. and at additional mailing offices. POSTMASTER: Send address changes to Membership & Subscription Services, PO Box 3337, Columbus, OH, 43210.

SUBSCRIPTION PRICES 1984: Members, $22 per year; nonmembers (for personal use), $25 per year; institutions, $124 per year. Foreign postage, $8 additional per year/Air freight add $33; multiple year rates available on request. Single issues $10.50 for current year; $12.50 for prior years. Back volumes $146. Rates above do not apply to nonmember subscribers in Japan, who must enter subscription orders with Maruzen Company Ltd., 3-10 Nihon bashi 2-chome, Chuo-ku, Tokyo 103, Japan. Tel: (03) 272-7211.

SUBSCRIPTION SERVICE: Orders for new subscriptions, single issues, back volumes, and microfiche and microform editions should be sent with payment to Office of the Treasurer, Financial Operations, ACS, 1155 16th St., N.W., Washington, D.C. 20036. Phone orders may be placed, using Visa, Master Card, or American Express, by calling toll free (800) 424-6747 from anywhere in the continental U.S. Changes of address, subscription renewals, claims for missing issues, and inquiries concerning records and accounts should be directed to Manager, Membership and Subscription Services, ACS, P.O. Box 3337, Columbus, Ohio 43210. Changes of address should allow six weeks and be accompanied by old and new addresses and a recent mailing label. Claims for missing issues will not be allowed if loss was due to insufficient notice of change of address, if claim is dated more than 90 days after the issue date for North American subscribers or more than one year for foreign subscribers, or if the reason given is "missing from files."

ES&T
CONTENTS

Volume 18, Number 4, April 1984

FEATURES

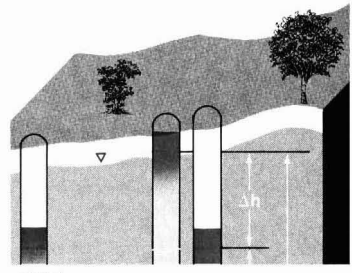

108A

REGULATORY FOCUS

OUTLOOK

DEPARTMENTS

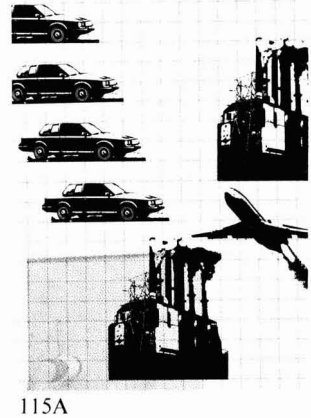

115A

124A

ESTHAG 18(4) 101A–132A
219–298 (1984)
ISSN 0013-936X

Credits: p. 104A, *ES&T*'s Julian Josephson; p. 114A, John Apai Photographers (Princeton, N.J.); p. 120A, Medical Documentation, Rancho Los Amigos Hospital (Downey, Calif.); p. 124A, courtesy ORBIS Press Agency (Prague, Czechoslovakia).
Cover: Barry Baron, Photo-Optik (Kensington, Md.); use of apparatus courtesy The George Washington University Medical Center (Washington, D.C.).

RESEARCH

219
Kinetics of monobromamine disproportionation–dibromamine formation in aqueous ammonia solutions. Guy W. Inman, Jr., and J. Donald Johnson*

The reaction observed is strongly catalyzed by phosphate and appears to have no ammonia dependence beyond that required for monobromamine formation.

224
Reactive foams for air purification. Susann M. Brander, Gudrun I. Johansson,* Bengt G. Kronberg, and Per J. Stenius

This work investigates whether the removal of gas pollutants from air by blowing the air through a foam bed is effective.

231
Comparison of solvent extraction and thermal–optical carbon analysis methods: Application to diesel vehicle exhaust aerosol. Steven M. Japar,* Ann C. Szkarlat, Robert A. Gorse, Jr., Emily K. Heyerdahl, Richard L. Johnson, John A. Rau, and James J. Huntzicker

A comparison of independent analytical methods for the determination of organic and elemental carbon is presented.

235
Acetone-sensitized and nonsensitized photolyses of tetra-, penta-, and hexachlorobenzenes in acetonitrile–water mixtures: Photoisomerization and formation of several products including polychlorobiphenyls. Ghulam Ghaus Choudhry and Otto Hutzinger*

Photochemical reactions of PCBs possessing four, five, and six chlorine substituents in the presence and absence of acetone at wavelengths ≥285 nm are studied.

242
Numerical simulation of a sedimentation basin. 1. Model development. Iraklis A. Valioulis and E. John List*

This computer model follows the spatial and temporal development of the influent particle size distribution toward the outlet of the tank.

248
Numerical simulation of a sedimentation basin. 2. Design application. Iraklis A. Valioulis and E. John List*

The model is used to study the importance of selective variables on the settling process and to demonstrate the computer simulation capabilities.

253
Analysis for trace elements in magnetohydrodynamic (MHD) pilot power plant effluents. Tom E. Clevenger,* Edward J. Hinderberger, Jr., Dennis A. Yates, and W. Dennis James

INAA and ICAP are evaluated as to their applicability for the multielement analysis of coal, slag, and fly ash.

■ 257
Dynamics of a fertilizer contaminant plume in groundwater. Michael J. Barcelona* and Thomas G. Naymik

The usefulness of a solute transport model for predicting contaminant transport and transformations is demonstrated.

262
Photochemical separation of xenon and krypton. Christine E. Geosling* and Terence Donohue

Stable XeF_2 is produced when a mixture of xenon, krypton, and fluorine gases is irradiated with near-ultraviolet light.

264
Aggregation and colloidal stability of fine-particle coal suspensions. Paul R. Schroeder* and Alan J. Rubin

Aggregation and colloidal stability of fine-particle coal suspensions in the presence of hydrogen ions, simple electrolytes, and aluminum sulfate are examined.

271
Characterization of surface species on coal combustion particles by X-ray photoelectron spectroscopy in concert with ion sputtering and thermal desorption. George E. Cabaniss and Richard W. Linton*

Surface chemical composition of coal ash particles is determined before and after inert ion (Ar^+) sputtering using XPS.

275
Octachlorostyrene in Lake Ontario: Sources and Fates. Ray Kaminsky and Ronald A. Hites*

This report confirms the hypothesis that OCS originates primarily from the waste product of electrolytic chlorine production.

280
Analysis of the characteristics of complex chemical reaction mechanisms: Application to photochemical smog chemistry. Joseph A. Leone and John H. Seinfeld*

This method allows one to determine the influence of individual reactions and species on the overall behavior of the reaction mechanism.

287
Summertime variations in polycyclic aromatic hydrocarbons at four sites in New Jersey. Ronald Harkov, Arthur Greenberg, Faye Darack, Joan M. Daisey, and Paul J. Lioy*

Examination of daily variation of 10 PAHs showed that meteorology had an overall influence on ambient levels but that the greatest effect was from local sources.

NOTES

291
Butyltin compounds and inorganic tin in sediments in Ontario. R. James Maguire

Results show that butyltin species and some methylated derivatives are present in the sediments of some harbors in Ontario.

CORRESPONDENCE

295
Comment on "Partition equilibria of nonionic organic compounds between soil organic matter and water." William G. MacIntyre* and Craig L. Smith

Cary T. Chiou,* Paul E. Porter, and Thomas D. Shoup

* To whom correspondence should be addressed.

■ This article contains supplementary material in microform. See ordering instructions at end of paper.

ES&T
EDITORIAL

Environmental R & D

A recent report by the National Science Foundation indicates that although the federal government has been the chief source of research and development funds in the U.S. for the past 20 years, industrial expenditures for R&D have now surpassed government expenditures, and industrial R&D spending continues to climb faster than government spending. According to the report, in 1983 industry spent $44.3 billion compared to $39.6 billion spent by the federal government.

Additionally, proposed legislation before Congress provides for extension of the present R&D tax credit incentive to encourage industry to undertake expanded R&D activities, which may require a long-term and relatively expensive commitment to projects which have greater risks associated with them. The legislation also includes incentives for expansion of corporate funding of basic research conducted at the nation's universities and for industrial support of scientific education programs at our colleges and universities to improve the development of scientifically skilled manpower. Under current law, the R&D tax credit is due to expire at the end of December 1985. The proposed legislation would make these incentives a permanent part of U.S. tax law.

The fact that industrial R&D expenditures are as high as they are and that industry seems willing to enter into collaborative and supportive programs with universities is a very healthy sign. Industry is to be commended for its efforts to date, and it is hoped that development of new initiatives along these lines will continue. This is of special concern in view of reports that our colleges and universities are suffering from a chronic shortage of faculty and a severe lack of modern scientific equipment. Furthermore, since federal expenditures have not kept pace with basic research needs, university basic research has suffered greatly over the past several years. Participation in these endeavors by industry should certainly be encouraged.

A corollary to these increased industrial expenditures has to do with how much of the industrial R&D budget is directed at environmental issues, either for basic research or for the development of more efficient and more sophisticated pollution control equipment. The industrial sector tends to be concerned that new developments will be used against it—in identifying new problems and in establishing more stringent effluent standards that will require use of more expensive pollution control devices. It would be satisfying to see a more progressive attitude on the part of industry—a greater willingness to devote its resources to long-term environmental research projects and to undertake collaborative efforts with universities to foster basic as well as applied environmental research. With the decline of federal research expenditures this need is as great in the environmental arena as it is in other scientific technological areas.

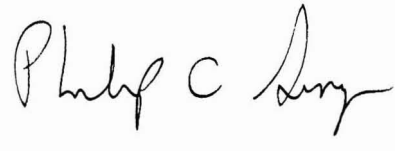

INTERNATIONAL

Canada officially registered deep disappointment with the U.S. announcement that efforts to combat acid rain would be limited solely to research for the foreseeable future. In a diplomatic note delivered to the Reagan administration, Canada asked the U.S. to explain how it intends to meet its obligations to Canada concerning transboundary air pollution. Canada believes that "the decision ignores principles contained in bilateral treaties directed at protecting the North American environment," said Allan J. MacEachen, deputy prime minister and secretary of state for External Affairs. MacEachen noted that when President Reagan visited Canada in 1981, he stated that both countries must cooperate to control transboundary air pollution.

WASHINGTON

Nuclear power in the U.S. is not likely to be expanded in this century beyond the reactors already under construction unless major changes are made in the technology, management, and levels of public acceptance, the Office of Technology Assessment (OTA) said in a recent report. Too many financial risks are now associated with nuclear power plants because of uncertainties in the growth in demand for electricity, high capital costs, operating problems, increasing regulatory requirements, and public opposition. "Nuclear power will not be a credible energy option for this country" unless confidence in it is restored, the report states.

In testimony before a Senate committee, acid rain controls have been endorsed by the American Public Power Association (APPA), the only national electric utility association in favor of immediate controls. However, the association believes that emissions from all mobile and stationary fossil fuel sources—not just power plants—should be taxed to pay for the controls. "As suppliers of electric power . . . our members are willing to pay their fair share," said Ruth Gonze, who testified for APPA. She urged Congress to adopt a financing program that would remain in effect until emission reduction goals are met. APPA represents more than 1750 local publicly owned electric utilities.

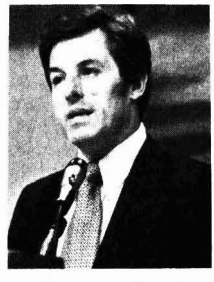

***Florio:** introduces Superfund bill*

Persons harmed by exposure to toxic substances would be allowed to recover medical and relocation expenses under a Superfund reauthorization bill introduced by Rep. James A. Florio (D-N.J.). The bill would also make permanent the $1.6-billion federal fund created by the Superfund law and add $1.8 billion to the fund each year for the first five years. It creates a new tax on generated wastes and provides federal funds to states for the long-term maintenance of Superfund sites. The bill also contains a mandatory schedule for the cleanup of Superfund sites.

Asbestos fibers in ambient air probably cause some cancer deaths each year, according to a recent study by the National Academy of Sciences. The study also suggests for the first time that other asbestoslike fibers such as certain forms of fiberglass and mineral wools may also be carcinogenic. However, the data on the other fibers are too uncertain to make a definite judgment. The report concludes that nine out of one million people in the general population would die from a lifetime exposure to the amount of asbestos generally found in the ambient air. It also states that the physical properties of asbestos appear to be related to adverse health effects and that substances used as asbestos replacements may cause the same problems.

Release of chlorofluorocarbons at current rates could reduce stratospheric ozone by 2–4% by late in the next century, according to a new report from the National Research Council of the National Academy of Sciences. This estimate is lower than previous estimates. In 1979 the council estimated an ozone reduction of 15–18%. In 1982, the estimate was 5–9%. The new estimate was derived from improved mathematical models and recent atmospheric research.

STATES

According to agency sources, EPA Administrator William Ruckelshaus is planning to approve relaxations in SO_2 control requirements in state implementation plans (SIPs) for several midwestern states. It is estimated that allowable SO_2 emissions will increase about 200 000 tons as a result of this action. The Clean Air Act requires the agency to approve SIP revisions if they will not result in violations of the national ambient air quality standards.

For the first time, a utility has voluntarily decided to install a scrubber to reduce SO_2 emissions. Boston Edison, one of the Northeast's largest electric utilities, will install a scrubber on a plant it is converting from oil to coal in New Boston, Mass. Originally, Boston Edison planned to convert two plants to coal, increasing annual emissions by 90 000 tons. After the *Boston Globe* published a study showing that local sources cause 15% or more of the acid rain problem in Massassachusetts and that the coal conversions would increase total

0013-936X/84/0916-0104A$01.50/0

state SO_2 emissions 25–30%, Boston Edison decided to convert only one plant to coal and install a scrubber on this plant.

The high rate of leukemia in Woburn, Mass., is related to the drinking water from two contaminated wells, according to a study by the Harvard School of Public Health. The three scientists who coordinated the study found positive associations between the amount of water consumed from the two wells and the incidence of childhood leukemia, fetal and newborn deaths, and various birth defects and illnesses. The two wells contained trichloroethylene and other toxic wastes and were shut down in 1979. They were two of four wells that supplied the town's drinking water.

New York State has announced new restrictions on the land burial of hazardous wastes that can be disposed of with some form of higher technology currently available. The regulations will apply not only to major commercial hazardous waste facilities but also to industries that dispose of their own wastes. Current higher technologies for waste disposal include liquid injection incineration, rotary kilns, molten salt thermal treatment, plasma arc reactors, and thermal treatment using supercritical water. Additionally, after March 1985, restrictions will be applied to waste streams containing halogenated, nitrogenated, and aromatic organic chemicals and certain other organic chemicals subject to federal toxic waste regulations.

The University of Alabama has formed a new research institute to study environmental issues related to hazardous and nonhazardous waste disposal. The institute consists of professors at major universities who are experts in geology, toxicology, chemistry, socioeconomics, and engineering. They will study the technical, social, and economic issues related to safe waste management and make the findings available to Congress, state legislatures, government agencies, and the public. They expect to develop a strategy for the management of spent solvents and solvent-contaminated wastes by January 1985. The group is supported by the university and a $390,000 grant from Waste Management, Inc. of Oak Brook, Ill.

AWARDS

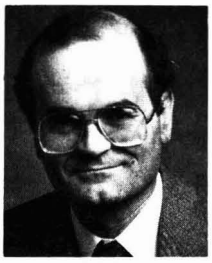

Benedek: AIChE award winner

The Larry K. Cecil Environmental Division Award of the American Institute of Chemical Engineers (AIChE) has been awarded to Andrew Benedek of Zenon Environmental Inc. (Burlington, Ontario, Canada). The award, which recognizes engineering contributions toward preservation or improvement of the natural environment, was given to Benedek for "contributions in developing improved analytical methods and novel water and wastewater treatment processes."

SCIENCE

Can fates of polynuclear aromatic hydrocarbons (PAHs) be predicted by mechanistic simulation models based on easily measured properties of homologous compounds? Several fates have been examined. Photolytic degradation seems to be the most important pathway, both experimentally and in simulations. On the other hand, the octanol–water partition coefficient is not "a good predictor of the behavior of PAHs in aquatic organisms," say John Giesy and his associates at Michigan State University. Their research was carried out for EPA's Environmental Research Laboratory (Athens, Ga.). They also note that PAH laboratory toxicity studies must be conducted under uniform lighting conditions if study results are to be realistic representations of field conditions.

Changes in how the toxicity of complex chemical mixtures is assessed may be in order, suggests Chris Reilly of Argonne National Laboratory (ANL, Argonne, Ill.). Reilly described experiments at ANL in which mice painted with a tar byproduct of coal gasification developed fewer cancers than mice painted with individual components of the tar. The separated chemicals were applied in concentrations identical to those in which they occur in the tar. "Apparently, the chemicals interacted so that the mixture was less toxic than the components," Reilly said. He noted that conventionally mixture toxicities are estimated by adding individual toxicities of the component chemicals.

Science-related issues concerning groundwater, geared to general public understanding, are set forth in "The Ground Water Information Pamphlet." The pamphlet was written under the auspices of the American Chemical Society's Committee on Environmental Improvement. It presents fundamental concepts concerning the chemistry of groundwater and helps the citizen begin to evaluate information about groundwater problems and to gauge implications of plans of action. Single copies are available from Jean Parr, Dept. of Public Affairs, American Chemical Society, 1155 16th St., N.W., Washington, D.C. 20036; 202-872-8725.

The ongoing debate about relationships between structure activity and toxicity of organic chemicals will continue at a conference on "Structure–Activity Relationships (SAR) and Toxicity Assessment," to be held at the National Bureau of Standards (Gaithersburg, Md.), June 6–8. The latest science, technology, and policy aspects will be discussed by leading U.S. and European authorities, who will consider SAR capabilities, limitations, benefits, and problems. For more information, contact T. L. Nally, Federal Regulatory Programs, ACS Dept. of Public Affairs, 1155 16th St., N.W., Washington, D.C. 20036; 202-872-8724.

Polychlorinated biphenyl (PCB) destruction up to 99.9999% is made possible by the advanced electric reactor (AER) according to its developer, J. M. Huber Corporation (Borger, Tex.). A destruction and removal efficiency of 99.999998% is claimed, along with no observation of hydrogen chloride, chlorine, volatile chlorinated hydrocarbons, dioxins, or furans at the stack, and "trace amounts" of particulate matter and oxides of nitrogen. The AER, which operates at temperatures of 4000–5000 °F, has a very low gas phase flow rate (about 500 scfm in a 150-t/d commercial-scale plant), with an absence of

oxygen in the process gases. The AER can process contaminated soils as well as gases and liquids, according to Huber.

Pollution control technology research and development may not be getting the attention they deserve, despite "revitalization of many programs in EPA since William Ruckelshaus took over," according to a resolution prepared by the Environmental Engineering Committee of EPA's Science Advisory Board. The resolution calls for EPA to exert more effort in this direction. The main thrusts of the effort would be to assess control technology improvements necessary to achieve environmental goals; to evaluate new and improved technologies continually; and to encourage EPA–private sector co-funding of projects to develop and demonstrate improved control technologies.

Liming an acidified lake

Spreading limestone powder in lakes made acid by acid precipitation can be done more efficiently with a method developed by Idemekaniska System AB (Hudiksvall, Sweden). The company says that six metric tons of lime can be spread in 15 min. The acid lake water is pumped into a boat where it is mixed with dry lime and then ejected in the form of a slurry over the lake's surface. The boat's design—its minimum draft is 0.5 m—allows it to be used even in very shallow waters. It weighs 2.5 tons and can travel at 7 knots. Sweden is presently wrestling with the problem of extensive acid precipitation and acidified lakes.

Suppression of toxic and respirable dusts that previously evaded control may now be possible. These include dusts containing such substances as lead and zinc oxides, coal, quartz, arsenic, pesticides, very fine limestone, and pharmaceuticals. Sonic Development Corporation (SDC, Mahwah, N.J.) says that it has achieved up to 90% control by first fogging a dust-generating area with micrometer-sized water droplets that are electrostatically charged. Their charge is opposite to that of the dust particles so they attract the dust and "knock it down, in place," explains Wayne Hartshorn of SDC. The firm reports suppression of coal dust up to 90%, lead oxide, about 80%; and fine limestone, 70%.

A method for removing trihalomethanes (THMs) from drinking water involves the use of ozone in chlorinated water, says the engineering firm of Briley, Wild & Associates, Inc. (BWA, Ormond Beach, Fla.). It is believed that THMs are formed by reactions of chlorine with humic and fulvic substances in raw water. BWA researchers say that the ozone removes those parts of the organic molecules which react with chlorine to form THMs. They maintain that the ozone–chlorine treatment brings THMs "far below the federal standard of 100 parts per billion." BWA developed the ozone process for the city of Belle Glade, Fla., which takes its water from Lake Okeechobee, a source heavily laden with humic and fulvic substances.

BUSINESS

Ocean thermal energy conversion (OTEC) plants of 100+ MWe are probably not on the horizon because of high costs and uncertainties concerning their economic viability. This view has been expressed despite the fact that the federal government has spent more than $200 million on OTEC over the past 10 years. Up to now, test plants of up to 100 kW have been operated, and those for no more than several months. OTEC could prove attractive in the 1–10-MWe range on tropical islands where comparative energy costs (oil, coal, or the like) would be very high, or where power and fresh water production may be combined. Aside from the U.S., only Japan has invested substantially in OTEC development.

An EPA contract to provide laboratory analysis of organically contaminated soil with "sophisticated analytical instrumentation" was awarded to Environmental Research Group, Inc. (ERG, Ann Arbor, Mich.). The 15-month, $550,000 contract calls for the use of gas chromatography with and without mass spectrometry and for use of reporting systems "exhibiting the factors EPA considers important criteria for choosing a reliable analytical laboratory." One of the principal areas of the contract will be the analysis of Superfund samples according to EPA-approved methods. Priority pollutants and other hazardous compounds would be detected to ppb levels.

"Nuclear power is today undergoing a major expansion in the U.S., and the recent wave of bad news about a handful of nuclear power plants under construction should not obscure this fact," says Carl Walske, president of the Atomic Industrial Forum (Bethesda, Md.). Walske predicted that by the end of this decade, "approximately one-fifth of our electricity will come from the atom, and it is likely that new nuclear power plants will be ordered."

The Zone I Emergency Response Cleanup Services (ERCS) contract was awarded to O.H. Materials (OHM, Findlay, Ohio). EPA awarded the one-year contract, valued at $66.5 million, for the period Feb. 1, 1984–Jan. 31, 1985. Zone I encompasses EPA Regions 1, 2, and 3. The contract involves emergency removals and remedial actions concerning hazardous and toxic materials under the Superfund law. In addition, OHM will be a first-tier subcontractor for ERCS Zone III, which encompasses EPA Region 5. The company plans to locate "response centers" in Springfield, Mass., and Richmond, Va.

"We are ahead of schedule in development of renewable and alternative energy sources," says G. J. Bjorklund, vice-president of system development for Southern California Edison (SCE, Rosemead). Detailing SCE's work in new technologies, Bjorklund cited wind, solar, biomass, and cogeneration developments by independent power producers as pacesetters in the shift to renewables. Other promising steps he named involve efforts toward commercial development of geothermal energy and fuel cells. SCE is committed to encouraging development of more than 2190 MW of electric generation from renewable and alternative sources by 1993.

ES&T FEATURES

Groundwater contaminant transport modeling

Its theory and the role it plays in evaluating, containing, and remedying contamination are discussed

George F. Pinder
Department of Civil Engineering
Princeton University
Princeton, N.J. 08544

The last decade has seen an extraordinary growth in the development and use of groundwater transport modeling. Whereas models in the 1960s were devoted almost exclusively to problems associated with groundwater *supply*, current modeling efforts are very often motivated by a desire to simulate subsurface contaminant movement. Moreover, advanced computer technology has helped the groundwater model evolve from a scientific curiosity to an important and widely used engineering tool.

Groundwater flow

Because groundwater contaminant transport is neither readily observed nor easily measured, the lay public views it as something approaching the

FIGURE 1
The saturated and unsaturated zones[a]

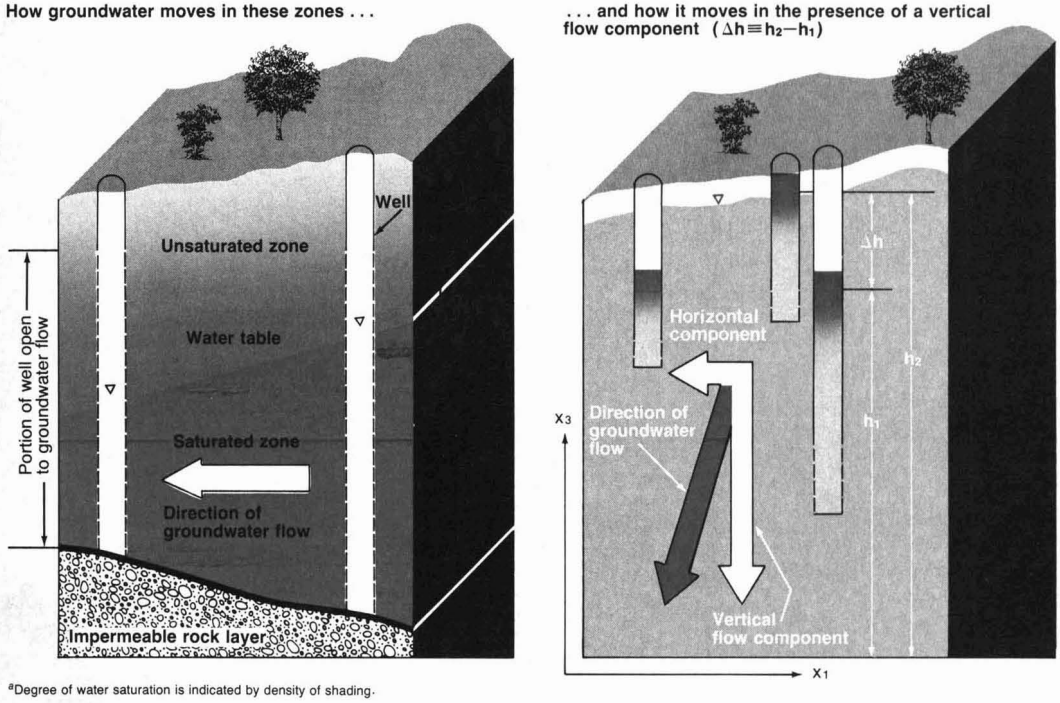

[a]Degree of water saturation is indicated by density of shading.

FIGURE 2
Species transport

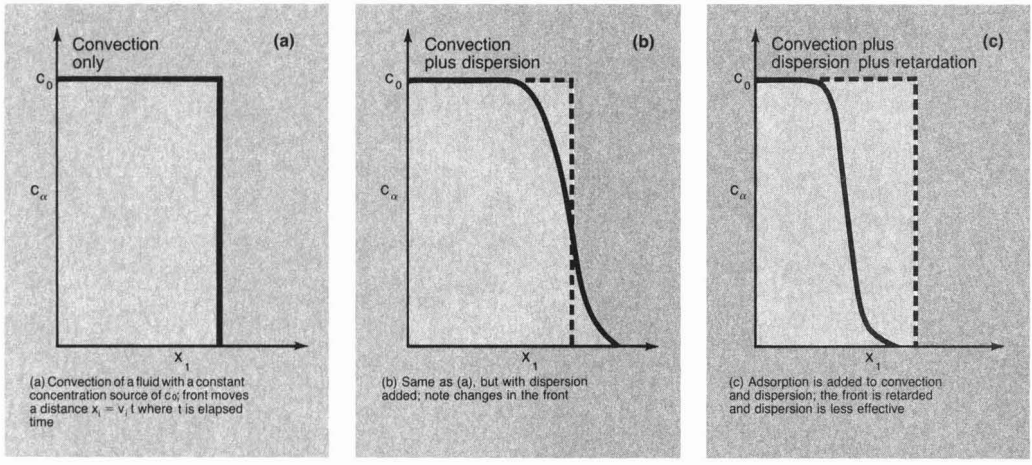

(a) Convection of a fluid with a constant concentration source of c_0; front moves a distance $x_1 = v_1 t$ where t is elapsed time

(b) Same as (a), but with dispersion added; note changes in the front

(c) Adsorption is added to convection and dispersion; the front is retarded and dispersion is less effective

metaphysical. Yet, because of the enormous impact this phenomenon has on the long-term viability of potable water supplies, contaminant transport is of tremendous scientific and practical importance.

Groundwater can be regarded as water occupying subterranean intergranular void spaces. Near the land surface, this water normally shares the available void space with air; this region is called the unsaturated zone (Figure 1). With depth, the proportion of water to air increases until the pore space is entirely saturated with water. While the water pressure in the unsaturated zone is normally less than atmospheric, in the saturated zone, it is generally greater than atmospheric. The level that represents the depth at which atmospheric pressure is encountered is designated as the water table, as shown in Figure 1.

The elevation (h) of the water table is, in a sense, a measure of the fluid potential, and is represented by the height to which water will rise in a well that penetrates the saturated zone. Because groundwater velocity in that zone is proportional to the fluid potential gradient, the direction of the maximum slope of the water table generally coincides with the direction of the horizontal component of groundwater flow.

The proportionality constant in this relationship is the ratio of the hydraulic conductivity of the groundwater reservoir to its porosity. The hydraulic conductivity (K_{ij}) is a measure of the friction losses incurred by groundwater in transit, while the porosity (ϕ) is a measure of the intergranular void space. Combining these terms, we obtain a relationship describing flow in the areal plane, or Darcy's law

$$v_i = -\frac{K_{ij}}{\phi} \cdot \frac{\partial h}{\partial x_j}, \; i, j = 1, 2 \qquad (1)$$

where (x_1, x_2, x_3) are principal axes and $\partial h/\partial x_j$ can be thought of as the slope of the water table in the horizontal x_i directions. Summation is assumed over repeated subscripts.

Although the concept of horizontal groundwater flow is easily understood when the water table is viewed as a potential surface, the vertical flow component requires additional explanation. The vertical groundwater flow velocity is also proportional to the fluid potential gradient. In fact, Equation 1 holds in this case as well; one simply allows the indexes i and j to range over the interval 1–3.

Now, however, one must discard the water table concept and think of h as the hydraulic head. The hydraulic head is readily measured as the elevation of the fluid level in a well which admits groundwater only over a small vertical increment. This is illustrated in Figure 1. Thus, the vertical gradient is established in the field by locating two such wells very near to each other in such a manner that they have access to the groundwater reservoir at two different vertical increments separated by a distance Δx_3. One then observes the change in hydraulic head Δh over this interval, i.e.,

$$v_3 = -\frac{K_{33}}{\phi}\frac{\partial h}{\partial x_3} \approx -\frac{K_{33}}{\phi}\frac{\Delta h}{\Delta x_3} \qquad (2)$$

In addition to the momentum balance relationship expressed by Equations 1 and 2, a complete mathematical description of groundwater flow requires a mass conservation principle. For the case of saturated groundwater of density ρ, mass conservation is given by:

$$\frac{\partial}{\partial t}(\phi\rho) + \frac{\partial}{\partial x_i}(\phi v_i \rho) = 0, \quad i = 1, 2, 3 \qquad (3)$$

where t is time. Although the first term in Equation 3 could be important for problems of water supply in which reservoir storage effects can be significant, this term can be safely neglected for most problems involving contaminant transport. The reason for this is the dramatic difference between the rate of propagation of a pressure front, which is described by the first term in Equation 3 and expressed in terms of ft/s, and the fluid velocity which is on the order of ft/d. Neglecting this term and combining Equations 1–3, we obtain the classical equation of groundwater flow:

$$\frac{\partial}{\partial x_i}\left(K_{ij}\frac{\partial h}{\partial x_j}\right) = 0, \quad i = 1, 2, 3 \qquad (4)$$

Solving Equation 4 requires the additional specification of boundary conditions expressed in terms of the dependent variable h. This information, along with the parameters K_{ij} and ϕ, is obtained from field investigations. Once h is obtained through the solution of Equation 4 for the entire region of interest, one can readily

FIGURE 3
Defining discrete elements

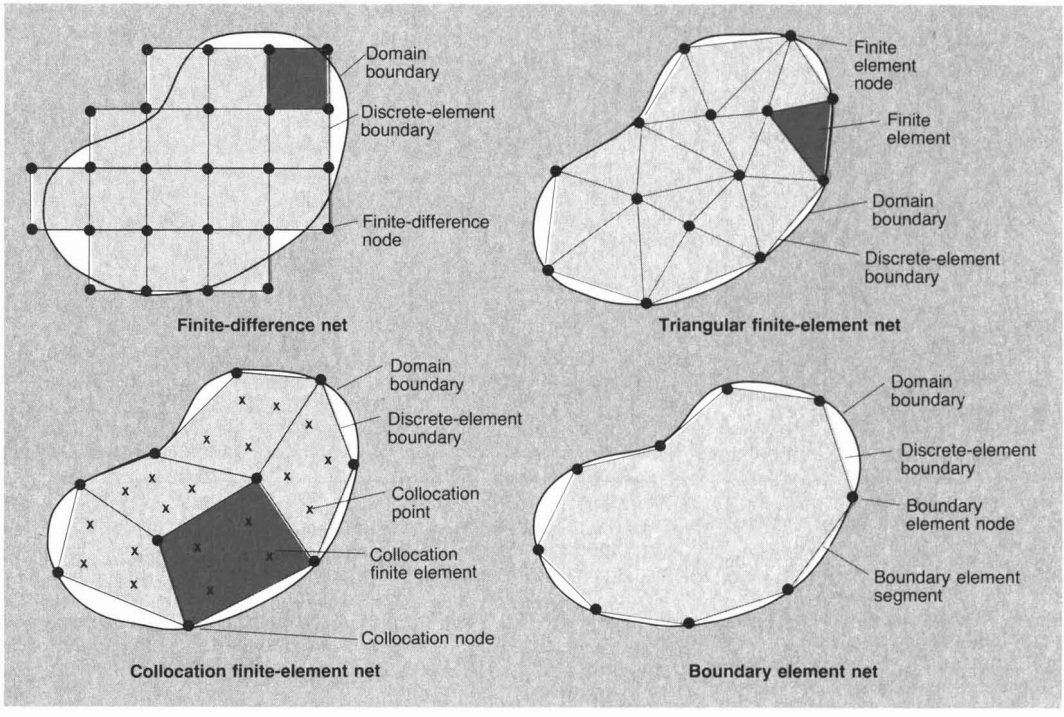

Note: Each node represents one equation per independent variable, except in the case of collocation, in which each collocation point represents one equation. The boundary element, collocation, and finite-element methods offer flexibility in geometric representation.

return to Equation 1 or 2 to retrieve the fluid velocity.

Solute transport

Although knowledge of the average velocity of fluids through pores v_i is necessary for the description of contaminant movement, it is *not* sufficient. The average pore velocity v_i does not account for the small-scale, rather tortuous pore-level behavior of the fluids. This highly complicated pore-level fluid flow pattern is important in contaminant transport because it tends to spread the solute in the fluid while the solute is being convected through the porous medium.

The mass flux $J_{\alpha i}$ is, therefore, given in terms of the mass concentration of a species α per unit volume of the fluid phase, c_α, as

$$J_{\alpha i} = v_i c_\alpha - D_{ij} \frac{\partial}{\partial x_j} c_\alpha \qquad (5)$$

where D_{ij} is the dispersion coefficient and the gradient of the fluid density is assumed to be small. The first term on the right side of Equation 5 describes the convection of species α, and the second defines the dispersion. Molecular diffusion is incorporated into the functional form of D_{ij}.

The conservation of mass for species α is given as:

$$\frac{\partial}{\partial t}(\phi c_\alpha) + \frac{\partial}{\partial x_i}(\phi J_{\alpha i}) = -f_\alpha \qquad (6)$$

where f_α is the transfer of species from the liquid to the solid phase. An equation analogous to Equation 6 can also be written for the solid phase, that is, the soil grains and rock matrix; by expressing the concentration of species on the solid phase as c_α^s, we obtain

$$\frac{\partial}{\partial t}[(1-\phi)c_\alpha^s] = f_\alpha \qquad (7)$$

because the grains are assumed to have negligible velocity. Equation 7 is normally combined with an empirical relation known as the *linear adsorption isotherm*

$$c_\alpha^s = \rho_s K_{D\alpha} c_\alpha \qquad (8)$$

where ρ_s is the density of the solid phase, and $K_{D\alpha}$ is the *distribution coefficient,* which describes the adsorption of species on the solid phase. The commonly used transport equation is the combination of Equations 5–8:

$$\frac{\partial}{\partial t}[\phi c_\alpha + (1-\phi)\rho_s K_{D\alpha} c_\alpha] + \frac{\partial}{\partial x_i}(\phi v_i c_\alpha) - \frac{\partial}{\partial x_i}\left(\phi D_{ij}\frac{\partial c_\alpha}{\partial x_j}\right) = 0 \qquad (9)$$

The three phenomena, convection, dispersion, and retardation, are illustrated schematically in Figure 2.

Although Equation 9 describes species transport in many commonly encountered groundwater systems, it specifically omits radioactive decay and kinetic chemical reactions. These topics are beyond the scope of this presentation; however, they are discussed in Huyakorn and Pinder, 1983. As in the case of Equation 4, describing fluid flow, the species transport equation (Equation 9) also requires additional information—in this case, initial and boundary conditions and parametric data. Equations 1, 2, 4, and 9 constitute the mathematical

FIGURE 4
Field investigation of groundwater contamination[a]

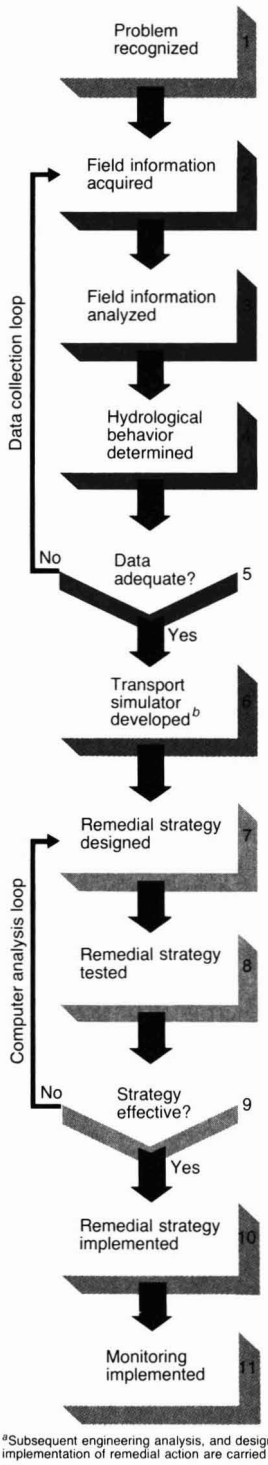

[a]Subsequent engineering analysis, and design and implementation of remedial action are carried out.

[b]The transport simulator plays a central role.

foundation of the contaminant transport model. Now, the methodology available to solve these equations can be considered.

Numerical simulation

The mathematical model composed of Equations 1, 2, 4, and 9 can generally be solved only by means of a numerical approach. The common characteristic of all numerical approaches is their transformation of a set of partial differential equations into a set of discrete equations. These, in turn, are typically expressed in terms of matrix equations that, for problems of practical significance, must be solved with a digital computer. The discrete equations are associated with a subdivision of a region of interest, usually a specified segment of the groundwater reservoir, into smaller regions often called *elements*. Several typical methods of defining discrete elements are illustrated in Figure 3, along with the associated numerical procedure.

The numerical solution procedure can be carried out with two distinct steps. First, the governing equations, along with the appropriate initial and boundary conditions, are approximated through a suitable numerical scheme. Common numerical approaches include the finite difference, finite element, and collocation methods, as well as the method of characteristics. In addition, the boundary element method, a relatively new approach, offers significant computational advantages for certain types of problems.

Of these, the finite-difference approach and its close relative, the integrated finite-difference method, are the most intuitively simple and computationally straightforward methods in general use. The finite-element method allows a more flexible subdivision of the region. The element geometry in two dimensions, for example, can be triangular, as well as rectangular; one method even permits the use of quadrilaterals with curved sides.

The collocation approach, like the finite-element method, is based on the method of weighted residuals. It differs from the finite-element method in important, but rather subtle ways, which this presentation is too brief to describe. Additional insight into all three methodologies can be found in Lapidus and Pinder, 1982, and Botha and Pinder, 1983, as well as in other, more comprehensive volumes dedicated to individual techniques (see, for example, Pinder and Gray, 1977; Wang and Anderson, 1983; Remson et al., 1971).

The method of characteristics is quite different from the preceding three because it does not rely on the same mathematical underpinnings. It is attractive because of its conceptual simplicity and because it requires little mathematical sophistication to understand, program, and apply in the field. Because of the lack of mathematical rigor associated with this scheme, care must be exercised to avoid misuse and abuse of this method in practical applications.

The boundary element method relies on a reduction in dimensionality to enhance efficiency. In essence, it reduces a three-dimensional problem to two dimensions and a two-dimen-

FIGURE 5
Groundwater transport model formulation and utilization

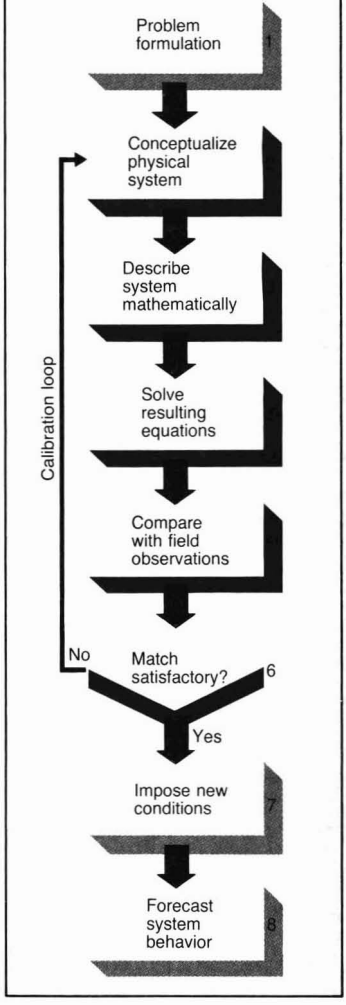

sional problem to one dimension. It is suited primarily to steady-state problems wherein field parameters can be assumed to be constant over large regions. An excellent description of the application of this method to groundwater flow is found in Liggett and Liu, 1983.

The second step in numerical simulation is the solution of the resulting algebraic equations. The efficacy of the simulator will often hinge on the efficiency of the equation-solving algorithm. Because the matrix structure of these equations depends on the approximation method, and the solution strategy, in turn, depends on the matrix structure, the methods of approximation and solution are very closely tied to one another. The alternating-direction methods, for example, employ approximation procedures that allow the overall algebraic problem to be subdivided into smaller problems with a concomitant enhancement in computational efficiency.

The combination of the governing equations, approximation procedure, and algebraic equation solver constitutes the mathematical apparatus of the groundwater simulator. To this point, the simulation is not problem specific, but rather is applicable to any field situation in which the basic porous-medium physics are described by the proposed governing equations. The task remains to provide the problem-specific initial and boundary conditions and parametric information required to complete the mathematical model.

Transport modeling

Transport modeling can be thought of as the practical use of the foregoing mathematical apparatus in the field. It should form an integral part of most groundwater contamination investigations and analyses. As the quantitative vehicle for making contaminant behavior forecasts, it has found application in evaluating the effectiveness of proposed remedial schemes. In litigation, contaminant transport models have also been used to demonstrate the history of human ingestion of groundwater contaminants that have been observed recently in active wells.

The role of the transport model in a typical field investigation and the associated analysis is outlined in the flow chart of Figure 4. Although recent legislation has encouraged precautionary field investigations, the discovery of groundwater contamination has more often been accidental.

Once the problem is recognized,

FIGURE 6
Investigating contamination at Price's Landfill

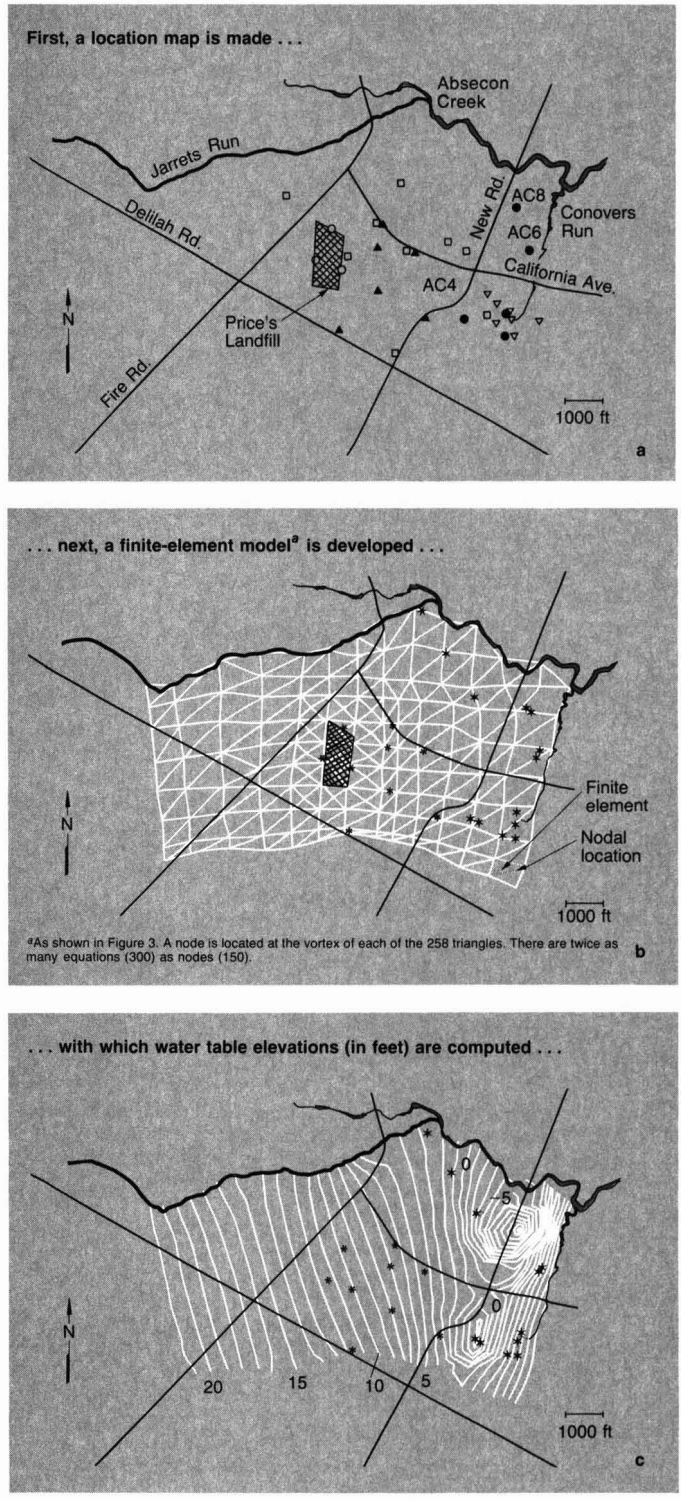

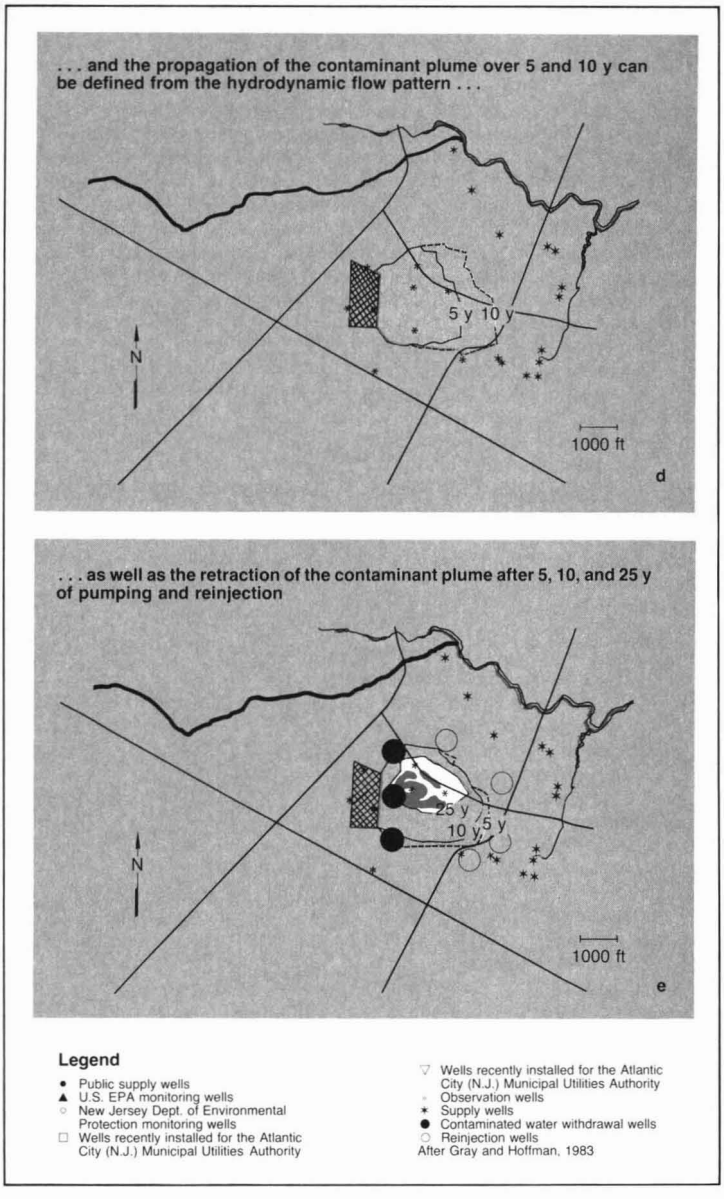

data are collected (Figure 4, boxes 1–4). However, the data acquired are often subject to equivocal interpretations, and additional field investigations (box 5) may be needed.

After any such investigations, when the physical system, including the hydrodynamics, is properly understood, the transport modeling phase is normally begun (box 6). Occasionally, modeling is initiated earlier, and preliminary results are used to enhance the data collection program.

Remedial design activities start after completion of the transport model (box 7). The model is used to test various remedial strategies proposed by the experienced hydrologist (box 8). On the basis of modeling forecasts, various mitigative strategies are evaluated and ranked according to technical merit (box 9).

After the examination of all reasonable alternatives, a remedial scheme is selected, based on technical, sociopolitical, and economic criteria (box 10). Because many, if not most remedial designs require the use of relatively new technology in a little-understood environment, a comprehensive monitoring program is considered an integral part of the overall investigative and remedial program (box 11).

While the general concept of a field investigation preceding model development and mitigative design is a desirable course of action, it is occasionally necessary to go through the data collection loop again after model development has been initiated. The principal reasons are:

- a recognition, via the model, that important data gaps exist;
- a discovery that a remedial design requires behavior forecasting beyond the original model boundaries;
- the demands of the designer of the remedial scheme, or the onset of litigation, which require a more detailed simulation in a region where relatively sparse data were considered adequate for the proposed use of the original model; and
- the deliberate design of the data collection program to proceed in parallel with the model development such that the model results would provide guidance in the optimal allocation of limited financial resources.

Modeling strategy

The design and implementation of a transport modeling strategy can also be presented by using the flow chart concept. Once the decision to construct a simulator is made, the first task is to establish the scope of the problem (Figure 5, box 1). This is very important, because the geometric size, mathematical sophistication, and degree of detail of the model will determine how it is to be used.

With the problem clearly delineated, the next step is to use the available geological and hydrological information to conceptualize the physical system (box 2). At this point, the geologist, hydrologist, and mathematical modeler must work together closely to avoid any basic misinterpretation which could be inadvertently carried through the analysis. The conceptual model of the system is now translated into physical-mathematical statements such as Equations 1, 2, 4, and 9, on which are imposed initial and boundary conditions (box 3). These equations are approximated with the aid of one of the numerical schemes outlined above, and the resulting set of algebraic equations is solved (box 4) with the digital computer. The solutions obtained through different parametric input, such as hydraulic conductivity, are now compared with field observations (box 5).

If the match is "satisfactory," the model is ready for behavior forecasting. A poor match requires the use of different parameters, boundary conditions, or, in the worst case, a com-

plete reevaluation of the conceptual model of the system (box 6).

"Satisfactory" means different things to different people, so it is important to keep in mind the problem definition in box 1 in order to establish an acceptable calibration level. The model, once calibrated, can be used to predict contaminant movement under various new hydrodynamic conditions (boxes 7 and 8). Typical new hydrodynamic conditions would consist of scavenger and injection wells, drains, walls of low hydraulic conductivity, and impermeable caps.

Field application

Price's Landfill is located in Pleasantville, N.J. After use as a sand and gravel pit from 1960 to 1968, it was converted to a landfill and subsequently received various forms of sanitary and industrial wastes until 1972. The landfill, which extends to within 2 ft of the water table, is underlain by a sand aquifer approximately 80 ft thick. A clay unit separates this aquifer from a lower unit; both the upper and lower aquifers are used for water supply. Unfortunately, the landfill is located approximately 3500 ft upgradient of several public supply wells for Atlantic City. The wells with prefix "AC" in Figure 6 are public supply wells drawing water from the upper aquifer.

The discovery of organic contaminants in many of the monitoring wells shown in Figure 6a gave rise to litigation and a concomitant flurry of geohydrological studies. As part of the ensuing investigations, several numerical simulators were developed. The modeling effort by Gray and Hoffman, 1983, provides an interesting example of the application of transport simulation and will be considered in light of Figure 5.

The problem at the site of Price's Landfill was to establish the current extent of contamination; to forecast the behavior of the plume, particularly its impact on the Atlantic City wells; and to evaluate the effectiveness of proposed remedial schemes. The *plume* is defined here as the groundwater domain containing nonreacting, nonsorbing solutes emanating from the landfill.

Since at the time of the study, no chemical contamination had been found in the lower aquifer, the upper or Cohansey aquifer was of principal concern. Because of the geohydrological aspects of the Cohansey aquifer, a vertically integrated two-dimensional model was selected. Later models of the site employed a three-dimensional formulation to examine migration through the clay.

The boundary conditions imposed on the governing Equations 1, 2, 4, and 9 can be discussed more easily with the aid of Figure 6b. This figure illustrates the model domain, which has been subdivided through the use of triangular finite elements. The northern and northeastern borders of the model coincide with the surface water bodies, namely Jarret's Run, Absecon Creek, and Conovers Run (see Figure 6a for locations). Water levels corresponding to the elevations of their surfaces were specified in the model as constant-head boundary conditions. The southern boundary is collinear with a flow line; thus, a condition of no flow into the model was specified. The western boundary was sufficiently remote from the existing and proposed pumping wells that a specified water level would not influence the drawdown forecasts.

The finite-element method was used to solve the governing equations, and the solutions for the water levels were compared against field observations. The water level solution considered to be an acceptable match is illustrated in Figure 6c. The water level contours indicate a regional flow to the east. In the neighborhood of large pumping centers, a distinct cone of depression (lowering of the water table in the vicinity of a pumping well) is observed.

The water level solution of Figure 6c is used to generate a groundwater velocity distribution which, in turn, is employed in the solution of contaminant transport equations. The boundary conditions selected for the transport equation are a specified concentration along the eastern edge of the landfill site and zero concentration along the model perimeter. The calculated time evolution of the contaminant plume geometry, as defined by a conservative chemical species, is presented in Figure 6d. The contour that defines the perimeter of the plume at each time interval represents 5% of the source concentration.

Remedial strategies

The model was subsequently used to examine remedial strategies. One such strategy assumed that the Atlantic City wells would cease pumping in the upper aquifer, but that three additional scavenger wells would be installed. These wells are indicated by the black dots in Figure 6c. Each pumped well produces 10 million gal/mo, of which 8 million gal/mo are reinjected, after treatment, at the wells identified by the circles in Figure 6e.

The dynamics of the plume are also illustrated in Figure 6e. Since the plume shrinks in response to this remedial scheme, it is apparent that the approach is a technically effective strategy. On the basis of field experience and principles delineated above, it is proposed that modeling should form an integral and important element of any and all groundwater contamination investigations.

Acknowledgment

Before publication, this article was reviewed for suitability as an *ES&T* feature by Douglas M. Mackay and Paul Roberts of Stanford University, Stanford, Calif. 94305.

References

Botha, J. F; Pinder, G. F. "Fundamental Concepts in the Numerical Solution of Differential Equations"; John Wiley: New York, N.Y., 1983.

Gray, G.; Hoffman, J. L. *Ground Water* **1983,** *21*(1), 7–21.

Huyakorn, P.; Pinder, G. F. "Computational Methods in Sub-Surface Flow"; Academic Press: New York, N.Y., 1983.

Lapidus, L.; Pinder, G. F. "Numerical Solution of Partial Differential Equations in Science and Engineering"; John Wiley: New York, N.Y., 1982.

Liggett, J. A.; Liu, P.L-F. "The Boundary Integral Equation Method for Porous Media Flow"; George Allen and Unwin: London, U.K., 1983.

Pinder, George F.; Gray, W. G. "Finite Element Simulation in Surface and Subsurface Hydrology"; Academic Press: New York, N.Y., 1977.

Remson, I.; Hornberger, G. M.; Molz, F. J. "Numerical Methods in Subsurface Hydrology"; John Wiley: New York, N.Y., 1971.

Wang, H. F.; Anderson, M. P. "Introduction to Groundwater Modeling"; Freeman: San Francisco, Calif., 1982.

George Pinder *is currently chairman of the department of civil engineering at Princeton University. After graduating from the University of Western Ontario in 1965 with a BS in geology, he attended graduate school at the University of Illinois, where he received his PhD in 1968. Upon graduation, he joined the U.S. Geological Survey Water Resources Division in Washington, D.C., until moving to Princeton University as director of the Water Resources Program in 1972. He has published approximately 100 papers on numerical simulation of subsurface flow and transport as well as four monographs on numerical analysis and subsurface flow.*

Assessing health effects of air pollution

The role of controlled studies of human volunteers is examined

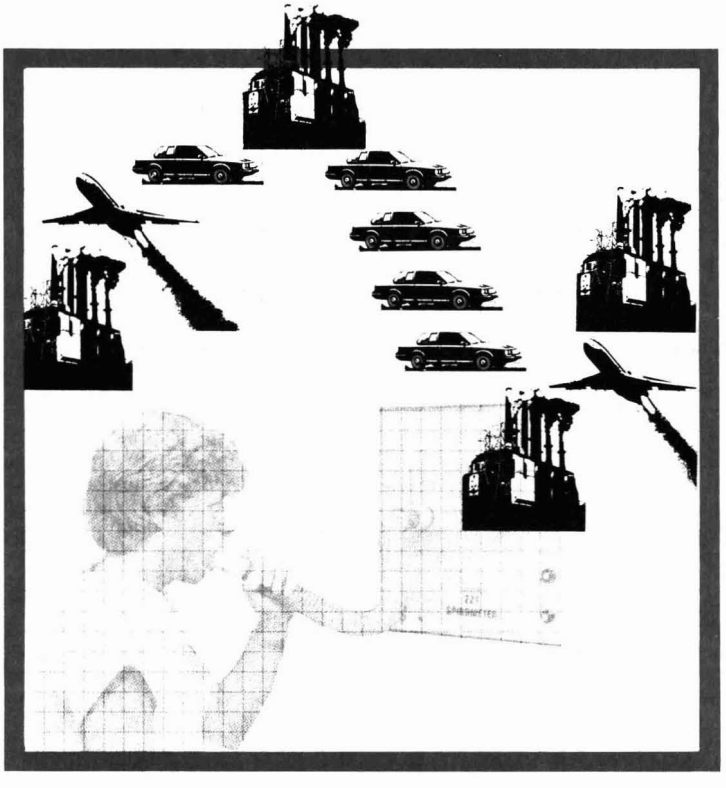

Jack D. Hackney
William S. Linn
Edward L. Avol
Environmental Health Service
Rancho Los Amigos Hospital
School of Medicine
University of Southern California
Downey, Calif. 90242

To set air quality standards adequate to protect public health, regulatory agencies need extensive, reliable scientific data on the health effects of air pollutants. For short-term standards especially, much of the necessary information is obtained by observing the responses of human volunteers who have been exposed deliberately to pollutants under controlled laboratory conditions. Despite its importance in the regulatory process, the field of controlled human studies remains unfamiliar to many in the environmental protection and health professions.

This article describes some current problems in assessing health risks from polluted air, the capabilities and limitations of controlled human studies in solving these problems, and the complementary relationship of controlled human studies to two other risk-assessment disciplines: animal toxicology and epidemiology. Emphasis is placed upon respiratory irritants common in ambient air, specifically photochemical oxidants and sulfur oxides. A number of other pollutants found in community or occupational environments also may be studied through human exposures, as indicated in Table 1.

What are controlled human studies?

Human exposure studies require contributions from the disciplines of atmospheric chemistry, environmental engineering, physiology, and clinical medicine. Scientific investigators must create within the laboratory a polluted air environment that is a reasonably realistic model of the polluted ambient environment of concern. They must then recruit volunteer subjects who are representative of the population at risk in the community. The subjects must be exposed to laboratory polluted air under conditions that are well controlled, well documented, and similar to ambient exposure conditions insofar as possible. Finally, the investigators must employ the most sensitive biomedical tests available to detect subjects' responses, if any, to the pollutant dose.

As in most medical experiments, subjects' responses to "treatment" must be compared against a control or placebo. Subjects should be "blind" to the difference between the actual exposure and control conditions, as should the experimenters who are actually measuring the results. Otherwise, the expectations of the people involved, or experimental stresses other than the pollutant itself, may provoke responses that could be mistaken for adverse effects of the pollu-

Table 1
Common ambient air pollutants studied by controlled human exposures

Substance	NAAQS [a]	"High" ambient concentrations [b]	Effects reported in controlled human studies
O_3	0.12 ppm (1 h)	0.3 ppm (1 h) in Los Angeles	Gradually developing (30–60 min) respiratory irritation above 0.3 ppm with light exercise, below 0.2 ppm with heavy exercise (*3*, *7–13*)
SO_2	0.14 ppm (24 h)	0.2–0.3 ppm (1 h) in some urban areas; above 1 ppm near some smelters	Rapidly developing (<5 min) airway constriction and symptoms in asthmatics below 0.5 ppm with heavy exercise (*31–37*)
CO	9 ppm (8 h)	20 ppm (1 h) in Los Angeles	Reduced oxygenation of body tissues due to formation of CO–hemoglobin, reduced exercise tolerance and mental performance, lowest effective dose controversial (*45*)
NO_2	None	0.3 ppm (1 h) in Los Angeles	Little effect below 1 ppm, except possible increase in some asthmatics' response to airway-constricting drugs (*46*)
Peroxyacetyl nitrate	None	<0.1 ppm (1 h) in Los Angeles [d]	Little effect near 0.2 ppm, in brief exposure with heavy exercise or 4-h exposure with light exercise (*14*, *15*)
H_2SO_4, $(NH_4)_2SO_4$	[c]	<50 $\mu g/m^3$ (2 h) in Los Angeles [d]	Little effect near 100 $\mu g/m^3$, except possible increase in rate of particle clearance from airways (*47*)
NH_4NO_3	[c]	<100 $\mu g/m^3$ (2 h) in Los Angeles [d]	Little effect near 200 $\mu g/m^3$, 2-h exposure with light exercise (*44*)
$Fe_2(SO_4)_3$	[c]	<25 $\mu g/m^3$ (2 h) in Los Angeles [d]	Little effect near 75 $\mu g/m^3$, 2-h exposure with light exercise (*48*)

[a] Short-term primary (health-based) National Ambient Air Quality Standard, averaging time in parentheses.
[b] Concentrations likely in moderately severe pollution episodes. "Worst-case" concentrations may be somewhat higher.
[c] NAAQS for total suspended particulate matter is 260 $\mu g/m^3$ (24 h). No standards for separate components.
[d] Few ambient monitoring data available.

tant exposure. Purified air with no added pollutants usually serves as the control atmosphere.

In some cases, it is impossible to blind subjects or staff members to the atmospheric conditions—for example, when the experimental pollutant has a distinctive odor at the test concentrations. Dose–response studies, in which subjects are exposed to more than one concentration of the experimental pollutant, help to overcome this problem. If an observed physiological effect increases in magnitude consistently with increases in pollutant dose, this supports the possibility of a direct causal association and opposes the possibility of a nonspecific, psychologically induced response.

Because physiological and clinical responses vary with the subjects and often with the measurement technique itself, statistical tests must be applied to determine whether differences between control and exposure conditions are meaningful. Statistically significant changes with exposure may not always have medical significance or imply risk to public health. They may represent an appropriate homeostatic response to an entirely tolerable stress, or may reflect a minor annoyance rather than a meaningful threat to health.

Conversely, failure to find statistically significant changes does not necessarily rule out risk to health. Negative results may be misleading if the experimental subjects or tests are not maximally sensitive or if the subject population is too small to allow statistical analyses to be meaningful. To overcome these problems, investigators often combine very sensitive subjects (such as people with preexisting respiratory disease), with very sensitive test procedures, and very severe pollution (such as concentrations attained in ambient air only rarely in the most polluted cities). Even with this worst-case experimental condition, however, negative results are not entirely definitive, since more sensitive tests or more sensitive people might be discovered later. Such an occurrence is discussed in the section on sulfur oxides.

Capabilities and limitations

Human exposure studies are usually empirical and descriptive in nature. They ask the questions: "Is there an effect from exposure to substance X?" "What sort of people are affected?" "How severe is the effect at a given exposure concentration?" "How long does it last?" Except in very limited contexts, not much is understood about the mechanisms of reaction between pollutant substances and the human body in terms of chemistry, pharmacology, or physiology. Broad unifying principles to predict effects of pollutant exposure are not generally available. In most cases, the only practical way to evaluate a suspected health hazard is to obtain specifically relevant experimental evidence.

Most human studies are intended to support air quality regulatory efforts directly. They are often funded either by regulatory agencies or by industries subject to regulation. Their results must be credible enough to withstand the intense scientific peer review and legal scrutiny that is conducted by all interested groups affected by regulatory decisions.

Requirements for credibility can be stated in terms of "three R's": scientific *rigor* or control of experimental variables, *relevance* to people's actual exposures and biological responses, and *redundancy*, that is, independent replication of experimental results (*1*, *2*). Toxicologic studies of laboratory animals can be well-controlled and independently replicated. However, their relevance to human health depends on how well the animal model represents human characteristics. The appropriateness of a particular animal model, either for normal human functioning or for a human disease process, often is in doubt.

Epidemiologic studies of air pollution are undeniably relevant to human health. Usually their scientific rigor is less than ideal, however, particularly with respect to characterization of the subjects' pollution exposures. Furthermore, because human behavior is seldom consistent among

ES&T

READER SURVEY

Spending Plans Study

For each of the following ten categories, please circle an appropriate number to indicate whether you anticipate spending more (M), less (L), or the same (S) during the next 12 months than you did during the past 12 months.

For example, if you spent nothing for Air Monitors in 1983 and plan to again spend nothing in 1984, your answer is S for "same" and you would circle #66 on the reply card.)

PRODUCT SPENDING PLANS

M = more
L = less
S = same

Air monitors & samplers
M:64 L:65 S:66

Air purification equipment
M:67 L:68 S:69

Water monitors & samplers
M:70 L:71 S:72

Water purification equip.
M:73 L:74 S:75

Waste disposal equipment
M:76 L:77 S:78

Water treatment chemicals
M:79 L:80 S:81

Construction services
M:82 L:83 S:84

Consulting services
M:85 L:86 S:87

Laboratory instruments
M:88 L:89 S:90

Lab reagents, gases
M:91 L:92 S:93

ES&T APRIL 1984 VALID THROUGH AUGUST1984

ADVERTISED PRODUCTS:

7	8	9	10	11	12	13	14	15	16	17
18	19	20	21	22	23	24	25	26	27	28
29	30	31	32	33	34	35	36	37	38	39
40	41	42	43	44	45	46	47	48	49	50
51	52	53	54	55	56	57	58	59	60	61
62	63	64	65	66	67	68	69	70	71	72
73	74	75	76	77	78	79	80	81	82	83
84	85	86	87	88	89	90	91	92	93	94

NEW PRODUCTS:

101	102	103	104	105	106	107	108	109	110	111
112	113	114	115	116	117	118	119	120	121	122
123	124	125	126	127	128	129	130	131	132	133
134	135	136	137	138	139	140	141	142	143	144
145	146	147	148	149	150	151	152	153	154	155
156	157	158	159	160	161	162	163	164	165	166
167	168	169	170	171	172	173	174	175	176	177
178	179	180	181	182	183	184	185	186	187	188
189	190	191	192	193	194	195				

NAME

TITLE

FIRM

STREET

CITY

STATE ZIP

PHONE ( )

TO VALIDATE THIS CARD, PLEASE CHECK ONE ENTRY FOR EACH CATEGORY BELOW:

Intensity of product need:
1. Have salesman call
2. Need within 6 months
3. Future project

Employees at this location:
1. Under 25
2. 25 - 29
3. 100 - 299
4. 300 - 499
5. 500 - 999
6. 1000 - 2999
7. Over 3000

Areas of your responsibility:
A. Air pollution only
B. Water pollution only
C. Waste treatment only
D. Air & Water pollution
E. Air & Waste treatment
F. Water & Waste treat
G. Air/Water/Waste
H. Other Environmental

Principal product to which my work relates:
A. Oil/Gas/Petroleum
B. Plastics/Resins
C. Rubber
D. Drug/Cosmetics
E. Food/Beverages
F. Textile/Fiber
G. Pulp/Paper/Wood
H. Soaps/Cleaners
I. Paint/Coating/Ink
J. Agrichemicals
K. Stone/Glass/Cement
L. Metals/Mining
M. Machinery
N. Auto/Aircraft
O. Instrument/Controls
P. Inorganic Chemicals
Q. Organic Chemicals
R. Other Manufacturing
S. Design/Construction
T. Utilities
U. Consulting Services
V. Federal Government
W. State Government
X. Municipal Governmen
Y. Education

This copy of ES&T is . . .
1. Personally addressed to me in my name
2. Addressed to other person or to my firm

Membership status:
1. I am an ACS member
2. Not an ACS member

Circle 94 for subscription form to ES&T

ES&T READER SURVEY

The extent to which our overall economy, governmental policy, and possible industrial recovery are influencing environmental control spending plans is unclear. In order to generate an indication of current trends, we invite you to participate in a survey by circling numbers on our reader service reply card and mailing your answers to us.

NO POSTAGE NECESSARY IF MAILED IN THE UNITED STATES

BUSINESS REPLY CARD

FIRST CLASS Permit #27346 Philadelphia, Pa.

POSTAGE WILL BE PAID BY ADDRESSEE

ENVIRONMENTAL SCIENCE & TECHNOLOGY

ES&T

P.O. BOX #7826
PHILADELPHIA, PA 19101

NO POSTAGE NECESSARY IF MAILED IN THE UNITED STATES

BUSINESS REPLY CARD

FIRST CLASS Permit #27346 Philadelphia, Pa

POSTAGE WILL BE PAID BY ADDRESSEE

ENVIRONMENTAL SCIENCE & TECHNOLOGY

ES&T

P.O. BOX #7826
PHILADELPHIA, PA 19101

ES&T READER SURVEY

The extent to which our overall economy, governmental policy, and possible industrial recovery are influencing environmental control spending plans is unclear. In order to generate an indication of current trends, we invite you to participate in a survey by circling numbers on our reader service reply card and mailing your answers to us.

ES&T APRIL 1984 VALID THROUGH AUGUST 1984

ADVERTISED PRODUCTS:

1	2	3	4	5	6	7	8	9	10	11
12	13	14	15	16	17	18	19	20	21	22
23	24	25	26	27	28	29	30	31	32	33
34	35	36	37	38	39	40	41	42	43	44
45	46	47	48	49	50	51	52	53	54	55
56	57	58	59	60	61	62	63	64	65	66
67	68	69	70	71	72	73	74	75	76	77
78	79	80	81	82	83	84	85	86	87	88
89	90	91	92	93	94					

NEW PRODUCTS:

101	102	103	104	105	106	107	108	109	110	111
112	113	114	115	116	117	118	119	120	121	122
123	124	125	126	127	128	129	130	131	132	133
134	135	136	137	138	139	140	141	142	143	144
145	146	147	148	149	150	151	152	153	154	155
156	157	158	159	160	161	162	163	164	165	166
167	168	169	170	171	172	173	174	175	176	177
178	179	180	181	182	183	184	185	186	187	188
189	190	191	192	193	194	195				

NAME

TITLE

FIRM

STREET

CITY

STATE ZIP

PHONE ( )

TO VALIDATE THIS CARD, PLEASE CHECK ONE ENTRY FOR EACH CATEGORY BELOW

Intensity of product need:

- ☐ 1. Have salesman call
- ☐ 2. Need within 6 months
- ☐ 3. Future project

Employees at this location:

- ☐ 1. Under 25
- ☐ 2. 25 - 29
- ☐ 3. 100 - 299
- ☐ 4. 300 - 499
- ☐ 5. 500 - 999
- ☐ 6. 1000 - 2999
- ☐ 7. Over 3000

Areas of your responsibility:

- ☐ A. Air pollution only
- ☐ B. Water pollution only
- ☐ C. Waste treatment only
- ☐ D. Air & Water pollution
- ☐ E. Air & Waste treatment
- ☐ F. Water & Waste treat.
- ☐ G. Air/Water/Waste
- ☐ H. Other Environmental

Principal product to which my work relates:

- ☐ A. Oil/Gas/Petroleum
- ☐ B. Plastics/Resins
- ☐ C. Rubber
- ☐ D. Drug/Cosmetics
- ☐ E. Food/Beverages
- ☐ F. Textile/Fiber
- ☐ G. Pulp/Paper/Wood
- ☐ H. Soaps/Cleaners
- ☐ I. Paint/Coating/Ink
- ☐ J. Agrichemicals
- ☐ K. Stone/Glass/Cement
- ☐ L. Metals/Mining
- ☐ M. Machinery
- ☐ N. Auto/Aircraft
- ☐ O. Instrument/Controls
- ☐ P. Inorganic Chemicals
- ☐ Q. Organic Chemicals
- ☐ R. Other Manufacturing
- ☐ S. Design/Construction
- ☐ T. Utilities
- ☐ U. Consulting Services
- ☐ V. Federal Government
- ☐ W. State Government
- ☐ X. Municipal Government
- ☐ Y. Education

This copy of ES&T is . . .

- ☐ 1. Personally addressed to me in my name
- ☐ 2. Addressed to other person or to my firm.

Membership status:

- ☐ 1. I am an ACS member
- ☐ 2. Not an ACS member

Circle 94 for subscription form to ES&T

ES&T
READER SURVEY

Reader Service Reply Card

It's computer processed for fast response to your inquiries

AND, IT'S FREE

FIGURE 1
"Missing links" between scientific disciplines concerned with assessment of health risks from air pollution

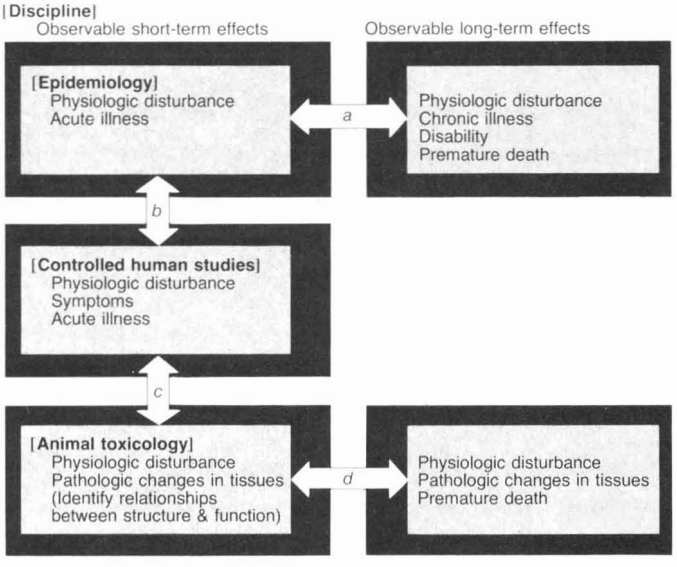

[a]Determine whether populations with atypical physiologic test results and/or high incidence of acute illness eventually develop high rates of disabling chronic disease or early death.

[b]Identify population subgroups whose members react clinically or physiologically to pollutants at atypically low doses.

[c]Identify animal "models," that is, similar responses of animals and humans to similar exposures.

[d]Determine relationship between acute effects of short-term exposures and chronic effects of prolonged or repeated exposures on structure and function of specific tissues and organs.

different times and places, epidemiologic studies are difficult to replicate.

To a certain extent, controlled human studies can avoid all of these problems. The characteristics of the subjects, exposure conditions, and responses to exposure can be documented reliably and in detail. Replication of exposure conditions is straightforward. Most limitations on human studies are ethical and practical, rather than scientific. No exposure that risks serious or irreversible illness can be contemplated. Internal body tissues other than blood samples usually cannot be examined. Subject populations are generally small. Only short-term exposures can be investigated, since volunteers cannot be expected to commit more than a few days or weeks to a study. This still leaves considerable latitude for useful investigation, as indicated in the following sections.

To investigate longer term or irreversible effects on human health, retrospective and prospective epidemiologic surveys are needed. To investigate biological mechanisms of response in detail, animal or cell-culture studies are needed. They allow effects to be observed at the tissue, cell, or molecular level—a difficult or impossible task in humans. Thus, controlled human studies complement rather than replace investigations in the other risk assessment disciplines.

A wide range of health risk questions must be answered, and each field of investigation can address only a fraction of them directly. Nevertheless, links among experimental findings from different disciplines can and should be established wherever possible, as indicated in Figure 1. One especially important but largely unresolved problem concerns a method of predicting long-term irreversible health effects by observing short-term reversible ones.

Methodology

Exposure facilities. The basic equipment required for exposure studies includes a source of purified air, a method of adding experimental pollutants (gases, aerosols, or both) to the purified air, a means of monitoring pollutant concentrations, and a facility for exposing subjects to the polluted air. Provision must also be made for appropriate control of temperature, humidity, light, and sound levels in the exposure environment.

Small-scale experiments may involve only one subject at a time, exposed through a mouthpiece or face mask. More elaborate studies may employ laboratory-sized exposure chambers large enough to house several subjects for extended periods. Mouthpiece or face mask exposures impose an unnatural mode of breathing, which in some circumstances may alter the subjects' responses to a pollutant. On the other hand, this method requires only simple equipment and small quantities of purified air and pollutant substances. Also, mouthpieces or masks make it easy to monitor subjects' breathing patterns, which may have important effects on physiological response.

Exposures in a large chamber allow the subjects to breathe naturally and engage in reasonably normal physical activity, thus considerably improving the relevance of the experimental conditions to the "real world." However, the costs to build and operate a state-of-the-art chamber are high, and only a few exist. Reference 3 describes the chambers in existence in 1977. Since then, new large-scale facilities have been put into operation at the University of North Carolina and the University of Rochester.

Figure 2, a schematic diagram of the air purification system in the authors' exposure laboratory, illustrates the various elements that may be needed (*4*). A high-temperature metal oxide catalytic agent, hopcalite, is employed to convert carbon monoxide and low-molecular-weight hydrocarbons to carbon dioxide. Additional hopcalite is used at ambient temperature in adsorption beds, which capture oxides of nitrogen. Each adsorption bed is periodically taken off-line and regenerated by heating. Activated carbon adsorbs most organic contaminants and catalytically decomposes ozone to molecular oxygen. Aluminum oxide pellets impregnated with potassium permanganate (trade name Purafil or Unisorb) are effective in removing oxides of nitrogen. High-efficiency paper particulate filters (HEPA filters) capture 99.9% of incident particles. This combination of equipment supplies the exposure chamber (volume 14 m^3) with air that contains only a few $\mu g/m^3$ of particles and undetectable or barely detectable levels of common pollutant gases, as determined by conventional ambient air monitoring instruments (see below) (*4*). The system's output is sufficient to allow approximately 15 air changes per hour in the chamber (see photo, p. 120A).

In less elaborate exposure cham-

FIGURE 2
Schematic representation of air purification system, pollutant generation system, and exposure chamber at Rancho Los Amigos Hospital, Downey, Calif.

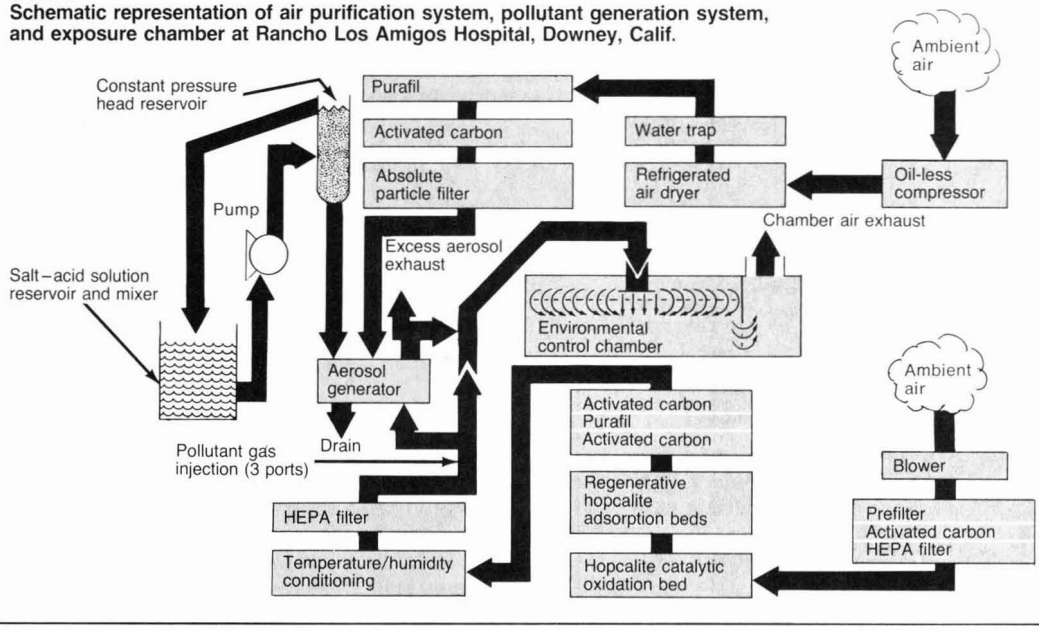

bers, typically only chemical adsorbents and HEPA filters are employed. Carbon monoxide is not removed efficiently by most such systems, but the large expense of a high-temperature catalyst and associated high-capacity air conditioning is avoided.

Air monitoring in laboratory exposure studies typically employs commercially available instruments of the types used in routine ambient air monitoring. Care must be taken to assure that air sampled by the instruments is representative of air breathed by the subjects. In some cases, pollutant concentrations may differ substantially at different points within the exposure facility.

Ozone is most commonly monitored by ultraviolet photometry, carbon monoxide and hydrocarbons by nondispersive infrared analyzers, and sulfur dioxide by flame photometry or ultraviolet photometry. Monitors for oxides of nitrogen typically are based on the chemiluminescent reaction of NO with O_3, which also may be exploited to monitor O_3. All these gas-monitoring techniques provide continuous readout and rapid response—essential to the safety of subjects. For aerosols, common ambient monitoring techniques involve collection of samples on filters and subsequent quantitative analysis, requiring hours or days to complete. Aerosol exposure studies thus need additional monitors with rapid response, such as optical particle counters or electrical-mobility analyzers.

Calibration procedures for monitoring equipment should be comparable to those used routinely by air quality regulatory agencies, so that health effect data, monitoring data, and standards will be expressed in the same terms. Inconsistencies can still arise: Most ozone health effect studies through the late 1970s employed the neutral buffered potassium iodide calibration method, reflecting federally approved practice. Ozone concentrations reported in these earlier publications must be multiplied by approximately 0.8 to make them consistent with the current federally approved ultraviolet photometer calibration method.

Pollutant gases such as SO_2 and NO_2 can be generated easily with source cylinders (usually low-concentration mixtures with nitrogen) and appropriate flow meters. Ozone can be generated either by ultraviolet lamps or by high-voltage discharge. Traces of nitrogen oxides may be produced inadvertently if ozone is generated from air rather than from 100% oxygen, but the concentrations are generally so low as to be toxicologically insignificant. Water-soluble particulate species such as sulfuric acid or ammonium sulfate may be generated by nebulizing aqueous solutions. Aerosols of insoluble particulate matter may be produced by Wright dust-feed generators or fluidized-bed generators, which thus far have been used to some extent in animal toxicology, but seldom in human studies.

Tests of biomedical response to exposure. The respiratory system is the first and foremost target of inhaled irritants and thus the primary focus of investigation in human exposure studies. In some cases, it is also important to examine the blood, either to detect a decrease in oxygenation resulting from respiratory disturbances, or to determine the biochemical consequences when inhaled pollutants, or their reaction products, pass completely through the respiratory tract and enter the circulation. So far, however, few effects on blood have been demonstrated unequivocally in controlled exposure studies, except for the formation of carboxyhemoglobin in exposure to carbon monoxide. Therefore, most attention is given to the respiratory tract itself. Objective quantitative measures of pulmonary mechanics, such as pressure, volume, and flow relationships, are fundamental to any controlled exposure study. Subjective responses—symptoms reported by the subjects—also are of considerable importance.

The most commonly used measures of pulmonary mechanical function are much the same as those used in clinical pulmonary laboratories to assist in the diagnosis of disease (*4*). Forced expiratory spirometry—re-

FIGURE 3

Tracings of flow-volume curves recorded in a healthy adult male volunteer who performed maximal forced expiratory maneuvers with heavy exercise before (a) and after (b) one hour's exposure to 0.32 ppm ozone[a]

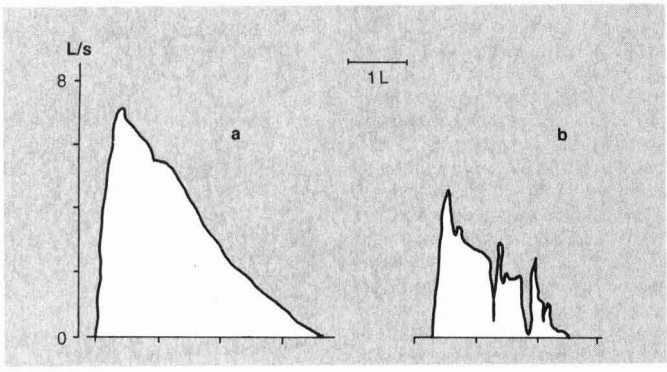

[a]Instantaneous expiratory flow rate in L/s is plotted as a function of expired volume. (Maximum inspiration is at the left. Volume scale is arbitrary since absolute lung volume cannot be measured in this test.) After exposure, chest discomfort prevents subject from breathing to extremes of lung volume, and forced expiration induces coughing, manifested by "spikes" in curve b.

cording the volume and flow rate of a maximal breath forced out—provides easily obtained, fairly reproducible indexes of overall respiratory physiological function (Figure 3). However, because the results depend on motivation as well as on several different aspects of physiological status, the test is not entirely objective and cannot readily identify the source of any disturbance in function.

A more specific test is provided by body plethysmography, in which the subject is enclosed in a sealed pressure-measuring chamber called a plethysmograph. The flow resistance of the airways can be measured in this manner (*5*). Resistance measurements are especially useful in detecting constriction of the bronchial passages, as occurs in asthma, for example. The technique is more complex than spirometry, however, and measurements are less reproducible.

Blood oxygenation is best evaluated by sampling arterial blood and polarographically determining its partial pressure of oxygen, but this process causes some discomfort to the subject. An indirect, nontraumatic alternative method involves spectrophotometric determination of oxyhemoglobin in capillary blood within the external ear, using an instrument known as an ear oximeter. Tests for more subtle effects of pollution on the respiratory tract include measuring the rate of clearance of inhaled tracer particles, and determining the response to standardized doses of an airway-constricting drug such as acetylcholine. These procedures are complex, and reproducibility is difficult to establish.

A distinction must be drawn between clinical and experimental uses of the aforementioned tests. The clinician usually tests one patient at a time, for the purpose of detecting chronic disease. For the clinician, a *positive* (abnormal) finding must be based on the statistical normal limits of the measurement, determined in a large, presumably healthy population. On the other hand, the experimenter usually tests several subjects before and after they are exposed to a pollutant, comparing each person's post-exposure measurement with his or her corresponding preexposure value, for the purpose of detecting a short-term, reversible change due to the exposure. A positive result is obtained if the subjects consistently show short-term function decrements attributable to the exposure—that is, if a statistically significant change in the group mean measurement is found.

Sometimes, even when a highly significant change is found for the group, all individual subjects' measurements remain well within normal limits. Thus, as suggested previously, there may be doubt and disagreement concerning the health significance (as opposed to the statistical significance) of a "positive" experimental finding. Investigators who conduct controlled human studies cannot always provide unequivocal answers to questions of health significance. Their primary job is to provide a reliable answer to the question of whether there is any effect from an exposure. The issue of health significance must be faced only when the answer is positive. Of course, any such answer—positive or negative—has meaning only within the context of the experiment that provided it.

Ozone and other oxidants

Although the history of exposing humans to O_3 in the laboratory goes back more than a century (*6*), the field did not attract much serious attention until the early 1970s. D. V. Bates and co-workers at McGill University performed some of the first modern O_3 studies. They employed a simple one-person exposure chamber, with a stationary bicycle on which the subject performed intermittent light exercise typical of outdoor activity (*7, 8*). Their subjects were healthy young adults. Irritation of the respiratory tract and decreases in forced expiratory performance developed gradually during the two-hour exposure periods, and disappeared slowly (over periods of hours) afterwards.

The effects were slight with an O_3 level of 0.3 ppm (by today's measurement methods), but considerably more severe at 0.6 ppm. Similar effects have been found in a number of other laboratories (*4, 9–11*). The irritation most noticeably affects the lower respiratory tract, causing coughing and chest pain, but upper respiratory disturbances also are possible. These results demonstrate unequivocally that undesirable effects can occur in typical healthy people with light activity at O_3 levels that are attainable in ambient air during severe oxidant pollution episodes. Subsequent work has attempted to identify physiological, behavioral, or atmospheric factors affecting the severity of the response.

By increasing ventilation, exercise increases the dose of O_3 inhaled at any given exposure concentration. A typical adult's ventilation rate may be about 6 L/min at rest, but can increase more than 10-fold with heavy exercise. Athletes or laborers undergoing prolonged heavy exercise may, therefore, have an especially high risk of developing respiratory irritation from O_3 exposure. In studies employing either continuous or intermittent heavy exercise, statistically significant clinical and physiological effects have been found at concentrations below 0.2 ppm (*12, 13*); concentrations of 0.3 ppm or higher are usually re-

quired to produce similar effects with intermittent light exercise.

Ozone is not the only powerful oxidant in photochemical pollution, so it is important to determine whether other species may present health risks. This is not an easy task. Oxidants other than O_3 generally occur in lower ambient concentrations, are more difficult to monitor, and are more difficult to generate in the laboratory than O_3 itself. Only peroxyacetyl nitrate (PAN) has been employed in controlled human studies. Little effect was found at concentrations of 0.24–0.27 ppm, which probably equal or exceed maximum ambient levels (*14, 15*).

Another way to assess the toxicity of air contaminants accompanying O_3 is to expose volunteers to ambient oxidant pollution and compare their responses to what would be expected in controlled exposures to O_3 alone at similar concentrations. A movable laboratory equipped with extensive air monitoring equipment, clinical support facilities, and an exposure chamber that can be ventilated with polluted ambient air or purified air, has been developed by the present authors (*16*). It has been employed in a neighborhood of metropolitan Los Angeles where oxidant levels are high. Volunteers recruited from the surrounding area showed mild but statistically significant irritant effects from ambient air, relative to control experiments with purified air (*17, 18*). Ozone, particulate nitrate, and particulate sulfate were prominent in the ambient air exposures; no on-site measurements of PAN or other trace photochemical oxidants were available. The biological effects were comparable to those seen in controlled O_3 studies, but without a direct comparison, it was not possible to confirm or deny an additional effect of the ambient mixture relative to O_3 alone.

Subsequently, a direct comparison was made: Healthy, heavily exercising adult volunteers were exposed to several controlled levels of O_3 as well as to purified air and ambient air. Their responses to ambient air, on the average, were nearly the same as predicted by the dose–response curves obtained from the controlled O_3 exposures (*13*). Thus, at least for typical healthy people exercising in Los Angeles-type smog, respiratory irritation seems entirely attributable to O_3.

Because preexisting respiratory impairment seems likely to increase the risk of ill effects from air pollution, volunteers with asthma (episodes of reversible airway obstruction) and others with chronic obstructive pulmonary disease (irreversible airway obstruction due to chronic bronchitis or emphysema) have been studied in O_3 exposures (*19–23*). Ethical concerns have limited the O_3 doses used in studies of people with chronic diseases to comparatively low levels, at which only slight or equivocal effects have been found. Thus, while direct comparisons have not been made, the available evidence suggests that people with respiratory diseases are not necessarily much more susceptible to O_3 than are healthy people. In fact, although substantial individual differences in reactivity to O_3 have been documented, very little progress has been made in identifying the biological characteristics that govern them. Reactivity is known to be modified by frequent exposure, however, as discussed later.

Ethical concerns have also inhibited studies of another potentially high-risk group—children. A few epidemiologic investigations of children have suggested physiological impairments even at only mildly elevated ambient oxidant levels, but factors other than air pollutants may have contributed to these apparent effects. No controlled O_3 studies with children have been published to date. However, successful studies of children exposed to SO_2 have been reported (*24*), and adolescents have been exposed to ambient air in our mobile laboratory. Information on the effects of O_3 in children may be available soon.

Adaptation to repeated O_3 exposures (also known by other terms, such as "tolerance" and "desensitization") is a well documented but poorly understood phenomenon. If volunteers are exposed on several days in succession to comparatively high O_3 concentrations, for example, 0.4 or 0.5 ppm with light exercise, their responses usually are most severe on the second day of exposure. Thereafter, responses diminish, and after three or four exposures the subjects are adapted—unresponsive to a dose of O_3 that previously produced substantial irritation.

Adaptation has been demonstrated using forced expiratory performance, response to airway-constricting drugs, and symptoms as measures of response (*25–27*). This lasts only a few days or weeks in the absence of frequent O_3 exposure, and develops incompletely or not at all in some people, even with daily exposure (*28–30*). The underlying biological mechanism of adaptation, its relevance to ambient O_3 exposure, and its long-term health consequences, if any, remain uncertain.

***Technician administers** spirometric (maximal forced expiration) test to subject in Rancho Los Amigos Hospital exposure chamber.*

Sulfur dioxide and particulates

Epidemiologic studies have often shown associations between elevated ambient levels of SO_2 and particulate matter, and increased rates of illness or premature death. Since SO_2 and particulates may be closely associated in the atmosphere, it is often difficult to separate their effects epidemiologically. This is not a problem in controlled experiments, which have studied the effects of SO_2 alone, various particulate species alone, and gas–particulate combinations.

Particulate pollution is exceedingly diverse and complex, and thus presents a vast array of questions about possible health effects, only a few of which have been investigated so far in human studies. To our knowledge, only slight and equivocal effects, if any, have been observed in exposure to any particulate species at a concentration likely to occur in ambient air. Until fairly recently the same could have been said about SO_2. A number of studies of SO_2 during the 1960s and 1970s indicated that increased airway resistance and symptoms of irritation could occur with exposure, but only at concentrations of 1 ppm or higher (above the common ambient range) in most subjects.

In 1980, however, D. Sheppard and associates of the University of California at San Francisco reported that asthmatic subjects were consistently and markedly more reactive to SO_2 than similarly exposed healthy subjects (*31*). These investigators

subsequently reported finding statistically significant increases in airway resistance in a group of moderately exercising asthmatics who were exposed to as little as 0.25 ppm for 10 min (*32*). Their reports renewed scientific and regulatory interest in the health effects of SO_2 and brought about a number of follow-up investigations, some of which are still in progress.

The first SO_2 exposures of asthmatics in our laboratory failed to show significant effects at 0.25 or 0.50 ppm (*33*). This inconsistency with the results of Sheppard et al. most likely related to differences in the mode of breathing during exposure (*34, 35*). Mouthpiece breathing, as employed originally by Sheppard's group, typically produces more severe responses than natural unencumbered breathing, which was employed by our group. The difference is at least partly explainable in terms of the high solubility of SO_2 in aqueous media. Natural breathing occurs at least partly through the nose, even during heavy exercise. The moist surfaces of the nasal cavity scrub SO_2 effectively, reducing the dose to the bronchial passages where constriction occurs.

But even natural breathing of SO_2 can cause some asthmatics to experience symptoms and increased airway resistance at concentrations at least as low as 0.4 ppm, with sufficiently heavy exercise (*36*). In some cases, constriction of bronchial passages may perhaps occur as a reflex response to nasal irritation, even if little SO_2 penetrates to the lower respiratory tract. The effects develop in less than five minutes, that is, much more quickly than the effects of exposure to O_3. Their severity appears to depend on the dose rate of SO_2 (concentration times the subject's ventilation rate), rather than on the total dose. In most asthmatic subjects, the effects disappear in less than an hour, with rest, even if SO_2 exposure continues (*37*). Many asthmatics experience symptoms and airway constriction with exercise even in very clean air, so care must be taken to differentiate the effects attributable to exercise from those attributable to SO_2.

Recent controlled SO_2 exposure studies leave little doubt that respiratory effects can occur at concentrations within the possible ambient range, in a particular small minority of the population—asthmatics who exercise heavily. Whether these "positive" findings have any connection with earlier positive epidemiologic findings (not related specifically to exercising asthmatics) is not yet clear.

A current concern: "acid fog"

Most human exposure studies have been conducted at moderate levels of relative humidity. However, in past episodes of extreme air pollution accompanied by substantially increased death rates, the weather was foggy. In London in December 1952, an episode lasting several days was associated with at least 3000 premature deaths in people with preexisting respiratory disease (*38*). Similar though smaller-scale incidents had occurred previously in Donora, Pa., and in the Meuse Valley of Belgium. No specific pollutant was ever identified as a cause of premature deaths and illnesses. Particulate and SO_2 levels are far lower today than they were in these instances and the effects of periods of extreme pollution on illness and death rates are no longer so obvious, although they may not have disappeared entirely.

Recent atmospheric studies, however, have redirected attention to possible health risks from fog-associated pollution, presenting a new challenge to the field of controlled human exposure studies. M. R. Hoffmann and coworkers at the California Institute of Technology collected fog water from a number of sites in southern California during winter nights and early mornings (*39*). They found substantial concentrations of acidic species in some of their samples, with pH values sometimes near 2 (compared with 5 or 6 in water from typical unpolluted fog). Nitrates appeared to be the predominant acidic species in most of these samples, reflecting the relatively high levels of oxides of nitrogen prevalent in urban southern California. In other industrialized urban areas, sulfates might be expected to predominate.

The total acidity of water from polluted California fogs may approach that of London's 1952 incident, although in California such extreme conditions typically persist for only a few minutes rather than for several days. Analysis of fog water by itself does not, of course, provide much information about the dose of potentially toxic pollutants inhaled by people breathing the fog. One still needs to know what the atmospheric concentration of inhalable pollutants is, and in what physical form the pollutants occur. Monitoring foggy atmospheres to obtain such information is difficult, but may be essential to understanding the health implications of acid fog.

The size of the water droplets in polluted fog may strongly affect the fog's respiratory toxicity. In theory, respirable droplets (a few micrometers or smaller in diameter) may concentrate soluble toxic gas or aerosol species, and when inhaled, may deposit preferentially at certain sites in the respiratory tract (*40*). Such hot spots of deposition might then receive far higher local doses of toxic agents than they would in the absence of water droplets. On the other hand, many fog droplets are too large to be in the respirable range. Any pollutants dissolved in these large droplets should be prevented from reaching the lower respiratory tract, in which case the fog might have a mitigating effect on the risk to health.

Nitrate and sulfate concentrations during pollution episodes in Los Angeles typically are on the order of tens of $\mu g/m^3$. Controlled exposures to sulfuric acid aerosol—presumably the most irritating sulfate—have shown little effect even at concentrations somewhat higher than this (*41–43*). Ammonium nitrate has shown no meaningful effect at 200 $\mu g/m^3$ (*44*), but nitric acid has not been studied. None of the aforementioned studies included fog, and most of them did not investigate a range of high-risk subject groups, such as heavily exercising asthmatics. Thus, neither the available evidence suggesting a health risk from acid fog nor the available contrary evidence is definitive.

New investigations will be needed either to confirm or to allay present concerns. Such experimental work is now being considered by several regulatory agencies and industry-sponsored research organizations. The biomedical aspects of acid fog exposure studies can be similar to previous studies of other pollutants, but the atmospheric aspects will be more complex. More extensive ambient air monitoring studies will be needed to provide more complete understanding of the physical and chemical properties of polluted fogs. In addition, techniques will have to be developed to generate and monitor polluted fogs in the laboratory.

Summary

Controlled exposure of human volunteers to air pollutants can provide the definitive scientific evidence of health risks that is essential to support air quality regulatory policy decisions. However, controlled studies are applicable only to short-term exposures with mild, temporary effects. Longer term exposures and effects

must be investigated through animal toxicology and epidemiology. To maximize overall understanding of air pollution hazards, links should be established between short- and long-term biological effects, and between different fields of investigation.

Among the numerous pollutants that have been studied in controlled exposures, only O_3 and SO_2 have shown clear untoward effects on the respiratory system at concentrations likely to be attained in polluted ambient air. The most obvious effect of O_3 is irritation of the lower respiratory tract, which develops and resolves slowly. This response is more or less proportional to the total O_3 dose: People who exercise heavily, and thus breathe heavily, for prolonged periods seem most susceptible. The typical effect of SO_2—constriction of the bronchial passages—has been observed at ambientlike exposure concentrations only in exercising asthmatics. This effect develops quickly and usually resolves quickly with rest. Its intensity seems to be proportionate to the dose rate, rather than the total dose, of SO_2. Acid fog has provoked concern recently over its possible effects on health. Controlled human studies provide a way to address this concern, but should be preceded by atmospheric monitoring studies and the development of new exposure methodology.

Acknowledgment

The authors' recent work mentioned here has been supported by the Electric Power Research Institute, Southern California Edison Co., the U.S. EPA, and Coordinating Research Council.

Before publication, this article was reviewed and commented on for suitability as an *ES&T* feature by Dr. Robert G. Tardiff, Life Systems, Inc., Arlington, Va. 22202; Dr. Julian B. Andelman, Department of Industrial Environmental Health Sciences, Graduate School of Public Health, University of Pittsburgh, Pittsburgh, Pa. 15261; and Dr. Richard G. Cuddihy, Inhalation Toxicology Research Institute, Lovelace Biomedical and Research Institute, Albuquerque, N.M. 87185.

References

(1) Hackney, J. D.; Linn, W. S. In "Measurement of Risks"; Berg, G. G.; Maillie, H. D., Eds.; Plenum Publishing Corp.: New York, N.Y., 1981; pp. 231–51.
(2) Hackney, J. D.; Linn, W. S. *Am. Rev. Respir. Dis.* **1979,** *119*, 849–52.
(3) "Ozone and Other Photochemical Oxidants"; National Academy of Sciences: Washington, D.C., 1977; pp. 388–415.
(4) Hackney, J. D. et al. *Arch. Environ. Health* **1975,** *30*, 373–90.
(5) DuBois, A. B.; Botelho, S. Y.; Comroe, J. H. *J. Clin. Invest.* **1956,** *35*, 327–35.
(6) Richardson, B. W. "Diseases of Modern Life"; Macmillan: London, England, 1876.
(7) Bates, D. V. et al. *Can. Med. Assoc. J.* **1970,** *103*, 833–37.
(8) Bates, D. V. et al. *J. Appl. Physiol.* **1972,** *32*, 176–81.
(9) Folinsbee, L. J. et al. *J. Appl. Physiol.* **1977,** *43*, 409–13.
(10) DeLucia, A. J.; Adams, W. C. *J. Appl. Physiol.* **1977,** *43*, 75–81.
(11) Kerr, H. D. et al. *Am. Rev. Respir. Dis.* **1975,** *111*, 763–73.
(12) McDonnell, W. F. et al. *J. Appl. Physiol.* **1983,** *54*, 1345–52.
(13) Linn, W. S. et al. *Am. Rev. Respir. Dis.* **1983,** *127* (No. 4, Part 2), 159.
(14) Raven, P. B. et al. *J. Appl. Physiol.* **1974,** *36*, 288–93.
(15) Gliner, J. A. et al. *J. Appl. Physiol.* **1975,** *39*, 628–32.
(16) Avol, E. L. et al. *J. Air Pollut. Control Assoc.* **1979,** 743–45.
(17) Linn, W. S. et al. *Am. Rev. Respir. Dis.* **1980,** *121*, 243–52.
(18) Linn, W. S.; Avol, E. L.; Hackney, J. D. In "Biomedical Effects of Ozone and Related Photochemical Oxidants"; Lee, S. D.; Mustafa, M. G.; Mehlman, M. A., Eds.; Princeton Scientific Publishers: Princeton, N.J., 1983; pp. 125–37.
(19) Linn, W. S. et al. *Am. Rev. Respir. Dis.* **1978,** *117*, 835–43.
(20) Silverman, F. *Environ. Health Perspect.* **1979,** *29*, 131–136.
(21) Solic, J. J.; Hazucha, M. J.; Bromberg, P. A. *Am. Rev. Respir. Dis.* **1982,** *125*, 664–69.
(22) Linn, W. S. et al. *Am. Rev. Respir. Dis.* **1982,** *125*, 658–63.
(23) Kehrl, H. R. et al. In "Biomedical Effects of Ozone and Related Photochemical Oxidants"; Lee, S. D.; Mustafa, M. G.; Mehlman, M. A., Eds.; Princeton Scientific Publishers: Princeton, N.J., 1983; pp. 213–25.
(24) Koenig, J. Q. et al. *Environ. Res.* **1981,** *25*, 340–48.
(25) Hackney, J. D. et al. *J. Appl. Physiol.* **1977,** *43*, 82–85.
(26) Folinsbee, L. J.; Bedi, J. F.; Horvath, S. M. *Am. Rev. Respir. Dis.* **1980,** *121*, 431–39.
(27) Dimeo, M. J. et al. *Am. Rev. Respir. Dis.* **1981,** *124*, 245–48.
(28) Horvath, S. M.; Gliner, J. A.; Folinsbee, L. J. *Am. Rev. Respir. Dis.* **1981,** *123*, 496–99.
(29) Linn, W. S. et al. *Am. Rev. Respir. Dis.* **1982,** *125*, 491–95.
(30) Kulle, T. J. In "Biomedical Effects of Ozone and Related Photochemical Oxidants"; Lee, S. D.; Mustafa, M. G.; Mehlman, M. A., Eds.; Princeton Scientific Publishers: Princeton, N.J., 1983; pp. 161–73.
(31) Sheppard, D. et al. *Am. Rev. Respir. Dis.* **1980,** *122*, 873–78.
(32) Sheppard, D. et al. *Am. Rev. Respir. Dis.* **1981,** *123*, 486–91.
(33) Linn, W. S. et al. *Environ. Res.* **1982,** *29*, 220–32.
(34) Kirkpatrick, M. B. et al. *Am. Rev. Respir. Dis.* **1982,** *125*, 627–31.
(35) Linn, W. S. et al. *Environ. Res.* **1983,** *30*, 340–48.
(36) Linn, W. S. et al. *Am. Rev. Respir. Dis.* **1983,** *127*, 278–83.
(37) Hackney, J. D. et al. *Environ. Res.*, in press.
(38) Ministry of Health. "Mortality and Morbidity during the London Fog of December 1952"; Her Majesty's Stationery Office: London, England, 1954.
(39) Waldman, J. M. et al. *Science* **1982,** *218*, 677–80.
(40) Bell, K. A.; Friedlander, S. K. *Staub-Reinhalt. Luft* **1973,** *33*, 178–85.
(41) Avol, E. L. et al. *Am. Rev. Respir. Dis.* **1979,** *120*, 319–27.
(42) Sackner, M. A. et al. *Am. Rev. Respir. Dis.* **1978,** *118*, 497–510.
(43) Horstman, D. et al. *Arch. Environ. Health* **1982,** *37*, 136–41.
(44) Kleinman, M. T. et al. *Environ. Res.* **1980,** *21*, 317–26.
(45) "Revised Evaluation of Health Effects Associated with Carbon Monoxide Exposure"; U.S. EPA: Research Triangle Park, N.C., in press.
(46) "Air Quality Criteria for Oxides of Nitrogen"; U.S. EPA: Research Triangle Park, N.C., 1982; pp. 15.8–15.21.
(47) "Air Quality Criteria for Particulate Matter and Sulfur Oxides"; U.S. EPA: Research Triangle Park, N.C., 1982; Vol. III, pp. 13.24–13.31.
(48) Kleinman, M. T. et al. *Am. Ind. Hyg. Assoc. J.* **1981,** *42*, 298–304.

Jack D. Hackney, M.D. *is chief of the Environmental Health Service at Rancho Los Amigos Hospital in Downey, Calif., and professor of medicine, University of Southern California School of Medicine. He received his M.D. from St. Louis University School of Medicine. He directs a number of research programs to determine the effects of atmospheric pollutants on the human lung. He was a member of the National Academy of Sciences committees on photochemical oxidants and diesel-engine emissions, and currently serves on the Environmental Health Committee of the EPA Science Advisory Board, as well as the State of California's Air Quality Advisory Committee.*

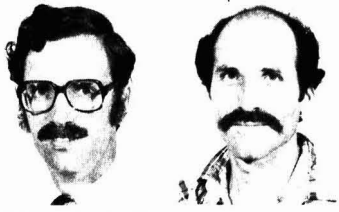

William S. Linn *(l.) is senior project scientist and coordinator of the Clinical Environmental Stress Testing Laboratory in the Environmental Health Service. He received his MA in chemistry from the University of California at Irvine. His current research interests concern the application of physiological and clinical tests to detect effects of air pollution, and the application of research results to public policy.*

Edward L. Avol *(r.) is environmental health engineer and director of the Aerosol/Chemistry Laboratory in the Environmental Health Service. He received his MS in environmental engineering from the California Institute of Technology in Pasadena. His responsibilities include the generation and characterization of all test atmospheres under investigation, and he is the developer and coordinator of the movable biosurveillance laboratory program. His current research interests include the health effects of air pollution on children and athletes, and devices for personal protection from air pollution exposure.*

EPA's FY'85 budget

Richard M. Dowd

The president's EPA budget for fiscal year 1985 carries a "good news, bad news" message for the agency's research and development program. The good news is that the research budget will increase by 14% over the previous year's level. President Reagan's budget increases funding for the entire agency both above his own request and congressional appropriations for 1984. This reverses the downward trend, both in dollars and in personnel, of the past three years.

The bad news is that, in the context of national environmental research needs, the proposed budget is still considerably below the levels of fiscal years 1980 and 1981, both in program resources and in personnel.

The one significant exception is Superfund, where dollar and personnel resources have been substantially increased. The Superfund budget shows an increase of $230 million and 350 work-years over the fiscal year 1984 appropriation, largely to expand the number of Superfund sites under construction and to increase the number of enforcement personnel.

As in the past, in fiscal year 1985 EPA's overall monitoring program will receive essentially no increase in funding (though a modest addition to the Air Office budget will increase monitoring for air toxics). The need for a major monitoring program for comprehensive measurement of ambient concentrations of potentially toxic chemicals in air, land, and water will again be unmet in 1985.

President Reagan has proposed a budget for EPA's Office of Research and Development (ORD) of $278 million; the budget for fiscal year 1980 was roughly $463 million (in 1984 dollars). Thus, although ORD's budget has increased from last year's level of $245 million, it is still at only 60% of the fiscal year 1980 level.

It is interesting to trace EPA's ORD funding over the past 10 years (see chart). The chart shows that, despite the good news (increases for fiscal year 1985 over the previous year), the overall level of total research and development expenditures is still at an almost historic low: roughly 50% of the average of fiscal years 1975 through 1981, in constant dollars.

Since research provides such a fundamental basis for regulatory action, it is useful to examine which program areas are proposed for increases and which still need additional funding.

Acid rain is the primary area of increased research funding in fiscal year 1985. The president's budget proposes a $34.4-million acid rain research program, an increase of $19 million over the level of fiscal year 1984. This effort constitutes more than 50% of the government's acid rain program, which will total $55 million in 1985.

Other increases in the ORD budget consist of salaries and expenses for a larger staff. Extramural funding for other research programs remains essentially constant, with some changes in priorities. More emphasis will be placed on toxic pollutants research, particularly health and risk assessments of potential hazardous air pollutants in order to list chemicals under NESHAPS; increasing work on hazardous waste, particularly engineering and technology evaluation; and continued development of test methods for new toxic chemicals—although an increase of $2.7 million for the latter can hardly be characterized as large.

Richard M. Dowd, PhD, is a Washington, D.C., consultant to Environmental Research and Technology, Inc.

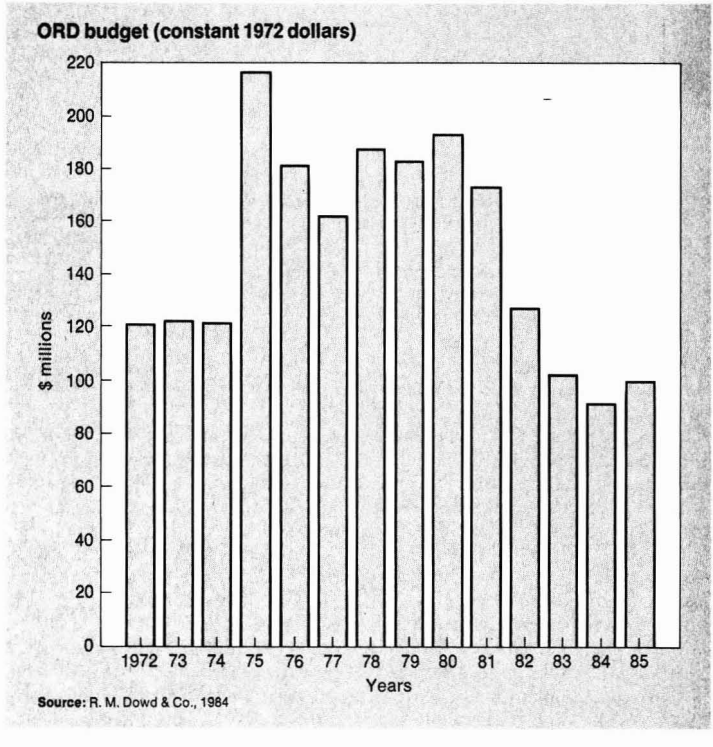

0013-936X/84/0916-0123A$01.50/0

ES&T
OUTLOOK

Water quality uncertainties

The movement of toxics underground and the health effects of certain organic toxics are not well understood

The dominant impression conveyed by a water conference held in late January in Philadelphia is that scientists understand very little about certain aspects of water quality, particularly groundwater quality. The amount of groundwater that is contaminated is not known; in many cases the movement of toxics through the ground and in the aquifers is extremely difficult—if not impossible—to predict; and the human health effects, if any, caused by many organic contaminants are known either vaguely or not at all.

The conference, entitled "The Fate of Toxics in Surface and Ground Waters," was the Second National Water conference. It was sponsored by the Academy of Natural Sciences, the American Water Works Association, and the Water Pollution Control Federation.

The speakers held diverse views about the seriousness of current groundwater contamination. Former EPA Deputy Administrator John Quarles of the Washington law firm of Morgan Lewis & Bockius seemed to have a very optimistic attitude toward the subject. He said that "most of the contamination that does exist is highly localized," and the majority of the aquifers that have been contaminated can't be cleaned up. "In most respects, that won't make any difference," he noted, because the "groundwater that is contaminated won't be needed." But contaminated isolated residential wells are a problem, he admitted.

Glenn Paulson of the National Audubon Society holds a rather different view of groundwater. He mentioned an unreleased EPA survey of groundwater in 954 cities greater than 10 000 people which found contamination in 29% of the underground water supplies and said that there are large numbers of industrial impoundments and hazardous waste sites which could cause contamination over time.

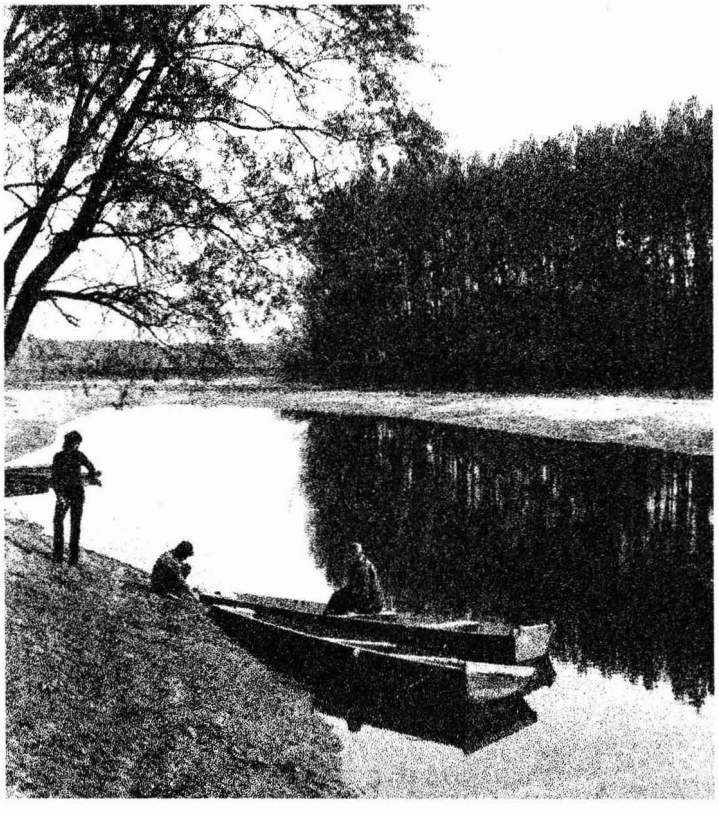

Many of the speakers mentioned that, according to current estimates, 1–2% of the groundwater in the U.S. is contaminated. This figure is not based on a comprehensive survey of groundwater quality because none has been done. Marian Mlay, acting director of EPA's groundwater office, said that it would cost half a billion dollars to do an accurate survey.

Some observers consider the 1–2% figure low or uncertain when viewed in light of the number of hazardous waste sites, surface impoundments, underground injection wells, and gasoline storage tanks—many of them leaking—in the U.S. Ruth Patrick, senior curator at the Patrick Center for Environmental Research, Academy of Natural Sciences, mentioned that tens of thousands of sites have

0013-936X/84/0916-0124A$01.50/0

received hazardous wastes and hundreds of sites are continuing to receive them. In addition, surface impoundments containing toxic liquids number approximately 59 000, according to an EPA review in the late 1970s cited by Paulson.

Many of these surface impoundments and hazardous waste sites, even those that contain a small amount of toxic material, could become sources of groundwater contamination if the sites described by John Cherry of the University of Waterloo are representative. He told about experiments in which an aquifer was contaminated by just a few milliliters of a halogenated hydrocarbon so that it exceeded drinking water standards. "It only takes a drum or two, given time, given dispersion, given dissolution, to produce large domains of contaminated groundwater when we are looking at halogenated hydrocarbons that are of concern at ppb levels," he said.

A number of the speakers mentioned sources of surface and groundwater contamination that up to the present have not been highly visible concerns of the general public. Patrick said that spraying or spreading sludges on land may cause contamination from the water that passes through the sludge and enters the ground and hence the ground or surface water. She also noted that improperly designed or maintained septic tanks often pollute water not only with human waste, but with metals and complex organic compounds that are used in the home. She especially emphasized nonpoint sources. "Feedlots where a thousand or more head of cattle are fattened" were mentioned in particular as important nonpoint sources of nitrates that often seep directly into groundwater. Nitrate concentrations as low as 50 mg/L can cause intestinal upsets in children or the birth of blue babies if the expectant mother drinks the water.

Unpredictable movement

Cleanup activities to prevent the contamination of aquifers are often predicated on the assumption that scientists have some ability to predict what happens to contaminants once they enter the ground. Cherry described a number of situations in which such predictions are impossible or nearly so. Sand and gravel are often considered the most predictable media for contaminant movement. However, in these media, " 'blobs' of contaminants split off into separate blobs in unpredictable ways, but the movement of each individual blob can be predicted more accurately," Cherry said. Those contaminants that he calls sinkers or floaters—those heavier or lighter than water—are a special problem. They seem to be almost entirely unpredictable, even in sand and gravel.

The movement of contaminants in clay is sometimes even more difficult to predict. It is generally believed that clay is a good place to put toxics because in the laboratory they move so slowly through clay that their movement is virtually zero. In the field, however, the situation is often quite different. Here, the clay is usually cracked, at least down to a considerable depth, so the pollutants may move just as fast through clay as they do through sand and gravel. Cherry showed many sites where clay was deeply fractured from weather or from tunnels created by decayed tree roots. He described a site in Oregon where drums containing liquids were bulldozed into trenches in clay soil. From these, a plume of 2,4-dichlorophenol was moving 100 ft/y at a concentration of mg/L—a high level.

Fractured rock is an equally serious problem, he noted. It is a medium where it is almost impossible to predict the movement of plumes. Cherry also said that knowing where the inorganic contaminants go tells you very little about the movement of organic contaminants and therefore these need to be monitored. As a result of these observations, Cherry said, "I think there are going to be a lot of cleanup activities that are going to be done in the absence of very good scientific information." This will lead to "many, many more wells and water supply systems going bad" because of groundwater contamination that is unpredictable and unexpected.

Wayne Pettyjohn of Oklahoma State University spoke in a similar vein. He noted that it has become "common practice within the past few years to develop manuals and techniques for regulatory personnel . . . to predict concentration distributions in the subsurface" and that many of these techniques involve the use of computer programs. When computer programs are used to predict the movements of contaminants underground, he said, the results are often extremely uncertain or limited because the inputs to the program are often very uncertain, limited, or simply unavailable. He advised that it is far more realistic to enter data into computer programs that have lower and upper bounds of uncertainty so that the results are expressed in a kind of risk probability curve rather than as definite numbers.

Lial Tischler, vice president and manager, Southwest Operations, Engineering-Science, Inc., noted research needs in the area of waste treatment. He said that "the proper conditions of biodegradation, or possibly adsorption, of many complex organic compounds are still not well understood." On the other hand, he concluded from a review of the literature that the number of organic compounds that are resistant to biodegradation is much smaller than was believed a few years ago.

Unknown health effects

Many of the speakers emphasized how little is known about the effects of organic water contaminants on human health. Gordon Wolman of Johns Hopkins University said, "I think it is safe to say that the data on the health effects of hazardous wastes, particularly the chronic effects, are exceedingly limited." William Lynch, president of the American Water Works Association, echoed the same idea. "We can identify substances in water with incredible accuracy, but as to their significance as potential threats to human health, we have only some very shaky extrapolations from some very vague ideas."

Abel Wolman, professor emeritus at Johns Hopkins University, mentioned that many of the diseases that could be caused by organic chemicals in water are in the carcinogenic group and that if we wait for epidemiological evidence, we might have to wait 60 years. "Sufficient data are turning up to indicate that toxics in water exist and that their presence is certainly not salutary," he said. He expressed particular concern about the genetic damage that chemicals in the water might cause to future generations. "The genetic risk causes special concern," he said, "because . . . the bulk of the risk is not to our immediate children but to our remote grandchildren."

Dr. Norton Nelson of New York University Medical Center noted that sometimes the attention given to toxic chemicals has been inflated, but that "there is enough actuality for these to be of concern." He said that the medical center is especially concerned about chronic exposures to various chemicals and mentioned in particular trihalomethanes (THMs) in drinking water. He observed that in epidemiological studies of THMs, positive results abound and that none of the results are negative, although none of the studies are as definitive as epidemiologists would like to see. He

mentioned Kenny Crump's (Science Research Systems) idea that rather than THMs, the cause of the cancers may be the nonvolatile organic compounds and other volatile organic compounds not yet tested that often coexist in water with THMs.

To test the effects of contaminants on aquatic organisms, John Cairns, Jr., of Virginia Polytechnic Institute recommended that scientists begin multispecies testing followed by validation in the field. Single-species tests in the laboratory have been relied on almost exclusively in the past. In the natural environment, we sometimes see fish swimming around in 10 times the "lethal doses" that were calculated using single-species tests in the laboratory, Cairns observed. Therefore, he believes that the single-species test may be vastly overprotective. He said the first suitable multispecies toxicity tests are now available for both aquatic and terrestrial systems.

Society's response

Scientists and other experts in the water field seem to agree that little is known about the human health effects of many organic contaminants found in water, but they disagree greatly about how much society should be willing to pay to clean up the water supplies or how urgent a priority it should be.

Earnest Gloyna, president of the Water Pollution Control Federation, defines acceptable pollution control as controlling those pollutants that cause demonstrable harm. But some scientists point out that, if it takes several decades to demonstrate an actual cause and effect relationship between certain organic chemicals and cancer, many cancers will have to occur before these pollutants are controlled.

Abel Wolman's approach to the question is entirely different from Gloyna's. His philosophy can be summed up in a few words: "Take it out." He said that as a result of a National Science Foundation inquiry, he was drawn to an old maxim "that the consumer should be given the benefit of the doubt when contaminants are being assessed." He also believes that keeping contaminants out of drinking water is not nearly as expensive as some suggest, especially when you consider that drinking water is a cheap commodity, now costing an average of 25 cents a ton.

The proceedings of the conference will be available this month from the Academy of Natural Sciences, Philadelphia, Pa. 19103.

—Bette Hileman

ES&T PRODUCTS

Radiation exposure standards
Direct-reading standards are accurate to ±2%. They do not have to be corrected for temperature and barometric pressure because they are sealed ion chambers. Dosimeter **101**

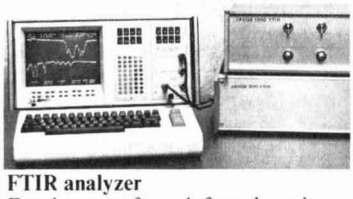

FTIR analyzer
Fourier transform infrared analyzer consists of a portable interferometer, which uses a rotating optical element. The optical sensing head can be battery operated, and up to four interferometers can be controlled from a central data station. The spectral resolution of the analyzer is better than 5 cm^{-1}. Janos Technology **102**

Liquid-metering system
This unit provides automatic continuous set-point control of process variables in chemical or biological systems. Easily programmed, it can be interfaced directly with process monitor instrumentation. One of the typical applications is in wastewater control. Ivek **103**

Precision laboratory balances
Four models of balances are designed to accept LabPac, Mettler plug-in software. LabPac allows the balances to be used for net total weighing, percentage determination, animal weighing, mean value, and standard deviation. Two of the models have a fine weighing range that can be recalled at the touch of a button. Mettler Instrument **104**

Micro-bellows metering pumps
Designed for laboratory and chromatographic applications, these pumps handle corrosive and difficult-to-handle liquids and gases. The capacities are from 3 to 25 000 mL/h, the adjustable flow rates are constant, and only stainless steel or Teflon touches the material being pumped. Andersen Samplers **105**

Ion chromatograph
This system is especially designed for applications where high sample throughput, sensitivity, and rugged reliability are primary considerations. Standard features include a chemically inert flow system, mechanical pulse damping, and a nonmetallic pump with flow rates from 0.53 to 5.3 mL/min. Dionex **106**

Laboratory potentiostats
Both models perform all advanced techniques of potential or current control in electrochemical cells and can accurately measure extremely low current. The power output of both is sufficient for most laboratory work. X–Y recorders with an input resistance higher than 1×10^{-6} ohms can be connected to the output terminals. Brinkmann Instruments **107**

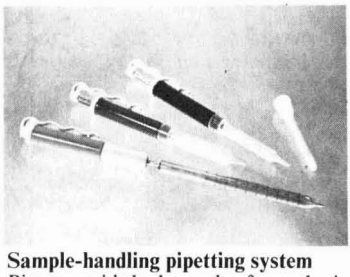

Sample-handling pipetting system
Pipets avoid the hazards of mouth pipetting and are convenient for the dispensing, transferring, and holding of macro-scale samples. They can be used with disposable Sarpette tips or adapted for standard glass or plastic pipets. Sarstedt **108**

Need more information about any items? If so, just circle the appropriate numbers on one of the reader service cards bound into this issue and mail in the card. No stamp is necessary.

***Companies interested in a listing** in this department should send their releases directly to* Environmental Science & Technology, *Attn: Products, 1155 16th St., N.W., Washington, D.C. 20036*

ES&T LITERATURE

Corrosion control. Brochure covers cooling water chemistry and corrosion control. Ask for "Cooling Water . . . Its Chemistry and Fundamentals." Wright Chemical **151**

Chromatography. *The Supelco Reporter,* Vol. III, No. 1, features chromatography for measuring inorganic acid mists, dinitroaniline herbicides, and other materials. New products are also described. Supelco **152**

Air purifiers. Literature describes ET-2 air purifier for smaller rooms and the ET-12 commercial air purifier for larger spaces. Ecology Tech **153**

Wastewater treatment. Information on "Integrated Wastewater Treatment" explains why steps are interdependent and how this concept can make treatment more cost-effective. ChemLink **154**

pH measurement. Booklet, "pH in Plain Language," explains the importance of pH measurements, methods used, instrument care, and how to use a pH meter. Chemtrix **155**

Atomic absorption (AA). Brochure describes S-11 and S-12 AA spectrophotometers with video display unit and background correction. Instrumentation Laboratory **156**

Turbidity standards. Information describes turbidity standards, which are the only EPA-approved alternative standards to formazin. Advantages set forth include longer life and lower costs. Amco Polymerics **157**

Asbestos. Literature sets forth technical considerations in air monitoring during asbestos removal projects, as well as the hazardous nature of asbestos and its ramifications. ATC **158**

Pollution reference standards. Product Bulletin No. 123 lists reference standards covering many areas of environmental pollution. Catalog numbers, descriptions, and prices are given. Foxboro **159**

Polarographic analysis. Catalog features Model 384B polarographic analyzer, which can determine metals, anions, and organics as low as 1 μg/L by square-wave voltammetry. EG&G Princeton **160**

Aerosol generator. Brochure describes Model 3450 aerosol generator, a source of monodisperse particles in the 1–200-μm range. It is used as an aerosol generation standard for research, calibration, and other needs. TSI **161**

Jet air cleaning. Fabric filter systems with pulse-jet air cleaning capabilities are described. The company claims they are more efficient and make use of total available filter area. Bact Engineering **162**

Flow meters. Brochure illustrates in-line flow meters that can work from 0.05 to 300 gal/min. Most are rated at 3000 psi and 240 °F, some at higher temperatures. Hedland **163**

HPLC columns. Catalog lists high-performance liquid chromatography columns with a selection guide, sample chromatograms, and other items. Publication is called "HPLC Columns." IBM Instruments **164**

Gas sampler. Bulletin 2333 describes five-gas sampler for SO_2, NO_2, hydrogen sulfide, ammonia, and aliphatic aldehydes. Andersen Samplers **165**

Gauges and valves. G83-84 catalog lists gauges, valves, viscosimeters, flow meters, and many other items, including five new products. Gilmont Instruments **166**

AA accessories. Catalog lists atomic absorption (AA) accessories and supplies at competitive prices. Instrument line is also listed. BUCK Scientific **167**

Water analysis. 1984/85 Water Analysis Catalog lists more than 2500 items for water analysis, including test kits, meters, reagents, apparatus, and other needs in the water- and wastewater-testing field. Prices hold until Jan. 1, 1985. Thomas Scientific **168**

Water treatment polymers. TECHNIFAX 137 sets forth requirements for successful storage, handling, and feeding of all types of water treatment polymers. Nalco Chemical **169**

Membrane linings. Brochure, "Nerva-Tite Flexible PVC Membrane Linings," describes linings for ponds, reservoirs, pits, lagoons, drying beds, and lakes where leakage could be a problem. Rubber & Plastics Compound Co. **170**

Wastewater samplers. Brochure features TC-2 continuous-flow wastewater samplers, which can take samples even under maximum natural turbulence. Easy setup. Sonford Samplers **171**

Resource recovery consulting. Brochure describes capabilities for complete or "a la carte" consulting and engineering services for resource recovery, pollution, and discharge problems. Other services encompass assistance with regulatory compliance. OMI International **172**

Geophysical instruments. 1984–85 catalog lists a variety of meteorological, environmental control, and hydrological systems and instruments, and provides charts and tables. WEATHERtronics **173**

Hazardous substances data. Brochure gives case histories in which HAZARDLINE, a hazardous substances data base, played a major role in counteracting effects of chemical spillages, identifying health hazards, and performing other services. Occupational Health Services **174**

***Need more information** about any items? If so, just circle the appropriate numbers on one of the reader service cards bound into this issue and mail in the card. No stamp is necessary.*

***Companies interested in a listing** in this department should send their releases directly to* Environmental Science & Technology, *Attn: Literature, 1155 16th St., N.W., Washington, D.C. 20036*

ACS Membership Application 1984

AMERICAN CHEMICAL SOCIETY • 1155 Sixteenth Street, N.W., Washington, D.C. 20036/(202) 872-4600
TTY: (202) 872-8733

Applicant

Mr., Mrs. (Name) _____
Dr., Miss, Ms. (Please type or print) Family Name First Middle

Mailing Address _____
Number and Street

_____ Telephone _____
City State Zip Code / Country Area Code

Academic Training

Name of College or University (Including current enrollment)	City and State	Curriculum Major	Years of Attendance	Title of Degree(s) Received or Expected	Date Degree Received or Expected

Courses Completed

Please list completed courses (by title) in the chemical sciences (Attach separate sheet or transcript if more space is needed.) *Not required of those with a bachelor's, masters or doctor's degree in a chemical science or those with a doctor's degree in a science closely related to chemistry with demonstrated significant experience in the practice of a chemical science.*

Quarter hour credits should be multiplied by two-thirds. If school did not use a credit hour system, please estimate credits on basis of 15 lecture clock hours or 45 laboratory clock hours as equivalent to one semester hour credit.

Course Title	Semester Hours	Course Title	Semester Hours	Course Title	Semester Hours

Nomination

Nomination by two ACS members (not necessary for former members; student affiliation does not constitute former membership). If this presents difficulty, please contact the Washington office.

We recommend _____ for membership in the American Chemical Society.
(Name of Applicant)

ACS Member: _____
(Signature) (Printed Name)

ACS member: _____
(Signature) (Printed Name)

This space for use of:
ADMISSIONS COMMITTEE

1 2
3 4 N

Local Section/Division

Statistical Information

Mr., Mrs. (Name) _____
Dr., Miss, Ms. (Please type or print) Family Name First Middle

Mailing Address _____
Number and Street

_____
City State Zip Code/Country

Date of Birth _____ Sex ☐ F ☐ M
(Information needed for statistical purposes)

Previous Membership

I have ☐ have not ☐ previously been a member.

I have ☐ have not ☐ previously been a student affiliate.

Office Use Only

AMC _____
MJR _____
DEL _____
MED _____
CSD _____
PNI 5446E
CLD _____
CNS _____
CNR _____
TEC _____
WTD _____

Professional Experience

Employer	Job Title	Functions	% Time on Chemical Work	Inclusive Dates of Employment (Mo. & Yr.)

Dues/Subscriptions/Divisions

There are four start dates for membership: 1 January, 1 April, 1 July and 1 October. We are anxious to begin your membership as soon as possible and will therefore enroll you immediately upon approval by the Admissions Committee. Dues for 1984 are $65.00. Your membership will begin at the nearest quarter and you will be billed accordingly. *Please send no money now.*

Student Dues

If you are a student majoring in the chemical sciences a 50% reduction on membership is available. To apply you must be registered for at least six credit hours as an undergraduate or be enrolled as a full-time graduate student.

I am ☐ an undergraduate student enrolled as described above.
☐ a graduate student enrolled as described above.

_____
Name of College or University

National Affiliation

National affiliates pay three-quarters dues (i.e. $48.75) and likewise will receive a prorated bill based on the quarter national affiliation begins.

Husband/Wife Dues

If you are the spouse of a member receiving C&EN, 23% (or the prorated amount) will be deducted from your bill. This is the portion that is allotted for C&EN. If you are eligible, please give the name of your spouse and his/her membership number.

_____
Spouse's Name Membership Number

If you wish to subscribe to an ACS publication or join an ACS division please list the publication(s)/division(s) below.

_____ _____
_____ _____

Remember, send no money now.

Agreement

I agree to restrict for my own personal use all publications to which I subsribe at member rates. I understand that membership dues are payable annually unless my signed resignation is received by the Executive Director before January 1 of the year for which the resignation is to take effect.

_____
(Date) (Signature of Applicant)

professional consulting services directory

CLASSIFIED SECTION ■ POSITIONS OPEN

The Water Resources Program in the Department of Civil Engineering at Princeton University invites applications for an appointment to the professional research staff at the rank of Research Associate. The position requires extensive laboratory experimental analyses in connection with our toxic and hazardous waste research particularly dealing with aspects of biodegradation of organic chemicals in aquifers and subsurface soil systems. The applicant must have a doctoral degree with demonstrated research scholarship in biochemistry, engineering with emphasis in biochemistry and biological systems, or a related discipline. Submit resume and three references to Raymond A. Ferrara, Director, Water Resources Program, Department of Civil Engineering, Princeton University, Princeton, New Jersey 08544.

Princeton University is an Equal Opportunity/Affirmative Action Employer.

Faculty Position, Tenure Track, Environmental Chemistry. The Raymond Walters General and Technical College, a 2-year suburban campus of the University of Cincinnati, solicits applications to fill the position of instructor or assistant professor of Chemistry. Rank commensurate with education and experience. Minimal qualifications include advanced degree in Chemistry, Chemical Engineering, or Environmentally related program, with recent experience and/or graduate training specifically in chemistry of the environment. Teaching responsibilities in chemical analysis of environmental pollutants and in introductory chemistry courses. Forward complete curriculum vita including the names and phone numbers of three references to: Dr. Robert Thomas, Chemistry Department, 9555 Plainfield Road, Cincinnati, Ohio 45236. RWC/UC is an Affirmative Action-Equal Opportunity Employer. Closing date: April 16, 1984.

DEPARTMENT OF CHEMISTRY
FACULTY POSITION ANNOUNCEMENT

SOUTHERN UNIVERSITY, Baton Rouge, Louisiana 70813, Dr. Wilbur B. Clark, Chairman, Department of Chemistry, Telephone (504) 771-3930.

Applications are invited for the following position at the Assistant Professor level beginning August, 1984. Doctorate required.

Environmental chemist with a strong background in organic chemistry and instrumentation. Teaching duties include areas of specialty as well as general chemistry.

Applicants must have the potential and determination to establish a strong and productive research program for graduate and undergraduate students. The proposed research should deal with problems of air/water pollution and related environmental topics. Additional duties include advisement, committee assignments, and developing activities in the area of community service. Applicants should submit a resume, transcript, a brief description of their research plans, and arrange to have three letters of recommendation sent to the Chairman. Salary will be commensurate with educational background and experience. Closing date is April 25, 1984.

AN AFFIRMATIVE ACTION/EQUAL OPPORTUNITY EMPLOYER

RESEARCH ENVIRONMENTAL CHEMIST

Aquatic Chemistry Section, seeks a senior level (Ph.D. experienced) candidate to actively pursue research in the chemistry of natural waters. Prefer strong analytical background environmental engineering or experience in investigating metal—natural ligand interactions in water/sediment or gound-water systems. Strong communication skills and drive to establish an active research group are essential. Resumè and three letters of reference should be sent to Dr. Michael J. Barcelona, Aquatic Chemistry Section, State Water Survey, Box 5050, Station A, Champaign, IL 61820. The State of Illinois is an Affirmative Action Equal Opportunity Employer.

ATTENTION
ENGINEERS AND SCIENTISTS
OWN A COMPANY IN FLORIDA

Due to the death of a partner, a nationally known engineering/science consulting firm in Florida is seeking a qualified.

- **Water Quality Modeler**
- **Water Supply and Treatment Engineer**
- **Environmental Engineer**
- **Environmental Scientist**

To assume an ownership position.

Respond in confidence to:

OPPORTUNITY
11011 N.W. 12th Place
Gainesville, FL 32606

CLASSIFIED ADVERTISING RATES

Rate based on number of insertions used within 12 months from date of first insertion and not on the number of inches used. Space in classified advertising cannot be combined for frequency with ROP advertising. Classified advertising accepted in inch multiples only.

Unit	1-T	3-T	6-T	12-T	24-T
1 inch	$100	$95	$90	$85	$80

(Check Classified Advertising Department for rates if advertisement is larger than 10".)

SHIPPING INSTRUCTIONS: Send all material to

Environmental Science & Technology
Classified Advertising Department
25 Sylvan Rd. South
Westport, CT. 06881
(203) 226-7131

INDEX TO THE ADVERTISERS IN THIS ISSUE

Advertising Management for the American Chemical Society Publications

CENTCOM, LTD.

Thomas N. J. Koerwer, President
James A. Byrne, Vice President
Alfred L. Gregory, Vice President
Clay S. Holden, Vice President
Benjamin W. Jones, Vice President
Robert L. Voepel, Vice President
Joseph P. Stenza, Production Director

25 Sylvan Road, South
P.O. Box 231
Westport, Connecticut 06881
(Area Code 203) 226-7131
Telex No. 643-310

ADVERTISING SALES MANAGER
JAMES A. BYRNE

ADVERTISING PRODUCTION MANAGER
GERI P. ANASTASIA

SALES REPRESENTATIVES

Philadelphia, Pa. . . . Dean A. Baldwin, CENTCOM, LTD., GSB Building, Suite 425, 1 Belmont Ave., Bala Cynwyd, Pa 19004 (Area Code 215) 667-9666

New York, N.Y. . . . Dean A. Baldwin, CENTCOM, LTD., 60 E. 42nd Street, New York 10165 (Area Code 212) 972-9660

Westport, Ct. . . . Edward M. Black, CENTCOM, LTD., 25 Sylvan Road South, P.O. Box 231, Westport, Ct. 06881 (Area Code 203) 226-7131

Cleveland, Oh. . . . Bruce Poorman, CENTCOM, LTD., 325 Front St., Suite 2, Berea, OH 44017 (Area Code 216) 234-1333

Chicago, Ill. . . . Bruce Poorman, CENTCOM, LTD., 540 Frontage Rd., Northfield, Ill 60093 (Area Code 312) 441-6383

Houston, Tx. . . . Dean A. Baldwin, CENTCOM, LTD., (Area Code 713) 667-9666

San Francisco, Ca. . . . Paul M. Butts, CENTCOM, LTD., Suite 112, 1499 Bayshore Highway, Burlingame, CA 90410. Telephone 415-692-1218

Los Angeles, Ca. . . . Clay S. Holden, CENTCOM, LTD., 3142 Pacific Coast Highway, Suite 200, Torrance, CA 90505 (Area Code 213) 325-1903

Boston, Ma. . . . CENTCOM, LTD. (Area Code 212) 972-9660

Atlanta, Ga. . . . Edward M. Black, CENTCOM, LTD., Phone (Area Code 203) 226-7131

Denver, Co. . . . Paul M. Butts, CENTCOM, LTD. Telephone 415-692-1218

United Kingdom:
Reading, England—Technomedia, Ltd. . . . Wood Cottage, Shurlock Row, Reading RG10 OQE, Berkshire, England 0734-343302
Lancashire, England—Technomedia, Ltd. . . . c/o Meconomics Ltd., Meconomics House, 31 Old Street, Ashton Under Lyne, Lancashire, England 061-308-3025

Continental Europe . . . Andre Jamar, Rue Mallar 1, 4800 Verviers, Belgium. Telephone (087) 22-53-85. Telex No. 49263

Tokyo, Japan . . . Shuji Tanaka, International Media Representatives Ltd., 2-29, Toranomon 1-Chrome, Minatoku, Tokyo 105 Japan. Telephone: 502-0656

ES&T RESEARCH

Kinetics of Monobromamine Disproportionation–Dibromamine Formation in Aqueous Ammonia Solutions

Guy W. Inman, Jr.,[†] and J. Donald Johnson*

Department of Environmental Sciences and Engineering, School of Public Health, The University of North Carolina at Chapel Hill, Chapel Hill, North Carolina 27514

■ Dibromamine is a major constituent of brominated wastewater and a toxic, though unstable, intermediate produced by the chlorination of seawater containing ammonia. Factors affecting the rate of dibromamine formation are relevant to the optimization of disinfection and antibiofouling processes that employ bromine either directly or indirectly from bromide oxidation. The formation kinetics have been studied by the method of initial rates in solutions wherein ammonia was present in molar excess over oxidizing bromine. The reaction was observed to be strongly catalyzed by phosphate and to have no ammonia dependence beyond that required for monobromamine formation. The empirical rate law was found to be $d[NHBr_2]/dt|_{t=0} = k_c[H^+][PO_4][Br^0_T]^2 + k_u[H^+][Br^0_T]^2$ where $[PO_4]$ = total phosphate concentration, $[Br^0_T] = [HOBr]^0 + [OBr^-]^0$, $k_c = 9.9 \times 10^{11}$ M^{-3} s^{-1}, and $k_u = 2.4 \times 10^8$ M^{-2} s^{-1} at 25 °C.

Introduction

Bromine has been proposed as an alternative disinfectant for drinking water, wastewater, swimming pools, and cooling water (*1–3*). Hypobromous acid, formed when chlorine oxidizes bromide, is also the active chemical constituent of chlorinated seawater. Most waters that require disinfection typically contain significant quantities of ammonia which rapidly reacts with bromine or hypobromous acid according to the following net reactions:

$$HOBr + NH_3 \rightarrow NH_2Br + H_2O \quad (1)$$

$$HOBr + NH_2Br \rightarrow NHBr_2 + H_2O \quad (2)$$

$$HOBr + NHBr_2 \rightarrow NBr_3 + H_2O \quad (3)$$

Dibromamine, $NHBr_2$, and tribromamine, NBr_3, are the major products produced at pH values less than 8.5 and molar concentrations of bromine equal to or greater than 5 times the ammonia concentration (*4*). Galal-Gorchev and Morris (*5*) showed that all three bromamines form in aqueous solution and given well-defined UV spectra. They noted the difficulty of kinetic measurement of formation and decomposition rates because of the sequential nature and rapidity of the reactions and the instability of the products produced. Cromer et al. (*6*) measured dibromamine decomposition kinetics. Because of the instability of dibromamine, the formation kinetics of dibromamine have been followed by the method of initial rates. A stopped-flow system was used to measure the formation of dibromamine after the very rapid initial formation of monobromamine. The disappearance of NH_2Br and appearance of $NHBr_2$ were followed by monitoring the wavelength of maximum absorbance of each compound at 232 and 278 nm, respectively. The effect of excess ammonia, pH, chloride, and phosphate was determined.

Experimental Section

Reagents. Hypochlorite stock solutions were prepared by diluting Fisher Reagent-grade sodium hypochlorite (5%). Their titers were determined by amperometric titration. Hypobromite solutions (10–20 mM) were prepared by mixing stoichiometric amounts of NaOCl stock with a known amount of potassium bromide and allowing 24 h for the reaction to go to completion. The pH was adjusted to 11.2 with 0.25 N NaOH and the stock stored in the dark. Concentrations were determined both by spectrophotometry from the absorbance at 329 nm, λ_{max} for OBr^-, and more accurately by amperometric titration with phenylarsine oxide. A 0.20 M potassium phosphate buffer stock was prepared by adding enough 0.02 M KH_2PO_4 to 0.20 M K_2HPO_2 until the desired pH was obtained. The reagents were Mallinckrodt analytical reagent-grade $K_2HPO_4 \cdot 3H_2O$ and Fisher primary standard KH_2PO_4. The stocks were filtered (0.45 μm), chlorinated, and irradiated with UV light in order to eliminate trace amounts of reducing agents. A 2.50 M stock of NaCl was prepared from Fisher biological grade sodium chloride and demand-free water. The solution was filtered (0.945 μm), chlorinated, and then dechlorinated with UV light.

Apparatus. A potentiostat–electrometer circuit was constructed from RCA CA-3140 operational amplifiers and used in conjunction with a rotating platinum hook electrode (Sargent S-30421), a saturated calomel reference, and a Houston Model X-Y recorder. A detailed description of the two-electrode system and circuitry is given elsewhere (*7*). An Orion Model 601A digital pH meter was used to measure and monitor the pH of reagents and reaction solutions. An Orion conbination pH electrode was used for all pH measurements made in low ionic media. A Fisher glass electrode (623) was used in conjunction with a Fisher reference electrode (423) in saline solutions. The stopped-flow system consisted of the optics from a Beck-

[†] Present address: Analytical Resources, P.O. Box 2642, Greenville, NC 27834.

0013-936X/84/0918-0219$01.50/0

man DU UV–vis spectrphotometer, a Beckman 96280 deuterium source, a Hammamatsu R-106 potted photomultiplier tube, Pacific Instruments high-voltage power supplies, an Aminco-Morrow stopped-flow mixing device, a thermistor temperature sensor, and associated photometric amplification circuitry. The photomultiplier current was processed by a two-stage operational amplifier circuit with variable gain and offset (*7,8*). The first stage converted the current to a voltage, and the second stage amplified the signal to fill the ±10-V window of an analog-to-digital converter (ADC). The ADC, a Data Translation Model DT-2762, was part of a microcomputer data acquisition system dedicated to the stopped-flow spectrophotometric system. The data system was comprised of a Charles River Data Systems LSI-11/2 microcomputer, the ADC board, a programmable real-time clock, 32 KB of memory, and an LA-36 Decwriter terminal.

The temperature of all solutions and the stopped-flow cell was controlled at 25.0 ± 0.2 °C by using a constant temperature bath.

Methods. Total oxidant concentrations were determined by amperometric titration using phenylarsine oxide as a titrant according to standard procedures (*9*). However, the KI was always added first to the diluent water and the pH 4 buffer added immediately prior to adding the sample aliquot.

Although absolute absorbance values could not be obtained directly from the stopped-flow system, absorbance changes, ΔA, relative to product absorbances at final equilibrium were obtained from the equation (*8*)

$$\Delta A = \pm\log\frac{(E_\infty - \mathrm{EOS2} + \mathrm{EOS1})\mathrm{GAIN}}{(E_2 - \mathrm{EOS2} + \mathrm{EOS1})\mathrm{GAIN}} \qquad (4)$$

where each variable in the expression has the following definition: E_∞ is the second stage output voltage at "$T = \infty$" or complete reaction. In practice, E_∞ was taken as the average value of the last 10 points on the decomposition curve. EOS1 is the offset voltage applied to the first stage. This value was always −2.000 ± 0.001 V. EOS2 is the offset voltage applied to the input of the second stage in order to ensure that E_2 was ±8.000 V. A positive value is required if a product appearance is being monitored and a negative value for a disappearance. GAIN is the gain of the second stage. E_2 is the final output voltage. So that ΔA was always positive, eq 4 was given a positive sign for disappearance and a negative sign for an appearance.

Monobromamine Formation. Concentrations of NH_2Br (eq 5) and OBr^- (eq 6) were computed from stopped-flow ΔA values at the respective wavelengths of 278 and 329 nm from the from following equations:

$$[\mathrm{OBr}^-] = \Delta A_{329}/(\epsilon^{\mathrm{OBr}}_{329} - \epsilon^{\mathrm{M}}_{329}/C) \qquad (5)$$

$$[\mathrm{NH_2Br}] = (\Delta A^0_{278} - \Delta A_{278})/(\epsilon^{\mathrm{M}}_{278} - \epsilon^{\mathrm{OBr}^-}_{278}C) \qquad (6)$$

where $C = 1/(1 + [\mathrm{H}^+]/K_a^{\mathrm{Br}})$ and $K_a^{\mathrm{Br}} = [\mathrm{H}^+][\mathrm{OBr}^-]/[\mathrm{HOBr}] = 2.0 \times 10^9$ M (*10*). These equations were derived on the assumption that the reaction goes to completion. Values for ΔA^0 were obtained by extrapolation of ΔA plots to zero time. Values for the molar extinction coefficients are given in Cromer (*6*) except new values (ϵ^{M}) were estimated for monobromamine to be 163 and 45.9 M^{-1} cm^{-1} at 232 and 329 nm, respectively. The coefficient (ϵ^{OBr}) for OBr^- at 278 nm was found to be 30.3 M^{-1} cm^{-1}.

Monobromamine Disproportionation–Dibromamine Formation. The concentrations of dibromamine in the presence of monobromamine and excess ammonia were computed by using eq 7. Derivation of eq 7 is based on the assumption that oxidizing bromine is conserved during

$$[\mathrm{NHBr_2}] = (\Delta A^0_{232} - \Delta A_{232})/(\epsilon^{\mathrm{Di}}_{232} - 2\epsilon^{\mathrm{M}}_{232}) \qquad (7)$$

the course of the reaction and that 1 mol of $NHBr_2$ is produced for every mol of NH_2Br that disproportionates ($[\mathrm{Br}^0_T] = [\mathrm{NH_2Br}] + [\mathrm{NHBr_2}]$). Equation 8 yields the rate

$$\frac{-\mathrm{d}[\mathrm{NHBr_2}]}{\mathrm{d}t} = -1/(\epsilon^{\mathrm{Di}}_{232} - 2\epsilon^{\mathrm{M}}_{232})\frac{\mathrm{d}(\Delta A_{232})}{\mathrm{d}t} \qquad (8)$$

of dibromamine formation. An alternate expression requiring ΔA values at two wavelengths and not based on assumption about stoichiometry is given by eq 9. Both

$$\frac{\mathrm{d}[\mathrm{NHBr_2}]}{\mathrm{d}t} = \frac{\epsilon^{\mathrm{M}}_{278}}{\epsilon^{\mathrm{M}}_{278}\epsilon^{\mathrm{Di}}_{232} - \epsilon^{\mathrm{M}}_{232}\epsilon^{\mathrm{Di}}_{278}}\left[-\frac{\mathrm{d}(\Delta A_{232})}{\mathrm{d}t} - \frac{\epsilon^{\mathrm{M}}_{232}}{\epsilon^{\mathrm{M}}_{278}}\frac{\mathrm{d}(\Delta A_{278})}{\mathrm{d}t}\right] \qquad (9)$$

equations were derived on the assumption that monobromamine does not disproportionate completely but approaches an equilibrium with dibromamine. In practice, the differences between rates computed with each equation were negligible; therefore, eq 8 was normally used since the necessary data could be obtained at one wavelength. In all cases, initial rates were calculated by fitting an exponential function to the early portion (5–10% of complete reaction) of absorbance, absorbance change, or concentration vs. time curves.

Procedures. The following general procedure was followed in all experiments to measure the formation rates of mono- and dibromamine. Two reactant solutions, one containing ammonium chloride and the other containing hypobromous acid/hypobromite, were prepared by adding an appropriate amount of stock solution to a 300-mL beaker. According to the desired experimental conditions, aliquots of phosphate buffer and sodium chloride were added, and the solution was diluted to 240 mL with demand-free water. The pH was then adjusted to the desired value with either 0.1 N HCl or 0.1 N NaOH. The solution was then transferred to a 250-mL volumetric flask (clear glass for NH_4Cl and amber for HOBr) and diluted to 250 mL. The concentration of oxidizing bromine in the reactant solution was determined amperometrically before and after a set of stopped-flow kinetic runs. Both solutions were introduced into the reservoir syringes of the stopped-flow mixing device, and the mixing chamber/quartz cell was purged with reatant solution. This step was repeated 4 times before a set of runs were begun and data acquired. Reactant solutions inside the reservoir syringes were equilibrated for 5 min, and the monochromator was set for either 232, 258, or 278 nm. A number of test runs were made while observing the second stage photometer output on an oscilloscope. During these runs the slits on the Beckman DU and the second stage gain were adjusted until the signal filled the ±10-V window of the ADC. At this point, the data acquisition program, STPFLO, was executed and data acquisition begun. Five replicate runs were made and the raw data stored on a floppy disk. Following a series of stopped-flow runs, 50-mL portions of each reactant solution were manually mixed with vigorous stirring, and the pH of the mixture was measured.

Additional experiments were also done to measure the equilibrium between mono- and dibromamine by measuring the absorbances at 232 and 278 nm. A manual mixing device (*6*) was used to introduce initial concentrations of bromine and ammonia into a 1-cm cell in a Cary

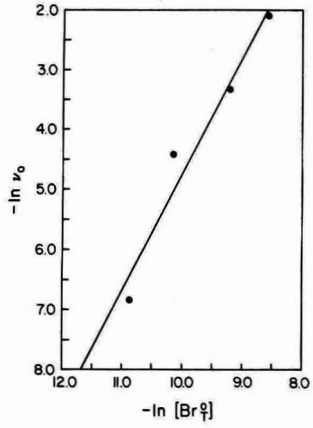

Figure 1. Order of dibromine formation with respect to the initial concentration of total bromine [Br_T^0]. Initial rate ($\nu_0 = -d(\Delta A_{232})/dt$) in absorbance units per second. Initial concentration of total oxidizing bromine [Br_T^0] in molar. Slope = 1.94, intercept = 14.66, and r^2 = 0.95.

210 to 300 nm from 45 s after reaction until 15 min.

Results and Discussion

In order to resolve rate constants for the formation of dibromamine, it was necessary to rely almost solely on the method of initial rates. Past work (*6*) has shown that dibromamine decomposition was well under way within a minute or so after formation. Furthermore, preliminary experiments revealed a complex time dependence for the absorbance changes associated with the appearance of dibromamine. Additional constraints were placed on the pH range of the experiments. Since initial rate were being used, it was imperative that the rate of formation of monobromamine, NH_2Br, must be forced to be much greater than the rate of formation of dibromamine. Experiments confirmed that pH values above 7 were necessary to completely resolve the two reactions. Because of the limited buffer capacity of phosphate, the upper pH limit was restricted to 8.5.

Monobromamine Formation Rate. Experiments were done to confirm that the rate of monobromamine formation was fast enough so as to have an insignificant effect of the measurement of the rate of dibromamine formation. Two experiments were done at 329 nm and pH 11.0 with $[OBr^-]^0 = 0.143$ mM and $[NH_3]^0 = 0.300$ mM. Four more runs were made at 278 nm and pH 6.0 with $[HOBr]^0 = 0.100$ mM and $[NH_4^+]^0 = 0.200$ mM. On the basis of the assumption that the mechanism for monobromamine formation between pH 7 and pH 8 is identical with that of monochloramine formation (*11*), the rate constant, k_1, was found to be $(4 \pm 1) \times 10^7$ M^{-1} s^{-1}, where k_1 is defined according to the rate equation

$$d[NH_2Br]/dt = k_1[NH_3][HOBr] \qquad (10)$$

Monobromamine formation rates computed for the pH range 7–8.5 were much larger than the rates observed for dibromoamine formation. Therefore, it would be possible to resolve rate constants for the two reactions.

Order with Respect to Oxidizing Bromine. The order with respect to the initial concentration of total bromine (OBr^- + HOBr) was determined at pH 7.0 for concentrations between 0.019 and 0.190 mM. The phosphate concentration, 20 mM, determined the ionic strength, and the excess ammonia concentration was 1.81–1.96 mM. The least-squares slope, 1.94, of the logarithm of initial rate vs. logarithm of concentration suggests an order with respect to concentration of 2 (see Figure 1).

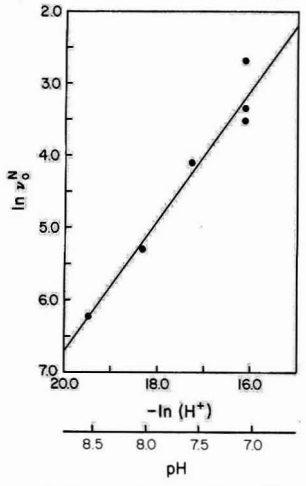

Figure 2. Order of dibromamine formation with respect to (H^+). Normalized initial rate ($\nu_0^N = \nu_0(0.1\ mM)^2/[Br_T^0]^2$) in absorbance units per second for a 0.1 mM total oxidizing bromine solution. Hydrogen ion activity (H^+) in molar. Slope = 0.902, intercept = 11.34, and r^2 = 0.95.

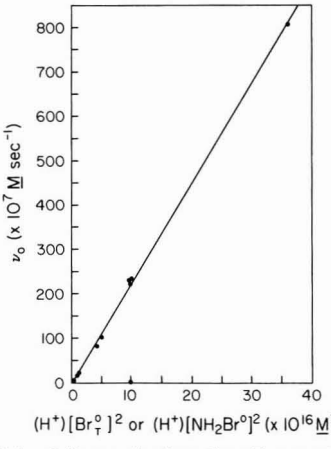

Figure 3. Order of dibromamine formation with respect to (H^+)[Br_T^0]^2 or (H^+)[NH_2Br^0]^2. Initial rate ($\nu_0 = +d[NHBr_2]/dt$) in molar per second. Slope = 2.26×10^{10} M^{-2} s^{-1}, intercept = 1.42×10^7 M s^{-1}, and r^2 = 0.999. Total phosphate = 0.02 M, pH 7.0–8.4, and [Br_T^0] = 0.019–0.190 mM.

Order with Respect to Hydrogen Ion. The order with respect to hydrogen ion concentration was found to be 1 over the pH range 7.0–8.4 (Figures 2 and 3). Below pH 7 the observed initial rates no longer responded linearly to pH changes (Figure 4). A possible cause was intrusion of the monobromamine formation reaction curve into the beginning of the dibromamine formation reaction. However, as will be discussed later, there may be other contributing factors.

Order with Respect to Excess Ammonia. The concentration of excess ammonia had no effect on the initial rate of dibromamine formation. However, it strongly affected the equilibrium between monobromoamine and dibromamine. At higher ammonia concentrations there was a higher proportion of monobromamine present when the dibromamine reaction had reached completion. This

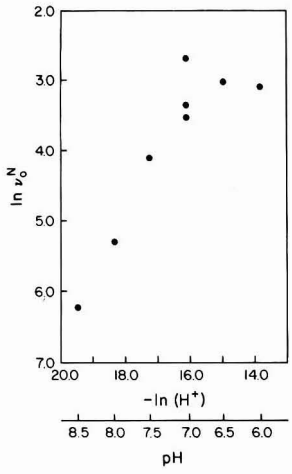

Figure 4. Low pH order of dibromamine formation with respect to (H^+). Normalized initial rate ($\nu_0^N = \nu_0$ (0.1 mM)^2/[Br_T^0]) in absorbance per second for a 0.1 mM total oxidizing bromine solution. Hydrogen ion activity (H^+) in molar. Slope = 0.619, intercept = 6.36, and r^2 = 0.80.

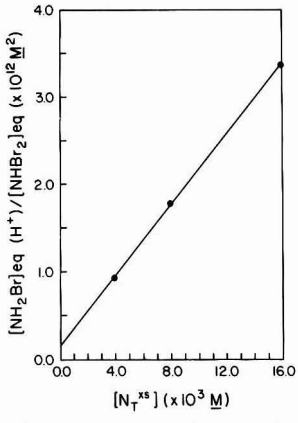

Figure 5. Dependence of bromamine ratio at equilibrium on excess ammonia (N_T^{xs}). pH 7.0. Slope = 2.02 × 10^{-10} M, intercept = 1.52 × 10^{-13}, and r^2 = 0.99.

is shown graphically in Figure 5 where the ratio of $[NH_2Br]_{eq}^2/[NHBr]_{eq}$ is plotted against the excess ammonia concentration at constant pH 7.0. The slope of Figure 5 is the equilibrium constant for eq 11. K_{eq} = 2.02 × 10^{-10} M at 25.0 ± 0.2 °C.

$$NHBr_2 + NH_4^+ \underset{}{\overset{K_{eq}}{\rightleftharpoons}} 2NH_2Br + H^+ \qquad (11)$$

Order with Respect to Phosphate. The first-order effect of phosphate on the formation of dibromamine was discovered during a series of runs to determine the effect of varying chloride concentrations. In order to obtain a low ionic strength for some runs, the phosphate buffer concentration was reduced, and the result was an extreme decrease in the rate of $NHBr_2$ formation. As Figure 6 shows, the chloride effect is egligible whereas the dependence on phosphate is marked. A plot of normalized initial rate vs. total phosphate revealed a linear dependence and a small intercept (see Figure 7). In order to more accurately compute a rate constant for the uncatalyzed reaction suggested by this intercept, an experiment was done at pH 7.55 with no phosphate buffer. In spite of the lack of

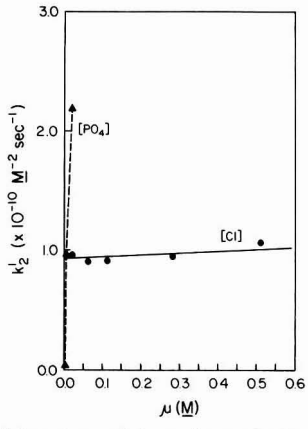

Figure 6. Salt dependence of observed second-order rate of dibromamine formation rate constant, k_2'. Phosphate dependence (▲). Chloride dependence (●). Ionic strength, μ, in molar.

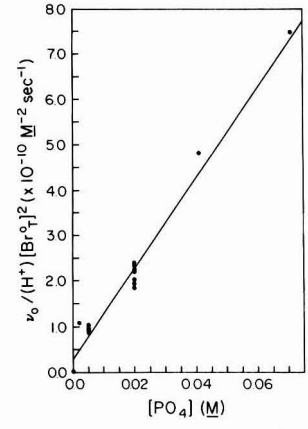

Figure 7. Experimental rate constant ($\nu_0/(H^+)[Br_T^0]$) dependence on phosphate concentration. Slope = 9.94 × 10^{11} M^{-3} s^{-1}, intercept = 2.91 × 10^9 M^{-3} s^{-1}, and r^2 = 0.97.

buffer the pH variation was no more than ±0.04 unit throughout the reaction which required approximately 16 min to reach equilibrium. If 0.02 M phosphate had been present, the reaction would have been complete in 30 s, and dibromamine would have begun decomposing. Phosphate apparently affects the stability as well as the formation of dibromamine. Past studies (*6*) on the decomposition of dibromamine in phosphate-buffered systems should be reexamined in light of this discovery. Future studies of monobromamine and dibromamine formation and decomposition should also consider possible effects of other oxyanions.

Rate Law. On the basis of the results shown graphically in Figures 3 and 8, the empirical rate law for the rate of dibromamine formation over the pH range 7.0–8.5 was found to be

$$d[NHBr_2]/dt = k_c(H^+)[PO_4][Br_T^0]^2 + k_u(H^+)[Br_T^0]^2 \qquad (12)$$

where $[PO_4]$ is the total phosphate concentration, $[Br_T^0]$ is the total initial oxidizing bromine, k_c = 9.9 × 10^{11} M^{-3} s^{-1}, and k_u = 2.4 × 10^8 M^{-2} s^{-1} at 25 ± 0.2 °C. The uncatalyzed rate constant was estimated from the initial rate of dibromamine formation depicted in Figure 8.

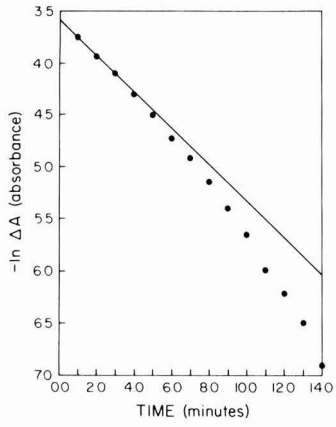

Figure 8. Dibromamine formation at 232 nm for pH 7.55, $[N_T^0] = 2.0$ mM, and $[Br_T^0] = 0.088$ mM in the absence of buffer or salt.

Reaction Mechanism. The following reaction scheme represents a possible mechanism for $NHBr_2$ formation that is consistent with the observed rate law:

$$HOBr + NH_3 \xrightarrow{k_1} NH_2Br \quad (13)$$

$$NH_2Br + H^+ \underset{}{\overset{k_{H1}}{\rightleftharpoons}} NH_3Br^+ \quad (14)$$

$$NH_3Br^+ + NH_2Br \xrightarrow{k_3} [NH_3Br\cdots NH_2Br]^+ \rightarrow NHBr_2 + NH_4^+ \quad (15)$$

$$NH_3Br^+ + PO_4^{-n} \underset{}{\overset{K_+}{\rightleftharpoons}} [NH_3Br\cdots OPO_3]^{1-n} \quad (16)$$

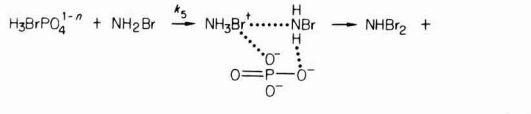

(17)

where PO_4 represents $H_2PO_4^-$, HPO_4^{2-}, or PO_4^{3-} and n is the charge on phosphate. The protonation step (eq 14) is consistent with the known behavior of monochloramine at low pH (*12*). Since monobromamine is a stronger base, the protonated form should be present in greater concentrations at higher pHs. Phosphate probably stabilizes the bromammonium ion, facilitates nucleophilic displacement of Br^+, and may also accept a proton as dibromamine is formed. The theoretical rate expression derived from the mechanism is

$$d[NHBr_2]/dt = k_3[NH_3Br^+][NH_2Br] + k_5[NH_3BrPO_4^{-n}][NH_2Br] \quad (18)$$

When the appropriate equilibrium equations are substituted, the rate may be expressed in terms of NH_2Br and H^+.

$$d[NHBr_2]/dt = k_3K_{H1}[H^+][NH_2Br]^2 + k_5K_{H1}K_P[H^+][PO_4][NH_2Br]^2 \quad (19)$$

Since either HPO_4^{2-}, $H_2PO_4^-$, or PO_4^{3-} probably catalyzes the reaction, there should be a negligible dependence of the phosphate effect on pH. For this reason, the terms $K_P[PO_4]$, which represents a composite of other terms, may be utilized in the rate equation. The expression may be written to include $[Br_T^0]$ if the following assumption is made

$$[Br_T^0] = [NH_2Br] + [NH_3Br^+] + [NH_3BrPO_4^{-n}] \quad (20)$$

and substituting equilibrium equations produce

$$[Br_T^0] = [NH_2Br] + K_{H1}[NH_2Br](H^+) + K_{H1}K_P[NH_2Br](H^+)[PO_4] \quad (21)$$

$$[Br_T^0] = [NH_2Br][1 + K_{H1}(H^+) + K_{H1}K_P(H^+)[PO_4]] \quad (22)$$

The rate expression becomes

$$\frac{d[NHBr_2]}{dt} = \frac{k_3K_{H1}(H^+)[Br_T^0]^2 + k_5K_{H1}K_P(H^+)[PO_4][Br_T^0]^2}{1 + K_{H1}(H^+) + K_{H1}K_P(H^+)[PO_4]} \quad (23)$$

which at high pH where the variables in the denominator are less than 1 reduces to

$$d[NHBr_2]/dt = k_3K_{H1}(H^+)[Br_T^0]^2 + k_5K_{H1}K_P(H^+)[PO_4][Br_T^0]^2 \quad (24)$$

where $k_c = k_5K_{H1} = 9.9 \times 10^{11}$ M^{-3} s^{-1} and $k_u = k_3K_{H1} = 2.4 \times 10^8 M^{-2}$ s^{-1}. At low pH when the variable terms in the demoninator are dominant, the initial rate should be invariant with pH. This behavior was only suggested in our low pH data due to interferences from monobromamine formation.

Conclusions

Over the pH range 7–8.5 the rate of monobromamine formation was very rapid compared to the rate of monobromamine disproportionation and subsequent dibromamine formation. Below pH 7 the rate of dibromamine formation was difficult to measure independent of monobromamine formation, but the proposed rate equation predicts a decrease in pH dependence of lower pH. Above pH 7 dibromamine formation was first order in hydrogen ion and second order in monobromamine or initial bromine in the presence of excess ammonia. Ammonia had no effect on the rate of dibromamine formation but increased the rate of the back-reaction of monobromamine. As predicted in earlier qualitative studies (*4*) monobromamine and dibromamine are in equilibrium, although the mixture decomposes. The formation of dibromamine is also independent of chloride ion but highly dependent on phosphate. In fact, the phosphate catalysis terms dominate experimental rates measured in phosphate-buffered solutions. Phosphate catalysis must also affect the rate of dibromamine decomposition. A possible decomposition mechanism may involved protonated di- and tribromamine molecules which would be stabilized by phosphate. Other oxyanions such as carbonate should also be considered in any future work for possible effects. The low concentrations of phosphate found in environmental samples probably would not be significant compared to the high buffer concentrations used in the laboratory. If ions such as carbonate behave similarly, the environmental significance would be higher. For this reason, extrapolation of these and earlier results to natural and wastewater bro-

mination should be done with care.

Registry No. $NHBr_2$, 14519-03-0; NH_3, 7664-41-7; NH_2Br, 14519-10-9; PO_4, 14265-44-2.

Literature Cited

(1) Bongers, L. H.; Burton, D. T.; Liden, L. H.; O'Connor, T. P. In "Water Chlorination–Environmental Impact and Health Effects"; Jolley, R. L.; Gorchev, H.; Hamilton, D. H., Eds.; Ann Arbor Science: Ann Arbor, MI, 1977; Vol. 2, Chapter 58, pp 735–752.
(2) Farkas-Himsley, H. In "Bromine and Its Compound"; Jolles, Z. E., Ed.; Academic Press: New York, 1966; Part VI, Chapter 2, pp 554–562.
(3) Mills, J. F. In "Chemistry of Wastewater Technology"; Rubin, A. J. Ed.; Ann Arbor Science: Ann Arbor, 1978; Chapter 13, pp 199–212.
(4) Johnson, J. D.; Overby, R. *J. Sanit. Eng. Div., Am. Soc. Cir. Eng.* **1971**, *97*, 617–628; *J. Environ. Eng. Div.* (Am. *Soc. Civ. Eng.*) **1973**, *99*, 371–373.
(5) Galal-Gorchev, H. A.; Morris, J. C. *Inorg. Chem.* **1965**, *4*, 899–905.
(6) Cromer, J. L.; Inman, G. W.; Johnson, J. D. In "Chemistry of Wastewater Technology"; Rubin, A. J., Ed.; Ann Arbor Science: Ann Arbor Science: Ann Arbor, 1978; Chapter 14, pp 213–225.
(7) Morgenthaler, L. P. "Basic Operational Amplifier Circuits for Analytical Chemical Instrumentation"; McKee-Pedersen (Pacific) Instruments: Danville, CA, 1968; p 63.
(8) Braddock, J. N. Dissertation, University of North Carolina, Chapel Hill, NC, 1973, Appendix A.
(9) American Public Health Association "Standard Methods for the Examination of Water and Wastewater", 13th ed.; American Public Health Association: Washington, DC, 1971; pp 115–116.
(10) Kelley, C. M.; Tartar, H. W. *J. Am. Chem. Soc.* **1956**, *78*, 5752.
(11) Weil, I.; Morris, J. C. *J. Am. Chem. Soc.* **1949**, *71*, 3123.
(12) Gray, E. T., Jr.; Margerum, D. W.; Huffman, R. P. In "Organometals and Organometalloids: Occurrence and Fate in the Environment; Brinckman, F. E.; Bellama, J. D.; Eds.; Americal Chemical Society: Washington, DC, 1978; ACS Symp. Ser. No. 82, pp 264–277.

Received for review August 16, 1982. Accepted August 29, 1983. This work was supported by the Nuclear Regulatory Commission, Division of Safeguards, Fuel Cycle and Environmental Research, Office of Nuclear Regulatory Research, Contract NRC-04-77-11.

Reactive Foams for Air Purification

Susann M. Brander, Gudrun I. Johansson,* Bengt G. Kronberg, and Per J. Stenlus

The Institute for Surface Chemistry, S-114 86 Stockholm, Sweden

■ The use of water-based foams for removal of gaseous pollutants from air has been investigated. Hydrogen sulfide, formaldehyde, and acetaldehyde can effectively be absorbed in a foam containing substances that react chemically with the gaseous pollutant. The influence of the foam characteristics on the absorption of gas has been studied for a single continuously flowing liquid film. Formaldehyde, acetaldehyde, and propionaldehyde were used as model compounds. It was found that the chemical structure of the foaming agent did not influence the rate of gas absorption. To achieve efficient absorption of slightly soluble gases, it was necessary to use a high renewal rate of the liquid film. The presence of a liquid-crystalline phase in the film increased the solubility of hydrophobic gas molecules.

Introduction

The aim of this work has been to investigate if gas pollutants can effectively be removed from air by blowing the air through a foam bed. The removal can be achieved either by simple absorption or by a chemical reaction, in the liquid foam lamella.

In order to investigate the effect of foaming agents on the gas pollutant absorption, we have also studied the absorption into a single continuously flowing liquid film.

Reactive foams have been used by Viles (*1*) and Silverman (*2*, *3*) to encapsulate air contaminated with radioactive materials and by Pozin (*4*) and Helsby and Birt (*5*) for absorption of CO_2. Several patents deal with the removal of nitrous oxides (*6*) or particles (*7–10*) from air by a foam technique.

The main advantage of using a foam as an absorption medium is the large contact area between the gaseous and the liquid phase (*1*, *11*). In addition, the rapid destruction and renewal of bubbles in a dynamic foam lead to efficient mass transfer (*12*). A low liquid/air ratio can be maintained (typically, 6×10^{-6} m^3/m^3) (*13*). This implies that a pollutant can be removed from a large gaseous volume to a very small liquid volume. With the proper choice of foam density, foam height, and process equipment the pressure drop in a foam column can be kept quite low, i.e., less than 0.5 kPa (*11*, *13*).

In a brief survey Jackson (*12*) has compared the mass transfer operations in a foam with other equipment such as packed towers. For many processes, e.g., absorption of N_2O_3 or conversion of SO_2 into H_2SO_4, he found a 10–100-fold increase in the absorption rate coefficient.

Model equations for the calculations of the mass transfer (*11*, *14*, *15*) or foam ratio (*16*) from measurable physical quantities in dynamic foam columns have been proposed. Weissman (*17*) found that the mass transfer is decreased by high foam stability and high viscosity of the liquid in the foam. This is probably due to a decreased gas/liquid contact and an increased diffusion barrier.

According to Cullen (*18*), impurities in technical surface active agents may cause up to 25% variation in the absorption of gas into a flowing liquid film. Sidorova (*19*) found that the mass transfer coefficient for desorption of NH_3, SO_2, CO_2, and N_2 from the liquid in a foam increased with increasing solubility of the gases.

Experimental Conditions and Equipment

Chemicals. Table I lists the surfactants used as foaming agents. Formaldehyde, HCHO (35%), acetaldehyde, CH_3CHO (for synthesis), and propionaldehyde, CH_3CH_2CHO (purum), were obtained from Merck AG. The hydrogen sulfide, H_2S, was supplied by AGA, Stockholm. Other chemicals were of reagent grade.

Foam Column. Figure 1 is a schematic drawing of the foam column. A foam bed of 500–600 cm^3 was generated at room temperature (22 ± 1 °C) by passing a gas flow (V^g)

 0013-936X/84/0918-0224$01.50/0

Table I. Foaming Agents

type of surfactant	trade name	manufactured by	quality, %	cmc, g/dm$_3$
sodium decyl sulfate ($NaC_{10}SO_4$)		Merck AG	99 (p.a.)	8.64
sodium dodecyl sulfate ($NaC_{12}SO_4$)		Merck AG	99	2.36
sodium tetradecyl sulfate ($NaC_{14}SO_4$)		Merck AG	99	0.65
polyethylene glycol (9-10)-*p*-octylphenol	Triton X-100		technical	0.15
hexadecyltrimethylammonium bromide, CTAB		Fluka AG	purum	0.34
sodium decyl sulfate	Empicol 0137	Albright & Wilson	90	2.0-2.2[a]
sodium dodecyl sulfate	Empicol LZV	Albright & Wilson	85	0.42[a]
sodium alkyl sulfate (C_{12}-C_{14})	Sulfatol 33	Aarhus Oljefabriker		0.58[a]
secondary sodium alkanesulfonate (C_{13}-C_{18})	Hostapur SAS60	Hoechst AG	60	0.33[a]
sodium alkylbenzene sulfonate	Berol 496	Berol Kemi AB	80	0.32[a]
sodium alkyl ether sulfate	Berol 475	Berol Kemi AB	39-41	0.16[a]
ethoxylated primary alcohol (30 e.o.)	Berol 081	Berol Kemi AB	100	0.01[a]
alkylphenol-ethylene oxide (14. e.o.)	Berol 263	Berol Kemi AB	100	0.035[a]

[a] These cmc values are measured with a Du Noüy ring balance at 22 °C. Other cmc values are taken from Mukerjee and Mysels (*27*) standard reference data of cmc values.

Table II. Absorption of Form- and Acetaldehyde in Foam[a]

foaming agent	concn of foaming agent, g/dm^3	concn of aldehyde in the gas, vol %	removed pollutant, %
	HCHO[b]		
sodium decyl sulfate	0.060	0.02	98.4
sodium decyl sulfate	0.060	0.1	97.9
sodium decyl sulfate	0.060	0.14	96.9
sodium decyl sulfate	0.060	0.33	97.5
sodium decyl sulfate	0.060	0.017	87.5[d]
sodium decyl sulfate	0.060	0.02	90.2[e]
Sulfatol 33	0.030	0.1	97.8
Sulfatol 33	0.030	0.1	99.2[f]
Empicol LZV	0.066	0.1	96.7
Empicol 0137	0.256	0.1	98.3
Berol 496	0.017	0.1	96.1
Berol 081	0.046	0.1	96.9
Berol 263	0.013	0.1	97.1
Berol 475	0.049	0.1	80.5
Hostapur SAS60	0.027	0.1	80.5
	CH_3CHO[c]		
sodium decyl sulfate	0.060	0.05	75.2
sodium decyl sulfate	0.060	0.2	74.4
sodium decyl sulfate	0.060	0.21	85.9
sodium decyl sulfate	0.060	0.07	99.6[f]
sodium decyl sulfate	0.060	0.26	99.8[f]
sodium decyl sulfate	0.060	0.36	99.3[f]
sodium decyl sulfate	0.060	0.32	92.5[d,f]

[a] V^l/V^g = 0.015 m^3/m^3, and V^g = 0.6 m^3/h. No reactant in solution (if not otherwise indicated). [b] Mean values of two to three determinations. [c] Analysis during first 10 min of experiment. [d] V^g = 1.2 m^3/h; V^l/V^g = 0.0075 m^3/m^3. [e] V^g = 1.2 m^3/h; V^l/V^g = 0.015 m^3/m^3. [f] $Na_2S_2O_5$ added.

through a glass filter, into the absorption liquid. The absorption liquid was an aqueous solution of the foaming agent and the reactant with a total volume of 150–200 cm^3. The concentration of the foaming agent was adjusted to give the desired foam height and, hence, was varied as shown in the second column of Table II. The foam expansion factor (foam volume/liquid volume) was between 4 and 6. The foam level was kept constant by recirculating the drained liquid at constant flow (V^l) and spraying it on top of the foam bed. Solid reaction products were removed with glass wool filters.

The gas flow was a mixture of air and pollutant. Samples for analysis were absorbed in liquid and analyzed. In each experiment, which lasted for 30–60 min, the input flow was analyzed at the beginning and at the end. The output flow was analyzed 2–3 times during the experiment.

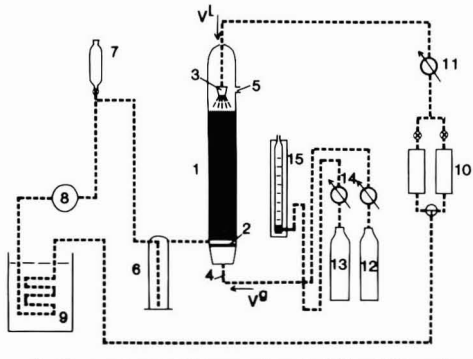

Figure 1. Foam column. (1) Foam column (height = 0.58 m; diameter = 0.05 m), (2) glass filter (porosity 1), (3) sprayer, (4) gas inlet, (5) gas outlet for analysis, (6) vessel for the foam liquid, (7) dropping funnel for additives, (8) pump for recirculating liquid, (9) thermostatic water bath, (10) glass wool filters, (11) flowmeter, liquid, (12) air, (13) gaseous pollutant, (14) flowmeters, gas, and (15) mercury manometer.

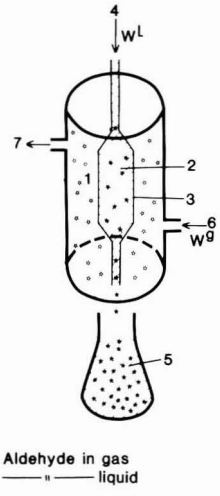

Figure 2. Liquid film equipment. (1) Gas box (~0.6 dm^3), (2) liquid film (~7 cm^2), (3) Pt frame, (4) liquid flow, inlet, (5) sampling of liquid for analysis, (6) gas flow, inlet, and (7) gas flow, outlet.

Apparatus for the Study of a Liquid Film. The absorption of gaseous aldehydes into a single liquid film was studied in the apparatus shown in Figure 2. The solution flows into the gas box and spreads as a liquid film

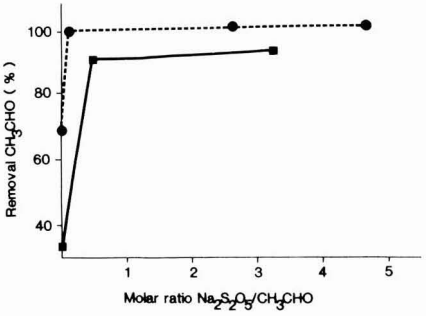

Figure 3. Percent removal of acetaldehyde in a foam with $Na_2S_2O_5$ as a reactant. Concentration of CH_3CHO in air = 0.3–0.4 vol%. (●) V^g = 0.6 m³/h, and V^l/V^g = 0.015 m³/m³; (■) V^g = 1.2 m³/h, and V^l/V^g = 0.0075 m³/m³.

over a platinum frame. The liquid flow rate, W^l (cm³/min), is regulated with a peristaltic pump and collected for analysis outside the box. The gas passes the liquid film in counterflow and can be collected for analysis as in the foam column. The gas flow, W^g (10 dm³/min), was measured with a flowmeter. The experiments were carried out at room temperature (22 ± 1 °C).

Preparation of Gaseous Mixtures. The hydrogen sulfide was introduced into the air stream from a gas cylinder. The aldehydes were mixed with air by passing an air stream through an aqueous solution of the aldehyde. The concentration of aldehyde in the gas was varied by changing the concentration of aldehyde in the solution, the flow rate of the air, and the temperature of the solution.

Chemical Analysis. The sample collection and analysis of the aldehydes followed standard methods recommended by the Swedish National Board of Occupational Safety and Health (*20*). Formaldehyde was analyzed by a spectrophotometric method in which a chromotropic acid forms a colored complex with formaldehyde. In the film experiments another spectrophotometric method was used for acet- and propionaldehyde; 3-methyl-2-benzothiazolinone hydrazone (MBTH) was reacted with the aldehydes to a colored complex. In the foam column experiments the titrimetric hydrogen sulfite method was used to determine the concentration of acetaldehyde (*20*).

To determine the concentration of absorbed hydrogen sulfide, the method described by Skoog and West (*21*) was used. CdS is precipitated from a $Cd(NH_3)_4^{2+}$ solution followed by titration of the remaining Cd^{2+}.

Results and Discussion

Experiments with the Foam Column. In Table II are listed the results of several experiments in which aldehydes were absorbed into foams with different foaming agents. $Na_2S_2O_5$ was used as a reactant in the foam liquid. Because of its large solubility in water, formaldehyde was removed very efficiently (96–98%) without any reactant. Addition of $Na_2S_2O_5$ increases the absorption to >99%. Efficient removal of acetaldehyde, >99%, is obtained only by addition of $Na_2S_2O_5$. This efficiency lasts as long as the molar ratio $Na_2S_2O_5$ (in the foam liquid)/CH_3CHO (in the gas) is >0.5 Figure 3. Absorption of acetaldehyde into solutions without $Na_2S_2O_5$, however, decreases rapidly with time (Table II).

The absorption of formaldehyde and acetaldehyde is dependent on the foaming agent (Table II) and its foam-stabilizing effect. This effect was investigated by shaking 10 cm³ of solution in glass tubes for 1 min. Table III shows the time required for the foam to decrease to 75% of its initial height, $t_{0.75}$. Berol 465 and Hostapur SAS 60 give much higher $t_{0.75}$ vaues than the other foaming agents. They also give poorer absorption of formaldehyde. The reason for this is probably that stable foams imply a decreased surface renewal of the foam films. The importance of surface renewal for gas absorption is discussed further in connection with the film experiments.

Table III. $t_{0.75}$ Values for the Foaming Agents

foaming agent	concn, g/dm³	$t_{0.75}$, min
sodium decyl sulfate	0.060	<5
Sulfatol 33	0.030	<5
Empicol LZV	0.066	20
Empicol 0137	0.256	<5
Berol 496	0.017	<5
Berol 081	0.046	60
Berol 263	0.013	60
Berol 475	0.049	270
Hostapur SAS60	0.027	130

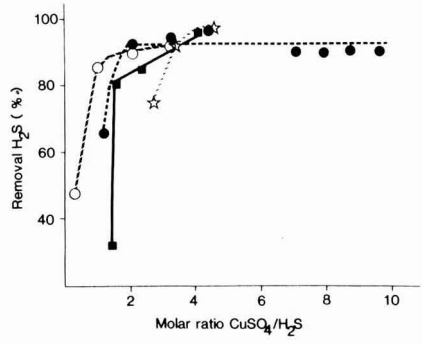

Figure 4. Removal of hydrogen sulfide in a foam with $CuSO_4$ as a reactant. V^g = 0.6 m³/h, and V^l/V^g = 0.015 m³/m³. Concentration of H_2S in air: (☆) 0.22 vol %, (●) 0.1 vol %, (■) 0.054 vol %, and (○) 0.026 vol %.

The removal capacities of both form- and acetaldehyde decrease if the flow rate of the gas increases (Table II). The experiment was conducted with two gas flows. The residence times of the gas in the foam (foam volume/gas flow) were approximately 3.5 and 1.75 s, respectively. These are several orders of magnitude larger than the estimated time for diffusion of a gas molecule across an average foam bubble. Thus, diffusion through the gas cannot be the limiting factor for absorption. Our conclusion is that too high flow rates lead to a decreased contact area due to the formation of holes and channels in the foam.

The liquid flow rate seemed to have minor influence on the removal capacity, which probably was due to the fact that a high liquid flow was needed to regulate the foam height.

Hydrogen sulfide was removed from the gas by precipitation of CuS ($CuSO_4$ was added to the foam liquid). The precipitation product, CuS, did not affect the stability of the foam. Above a limiting molar ratio $CuSO_4/H_2S$ absorption becomes independent of the $CuSO_4$ concentration. Maximum absorption efficiency with this foam column is >90% and requires a molar ratio $CuSO_4/H_2S$ higher than 2 (Figure 4).

It was found that the pressure drop over the foam column (glass filter plus foam bed) was considerably higher in the H_2S experiments (>6 kPa) than for the aldehydes (~2 kPa).

Figure 5 shows that the pressure drop increases and the removal of hydrogen sulfide decreases rapidly when the liquid/gas flow ratio is reduced. This is explained by the

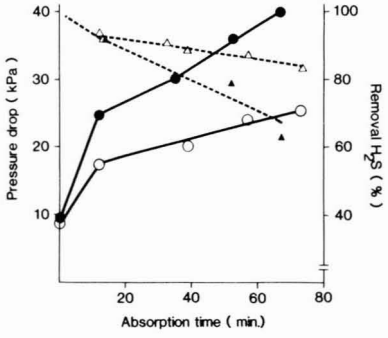

Figure 5. Comparison of pressure drop (—) and percent removal of hydrogen sulfides (---) as a function of absorption time in the foam column. $CuSO_4$ was used as a reactant for H_2S. Molar ratio $CuSO_4/H_2S$ = 2.5–5.0, concentration H_2S = 0.054 vol % and V^g = 0.6 m^3/h. (○, △) V^l/V^g = 0.015 m^3/m^3; (●, ▲) V^l/V^g = 0.0075 m^3/m^3.

increased amount of precipitated CuS in the column which increases the flow resistance in the filter as well as in the foam. We conclude that efficient absorption of gaseous pollutants with reactants that form solid products is also possible, but it is necessary to ensure an efficient removal of the precipitate from the foam column.

Experiments with a Single Foam Film. The absorption of gaseous pollutants in the foam column is obviously dependent not only on the properties of the foam lamella and the solubility (absorption capacity) of the impurities in the foam liquid but also on the parameters of the equipment used such as foam height, gas/liquid flow ratio, pressure drop, volume ratio of the foam, etc. In order to study the absorption process independently of these parameters, we also investigated absorption into a single liquid film as a model for the foam lamella in the experimental setup shown in Figure 2.

Theoretical Considerations. The cell in Figure 2 is not designed to ensure that equilibrium prevails in all experiments. Rather, it allows one to draw conclusions concerning the rate-determining factors in different cases. To show this, we will derive equations for equilibrium conditions and compare the calculated and experimental results.

If the distribution of aldehyde molecules between the gas and the liquid phase reaches equilibrium, Henry's law may be used:

$$p_A = k_H X_A = C_A^g RT \tag{1}$$

where p_A is the aldehyde partial pressure, X_A is the mole fraction of aldehyde in water, C_A^g is the aldehyde concentration in the gas phase, k_H is the Henry law constant, and R and T have their usual meaning. At low concentrations

$$X_A \simeq C_A^l \bar{V}_{H_2O} \tag{2}$$

where C_A^l is the molar concentration of aldehyde in the liquid and $\bar{V}_{H_2O}$ is the molar volume of water.

Inserting eq 2 into eq 1 we obtain

$$C_A^l = \frac{RT}{k_H \bar{V}_{H_2O}} C_A^g = K C_A^g \tag{3}$$

Experimentally, however, the flow rate rather than the concentration of aldehyde is of interest. The aldehyde flow, Q, is related to the gas or liquid flow, W, by

$$Q^g = C_A^g W^g \qquad Q^l = C_A^l W^l \tag{4}$$

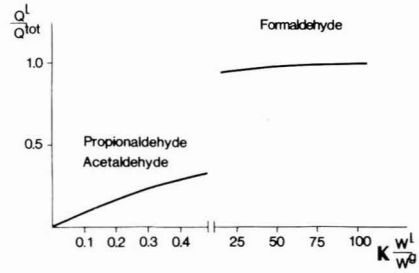

Figure 6. Calculated liquid uptake of aldehyde as a function of liquid flow rate. The working areas for form-, acet-, and propionaldehyde at constant gas flow (10 dm^3/min) are indicated in the figure.

where g and l denote gas and liquid, respectively. Therefore, at equilibrium

$$\frac{Q^l}{Q^g} = K\frac{W^l}{W^g} \tag{5}$$

The total aldehyde flow in the gas box is expressed by

$$Q^{tot} = Q^g + Q^l \tag{6}$$

Combining eq 5 and 6 gives

$$Q^l = Q^{tot}\frac{K(W^l/W^g)}{1 + K(W^l/W^g)} \tag{7}$$

Thus, at constant flow rates of gas and liquid the aldehyde uptake in the liquid, Q^l, should depend linearly on the aldehyde concentration in the gas phase, or Q^{tot}, with a slope given by the constants in eq 7.

Equation 7 can also be used to predict the dependence of the aldehyde uptake in the liquid on the flow rate of the liquid film. Figure 6 shows the predicted relative aldehyde uptake in the liquid film, Q^l/Q^{tot}, as a function of the liquid flow rate, or $K(W^l/W^g)$, keeping the gas flow rate, W^g, constant. In this calculation k_H = 7.14 mmHg for formaldehyde (*22*), $k_H = 2.3 \times 10^3$ mmHg for acetaldehyde (*23*), and $k_H = 5.6 \times 10^3$ mmHg for propionaldehyde (*24*) were used. The figure shows clearly that, keeping Q^{tot} constant, there are two extreme cases:

(i) $K(W^l/W^g) \ll 1$; i.e., k_H is large. The aldehyde uptake in the liquid will be directly proportional to the liquid flow rate, and the small equilibrium value of the aldehyde concentration in the liquid phase is immediately reached. Hence, the liquid film works at a maximum capacity. An increase in the liquid flow rate therefore increases the aldehyde uptake because a larger liquid volume per unit time is exposed to the gas. This is the case of acet- and propionaldehyde as will be discussed below.

(ii) $K(W^l/W^g) \gg 1$; i.e., k_H is small. The aldehyde uptake in the liquid will be almost independent on the liquid flow rate and almost equal to the maximum possible value (Q^{tot}). In this case the absorption capacity of aldehyde in the liquid is very large, and the aldehyde content of the gas in equilibrium will be very low. This is the case of formaldehyde as will be discussed below.

An intrinsic efficiency, f, of gas uptake in the film may be defined by

$$f = \frac{P_A^{tot} - P_A^{out}}{P_A^{tot} - P_A^g} = \frac{Q^l(\text{exptl})}{Q^l(\text{calcd})} \tag{8}$$

where P_A^{tot} is the initial partial pressure of the aldehyde and P_A^{out} is the experimental partial pressure in the gas outlet. P_A^g and Q^l(calcd) are the calculated partial pressure of the

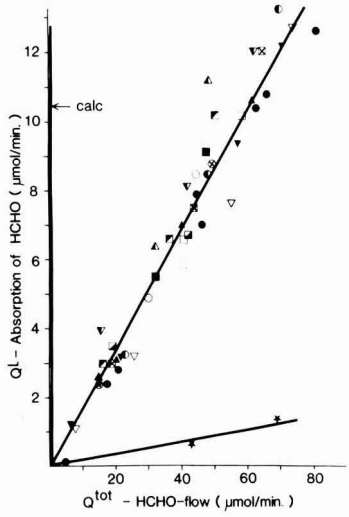

Figure 7. Uptake of formaldehyde into a flowing liquid film, Q^l (W^l = 2.5 × 10^{-3} dm^3/min), at various concentration of aldehyde in the gas flow, Q^{tot}. The following surface active agents and concentrations (g/dm^3) were used as film stabilizers: (○) $NaC_{10}SO_4$ (7.5), (◑) $NaC_{10}SO_4$ (5.12), (●) $NaC_{12}SO_4$ (1.8), (◐) $NaC_{12}SO_4$ (1.2), (△) $NaC_{14}SO_4$ (0.25), (▲) Triton X-100 (0.05), (▽) Empicol LZV (0.066), (▼) Empicol LZV (0.264), (half-filled up triangle) Empicol 0137 (1.12), (half-filled down triangle) Hostapur SAS60 (0.08), (□) Berol 496 (0.113), (■) Berol 081 (0.046), (left half-filled squares) Berol 475 (0.05), (right half-filled squares) Berol 263 (0.01), (⊗) Sulfatol 33 (0.294), (crossed box) CTAB (0.192), (solid star) CTAB + hexanol (32 + 32). The calculated lines show the maximal absorption of the aldehydes into the film at equilibrium conditions.

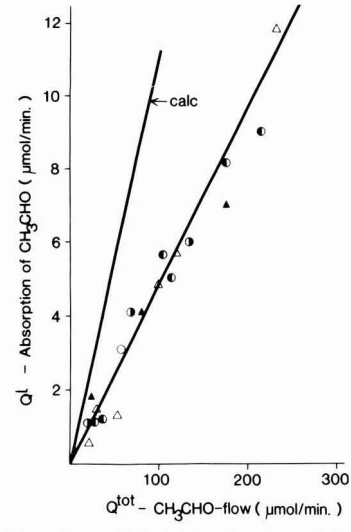

Figure 8. Uptake of acetaldehyde into a flowing liquid film, Q^l (W^l = 2.5 × 10^{-3} dm^3/min), at various concentrations of aldehyde in the gas flow, Q^{tot}. See Figure 7 for symbol and details.

aldehyde in the outlet and the calculated liquid uptake of the aldehyde assuming equilibium conditions.

Influence of Type of Surfactant in the Film. Figures 7–9 show the uptake of form-, acet-, and propionaldehyde into the liquid films formed by 12 different surfactants with varying concentrations. No reactant was added to the film liquid. In all experiments the flow rate of the liquid film, W^l, was 2.5 × 10^{-3} dm^3/min. Neither

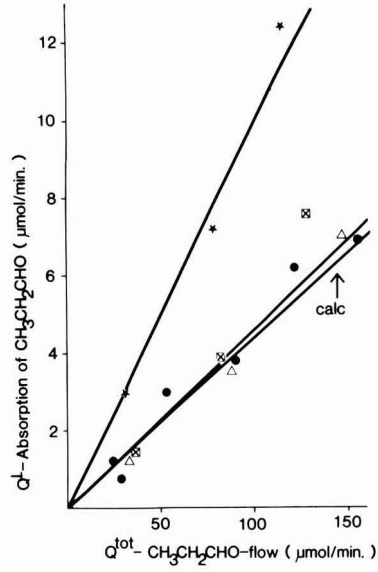

Figure 9. Uptake of propionaldehyde into a flowing liquid film, Q^l (W^l = 2.5 × 10^{-3} dm^3/min), at various concentrations of aldehyde in the gas flow, Q^{tot}. See Figure 7 for symbols and details.

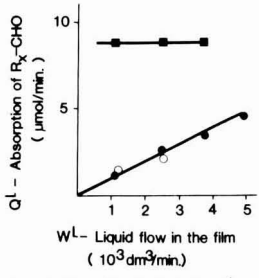

Figure 10. Aldehyde uptake in the liquid film, Q^l, as a function of the flow rate of the film, W^l. W^g = 10 dm^3/min. (■) HCHO, (●) CH_3CHO, and (○) CH_3CH_2CHO.

the chemical composition nor the concentration of surfactant has any significant effect on the rate of absorption as long as the surfactant is dissolved in homogeneous solution below the critical micelle concentration, cmc. (The values of cmc are given in Table I. The results for CTAB–hexanol are discussed below). Since there is no variation in the aldehyde uptake on changing surfactant, we conclude that the variations in efficiency of absorption indicated in Table II must be due to variation in the properties of the foam bed. It is also obvious that the rate of transport across the surfactant film cannot be a rate-determining step in the absorption process.

Using eq 7, we can calculate the aldehyde uptake in the film at equilibrium as a function of Q^{tot}. The predicted uptake is shown in Figures 7–9. The predicted slopes are respectively 5, 0.1, and 0.04 for form-, acet-, and propionaldehyde. The experimental slopes are 0.18, 0.05, and 0.04, respectively. The predicted faster uptake of the formaldehyde is confirmed experimentally. The intrinsic efficiencies according to eq 8 are 0.04 for formaldehyde, 0.5 for acetaldehyde, and ~1 for propionaldehyde. Hence, in the case of formaldehyde the system is far from equilibrium, and the experimental line in Figure 7 probably describes the maximum uptake made possible by the design of the gas box.

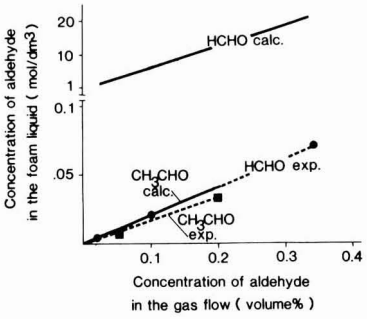

Figure 11. Theoretical possible absorption at equilibrium conditions (calcd) compared with experimental results for absorption of form- and acetaldehyde in the foam column. $V^g = 0.6$ m^3/min, and $V^l/V^g = 0.015$ m^3/m^3.

Influence of the Liquid Flow Rate in the Film. Figure 10 shows clear differences between formaldehyde and the two other compounds. The uptake of formaldehyde is independent of the liquid flow rate, corresponding to $K(W^l/W^g) \gg 1$ (Figure 6). (With $W^g = 10$ dm^3/min and $W^l = 2.5 \times 10^{-3}$ dm^3/min, $K(W^l/W^g) = 36$ for formaldehyde.) Thus, the uptake in the film confirms that conditions for formaldehyde are far from equilibrium.

The uptake of acet- and propionaldehyde, on the other hand, increases linearly with increasing flow rate. This corresponds to $K(W^l/W^g) \ll 1$ (Figure 6). (With $W^g = 10$ dm^3/min and $W^l = 2.5 \times 10^{-3}$ dm^3/min, $K(W^l/W^g) = 0.11$ for acetaldehyde and 0.046 for propionaldehyde). The conclusion is that the uptake of both acet- and propionaldehyde is at its maximum possible value; i.e., the rate of uptake is determined by the rate of flow in the lamella, and there is equilibrium between gaseous and dissolved aldehydes.

Equilibrium Calculations for the Foam Column. Using eq 3 for equilibrium calculations in the foam columns shows that similar conditions as in the film prevail. Formaldehyde is far from maximum uptake and acetaldehyde much closer (Figure 11). The experimental values $C_{A(l)}$ were calculated by assuming a liquid volume of 0.2 dm^3 in the foam and for the measured removal capacities after 10 min of absorption.

Lamellar Liquid Crystal in the Film. For slightly soluble gases the absorption may be increased by (a) increasing the solubility of the gas in the liquid film or (b) adding a reagent that removes the free dissolved compound by a chemical reaction. The latter possibility was demonstrated by the experiments with pyrosulfate or copper sulfate. The former possibility was demonstrated in the film experiments by using a foam agent in such concentrations that a lamellar liquid-crystalline phase occurs in the film.

Figure 12 shows the three-component phase diagram for the system water/cetyltrimethylammonium bromide (CTAB)/hexanol at 20 °C (*25*). In this system two types of lyotropic liquid crystals are formed. The hexagonal structure (E) which is in equilibrium with concentrated (micellar) aqueous solution (L_1) is able to incorporate about 5 wt % hexanol. The other liquid-crystalline structure (D) is lamellar and is formed only by all three components together at this temperature. In addition, solutions of CTAB and water in hexanol occur (area L_2). The D-phase region extends to very high concentrations of water (≈95%) and at these very high water contents is in equilibrium with an aqueous micellar solution. It is very easy to form a stable film from CTAB/hexanol/water mixtures in which this type of equilibrium obtains (marked

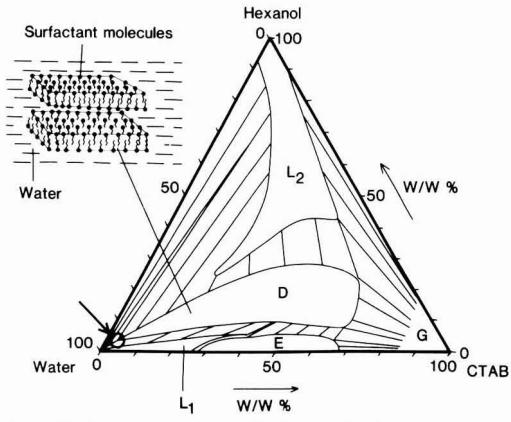

Figure 12. Phase diagram of CTAB/hexanol/H_2O.

with a ring in the left corner of the phase diagram in Figure 12). The absorption of formaldehyde and propionaldehyde into such lamellae is shown in Figures 7 and 9, respectively. The absorption of the highly water-soluble formaldehyde is much less than in water, while propionaldehyde absorption increases strongly.

It was shown by Saito and Friberg (*26*) that when foam lamellae are prepared from mixtures of the type described above, they consist of multilayers of the lamellar liquid-crystalline phase. Such a lamella will offer an amphiphilic environment into which an amphiphilic molecule, like propionaldehyde, can be incorporated with its hydrophobic parts in contact with the hydrophobic parts of the multilamellar structure, and the hydrophilic part in the polar layer. A strongly polar compound like formaldehyde, on the other hand, would not be incorporated in this way, and the volume of the aqueous environment into which the formaldehyde can be dissolved would be much less in a lamella containing a liquid-crystalline phase than in an aqueous lamella which is stabilized by a single surfactant layer. This clearly explains the reversed absorption capacities for form- and propionaldehyde.

Conclusions

The results from the column experiments together with the absorption studies in a single liquid film indicate the following conclusions about the foam characteristics:

(i) The chemical composition of the foaming agent does not influence the rate of absorption, probably because thick foam lamellae that would decrease the permeability of the gas do not develop in the time available in a dynamic foam.

(ii) The rate of surface renewal in the foam is important for slightly soluble gases. Such gases reach equilibrium conditions in the foam lamella very rapidly. In this case an increased surface renewal increases the rate of absorption. A high surface renewal is obtained if the stability of the foam is low. Then mechanical agitation such as caused by gas flow or a water spray will break the foam lamellae easily and new gas/liquid contact areas are continuously created. Thus, the choice of foaming agent is important in the sense that it controls the foam stability.

(iii) A reactant mixed into the foam is an effective way to increase the gas absorption. This is particulary important for the slightly soluble gases. Another possibility is to increase the solubility of the gas in the lamella. For this purpose liquid crystals can be utilized in the case of hydrophobic gas molecules. As liquid-crystalline phases also enhance the foam stability, thus decreasing the rate of surface renewal, the optimum combination of the dif-

ferent parameters will be specific to every system.

(iv) Precipitated reaction products must be effectively removed from the foam, so that pressure drop and removal capacity are not negatively affected. The main advantage of particulate reaction products is that they can easily be removed by filtration from the foam solution.

The foam technique seems to be applicable to different types of pollutants. The problem of obtaining a high absorption efficiency of the foam is probably a question of finding an effective reactant for the pollutant. If this can be found, the foam technique has great advantages in combining a large surface area with a low pressure drop and a low water consumption. A practical problem, however, is that holes and channels may rather easily be created because of the mechanical weakness of the foam.

Acknowledgments

The contributions of Gunilla Gillberg to the initial stages of the work are gratefully acknowledged.

Nomenclature

V^g	gas flow in the foam column, m^3/min
V^l	liquid flow in the foam column, m^3/min
V^l/V^g	liquid/gas flow ratio in the foam column, m^3/m^3
W^l	liquid flow in the film, dm^3/min
W^g	gas flow around the film, dm^3/min
Q^l	velocity of aldehyde absorption in the film, $\mu mol/min$
Q^{tot}	initial aldehyde flow in the gas, $\mu mol/min$
Q^g	aldehyde flow in the gas after absorption in the film at equilibrium conditions, $\mu mol/min$

Registry No. $Na_2S_2O_5$, 7681-57-4; $CuSO_4$, 18939-61-2; H_2S, 7783-06-4; HCHO, 50-00-0; CH_3CHO, 75-07-0; CH_3CH_2CHO, 123-38-6; $NaC_{10}SO_4$, 142-87-0; $NaC_{12}SO_4$, 151-21-3; $NaC_{14}SO_4$, 1191-50-0; CTAB, 57-09-0; Triton X-100, 9002-93-1; Sulfatol 33, 88495-87-8; Berol 496, 88495-86-7; Berol 475, 67894-03-5; Berol 081, 88495-84-5; Berol 263, 88495-85-6.

Literature Cited

(1) Viles, F. J.; Bulba, E.; Lynch, J. J.; First, M. V. *U.S. At. Energy Comm.* **1968**, *NYO-841-14*, 1–29.
(2) Silverman, L. *U.S. At. Energy Comm.* **1962**, *TID-7641*, 169–184.
(3) Silverman, L. U.S. Patent 3 338 665, 1967.
(4) Pozin, M. E.; Kopylev, B. A.; Tarat, E. A., *J. Appl. Chem.* **1958**, *32*, 1033–1038.
(5) Helsby, F. W.; Birt, D. C. P. *J. Appl. Chem.* **1955**, *5*, 347–352.
(6) Yoshioka, K.; Matsumoto, M. Jpn. Tokkyo Koho Patent 73 01 296, 1973.
(7) Okabe, A.; Ishii, T. Japan Kokai Tokkyo Koho Patent 73 24 962, 1973.
(8) Huppke, G. P.; McIlvaine, R. L. Ger. Offen. Patent 2 231 895, 1973.
(9) Bröll, R.; Thomas, H. Ger. Offen. Patent 2 243 241, 1974.
(10) Javorsky, B. S.; Winberg, H. T. Ger. Offen. Patent 2 231 911, 1973.
(11) Workman, W. L.; Calvert, S. *AIChE J.* **1966**, *12* (15), 867–876.
(12) Jackson, I. *Br. Chem. Eng.* **1963**, *8* (5), 319–321.
(13) Javorsky, B. S. *Filtr. Sep.* **1972**, *9* (2), 173–175.
(14) Maminov, D. V.; Mitriskov, A. Ya. *Int. Chem. Eng.* **1969**, *9* (4), 642–644.
(15) Muklenov, I. P. *J. Appl. Chem.* **1958**, *31*, 1328–1333.
(16) Rubin, E.; LaMantia, C. R.; Gaden, E. L., Jr. *Chem. Eng. Sci.* **1967**, *22* (8), 1117–1125.
(17) Weissman, E. Y.; Calvert, S. *AIChE J.* **1965**, *11* (2), 356–363.
(18) Cullen, E. J.; Davidson, J. F. *Chem. Eng. Sci.* **1956**, *6* (2), 49–56.
(19) Sidorova, L. S.; Tubolkin, A. F.; Tumarkina, E. S. Zh. Prikl. Khim. (*Leningrad*) **1969**, *42* (9), 1925–1929.
(20) Skare, I.; Dahlner, B. "Determination of Aldehydes in Air"; Arbete och Hälsa: Stockholm, 1973; Vol. 6 (Swedish).
(21) Skoog, D. A.; West, D. M. "Fundamentals of Analytical Chemistry", 1st ed.; Holt, Rinehart and Winston: London, 1966; p 275.
(22) Walker, J. F. "Formaldehyde", 3rd ed.; Reinhold: New York, 1964; p 113.
(23) Timmermans, J. "Physico-Chemical Constants of Binary Systems"; Interscience: New York, 1960; Vol. 4, p 21.
(24) Buttery, R. G.; Guadagni, D. G.; Okano, S. *J. Sci. Food Agric.* **1965**, *16*, 691–692.
(25) Ekwall, P. "Advances in Liqid Crystals"; Brown, G. H., Ed.; Academic Pres: New York, 1975; Vol. 1, p 117.
(26) Saito, H.; Friberg, S. "Foams", Akers, R. J., Ed.; Academic Press: New York, 1976; pp 33–38.
(27) Mukerjee, P.; Mysels, K. J. "Critical Micelle Concentrations of Aqueous Surfactant Systems"; U.S. National Bureau of Standards: Washington, DC, 1971; NSRDS-NBS 36.

Received for review October 20, 1982. Revised manuscript received May 5, 1983. Accepted September 6, 1983. This work was made possible through a grant from the Swedish Board for Technical Development.

Environ. Sci. Technol. 1984, 18, 231–234

Comparison of Solvent Extraction and Thermal–Optical Carbon Analysis Methods: Application to Diesel Vehicle Exhaust Aerosol

Steven M. Japar,* Ann C. Szkarlat, and Robert A. Gorse, Jr.

Research Staff, Ford Motor Company, Dearborn, Michigan 48121

Emily K. Heyerdahl, Richard L. Johnson, John A. Rau, and James J. Huntzicker*

Department of Environmental Science, Oregon Graduate Center, Beaverton, Oregon 97006

■ Filter samples of particulate emissions from two diesel automobiles were analyzed by solvent extraction with a hot toluene/1-propanol mixture, by thermal–optical carbon analysis, and by X-ray fluorescence analysis. On the average, carbon accounted for 83% of the particulate matter, and organic carbon comprised 70% of the extractable mass. The ratio of elemental carbon as measured by the thermal–optical technique to unextractable mass was 1.05 ± 0.04. For most of the filters the unextractable mass was predominantly elemental carbon. However, for the filters with the largest amounts of unextracted material the elements Fe, S, Al, Si, and Ca were present in significant amounts (0.3–5% each of the unextractable mass when expressed as oxides).

Introduction

It has become apparent in recent years that carbonaceous aerosols play an important role in the chemistry and physics of the atmosphere. Carbonaceous aerosols have been implicated in the problem of climate modification (submicron elemental carbon particles can change the radiative transfer properties of the atmosphere), potential health effects (a number of particle-bound organic compounds found in the atmosphere are known mutagens), and visibility reduction (elemental carbon is an efficient light absorber, and both organic and elemental carbon aerosols scatter light). Because of this, a number of efforts have been made to develop rapid and simple analytical methods to determine the elemental, organic, and total carbon content of aerosols. These techniques include solvent extraction (*1–7*), thermal combustion (*8–13*), optical methods (*14–21*), and acid digestion (*22–24*).

Comparisons of several of the analytical techniques have been reported by Cadle and Groblicki (*6*) and Stevens et al. (*25*). Cadle and Groblicki (*6*) note that each of the analytical techniques defines organic and elemental carbon in an operational manner; i.e., there is no accepted, standard analytical definition of organic and elemental carbon. Consequently, it is of interest to compare independent analytical methods for the determination of organic and elemental carbon. This report presents the results of such a comparison between a solvent extraction method (*1*) and a thermal–optical technique (*8, 9*) on samples of diesel vehicle exhaust aerosol.

Experimental Section

Diesel vehicle exhaust particulate samples were collected on a chassis dynamometer/dilution tube facility (*26*). The vehicles, a 1979 2.3-L Opel and a 1980 2.3-L Peugeot, were run, using no. 2 diesel fuel, over a series of cruises between 20 mph and 60 mph, as well as over a portion of the Federal Test Procedure (FTP), a test cycle which includes idles, cruises, and hard accelerations to speeds in excess of 50 mph.

Samples were collected on two different filters simultaneously: 47-mm Teflon-backed Teflon membrane filters (1.0 μm pore size "Zefluor", Ghia Corp.) were used to collect samples for solvent extraction, mass measurement, and X-ray fluorescence analysis while 47-mm glass fiber filters (type AE, Gelman Corp.) were used to collect samples for carbon analysis. It has been found on the basis of a large number of vehicle tests that both filters are equally efficient in the collection of submicron aerosol emitted from diesel vehicles. The Teflon filters were used for the solvent extraction and mass measurements because they minimize artifact formation due to sorption of gaseous oxides of nitrogen and sulfur.

Solvent Extractions. The organic-soluble fraction of the particulate emissions was determined by 20-h Soxhlet extractions of the Teflon filter samples in 1:1 (v/v) mixtures of toluene/1-propanol. This solvent system is highly efficient for the removal of adsorbed organic material from diesel particulate material (*1*). To minimize loss of particulate material during the extractions, the sample filters were wrapped in a second Teflon filter. The extractable mass was determined by the difference in the two-filter weight before and after extraction.

X-ray Fluorescence Analysis. Several of the Teflon filters which had been extracted were subjected to energy dispersive X-ray fluorescence analysis using an ORTEC-TEFA instrument. Concentrations of Fe, Zn, Pb, Al, Si, S, and Ca were determined. The results were only semiquantitative, however, because the solvent extraction procedures produced both a nonuniform deposit of particulate material on the filter and wrinkled filters. The latter effect resulted in a nonuniform distribution of distances between the X-ray source and filter and between the X-ray detector and filter.

Thermal–Optical Carbon Analysis. The thermal–optical carbon analyzer (*8, 9*) is unique among thermal methods in that it explicitly corrects for the pyrolytic conversion of organic to elemental carbon (i.e., carbonization) which occurs during the organic analysis step in most thermal methods. In the thermal–optical approach a single glass fiber filter disk (0.25 cm^2 in area) was placed in a quartz boat in the cool end of the analyzer. After purging with He, the boat was inserted into the volatilization oven in which the initial temperature was 350 °C. Organic carbon that volatilized under these conditions flowed through a MnO_2 bed at 1000 °C where it was oxidized to CO_2. (For some analyses this step was conducted in a 2% O_2–98% He atmosphere. Continuous monitoring of the filter reflectance as described below indicated no oxidation of elemental carbon under these conditions.) The CO_2 was subsequently reduced to CH_4 and measured with a flame ionization detector. Further volatilization and measurement of the remaining organic carbon were achieved at 600 °C. Elemental carbon was analyzed by lowering the temperature to 400 °C, changing the atmosphere to 2% O_2–98% He, and measuring the amount of

0013-936X/84/0918-0231$01.50/0

Table I. Chemical Analysis of Vehicle Particulate Emissions[a]

run	vehicle	condition[c]	mass, μg/cm²			carbon, μg of C/cm²		
			total[b]	unextr.	extract.	total	elemental	organic
1	2.3-L	FTP	296.7	164.2	132.5	253	181	72
2	Opel	C-50	497.6	156.9	340.7	428	156	272
3		C-30	300.0	109.8	190.2	202	115	87
4		C-50	491.9	111.4	380.5	393	132	262
5		C-50	221.1	87.0	134.1	175	96	79
6		C-30	200.0	82.9	117.1	149	90	59
7		C-40	213.0	78.9	134.1	154	86	68
8		FTP	203.3	161.8	41.5	196	170	26
9		FTP	281.3	230.9	50.4	232	193	39
10		C-20	281.3	106.5	174.8	236	110	126
11		C-40	253.7	97.6	156.1	207	94	113
12		C-50	246.3	79.7	166.6	192	77	116
13		C-30	235.8	100.8	135.0	187	88	99
14		FTP	502.4	387.8	114.6	392	310	81
15		C-50	240.7	118.7	122.0	202	106	96
16		FTP	296.7	248.8	47.9	241	204	37
17		C-30	269.1	102.4	166.7	196	98	98
18		C-50	226.8	64.2	162.6	194	76	119
19		C-40	195.1	89.4	105.7	159	89	70
20		C-50	284.6	117.9	166.7	260	130	130
21		C-40	354.4	135.0	219.4	297	141	156
22		C-30	266.7	108.1	158.6	218	102	116
23		C-50	321.1	89.4	231.7	279	91	187
24		FTP	244.7	204.1	40.6			
25	2.3-L	FTP	125.2	76.4	48.8	153	97	56
26	Peugeot	C-40	321.1	131.7	189.4	271	128	143
27		C-50	386.2	111.4	274.8	343	138	205
28		FTP	97.1	48.0	49.1			
29		C-50	314.6	119.5	195.1	283	131	152
30		C-45	515.4	185.4	330.0	414	166	248
31		C-50	340.7	113.0	227.7	320	140	180
32		C-60	346.3	98.4	247.9	263	103	160
33		FTP	99.2	61.8	37.4	78	53	25

[a] Carbon concentrations are rounded to the nearest whole number. [b] Average area of deposition of the filters is 12.3 cm². For #28 the area is 10.2 cm². [c] FTP is a 505-second cycle including accelerations to 50 mph. C-50 is a 50 mph cruise.

CO_2 evolved at 400, 500, and 600 °C.

To correct for the pyrolytic conversion of organic to elemental carbon the filter reflectance was continuously monitored with a He–Ne laser (633 nm). The amount of elemental carbon combustion necessary to return the filter reflectance to its original value (i.e., before pyrolytic production of elemental carbon occurred) was taken to be the correction. The three-step elemental carbon combustion process permitted adequate resolution of the point when the filter reflectance returned to its original value. For the 56 measurements (including replicates) the average correction amounted to 3 ± 3% (1σ) of the total carbon on the filter. This is considerably less than usually observed for ambient air filters (*9*).

To assess the accuracy of the carbon analysis procedure for total carbon, known amounts of sucrose were deposited on filter disks and analyzed. The average ratio of measured to expected carbon was 1.01 ± 0.04 (95% confidence interval).

Results and Discussion

The results are presented in Table I in terms of mass (μg) or carbon (μg of C) loading per centimeter squared of filter. Replicate carbon analysis (two to five per sample) was performed on 13 filters. From these results the following analytical precisions (±1 standard deviation, n = 38) were determined by analysis of variance: organic carbon (OC), ±16%; elemental carbon (EC), ±5.4%; total carbon (TC = OC + EC), ±4.0%; OC/TC and EC/TC, ±0.027. The large uncertainty in organic carbon was caused by the three filters (numbers 9, 14, and 16) with the highest concentrations of elemental carbon (193, 310, and 204 μg of C/cm², respectively). For these filters small fractional uncertainties in elemental carbon due to uncertainties in the speciation between organic and elemental carbon resulted in large fractional uncertainties for organic carbon, which was the minor species for all three filters. When these filters were removed from the analysis of variance, the uncertainty for organic carbon dropped to ±7.1% while the uncertainties for elemental carbon, total carbon, OC/TC, and EC/TC remained essentially unchanged.

It is apparent from Table I that the nature of the particulate emissions is dependent on the vehicle operating conditions. For the Opel the extractable fraction of the total mass was 23 ± 4% for FTP's and 63 ± 2% for cruises where the uncertainties correspond to one standard error of the mean. For the Peugeot FTP runs the extractable mass was 42 ± 4% of the total and for cruises 66 ± 2%. These can be compared with the on-road vehicle results of Szkarlat and Japar (*27*) in the 1981 Allegheny Tunnel experiment in which extractable mass was 24% of the total mass associated with diesel vehicles (primarily trucks). For the FTP runs organic carbon comprised 19 ± 2% of total carbon for the Opel and 34 ± 2% for the Peugeot and for the cruise runs 53 ± 2% for the Opel and 58 ± 2% for the Peugeot. For all runs carbon (i.e., organic plus elemental) constituted 83 ± 2% of total mass. This is in good agreement with the results of Pierson and Brachaczek (*28*) for the 1977 Tuscarora Tunnel experiment (84% carbon) and with the results of Szkarlat and Japar (*27*) for the 1981 Allegheny Tunnel experiment (76%).

Elemental Carbon/Unextractable Mass Relationships. In comparing the results of the carbon analyses and

Table II. Statistical Analysis of Elemental Carbon (EC)/Unextractable (UEM) Data[a]

data set	$\overline{(EC/UEM)}$	EC = a(UEM) + b		
		a	b	r
(1) all filters	1.03 ± 0.06	0.74 ± 0.04	32 ± 5	0.96
(2) delete 14	1.03 ± 0.04	0.78 ± 0.05	9 ± 8	0.94
(3) delete 9, 14, and 16	1.05 ± 0.04	0.96 ± 0.07	9 ± 8	0.93
(4) delete 9, 14, 16, and 30	1.05 ± 0.04	1.05 ± 0.08	0.4 ± 9	0.93
(5) delete 9, 14, 16, 30, 1, and 8	1.05 ± 0.04	1.00 ± 0.10	5 ± 10	0.90
(6) delete 9, 14, 16, 30, 1, 8, and 2	1.05 ± 0.04	1.04 ± 0.12	1 ± 12	0.88

[a] Uncertainties in $\overline{(EC/UEM)}$ correspond to 95% confidence intervals for the mean and in the regression coefficients to one standard error. r is the linear correlation coefficient.

Table III. Elemental Concentrations ($\mu g/cm^2$) on Extracted Filters[a]

element	filter				
	14	15	16	30	31
Fe	9.7	0.45	9.0	0.14	0.14
Zn	0.50	0.23	0.34	0.20	0.10
Pb	1.0	1.2	0.87	0.10	0.04
Al	1.6	0.10	1.6	0.09	0.00
Si	3.0	0.38	3.3	0.26	0.21
S	3.4	0.86	2.4	0.52	0.23
Ca	2.8	0.35	1.8	0.15	0.16
total	22	3.6	19	1.5	0.88
total as oxides[b]	38	6.2	34	2.9	2.8
unextracted mass − elemental carbon	78 ± 17	13 ± 6	45 ± 11	19 ± 9	(−27 ± 8)

[a] The uncertainties in (unextracted mass − elemental carbon) were taken to be the 5.4% uncertainty in elemental carbon. [b] Assumed to be Fe_2O_3, ZnO, PbO, Al_2O_3, SiO_2, SO_4^{2-}, and CaO.

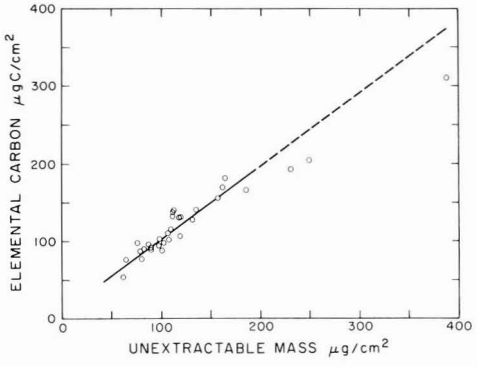

Figure 1. Relation between elemental carbon (thermal–optical method) and unextractable mass. The solid line corresponds to the regression relation of data set 3 in Table II which excludes filters 14, 16, and 9, the three points with the largest unextractable mass listed in descending order. The dashed line is an extrapolation of the solid line.

the extractions it can be assumed that the unextractable mass on the filter represents an upper limit to the mass of the elemental carbon determined by combustion. Deviations from a 1:1 relationship between the two values would be expected if a significant fraction of the emissions were unextractable organic or inorganic material, i.e., (elemental carbon)/(residual mass) < 1.

To investigate the relationship between elemental carbon and unextractable mass, the data were subjected to statistical analysis. As shown in Table II the average ratio of elemental carbon to unextractable mass was 1.03 ± 0.06 (±95% confidence interval) for all filters. Least-squares regression analysis, however, gave a slope of only 0.74. Further investigation revealed that the deviation from unit slope was strongly influenced by the three filters with the largest unextractable mass concentrations (filters 9, 14 and 16). When these three points were removed, the regression slope (data set 3) approached unity, and the average ratio of elemental carbon to unextractable mass increased slightly to 1.05 ± 0.04 (±95% confidence interval). Further removal of the high concentration runs produced only small changes in the regression coefficients and the average ratio. The elemental carbon/unextractable mass results are plotted in Figure 1 in which the solid line represents the regression results of data set 3 in Table II.

To investigate the large differences between unextractable mass and elemental carbon for filters 9, 14, and 16, a selected group of filters (14, 15, 16, 30, and 31) was analyzed for elemental content by X-ray fluorescence analysis. The results of the analysis are given in Table III. Filters 14 and 16 are clearly distinguished from filters 15, 30, and 31 by the concentrations of Fe, Al, Si, S, and Ca. When the elemental concentrations are expressed as oxides, the totals for filters 14 and 16 account for a significant share of the difference between elemental carbon and unextractable mass for these two filters. The sources of the major elements were not determined although it is likely that S originated from the fuel, Fe, Si, and Al from the exhaust train during the accelerations in the FTP cycle, and Ca from the motor oil (28). In experiments prior to the one reported here, aluminum-coated particulate traps fabricated from cordierite (an aluminosilicate mineral) had been used in the exhaust trains, and it is probable that the Al and Si observed in this experiment resulted from debris

Table IV. Statistical Analysis of Organic Carbon (OC)/Extractable Mass (EM) Data[a]

data set	$\overline{(OC/EM)}$	OC = a(EM) + b		
		a	b	r
(1) all filters	0.70 ± 0.05	0.75 ± 0.03	−7.5 ± 6.4	0.97
(2) delete 14	0.70 ± 0.05	0.75 ± 0.03	−7.6 ± 6.6	0.97
(3) delete 9, 14, and 16	0.70 ± 0.05	0.76 ± 0.04	−10.4 ± 7.5	0.97
(4) delete 9, 14, 16, and 30	0.70 ± 0.05	0.76 ± 0.04	−9.6 ± 7.9	0.96
(5) delete 9, 14, 16, 30, 1, and 8	0.71 ± 0.05	0.75 ± 0.04	−7.3 ± 8.8	0.96

[a] Uncertainties in $\overline{(OC/EM)}$ correspond to 95% confidence intervals for the mean and in the regression coefficient to one standard error. r is the linear correlation coefficient.

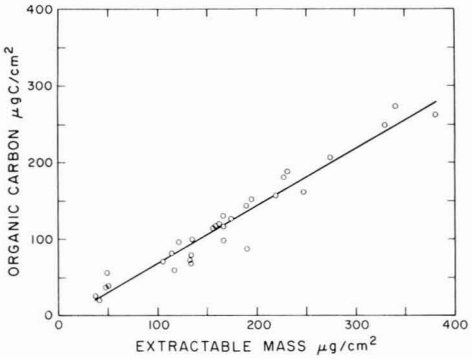

Figure 2. Relation between organic carbon (thermal–optical method) and extractable mass. The line corresponds to the regression relation of data set 1 in Table IV.

from the particulate traps which remained in the exhaust trains after the traps had been removed.

The slight excess of elemental carbon relative to unextracted mass (with filters 9, 14, and 16 excluded) could be due either to a systematic error in the carbon analysis speciation or to wash-off of elemental carbon particles from the Teflon filters during solvent extraction. Although the solvent extraction procedure was designed to minimize such wash-off, such a possibility cannot be excluded. The results of Johnson (*29*) suggested that wash-off of elemental carbon particles from fibrous filters occurred during extraction with a mixture of polar and nonpolar solvents.

Organic Carbon/Extractable Mass Relationships. Statistical analysis of the organic carbon/extractable mass data was also performed, and the results are given in Table IV and plotted in Figure 2. In contrast to the elemental carbon/unextractable mass relationship the organic carbon/extractable mass regressions are invariant with respect to the selective removal of various runs and, in particular, the removal of filters 9, 14, and 16. The slope of the regression line was 0.75, and the average ratio of organic carbon to extractable mass was 0.70 ± 0.05 (±95% confidence interval). Such a ratio is not unreasonable in view of other vehicle emission studies (*27*) and is due to the presence of both oxygenated organic compounds and (possibly) inorganic sulfates in the extracted mass.

Conclusion

Elemental carbon concentrations as determined by the thermal–optical carbon analysis procedure (*2*, *3*) were compared with the mass of material left on the filter after extraction with a hot toluene/1-propanol mixture. As a working hypothesis this residual mass was taken to be an upper limit to the concentration of elemental carbon on the filter. With the exception of the three most heavily loaded samples which were obtained under FTP conditions, the average ratio of elemental carbon to unextracted mass was 1.05 ± 0.04 (±95% confidence interval), and the slope of the regression line was 1.05. Thus, for most of the filters the unextractable mass was predominantly elemental carbon.

Acknowledgments

We thank Richard DeCesar of the Oregon Graduate Center for performing the X-ray fluorescence analysis.

Registry No. C, 7440-44-0; toluene, 108-88-3; 1-propanol, 71-23-8.

Literature Cited

(1) Schuetzle, D.; Lee, F. S.-C. In "Informational Report of the Measurement and Characteristics of Diesel Exhaust Emissions"; Perez, J. M.; Hill, F. J.; Schuetzle, D.; Williams, R. L., Eds.; Coordinating Research Council, 1980, Report No. 516.
(2) Pierson, W. R.; Russell, P. A. *Atmos. Environ.* **1979**, *13*, 1623–1628.
(3) Grosjean, D. *Anal. Chem.* **1975**, *47*, 797–805.
(4) Appel, B. R.; Colodny, P.; Wesolowski, J. J. *Environ. Sci. Technol.* **1976**, *10*, 359–363.
(5) Appel, B. R.; Hoffer, E. M.; Kothny, E. L.; Wall, S. M.; Haik, M.; Knights, R. L. *Environ. Sci. Technol.* **1979**, *13*, 98–104.
(6) Cadle, S. H.; Groblicki, P. J. In "Particulate Carbon: Atmospheric Life Cycle"; Wolff, G. T.; Klimisch, R. L., Eds.; Plenum Press: New York, 1982; pp 89–109.
(7) Daisey, J. M.; Leyko, M. A.; Kleinman, M. T.; Hoffman, E. *Ann. N.Y. Acad. Sci.* **1979**, *322*, 125–141.
(8) Johnson, R. L.; Shah, J. J.; Cary, R. A.; Huntzicker, J. J. In "Atmospheric Aerosol: Source/Air Quality Relationships"; Macias, E. S.; Hopke, P. K., Eds.; American Chemical Society: Washington, DC, 1981; ACS Symp. Ser. No. 167, pp 223–233.
(9) Huntzicker, J. J.; Johnson, R. L.; Shah, J. J.; Cary, R. A. In "Particulate Carbon: Atmospheric Life Cycle"; Wolff, G. T.; Klimisch, R. L., Eds.; Plenum Press: New York, 1982.
(10) Mueller, P. K.; Fung, K. K.; Heisler, S. L.; Grosjean, D.; Hidy, G. M. In "Particulate Carbon: Atmospheric Life Cycle"; Wolff, G. T.; Klimisch, R. L., Eds.; Plenum Press: New York, 1982, pp 343–370.
(11) Cadle, S. H.; Groblicki, P. J.; Stroup, D. P. *Anal. Chem.* **1980**, *52*, 2201–2206.
(12) Tanner, R. L.; Gaffney, J. S.; Phillips, M. F. *Anal. Chem.* **1982**, *54*, 1627–1630.
(13) Ellis, E. C.; Novakov, T. *Sci. Total Environ.* **1982**, *23*, 227–238.
(14) Lin, C.-I.; Baker, M.; Charlson, R. J. *Appl. Opt.* **1973**, *12*, 1356–1363.
(15) Delumyea, R. G.; Chu, L.-C.; Macias, E. S. *Atmos. Environ.* **1980**, *14*, 647–652.
(16) Japar, S. M.; Killinger, D. K. *Chem. Phys. Lett.* **1979**, *66*, 207–209.
(17) Japar, S. M.; Szkarlat, A. C. *Trans. Soc. Automot. Eng.* **1981**, *90*, 3624–3631.
(18) Roessler, D. M.; Faxvog, F. R. *J. Opt. Soc. Am.* **1979**, *69*, 1699–1702.
(19) Pleil, J. D.; Russworm, G. M.; McClenny, W. A. *Appl. Opt.* **1982**, *21*, 133–135.
(20) Rosen, H.; Hansen, A. D. A.; Dod, R. L.; Novakov, T. *Science (Washington, D.C.)* **1980**, *208*, 741–744.
(21) Heintzenberg, J. *Atmos. Environ.* **1982**, *16*, 2461–2469.
(22) McCarthy, R.; Moore, C. E. *Anal. Chem.* **1952**, *24*, 411–412.
(23) Kukreja, V. P.; Bove, J. L. *Environ. Sci. Technol.* **1976**, *10*, 187–189.
(24) Pimenta, J. A.; Wood, G. R. *Environ. Sci. Technol.* **1980**, *14*, 556–561.
(25) Stevens, R. K.; McClenny, W. A.; Dzubay, T. G.; Mason, M. A.; Courtney, W. J. In "Particulate Carbon: Atmospheric Life Cycle"; Wolff, G. T.; Klimisch, R. L., Eds.; Plenum Press: New York, 1982; pp 111–129.
(26) McKee, D. E.; Ferris, F. C.; Goeboro, R. E. Society of Automotive Engineers, 1978, Paper No. 780592.
(27) Szkarlat, A. C.; Japar, S. M. *J. Air Pollut. Control Assoc.* **1983**, *33*, 592–597.
(28) Pierson, W. R.; Brachaczek, W. W. *Aerosol Sci. Technol.* **1983**, *2*, 1–40.
(29) Johnson, R. L. M.S. Thesis, Oregon Graduate Center, 1981.

Received for review December 20, 1982. Revised manuscript received October 4, 1983. Accepted October 18, 1983.

All forward thinking environmental scientists depend on ES&T. They get the most authoritative technical and scientific information on environmental issues—and so can you! Have *your own* subscription delivered directly to you each month!

☐ **YES!** Enter my own subscription to *ENVIRONMENTAL SCIENCE & TECHNOLOGY* at the rate I've checked below: 1984

One Year Rates	U.S.	Foreign** (includes surface mail)
ACS Members—Personal*	☐ $ 22	☐ $ 30
Nonmembers—Personal*	☐ $ 25	☐ $ 33
Nonmembers—Institutions	☐ $121	☐ $129

☐ Payment Enclosed (Payable to American Chemical Society)
☐ Bill Me ☐ Bill Company Charge my: ☐ Mastercard ☐ VISA

Card #_____ Exp. Date_____

Interbank #_____ (MasterCard Only) Signature_____

or CALL TOLL FREE (800) 424-6747 (new orders)

Name_____

Employer_____ Job Title_____

Address_____

City_____ State_____ Zip_____

Employer's Business: ☐ Manufacturing Type of Products_____

☐ Academic ☐ Government ☐ Other_____

*Subscriptions at these rates are for personal use only.
**Payment must be made in U.S. currency by international money order, UNESCO coupons, U.S. bank draft, or order through your subscription agency. For nonmember subscription rates in Japan, contact Maruzen Co., Ltd.
Please allow 45 days for your first copy to be mailed. Redeem until December 31, 1984.

MAIL THIS POSTAGE-PAID CARD TODAY!

680 2507X

All forward thinking environmental scientists depend on ES&T. They get the most authoritative technical and scientific information on environmental issues—and so can you! Have *your own* subscription delivered directly to you each month!

☐ **YES!** Enter my own subscription to *ENVIRONMENTAL SCIENCE & TECHNOLOGY* at the rate I've checked below: 1984

One Year Rates	U.S.	Foreign** (includes surface mail)
ACS Members—Personal*	☐ $ 22	☐ $ 30
Nonmembers—Personal*	☐ $ 25	☐ $ 33
Nonmembers—Institutions	☐ $121	☐ $129

☐ Payment Enclosed (Payable to American Chemical Society)
☐ Bill Me ☐ Bill Company Charge my: ☐ Mastercard ☐ VISA

Card #_____ Exp. Date_____

Interbank #_____ (MasterCard Only) Signature_____

or CALL TOLL FREE (800) 424-6747 (new orders)

Name_____

Employer_____ Job Title_____

Address_____

City_____ State_____ Zip_____

Employer's Business: ☐ Manufacturing Type of Products_____

☐ Academic ☐ Government ☐ Other_____

*Subscriptions at these rates are for personal use only.
**Payment must be made in U.S. currency by international money order, UNESCO coupons, U.S. bank draft, or order through your subscription agency. For nonmember subscription rates in Japan, contact Maruzen Co., Ltd.
Please allow 45 days for your first copy to be mailed. Redeem until December 31, 1984.

MAIL THIS POSTAGE-PAID CARD TODAY!

680 2507X

NO POSTAGE
NECESSARY
IF MAILED
IN THE
UNITED STATES

BUSINESS REPLY CARD

FIRST CLASS PERMIT NO. 10094 WASHINGTON, D.C.

POSTAGE WILL BE PAID BY ADDRESSEE

American Chemical Society
Circulation Dept.
1155 Sixteenth Street, N.W.
Washington, D.C. 20036

NO POSTAGE
NECESSARY
IF MAILED
IN THE
UNITED STATES

BUSINESS REPLY CARD

FIRST CLASS PERMIT NO. 10094 WASHINGTON, D.C.

POSTAGE WILL BE PAID BY ADDRESSEE

American Chemical Society
Circulation Dept.
1155 Sixteenth Street, N.W.
Washington, D.C. 20036

Environ. Sci. Technol. 1984, 18, 235–241

Acetone-Sensitized and Nonsensitized Photolyses of Tetra-, Penta-, and Hexachlorobenzenes in Acetonitrile–Water Mixtures: Photoisomerization and Formation of Several Products Including Polychlorobiphenyls†

Ghulam Ghaus Choudhry‡ and Otto Hutzinger*

Laboratory of Environmental and Toxicological Chemistry, University of Amsterdam, 1018 WV Amsterdam, The Netherlands

■ Photochemical reactions of tetra-, penta-, and hexachlorobenzenes in the presence and absence of acetone as sensitizer at wavelengths ≥ 285 nm have been studied. The reductive dechlorination is the main photochemical pathway in both sensitized and nonsensitized photolyses. 1,2,4-Trichlorobenzene appears as the main photoproduct of the nonsensitized photolyses of 1,2,3,5-tetrachlorobenzene, while the major photoproduct of the sensitized irradiation of this substrate is 1,3,5-trichlorobenzene. The nonsensitized photoreactions of tetrachlorobenzenes yield photoisomerized chlorobenzenes and also give product chlorobenzenes containing more chlorine atoms than the starting material. Yields of up to several percent of polychlorobiphenyls (PCBs) are obtained in the case of sensitized irradiation of tetra- and pentachlorobenzenes, but this reaction is less significant in the case of direct photolysis.

Introduction

Polychlorobenzenes (PCBzs) are utilized on industrial scale (*1–5*). PCBzs have also been identified in the emissions from some municipal and industrial incinerators, e.g. (*6–8*), as well as in various water bodies (*9*). Moreover, acetone occurs in natural waters (*10*). Therefore, it is likely that in our environment aquatic systems contaminated with PCBzs also contain acetone.

Several reports on the studies of monochlorobenzene photolysis have been seen in the literature (*11, 12*). Parlar, Korte, and their co-workers have reported the solution phase photochemical ($\lambda \leq 254$ nm) reductive dechlorination of *o*-, *m*-, and *p*-dichlorobenzenes (*13, 14*) and their derivatives (*13–15*) containing one substituent such as CH_3, CH_2OH, OH, OCH_3, CHO, NH_2, NO_2, CN, and Ph. Choudhry et al. (*16*) have demonstrated the reductive dechlorination, isomerization, and formation of polychlorobiphenyls (PCBs) by exposing solutions of trichlorobenzenes in methanol and acetonitrile–water mixture with radiation of $\lambda \geq 285$ nm. The photoreduction of pentachlorobenzene in organic solvents like hexane, cyclohexane, acetone, and 95% ethanol by utilizing ultraviolet (UV) light of $\lambda = 253.7$ nm has been performed by Crosby and Hamadmad (*5*). Plimmer and Klingebiel (*4*) reported the reductive dechlorination of hexachlorobenzene in methanol and hexane carried out by light of wavelengths greater than 260 and 220 nm, respectively. Furthermore, Uyeta and his co-workers (*17*) have shown the photoformation of PCBs by irradiating neat mono-, di-, tri-, tetra- (except the 1,2,3,5-isomer), and hexachlorobenzenes by sunlight.

In view of our interest in the photochemical fate of halogenated pollutants (*16, 18*) we decided to further investigate the photochemistry of PCBzs possessing four, five, and six chlorine substituents. The present paper deals with acetone-sensitized and nonsensitized photochemistry of the three tetrachlorobenzenes, pentachlorobenzene, and hexachlorobenzene in different acetonitrile–water mixtures utilizing radiation of wavelengths ≥ 285 nm.

Experimental Section

Substrates and Standards. The substrate (**5**) and standard trichlorobenzenes (**7**) were supplied by Chemical Service, Inc., West Chester, and Koninklijke/Shell-Laboratorium, Amsterdam, respectively. All other compounds were purchased from Aldrich.

Solvents. Sources are described elsewhere (*18*).

Preparation of Solutions. Stock solution of a substrate was prepared with acetonitrile as solvent. To a portion of the stock solution was added water drop by drop with continuous manual shaking, until the required concentration of the substrate, i.e., ca. 1 mM/L, was achieved. In this manner, sample solutions of all substrates (compounds **1–5**) in water–acetonitrile using the maximum volume of water were made. For both types of photolysis, the ratios of acetonitrile–water used for the preparation of solutions were as follows: 1:1 (v/v) for PCBzs **1** and **2**; 6:4 (v/v) for PCBzs **3** and **4**; 9:1 for hexachlorobenzene (**5**). In the case of acetone sensitized irradiations (Table I), concentrations of substrates **1–5** were 1.204, 1.065, 1.112, 1.119, and 1.194 mM/L, respectively, while each solution contained 0.553 M/L acetone. For the direct photolyses (Table II), concentrations of tetrachlorobenzenes **1–3** were 1.112 mM/L, whereas those of penta- and hexachlorobenzene (**4** and **5**) were 1.119 and 1.194 mM/L, respectively.

Irradiation Equipment and Experiments. Detailed descriptions of irradiation equipment and experiments are given in ref 18. Irradiation times in the case of acetone-sensitized photoreactions of substrates **1**, **3**, and **4** were 4 h, while such sample solutions of substrates **2** and **5** were irradiated for 1.5 and 16 h, respectively. In the case of nonsensitized reactions, sample solutions of substrates **1**, **2**, and **4** were irradiated for 40, 36, and 24 h, respectively, while irradiation times for substrates **3** and **5** were 8 h.

Extraction Procedures. One milliliter of hexane each was added to photolyzed samples. After the samples were well shaken, the hexane layer was separated from the water–acetonitrile layer. A few drops of *n*-nonane were added to the hexane solution which was then reduced in volume to approximately 0.2 mL by using a rotary evaporator. The same procedure was also followed for unphotolyzed samples. *n*-Nonane was added to prevent loss of volatile compounds.

Gas Chromatography. Two types of GCs were used. Qualitative and quantitative analyses of the photolysates were carried out on a Hewlett-Packard 5830A instrument with a flame ionization detector equipped with an 18850 GC terminal. The following three types of columns and GC conditions on this gas chromatograph were used:

* Address correspondence to this author at the Chair of Ecological Chemistry and Geochemistry, University of Bayreuth, D-8580 Bayreuth, West Germany.

† This article is part 3 of the series "Photochemistry of Halogenated Benzene Derivatives". For part 2, see ref 18.

‡ Present address: Pesticide Research Laboratory, Department of Soil Science, The University of Manitoba, Winnipeg, Manitoba, Canada R3T 2N2.

0013-936X/84/0918-0235$01.50/0

column A, glass column (2 m × 0.2 cm) containing 5% Carbowax 20 M on 160–180 mesh Chromosorb WAW, temperature 1 (T_1) = 70 °C, time 1 (t_1) = 2 min, rate 8 °C/min, temperature 2 (T_2) = 240 °C, time 2 (t_2) = 30 min, carrier gas (N_2) flow = 24 mL/min, injection temperature = 260 °C, and FID temperature = 300 °C; column B, glass column (3 m × 0.2 cm) containing 10% Carbowax 20 M on 160–180 mesh Chromosorb WAW, T_1 = 80 °C, t_1 = 20 min, rate 8 °C/min, T_2 = 240 °C, t_2 = 40 min, carrier gas (N_2) flow = 18 mL/min, injection temperature = 260 °C, and FID temperature = 300 °C; column C, glass column (1.90 m × 0.2 cm) containing 3% Silicone OV 101 on 150–160 mesh Chromosorb WAW, T_1 = 80 °C, t_1 = 2 min, rate 8 °C/min, T_2 = 240 °C, t_2 = 40 min, carrier gas (N_2) flow = 25 mL/min, injection temperature = 260 °C, and FID temperature = 300 °C.

Photolyzed samples containing water were directly injected into column A for the determination of the disappearance of starting material and chlorobenzenes appearing as photoproducts. Column B was used for the quantitative analyses of the hexane extracts of photolysates, which contained 1,2,3,5- and 1,2,4,5-Cl_4-Bz (**2** and **3**, respectively). The Cl_4-Bz **2** and **3** were only partly resolvable on column B; the retention time of both compounds differed by 0.20 min. Quantitative analyses of the PCBs formed during the photolyses of substrates **1**–**4** were carried out on column C by injecting hexane extract of the corresponding photolysate. Chemical yields of photoproducts such as PCBzs and PCBs were calculated from the amount of photoconverted starting material. For the determination of yields of PCBzs, appropriate standard solutions of authentic chlorobenzenes were used, while for those of PCBs, the amount of undecomposed starting material present in a photolysate was utilized as internal standard. Polychlorobiphenyls from nonsensitized photolysates (Table II) were detected on a Packard 428 gas chromatograph utilized with a ^{63}Ni electron detector (ECD) and a capillary injection system according to Grob and Grob (*19*).

The fused silica capillary column (25 m × 0.25 mm i.d.) was coated with CP-SIL 7, film thickness being 0.4 μm (Chrompack). The pressure of the carrier gas (N_2) at the inlet of the column was 0.9 atm, the gas flow in the column being ca. 1–2 mL/min. The other GC conditions were the following: T_1 = 40 °C, t_1 = 4 min, rate = 39 °C/min, T_2 = 240 °C, t_2 = 40 min, injector temperature = 250 °C, and ECD temperature = 300 °C. Two minutes after injection the splitter was opened manually to flush the injector. The splitter was kept closed manually for 2 min before injecting each sample.

Gas Chromatography–Mass Spectrometry. Qualitative analysis was conducted on a Hewlett-Packard 5894 A mass spectrometer operating in the electron-impact mode at 70 eV. For the identifications of chlorobenzenes, especially di- and trichlorobenzenes present in a photolyzed sample, previously described (*18*) glass column and operating conditions were utilized.

Although some other photoproducts like PCBs could be identified on the above-mentioned column (0.2% Carbowax 20M (*18*), all photoproducts (except Cl_2-Bzs and some Cl_3-Bzs) (documented in Tables I and II) were qualitatively recognized on the GC-MS equipped with a fused silica capillary column (25 m × 0.25 mm i.d.), which was coated with CP-SIL 5, the film thickness being 0.4 μm (provided by Chrompack). The procedure of Grob and Grob (*19*) was followed for operating the capillary injection system. The GC conditions for this capillary system were the following: T_1 = 70 °C, t_1 = 0 min, and rates = 32 °C/min; after 2 min rate = 8 °C/min, T_2 = 300 °C, and t_2 = 30 min.

The mass (M) ranges were $100 \leq M \leq 500$. For the search of chlorine-containing photoproducts present in the total ion chromatogram (TIC) of a photolysate, the computer program for specific detection of organochlorine and organobromine compounds (*20*) was used (e.g., see Figure 1).

Identification of Photoproducts. Photoproducts like PCBzs were identified as mentioned previously (*18*). Because of unavailability of authentic standards, structures to all other photoproducts (Table I and II) were tentatively ascribed by interpreting their mass spectra.

Results

Acetone-Sensitized Photolysis. Results of irradiation of 1.1–1.2 mM/L solutions of 1,2,3,4-tetrachlorobenzene (1,2,3,4-Cl_4-Bz) (**1**), 1,2,3,5-Cl_4-Bz (**2**), 1,2,4,5-Cl_4-Bz (**3**), pentachlorobenzene (Cl_5-Bz) (**4**), and hexachlorobenzene (Cl_6-Bz) (**5**) in the presence of 0.553 M/L acetone as sensitizer at wavelengths (λ) ≥ 285 nm are recorded in Table I. Typical total ion chromatograms of the acetone-sensitized photolysates of the tetrachlorobenzenes (Cl_4-Bzs) (**1**–**3**) are shown in Figure 1. The peaks labeled with numbers represent the compounds which have been identified and are documented in Table I.

It is obvious from Table I that, as expected, the acetone-sensitized photolysis of the investigated chlorobenzenes leads mainly to reductive dechlorination. The usual reductively dechlorinated photoproducts of these substrates are chlorobenzenes containing one and two Cl atoms less than those of starting materials, the latter chlorobenzenes appearing as minor products. For example, tetrachlorobenzene **1** gives two trichlorobenzenes, 1,2,3-Cl_3-Bz (**6**) (9.2%) and 1,2,4-Cl_3-Bz (**7**) (32.6%) and two dichlorobenzenes, namely, 1,3-Cl_2-Bz (**10**) (5.2%) and 1,4-Cl_2-Bz (**11**) (1.5%), where the percentages in the parentheses represent the chemical yields of the corresponding product calculated on the basis of the amount of decomposed starting material. It is noteworthy that 49.3% of disappeared substrate **2** is photoconverted into 1,3,5-trichlorobenzene (**8**), the amount of which is approximately 10 times greater than those of the other two Cl_3-Bzs (**6** and **7**). Likewise, during the sensitized photoreaction of chlorobenzene **3**, in addition to trichlorobenzene **7** as principal product (25.3%), 1,3-Cl_2-Bz (**10**) appears in amounts about 2 times larger than that of 1,4-Cl_2-Bz (**11**), the yield of the latter dichlorobenzene amounting to 3.6%. In case of such photolysis of pentachlorobenzene (**4**), among the three Cl_4-Bzs, 1,2,3,5-Cl_4-Bz (**2**) is produced as chief product (52.8%), while the yield of the photoproduct 1,2,4-Cl_3-Bz (**7**) is about 3 times smaller than that of 1,3,5-Cl_3-Bz (**8**). Finally, 71% of the degraded hexachlorobenzene (**5**) undergoes photoconversion to pentachlorobenzene (**4**).

Table I and also Figure 1 clearly indicate that the photoreactions of these polychlorobenzenes (except Cl_6-Bz, **5**), sensitized by acetone provide considerable chemical yields of polychlorobiphenyls (PCBs). Compound **1** gives 2 heptachlorobiphenyls, most probably 2,2′,3,3′,4,4′,5-heptachlorobiphenyl (2,2′,3,3′,4,4′,5-Cl_7-BP) and 2,2′,3,3′,4,5,6′-Cl_7-BP (**12a** and **12b**; in Figure 1a) with a total chemical yield ($\sum$) of 3.74%, 10 hexachlorobiphenyls (10 Cl_6-BPs) (**13a**–**j**) ($\sum$ = ∼3.50%), and 5 pentachlorobiphenyls (**14a**–**e**) ($\sum$ = ∼0.87%), the yields being determined, as mentioned above, from the amount of the decomposed substrate. Similarly, tetrachlorobenzene **2** yields three heptachlorobiphenyls including 2,3,3′,4,4′,5′,6-Cl_7-BP, 2,2′,3,4,4′,6,6′-Cl_7-BP, and

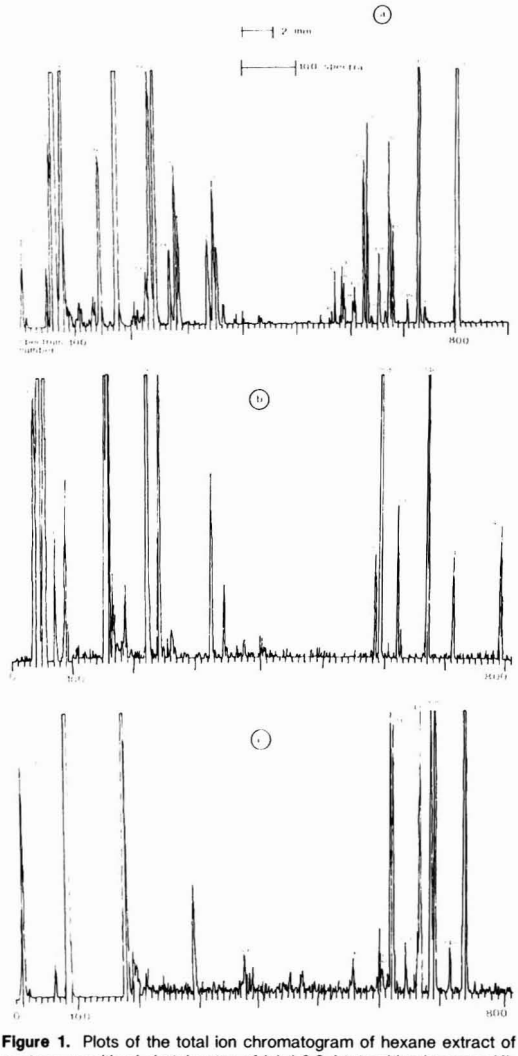

Figure 1. Plots of the total ion chromatogram of hexane extract of acetone-sensitized photolysates of (a) 1,2,3,4-tetrachlorobenzene (**1**), (b) 1,2,3,5-tetrachlorobenzene (**2**), and (c) 1,2,4,5-tetrachlorobenzene (**3**) subjected to the halogen test computer program (*20*) for searching chlorine-containing compounds. GC-MS equipped with a capillary column was used (see Experimental Section for further details).

2,2′,3,3′,4,5′,6-Cl_7-BP(**24a–c**) ($\sum$ = 7.01%), four Cl_6-BPs (**25a–d**) ($\sum$ = 4.69%), and a pentachlorobiphenyl (**26**) (0.64%). The sensitized irradiation of 1,2,4,5-Cl_4-Bz (**3**) results in the formation of 2,2′,3,4′,5,5′,6-Cl_7-BP (**33**) (4.19%), four Cl_6-BPs (**34a–d**) ($\sum$ = 6.78%), four Cl_5-BPs (**35a–d**) ($\sum$ = ca. 2.33%), and a tetrachlorobiphenyl (**36**) (0.32%). Three nonachlorobiphenyls (Cl_9-BPs), namely, 2,2′,3,3′,4,4′,5,6,6′-Cl_9-BP, 2,2′,3,3′,4,4′,5,5′,6-Cl_9-BP, and 2,2′,3,3′,4,5,5′,6,6′-Cl_9-BP (**40a–c**) of $\sum$ = 2.42%, along with a Cl_8-BP (**41**) (0.53%) and a Cl_7-BP (**42**) (0.49%) are formed in the case of sensitized photodegradation of pentachlorobenzene (**4**).

During acetone-sensitized photolyses of tetrachlorobenzenes **1–3** in H_2O–CH_3CN mixtures, no photoisomerized tetrachlorobenzenes are formed. However, in each case, photoisomerization leading to the production of chlorinated valence tautomers, possible valence-bond benzenes, has been noticed (see Table I and Figure 1). The status of the data does not permit us to decide whether these tautomers are benzvalene, Dewar, prismane, or (and) some other possible isomers. Thus, Table I indicates that a tetrachloro valence-bond benzene could be detected in the photolysates of **1** and **2** (see peaks 16 and 28 in Figure 1). Likewise, such irradiation of compounds **1–3** generates two, one, and one trichloro valence tautomers, respectively (peaks 15a,b, 27, and 37 in Figure 1).

In addition to the photoproducts described in the preceding paragraphs of this section, products like trichloroacetophenones and trichlorophenylacetonitriles are formed, when acetonitrile–water solutions of tetrachlorobenzenes **1–3** containing acetone as sensitizer are exposed to UV light. Moreover, in the case of substrates **1** and **2**, 1-(trichlorophenyl)-2-propanes (**23** and **31**, respectively) and unidentified compounds, viz., $C_8H_5Cl_2NO$ and C_8H_6ClNO (for **1** only) together with several other products are apparent (see Table I and Figure 1).

Finally, in order to detect polychlorophenols among the photoproducts, the sensitized photolysates of substrates **1–5** (given in Table I) were treated with the ethereal solution of diazomethane (CH_2N_2) and the ether plus acetonitrile layers were separated from the water layers. The concentrated organic extracts were analyzed on column A (see Experimental Section). Comparison of the retention times of both authentic standard and photoproducts gave evidence that either polychlorophenols are *not* formed during the acetone-sensitized irradiation of substrates **1–5** under the present circumstances or these phenols undergo further photoconversions.

Nonsensitized Photolysis. Again, reductively dechlorinated compounds appear as main products of nonsensitized irradiation of PCBzs (see Table II). For some substrates, distribution of such products is altered compared to that of acetone-sensitized photolysis. For instance, under these conditions, 1,2,4-trichlorobenzene (**7**) is produced as a major product of 1,2,3,5-Cl_4-Bz (**2**), showing a chemical yield (determined from the amount of disappeared starting material) of 24.3%. Furthermore, direct photolysis of chlorobenzenes **1–5** proceeds to yield reductively dechlorinated benzenes containing one and two chlorine atoms less than the starting materials. Such photoreactions of Cl_5-Bz (**4**) and Cl_6-Bz (**5**) produce this sort of products bearing even three Cl atoms less than the corresponding starting chlorobenzene. It is important to note that during direct photolyses of some substrates, especially 1,2,3,4-Cl_4-Bz (**1**) and Cl_5-Bz (**4**), photoproducts, e.g., 1,4-Cl_2-Bz (**11**) (from **1**) and 1,2,4-Cl_3-Bz (**7**) (from **4**) formed via losses of two Cl atoms are observed in large yields (30.4% and 12.7%, respectively) (see Table II). Finally, nonsensitized exposure of Cl_6-Bz (**5**) to UV light results in the generation of pentachlorobenzene (**4**) (76.8%) as principal product accompanied with the formation of 1,2,3,5-Cl_4-Bz (**2**) (1.2%), 1,2,4,5-Cl_4-Bz (**3**) (1.7%), and trichlorobenzene **7** (0.2%) in minor yields.

Contrary to acetone-sensitized photoreactions, in the case of nonsensitized irradiation of each isomer of tetrachlorobenzenes **1–3**, the process of photoisomerization with the eventual formation of isomerized Cl_4-Bzs also takes place. It can be seen from Table II that chlorobenzene **1** photoisomerizes to 1,2,3,5- and 1,2,4,5-Cl_4-Bz (**2, 3**), the chemical yields of which are 2.26 and 0.72%, respectively. Similarly, substrate **3** gives rise to the formation of two other isomers, namely, 1,2,3,4-Cl_4-Bz (**1**) (0.45%) and 1,2,3,5-Cl_4-Bz (**2**) (1.11%). However, during nonsensitized photolysis of the 1,2,3,5-tetrachlorobenzene (**2**), only one tetrachloro isomer, i.e., **1**, with a yield of 5.99%, could be detected as photoisomerized chlorobenzene. In addition

Table I. Acetone-Sensitized Photolysis of Polychlorobenzenes in Acetonitrile–Water Mixtures

no.	substrate, -chlorobenzene	disappearance of starting material, %	products[a] reductively dechlorinated,[b] %[d]	polychlorobiphenyls (PCBs),[c] %[d]	others
1	1,2,3,4-tetra-	78.4	1,2,3-Cl_3-Bz (**6**, 9.2); 1,2,4-Cl_3-Bz (**7**, 32.6); 1,3-Cl_2-Bz (**10**, 5.2); 1,4-Cl_2-Bz (**11**, 1.5)	2,2′,3,3′,4,4′,5-Cl_7-BP, 2,2′,3,3′,4,5,6′-Cl_7-BP (**12a**, 2.52; **12b**, 1.22); 10 Cl_6-BPs (**13a**, 0.29; **13b**, ?; **13c** and **13d**, 0.79; **13e**, tr; **13f**, 0.39; **13g**, 0.09; **13h**, 0.78; **13i**, 0.64; **13j**, 0.52); 5 Cl_5-BPs (**14a**, 0.25; **14b**, 0.30; **14c**, 0.20; **14d**, 0.09; **14e**, 0.03)	2 trichloro valence-bond benzenes (**15**); tetrachloro valence-bond benzene (**16**); dichlorophenyl cyanide (**17**); C_8H_4ClNO, $M^{+\cdot}$ = 167 (**18**); 3 $C_8H_5Cl_2NO$, $M^{+\cdot}$ = 201 (**19**); 2 trichloroacetophenones (**20**); trichlorocyanophenol (**21**); 2 (trichlorophenyl)acetonitriles (**22**); 1-(trichlorophenyl)-2-propanone (**23**)
2	1,2,3,5-tetra-	63.8	1,2,3-Cl_3-Bz (**6**, 5.3); 1,2,4-Cl_3-Bz (**7**, 4.9); 1,3,5-Cl_3-Bz (**8**, 49.3); 1,3-Cl_2-Bz (**10**, 1.8)	2,3,4′,4,4′,5′,6-Cl_7-BP, 2,2′,3,4,4′,6,6′-Cl_7-BP, 2,2′,3,3′,4,5′,6-Cl_7-BP (**24a**, 1.41; **24b**, 1.10; **24c**, 4.50); 4 Cl_6-BPs (**25a**, 0.16; **25b**, 0.74; **25c**, 0.11; **25d**, 3.68); Cl_5-BP (**26**, 0.64)	trichloro valence-bond benzene (**27**); tetrachloro valence-bond benzene (**28**); trichloroacetophenone (**29**); $C_8H_5Cl_2NO$, $M^{+\cdot}$ = 201 (**30**); 1-(trichlorophenyl)-2-propanone (**31**); (trichlorophenyl)acetonitrile (**32**)
3	1,2,4,5-tetra-	89.7	1,2,4-Cl_3-Bz (**7**, 25.3); 1,3-Cl_2-Bz (**10**, 8.1); 1,4-Cl_2-Bz (**11**, 3.6)	2,2′,3,4′,5,5′,6-Cl_7-BP (**33**, 4.19); 4 Cl_6-BPs (**34a**, 0.32; **34b**, 2.71; **34c**, 1.76; **34d**, 1.99); 4 Cl_5-BPs (**35a**, 0.18; **35b** and **35c**, 1.90; **35d**, 0.25); Cl_4-BP (**36**, 0.32)	trichloro valence-bond benzene (**37**); 2,4,5-trichloroacetophenone (**38**); (2,4,5-trichlorophenyl)acetonitrile (**39**)
4	penta-	53.8	1,2,3,4-Cl_4-Bz (**1**, 6.6); 1,2,3,5-Cl_4-Bz (**2**, 52.8); 1,2,4,5-Cl_4-Bz (**3**, 15.1); 1,2,4-Cl_3-Bz (**7**, 1.9); 1,3,5-Cl_3-Bz (**8**, 5.3); 1,3-Cl_2-Bz (**10**, 0.9)	2,2′,3,3′,4,4′,5,6,6′-Cl_9-BP, 2,2′,3,3′,4,4′,5,5′,6-Cl_9-BP, 2,2′,3,3′,4,5,5′,6,6′-Cl_9-BP (**40a**, 2.08; **40b**, 0.34; **20c**, tr); Cl_8-BP (**41**, 0.53); Cl_7-BP (**42**, 0.49)	
5	hexa-	29.1	Cl_5-Bz (**4**, 71.0); 1,2,3,4-Cl_4-Bz (**1**, 0.6); 1,2,3,5-Cl_4-Bz (**2**, 2.2); 1,2,4,5-Cl_4-Bz (**3**, 3.7)		

[a] Fragmentograms of the photoproducts of tetrachlorobenzenes are described in Figure 1. [b] Abbreviations like 1,2,3-Cl_3-Bz (**6**, 9.2) indicate that the product number **6**, namely, 1,2,3-trichlorobenzene with 9.2% chemical yield is produced. [c] Abbreviations like 2,2′,3,3′,4,4′,5-Cl_7-BP indicate 2,2′,3,3′,4,4′,5-heptachlorobiphenyl. [d] Percent is given in the parentheses.

Table II. Nonsensitized Photolysis of Polychlorobenzenes in Acetonitrile–Water Mixtures

no.	substrate, -chlorobenzene	disappearance of starting material, %	products,[a] % reductively dechlorinated	with increased chlorine contents	photoisomerized chlorobenzenes	polychlorobiphenyls	others
1	1,2,3,4-tetra-	56.5	1,2,3-Cl_3-Bz (**6**, 7.8); 1,2,4-Cl_3-Bz (**7**, 26.8); 1,2-Cl_2-Bz (**9**, 0.5); 1,3-Cl_2-Bz (**10**, 0.7); 1,4-Cl_2-Bz (**11**, 30.4)	hexachloro valence-bond benzene (tr)	1,2,3,5-Cl_4-Bz (**2**, 2.26); 1,2,4,5-Cl_4-Bz (**3**, 0.72)	2,2′,3,3′,4,4′,5-Cl_7-BP, 2,2′,3,3′,4,5,6′-Cl_7BP (**12a**, <0.01; **12b**, <0.01)[b]	trichloro valence-bond benzene, 2 $C_8H_5Cl_2NO$, $M^{+\cdot}$ = 201; 2 unidentified compounds
2	1,2,3,5-tetra-	48.1	1,2,3-Cl_3-Bz (**6**, tr); 1,2,4-Cl_3-Bz (**7**, 24.3); 1,3,5-Cl_3-Bz (**8**, 11.7); 1,3-Cl_2-Bz (**10**, 0.5); 1,4-Cl_2-Bz (**11**, 3.3)	1,2,3,4,5-Cl_5-Bz (**4**, 1.43)	1,2,3,4-Cl_4-Bz (**1**, 5.99)	2 Cl_7-BPs (**24b**, 1.40; **24c**, <0.01); 2 Cl_6-BPs (**25a**, <0.01; **25b**, <0.01); Cl_5-BP (**26**, 0.75)[b]	3 unidentified compounds

3	1,2,4,5-tetra-	98.3	1,2,4-Cl_3-Bz (7, 27.7); 1,3-Cl_2-Bz (10, 0.3); 1,4-Cl_2-Bz (11, 8.5)	1,2,3,4,5-Cl_5-Bz (4, tr)	1,2,3,4-Cl_4-Bz (1, 0.45); 1,2,3,5-Cl_4-Bz (2, 1.11)	2,2′,3,4′,5,5′,6-Cl_7-BP (33, 1.24); 3 Cl_6-BPs (34a, 0.31; 34c, 0.64; 34d, 0.24); 4 Cl_5-BPs (35a, 0.06; 35b and 35c, 0.49; 35d, <0.01)[b]	4 unidentified compounds
4	penta-	41.2	1,2,3,4-Cl_4-Bz (1, 3.7); 1,2,3,5-Cl_4-Bz (2, 13.5); 1,2,4,5-Cl_4-Bz (3, 2.8); 1,2,4-Cl_3-Bz (7, 12.7); 1,3,5-Cl_3-Bz (8, 1.0); 1,4-Cl_2-Bz (11, 6.7)			*c*	2 $C_8H_4Cl_3NO$, $M^{+\cdot}$ = 235 (tr)
5	hexa-	33.5	1,2,3,4,5-Cl_5-Bz (4, 76.8); 1,2,3,5-Cl_4-Bz (2, 1.2); 1,2,4,5-Cl_4-Bz (3, 1.7); 1,2,4-Cl_3-Bz (7, 0.2)				

[a] For the explanations of abbreviations, see footnotes *b* and *c* of Table I. [b] When glass capillary gas chromatography was used with an electron capture detector, the presence of additional appropriate hepta-, hexa-, and pentachlorobiphenyls in these photolysates could be observed with the aid of acetone-sensitized photolysates of corresponding starting tetrachlorobenzene (recorded in Table I) as the authentic standard. [c] PCBs like nona-, octa-, and heptachlorobiphenyls present in this photolysates were detected on glass capillary gas chromatography with ECD using acetone-sensitized photolysate of pentachlorobenzene as the authentic standard.

to photoisomerized chlorobenzenes, compound **1** also provides a trichloro valence-bond benzene.

During nonsensitized photolysis of these PCBzs, photoformation of PCBs is less significant as compared to the case of the acetone-sensitized photoreaction. In Table II, we have recorded only those PCBs which were observable on GC with FID (column C) as well as on the capillary GC-MS system. It should be noted that several additional isomers of PCBs of trace levels are detected, when directly photolyzed samples of compounds **1**–**4** are checked on a capillary column with ECD utilizing acetone-sensitized photolysates (from Table I) as standards. Moreover, in preliminary photolysis of 1,2,3,5-Cl_4-Bz (**2**) for 24 h in H_2O–CH_3CN (1:1 v/v) (5.61 mM/L), we have been able to identify one Cl_7-BP, four Cl_6-BPs, two Cl_4-BPs, and one Cl_3-BP among the photoproducts. Likewise, in another preliminary photoreaction of **4** for 24 h in H_2O–CH_3CN (4:6 v/v) (1.20 mM/L) containing benzene (6.0 mM/L), the generation of four Cl_4-BPs and one Cl_3-BP has been observed. Identifications of the PCBs produced during such preliminary studies were carried out on the previously described GC-MS (*18*). In addition to the above cited photoproducts, on exposing Cl_4-BZ (**1**) and Cl_5-Bz (**4**) to UV radiation without sensitizer, unidentified compounds like $C_8H_5Cl_2NO$ and $C_8H_4Cl_3NO$, two isomers of each, are also obtained, the products of the latter type being of trace levels (see Table II). It is unexpected that direct photolysis of tetrachlorobenzenes **1**–**3** proceeds also to provide more highly chlorinated photoproducts. Thus, substrate **1** gives hexachloro valence-bond benzenes, whereas chlorobenzenes **2** and **3** yield pentachlorobenzene (1.43% amd trace levels (tr), respectively).

Polychlorinated phenols were not among the photoproducts as shown by the method discussed above.

Discussion

Reductive Dechlorination. In general, the process of reductive dechlorination during both acetone-sensitized and nonsensitized photoreactions of the polychlorobenzenes ($Cl_nC_6H_{6-n}$, n = 4–6) in aqueous acetonitrile mixtures described above appears to proceed through the intermediacy of polychlorophenyl radicals (reaction 1)

$$Cl_nC_6H^{*}_{6-n} \xrightarrow[-Cl^{\cdot}]{} Cl_{n-1}\dot{C}_6H_{6-n} \xrightarrow{RH} Cl_{n-1}C_6H_{7-n} \qquad (1)$$

generated by the homolysis of C–Cl bonds. In reaction 1, RH represents a hydrogen-donating solvent. The tentative detection of products such as chlorophenylacetonitriles, 1-(chlorophenyl)-2-propanones, and chloroacetophenones (documented in Table I) by us as well as that of pentachlorobenzyl alcohol and tetrachlorobis(hydroxymethyl)-benzene from **5** in methanol by Plimmer and Klingebiel (**4**) strongly supports the concept of involvement of the polychlorophenyl radical as an intermediate species. Furthermore, our identifications of heptachlorobiphenyls in the case of Cl_4-Bzs **1**–**3** and nonachlorobiphenyls in the case of Cl_5-Bz (**4**) is more evidence that chlorophenyl radicals appear in these irradiations. It is interesting to mention that the isotopic composition of biphenyl formed by photodechlorination of 2-Cl_1-BP in equimolar solvent mixtures like CH_3CN–H_2O, CH_3CN–D_2O, and CD_3CN–H_2O led Bunce (*24*) to conclude that only about 10–20% of the hydrogen abstraction originates from water, whereas the rest comes from acetonitrile. According to him, among aqueous organic mixtures, acetonitrile appears to be a promising cosolvent.

Acetone has been detected in many natural waters (*10*). Since acetone is a well-known triplet sensitizer (*10*, *25*–*27*, and references cited therein), the product composition

from both types of photolyses of 1,2,3,5-tetrachlorobenzene (**2**) in an acetonitrile–water (1:1 v/v) mixture (see Tables I and II) is possibly understandable in terms of the following concept. When molecules of substrate **2** are in the first excited singlet state (S_1), homolysis of a C–Cl bond on position 1 (or 3) of compound **2** takes place, whereby 2,3,5-trichlorophenyl radicals are produced. These radical species subsequently abstract H atoms from the solvent to yield 1,2,4-Cl_3-Bz (**7**). When molecules of the starting chlorobenzene (**2**) have reached the first excited triplet state (T_1) through intersystem crossing from the S_1 state and by transfer of excitational triplet energy of molecules of acetone to the ground state molecules S_0 of substance **2** (in the case of acetone-sensitized reaction), the C–Cl bond on position 2 of Cl_4-Bz **2** is preferably homolytically cleaved leading to the production of 2,4,6-trichlorophenyl radicals, thereby 1,3,5-Cl_3-Bz (**8**) being eventually produced. However, acetone sensitization of **2** does also account for the formation of substantial amounts of 1,2,4-trichlorobenzene (**7**) (see Table I) which clearly cannot be explained by the presented concept. Direct photolysis of **2** could have led to Cl_3-Bz **7**, but this has to be ruled out by the fact that the sensitizer absorbed nearly all of the radiation available.

Our results on the direct photolysis of pentachlorobenzene (**4**) (1.1 mM/L) in *aqueous acetonitrile* (Table II) are different from the results of Crosby and Hamadmad (*5*) on **4** in *hexane* (1 g/L) at 254 nm. They obtained only two Cl_4-Bzs, namely, 1,2,4,5-Cl_4-Bz (**3**) (50%) and 1,2,3,5-Cl_4-Bz (**2**) (13%) at a ratio of ca. 4:1, while we gained these two isomers at a ratio of 1:5 accompanied with Cl_4-Bz **1**, two Cl_3-Bzs, viz., **7** and **8**, and Cl_2-Bz **11**. Likewise, Plimmer and Klingebiel (*4*) could identify among Cl_4-Bzs one tetrachloro isomer, probably compound **2**, as the photoproduct of the suspension of hexachlorobenzene **5** in methanol, while we have been able to detect 2 isomers, namely, **2** and **3**, in the nonsensitized photolysates of **5** (see Table II).

Further discussion on the reductive dechlorination of polychlorobenzenes (PCBzs) giving rise to the production of chlorobenzenes having one Cl and especially two Cl contents less than the starting PCBzs will be presented elsewhere (*28*).

Formation of Polychlorobiphenyls (PCBs). The detection of PCBs in our photochemical studies of tetra- and pentachlorobenzenes (**1**–**4**) can best be explained via free radical mechanisms. For instance, in the case of photolyses of 1,2,4,5-tetrachlorobenzene (**3**), light-excited molecules of substrate **3** yield 2,4,5-trichlorophenyl radicals (**43**), which then attack ground-state molecules of **3**, i.e., $\mathbf{3}^{S_0}$, to produce σ-complex intermediate **44**. Intermediate species **44** in a subsequent step suffered loss of the H atom to yield 2,2′,3,4′,5,5′,6-heptachlorobiphenyl (2,2′,3,4′,5,5′,6-Cl_7BP, **33**) (as explained in reaction 2).

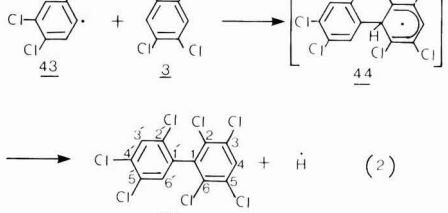

(2)

Although the structure designated as PCB **33** is tentative, only one isomer, heptachlorobiphenyl (Cl_7-BP), formed via reaction 2 is expected. In a previous study (*16*), we have detected and confirmed the presence of 2,3′,4,5′,6-Cl_5-BP in the photolyzed sample of 1,3,5-Cl_3-Bz (**8**) in solution phase. In the case of photolyses of chlorobenzenes **1** and **2**, two and three isomers of trichlorophenyl radicals are produced, respectively. Then chlorophenylation of $\mathbf{1}^{S_0}$ and $\mathbf{2}^{S_0}$ by these chlorophenyl radicals takes place, whereby two and three isomers of Cl_7-BP are formed, respectively. Likewise, the isomers of nonachlorobiphenyl (Cl_9-BP) in the case of **4** are formed through the intermediacy of three chlorophenyl radicals, namely, 2,3,4,5-, 2,3,4,6-, and 2,3,5,6-tetrachloro isomers. In this manner, the tentative structures of Cl_7-BPs generated from Cl_4-Bzs **1**–**3** and of Cl_9-BPs produced from Cl_5-Bz **4** were given. Similar chlorophenylation of the reductively dechlorinated photoproducts also seems to happen; thus, PCBs containing lower chlorine contents are formed. In addition, chlorophenyl radicals arising as a consequence of primary photochemical processes are also likely to attack a position bearing a Cl substituent of the ground-state molecules of the starting material, e.g., Cl_n-Bzs, as well as reductively dechlorinated photoproducts, viz., Cl_{n-1}-Bzs and Cl_{n-2}-Bzs, thereby Cl_{n-2}-BPs and Cl_{n-3}-BPs being eventually formed where n represents the number of Cl atoms in a starting chlorobenzene. Furthermore, hexa-, penta-, and tetrachlorobiphenyls found in the photolysates of **1**–**3** can be the consequence of the reductive dechlorination of the primary Cl_7-BPs. Similarly, photodechlorination of Cl_9-BPs in the case of photolysis of **4** can be taken into account in order to explain the appearance of octa and hepta isomers.

Photoisomerization. With the support of our own data and data from existing literature, detailed mechanisms explaining the process of photoisomerization in the case of tetrachlorobenzenes which leads to the production of tetrachloro valence-bond benzenes and eventually photoisomerized tetrachlorobenzene(s) will be discussed in another paper (*28*).

Miscellaneous Processes. During these photoconversions, the tentative identifications of chlorobenzene derivatives containing substituents like CH_2–CN (recorded in the last columns of Tables I and II) are possibly produced through the simple combination of chlorophenyl radicals with $\dot{C}H_2CN$, previously generated as a consequence of abstraction of the H atom from solvent CH_3CN by other free radicals. Likewise, the formation of trichloroacetophenones **20**, **29**, and **38** in the case of acetone-sensitized photolyses of Cl_4-Bzs is probably the result of an interaction between intermediate trichlorophenyl radicals and acetyl radicals ($CH_3\dot{C}$=O), the latter radicals being produced through the photolysis of acetone. The molecular ion ($M^{+}\cdot$), in the mass spectra of these acetophenones, exhibited the losses of masses of 15 (i.e., CH_3 group) and 43 (i.e., acetyl group), thereby providing the clear evidence for the presence of acetyl substituents. Isopropyltrichlorobenzenes can be considered alternative structures for products **20**, **29**, and **38**. However, under the present circumstances, the photoformation of chlorinated isopropylbenzenes seems unlikely. Likewise, 1-(trichlorophenyl)-2-propanones **23** and **31** are formed by the combination of corresponding trichlorophenyl radicals with $\dot{C}H_2C(O)CH_3$ radicals presumably generated via the abstraction of H atoms by the intermediate free radical species from acetone.

Environmentally Significant Conclusions

In the environment, the photodegradation of tetra- and pentachlorobenzenes is possibly accelerated by the presence of acetone or similar sensitizers, while such a photoreaction of hexachlorobenzene is ca. 2 times slower than its direct photolysis. For the evaluation of photochemical

fate of tetrachlorobenzenes present in aquatic environments, the process of photoisomerization needs to be considered. For instance, nonsensitized photolysis of 1,2,3,4-tetrachlorobenzene yields 1,2,3,5- and 1,2,4,5-tetrachloro isomers, each photoisomerized Cl_4-Bz being readily photodegradable and more effectively converted to polychlorobiphenyls than the starting tetrachlorobenzene. The identifications of PCBs and chlorinated phenylacetonitriles, acetophenones, 1-phenyl-2-propanones, etc., presumably formed through the intermediacy of polychlorophenyl radicals, show that relatively stable intermediate chlorophenyl radicals produced from PCBzs in the aquatic environment are likely to interact with the free radical centers of humic substances which are known to have 10^{17} to 10^{18} spins/g (*29*) and aryl aromatic compounds, viz., substituted benzenes derived from humic substances and lignins (*30*) and aromatic hydrocarbons frequently found in natural water bodies. Although the photogeneration of PCBs from PCBzs seems to be dependent on the concentration of the chlorobenzenes, the appearance of PCBs in the acetone-sensitized photolyses of 1,2,3,4-, 1,2,3,5-, and 1,2,4,5-tetrachlorobenzene and pentachlorobenzene with total chemical yields (calculated from the photodecomposed chlorobenzene) of ca. 8.11%, 12.34%, 13.62%, and 3.44%, respectively, indicates that acetone which occurs in many natural waters may play an important role in the photoformation of PCBs from PCBzs present in lower concentrations.

Acknowledgments

We thank H. Parlar of the Institute of Ecological Chemistry, Gesellschaft für Strahlen- und Umweltforschung mbH München, West Germany, and R. G. Zepp of the Environmental Research Laboratory, U.S. EPA, Athens, GA, for the critical comments on the manuscript.

Literature Cited

(1) Buser, H. R. *Chemosphere* **1979**, *8*, 415–424.
(2) Jansson, B.; Sundström, G.; Ahling, B. *Sci. Total Environ.* **1978**, *10*, 209–217.
(3) Crosby, D. G.; Wong, A. S.; Plimmer, J. R.; Woolson, E. A. *Science (Washington, D.C.)* **1971**, *173*, 748–749.
(4) Plimmer, J. R.; Klingebiel, U. I. *J. Agric. Food Chem.* **1976**, *24*, 721–723.
(5) Crosby, D. G.; Hamadmad, N. *J. Agric. Food Chem.* **1971**, *19*, 1171–1174.
(6) Choudhry, G. G.; Hutzinger, O. *Toxicol. Environ. Chem.* **1982**, *5*, 1–65.
(7) Olie, K.; Vermeulen, P. L.; Hutzinger, O. *Chemosphere* **1977**, *6*, 455–459.
(8) Eiceman, G. A.; Clement, R. E.; Karasek, F. W. *Anal. Chem.* **1979**, *51*, 2343–2350.
(9) Shackelford, W. M.; Keith, L. H. "Frequency of Organic Compounds Identified in Water"; 1976, EPA Report 600/4-76-062, pp 65, 66, 69, 70, 72–76, 247, 248.
(10) Choudhry, G. G.; Roof, A. A. M.; Hutzinger, O. *Toxicol. Environ. Chem. Rev.* **1979**, *2*, 259–302.
(11) Fox, M.-A.; Nichols, W. C., Jr.; Lemal, D. M. *J. Am. Chem. Soc.* **1973**, *95*, 8164–8166, and references cited therein.
(12) Arnold, D. R.; Wong, P. C. *J. Am. Chem. Soc.* **1977**, *99*, 3361–3366.
(13) Mansour, M.; Wawrick, S.; Parlar, H.; Korte, F. *Chem.-Ztg.* **1980**, *104*, 339–340.
(14) Mansour, M.; Parlar, H.; Korte, F. *Chemosphere* **1980**, *9*, 59–60.
(15) Mansour, M.; Parlar, H.; Korte, F. *Naturwissenschaften* **1979**, *66*, 579–580.
(16) Choudhry, G. G.; Roof, A. A. M.; Hutzinger, O. *Tetrahedron Lett.* **1979**, 2059–2062.
(17) Uyeta, N.; Taue, S.; Chikasawa, K.; Mazaki, M. *Nature (London)* **1976**, *264*, 583–584.
(18) Choudhry, G. G.; Roof, A. A. M.; Hutzinger, O. *J. Chem. Soc., Perkins Trans. 1* **1982**, 2957–2961.
(19) Grob, K.; Grob, G. *Chromatographia* **1972**, *5*, 3–12.
(20) Olie, K.; Hutzinger, O. In "Recent Developments in Mass Spectrometry in Biochemistry and Medicine"; Frigerio, A., Ed.; Plenum Press: New York and London, 1978; Vol. 1, pp 555–562.
(21) Olie, K.; Lustenhouwer, J. W. A.; Hutzinger, O. *Pergamon Ser. Environ. Sci.* **1982**, *5*, 227–244.
(22) Lahaniatis, E. S.; Bieniek, D.; Vollner, L.; Korte, F. *Chemosphere* **1981**, *10*, 935–943.
(23) Ahling, B.; Bjørseth, A.; Lunde, G. *Chemosphere* **1978**, *7*, 799–806.
(24) Bunce, N. J. *Chemosphere* **1978**, *7*, 653–656.
(25) Murov, S. L. "Handbook of Photochemistry"; Marcel Dekker: New York, 1973.
(26) Wagner, P. J.; Hammond, G. S. In "Properties and Reactions of Organic Molecules in their Triplet States"; Noyes, W. A., Hammond, G. S., Pitts, J. N., Eds.; Interscience Publishers: New York, London, Sydney, 1968; Adv. Photochem. Vol. 5, pp 22–156.
(27) Wagner, P. J. *J. Am. Chem. Soc.* **1966**, *88*, 5672–5673.
(28) Choudhry, G. G.; Webster, G. R. B., submitted for publication in *Can. J. Chem.*
(29) Choudhry, G. G. *Toxicol. Environ. Chem.* **1981**, *4*, 261–295.
(30) Choudhry, G. G. *Toxicol. Environ. Chem.* **1981**, *4*, 209–260.

Received for review December 30, 1982. Revised manuscript received September 9, 1983. Accepted October 28, 1983.

Environ. Sci. Technol. 1984, 18, 242–247

Numerical Simulation of a Sedimentation Basin. 1. Model Development

Iraklis A. Vallouls and E. John List*

W. M. Keck Laboratory of Hydraulics and Water Resources, Division of Engineering and Applied Science, California Institute of Technology, Pasadena, California 91125

■ A method for the numerical simulation of a rectangular sedimentation basin operating under steady or unsteady conditions is described. The computer model follows the spatial and temporal development of the influent particle size distribution toward the outlet of the tank. It is based on the fundamental mechanisms which govern particle motion and growth. The model accounts for the variability of the flow field and the particle size distribution in the tank and, from the local development of the particle size spectrum, predicts the overall performance of the settling basin.

1. Introduction

Settling is the most common unit treatment process in a wastewater treatment plant. Settling basins are used both as primary clarifiers to remove particulate matter and as secondary tanks following the activated sludge unit for biological floc removal. They are also used to settle the chemical floc in the chemical coagulation process.

Most settling tanks are sized on the basis of standard detention periods and overflow rates under ideal conditions (steady-state inflow, plug flow, and no particle flocculation) using a safety factor in the range 1.5–2 (*1*). Pilot units, or data from actual plants, are often used to develop relations between loading and performance. Oversized tanks occur frequently as a result of attempts to meet effluent standards under variable load conditions. The need for dynamic simulation arises, and numerous un-steady-state mathematical models for the performance of settling tanks under transient inflows have been developed (*2*).

Regression models (*3*) are empirical. They use data from operating tanks to derive a relationship between loading and effluent characteristics. Hydraulic scale models (*4*), if successful, are applicable only to the sedimentation basins they simulate. Dispersion models (*5*, *6*) use an experimentally determined eddy dispersion coefficient to characterize the flow field in the tank. Mechanistic models (*2*, *7*) assume a welll-mixed settling basin and use a one-dimensional unsteady diffusion equation to predict the effluent quality under variable load. The physical configuration of the tank is taken into account and the resuspension of sediment related empirically to the average cross-sectional mixing coefficient. Ramaley et al. (*8*) incorporated coagulation in simulating the settling basin in their numerical model for integral water treatment plant design. Their model does not account for scouring and turbulent transfer of mass through the tank; it assumes a constant density for all particle sizes and uses a collision efficiency of unity. Dick (*9*) noted that the utility of the model of Ramaley et al. is limited because of the simplifications involved.

Hazen's (*10*) early theory predicts that all particles with settling velocity greater than the overflow rate of the tank are removed provided that the flow is uniform, no short-circuiting currents or scouring occurs, and particles of uniform density and shape settle discretely. In reality, inlets, outlets, wind, and density differences induce currents or create dead regions in the tank. High forward velocities resuspend the deposits and reduce the efficiency of the basin. Regardless of surface loading coagulation is essential in achieving high suspended solid removal (*11*). Rigorous analysis of the performance of a settling basin must be based on the detailed spatial behavior of the fluid and the particles in the tank and take into account the fluid–particle and particle–particle interactions.

The aim of this computer simulation of a rectangular settling basin is to describe the spatial and temporal development of the influent particle size distribution toward the outlet of the tank. It is based on the fundamental mechanisms that govern particle motion and growth. The model accounts for the variability of the flow field and the particle size distribution in the tank and, from the local development of the particle size spectrum, predicts the overall performance of the settling basin.

2. Fundamental Mechanisms

In this section we discuss the basic features of the model.

(a) Flow Field. Any empirical or observed velocity distribution in the tank can be incorporated into the model. However, for this analysis the logarithmic velocity profile is used to demonstrate the model capabilities. We assume that the local mean longitudinal velocity through the tank is given by

$$u = \bar{u} + \frac{u^*}{\kappa}\left[1 + \ln\left(\frac{z}{H}\right)\right] \qquad (2.1)$$

where $\bar{u}$ is the cross-sectional mean velocity, u^* is the shear velocity, H is the depth of the tank, u the time-averaged velocity at the vertical coordinate z, and $\kappa = 0.38$ is von Karman's constant, reduced to account for the suspended mass (*12*).

The cross-sectional turbulent mixing coefficient $\hat{E}$ can be derived from the logarithmic velocity profile (*13*)

$$\hat{E} = \kappa u^* z\left(1 - \frac{z}{H}\right) \qquad (2.2)$$

Longitudinal turbulent mixing is neglected because it is insignificant when compared with the shear flow dispersion caused by the vertical velocity gradient (*13*).

An estimate of the rate of turbulent energy dissipation ϵ, per unit mass of fluid, can be obtained from (*14*)

$$\epsilon = \hat{E}\left(\frac{du}{dz}\right)^2 \qquad (2.3)$$

which agrees well with experimental results (*15*). ϵ is needed in the collision function for turbulent shear induced coagulation and for determining the maximum allowable floc size for a given shear strength.

(b) Coagulation. Particles in wastewater are classified as the following (*16*):

settleable	$>100\ \mu m$
supracolloidal	$1–100\ \mu m$
colloidal	$10^{-3}–1\ \mu m$
soluble	$<10^{-3}\ \mu m$

In the absence of coagulation a settling basin operating at a detention time of practical interest will remove only the settleable and some of the supracolloidal particles. However, flocculation transfers mass through the particle size spectrum toward larger particle sizes with a subsequent increase in the removal efficiency of the tank. Thus,

0013-936X/84/0918-0242$01.50/0

Table I. Collision Functions for the Three Particle Collision Mechanisms Considered[a]

	collision function $\beta(r_i,r_j)$	source
Brownian motion	$\frac{2kT}{3\mu}\frac{(r_i + r_j)^2}{r_i r_j}E_b(r_i,r_j) = 4\pi(D_i + D_j)(r_i + r_j)E_b(r_i,r_j)$	Smoluchowski (*18*)
turbulent shear	$2.3(r_i + r_j)^3(\epsilon/\nu)^{1/2}E_{sh}(r_i,r_j)$	Pearson et al. (*19*)
differential sedimentation	$\frac{0.7g(\rho_p - \rho_w)}{\mu}(r_i + r_j)^2\lvert r_i^2 - r_j^2\rvert E_{ds}(r_i,r_j)$	Findheisen (*20*)

[a] Values of β are for collision mechanisms acting individually. E_b, E_{sh}, and E_{ds} express the influence of hydrodynamic and other interparticle forces on the collision process. k, Boltzmann's constant; T absolute temperature; r_i,r_j, particle radii; μ, coefficient of fluid viscosity; D_i, particle diffusivity; ϵ, viscous dissipation rate per unit mass; ν, kinematic viscosity of fluid (μ/ρ_f); ρ_f, fluid density; ρ_p, particle density; g, acceleration of gravity.

particles in the size range traditionally referred to as suspended solids (>1 μm) may be generated within the tank from coagulation of colloidal material.

Brownian motion, fluid shear, and differential settling cause relative motion of the particles through the fluid and bring them into close proximity. Short-range interfacial forces act then between the particles to bring about their coalescence. Analytic estimates of the probability (collision function) $\beta(r_i,r_j)$ that two spherical particles of radii r_i and r_j will collide in unit time are shown in Table I; $\beta(r_i,r_j)$ represents the geometry and dynamics of the collision mechanisms. The collision efficiency $E(r_i,r_j)$ reflects the influence of hydrodynamic and van der Waals' forces on the collision probability of two approaching particles.

Published work on E deals with interactions between hard spherical particles. For Brownian diffusion induced collisions Valioulis and List (*17*) reported the best-fit approximation to their numerical calculations

$$E_b(r_i,r_j) = 0.4207 + 0.031\left(\frac{r_j}{r_j}\right) - 0.0009\left(\frac{r_i}{r_j}\right)^2 \qquad \frac{r_i}{r_j} \leq 20$$

$$E_b(r_i,r_j) = 0.652 + 0.0055\left(\frac{r_i}{r_j}\right) - (3.035 \times 10^{-5})\left(\frac{r_i}{r_j}\right)^2 \qquad 20 \leq \frac{r_i}{r_j} \leq 100 \quad (2.4)$$

where $r_i > r_j$ and for $A/(kT) = 1$; A is the Hamaker constant, k Boltzmann's constant, and T the absolute temperature. For particle size ratios larger than 100, where $r_j = 0.05$ μm is the minimum particle size considered here, Brownian diffusion is no longer important in inducing particle collisions (*21*).

Adler (*22*) used Stokes' equations to compute the collision efficiency $E_{sh}(r_i,r_j)$ for two unequal hard spheres in simple shear flow. His results are a function of the ratio of the size of the interacting particles r_i/r_j, where $r_i > r_j$, and either the van der Waals' energy of attraction (Table II) or the distance between the spheres at which collision is assumed to occur. The Monte Carlo simulation of the evolution of the particle size distribution by Pearson et al. (*19*) showed that, for particles much smaller than the Kolmogorov microscale, isotropic turbulent shear is equivalent in coagulation power to a rectilinear laminar shear, G, of magnitude 1.72 times the characteristic strain rate $(\epsilon/\nu)^{1/2}$ given by the rate of dissipation of turbulent kinetic energy, ϵ, per unit mass of fluid and the fluid kinematic viscosity ν. In primary clarifiers, even at high forward velocities, $(\epsilon/\nu)^{1/2}$ is rarely larger than 10 s^{-1} (*11*); ϵ is then on the order of 10^{-4} m^2/s^3 and the Kolmogorov length microscale $(\nu^3/\epsilon)^{1/4} = 3 \times 10^{-4}$ m. This suggests the use of Adler's results with $G = 1.72(\epsilon/\nu)^{1/2}$ for turbulent shear induced collisions between particles with sizes up to 10^{-4} m. For larger particles differential settling induced coagulation becomes dominant.

Table II. Approximations for Collision Efficiencies E_{sh} for Hard Spherical Particles in Laminar Shear

$$E_{sh} = \left(\frac{1 + bx}{1 + cx + dx^2}\right)\left(\frac{8}{(1 + 1/x)^3}\right) \qquad x = r_i/r_j,\ r_i \geq r_j$$

$A/(144\pi\mu r_i^3 G)$	a	b	c	d
10^{-2}	1.189	0.118	−3.431	0.331
10^{-3}	0.766	0.007	−0.006	1.547
10^{-4}	0.145	−0.0006	−1.137	0.775
10^{-5}	0.0017	−0.0001	−1.442	0.557

Neiburger et al. (*23*) obtained an analytic expression for theoretical collision efficiencies induced by differential sedimentation of hard spherical particles, computed assuming Stokes' flow (with the slip-flow correction), and modified to be consistent with experimental results:

$$E_{ds}(r_i,r_j) = E_0 + E_1 + E_2 + E_3 + E_4 \qquad (2.5)$$

where

$$E_0 = 0.95 - (0.7 - 0.005r_i)^4\,(7.92 - 0.12r_i + 0.001r_i^2)$$

$$E_1 = -\left(\frac{r_j}{r_i} - 0.5\right)^2$$

$$E_2 = -1.5\exp\left[-(0.0015r_i + 8)\frac{r_j}{r_i}\right]$$

$$E_3 = -(1 - 0.007r_i)\exp\left[-0.65r_i\left(1 - \frac{r_j}{r_i}\right)\right]$$

$$E_4 = 0 \qquad r_i < 20\ \mu\text{m}$$

$$= \exp\left[-30\left(1 - \frac{r_j}{r_i}\right)\right] \qquad r_i \geq 20\ \mu\text{m}$$

where $r_i > r_j$ and r_i and r_j are in micrometers. This expression can be used for $r_i > 10$ μm. Davis (*24*) computed collision efficiencies for two spherical particles smaller than 10 μm. His results suggest that efficiencies for collisions between particles r_i and r_j such that $r_j < r_i < 10$ μm are essentially equal to those with $r_j < r_i = 10$ μm.

In hydrosols only the smaller particles can be assumed nearly spherical. These particles coalesce and form loose aggregates rather than solid masses. The volume of the aggregate is larger than the sum of the volumes of primary particles it contains due to inclusion of water. The size–density relationship and the structure of the flocs depend on their physical and chemical characteristics. This has important implications with regard to particle–particle and

fluid–particle interactions. Floc densities observed (*9*, *25*), or computed numerically (*25*–*27*), indicate almost neutrally buoyant flocs for sizes larger than about 100 μm. For this model particles smaller than 3.5 μm in diameter are considered solid spheres with a density of 2650 kg/m^3. For larger particles the size–density relationship proposed by Tambo and Watanabe (*25*) is used:

$$\rho_f - \rho_w = \frac{1.3}{(200r_i)^{0.9}} \tag{2.6}$$

where ρ_f and ρ_w are the densities (kg/m^3) of the floc and the water, respectively, and r_i is the particle radius (μm). In order to assure a smooth variation of particle size with density, it is assumed in the simulation that eq 2.6 holds for $r_i \geq 1.75$ μm; all smaller particles have $\rho_f - \rho_w = 1650$ kg/m^3.

The very low aggregate densities are characteristic of particles with an expanded structure. Sutherland's (*28*) computer simulation of floc formation and observations under an electron microscope (*29*) revealed an open network of filaments joining denser regions. Collisions of such clusters create a chainlike framework. Vold (*26*) and Sutherland and Goodarz-Nia (*27*) characterized their numerically generated flocs by a core radius, where about 60% of the primary particles are contained, and by branches or tentacles with a mean length from 0.1 to 1 times the diameter of the core. Vold suggested that coagulation of such particle formations can involve only mechanical entanglement of their branches.

The above discussion suggests that the collision efficiencies for hard spheres can be used in the simulation of particles smaller than 3.5 μm in diameter but will underestimate the collision frequency between flocs. The increased chances of collisions of such nonspherical aggregates are accounted for in the simulation by assuming that they behave like solid spheres with a 20% larger effective coalescence radius. The value of 20% is only a rough estimate, suggested by the length of the tentacles observed in ref 27, and is used due to lack of better experimental information. The collision rate of Brownian diffusion induced collision is not altered by this assumption, since both the collision function and the efficiency depend only on the size ratio of the interacting particles. For shear-induced collisions and for particles larger than 3.5 μm in diameter, the best-fit approximation to Adler's (*22*) graphical results for the collision efficiency (assuming that coalescence occurs at an interparticle separation of $0.2r_i$) is used:

$$E_{sh}(r_i,r_j) = -0.4036 + 9.423\left(\frac{r_j}{r_i}\right) - 17.214\left(\frac{r_j}{r_i}\right)^2 + 9.444\left(\frac{r_j}{r_i}\right)^3 \tag{2.7}$$

where $r_i > r_j$. Hocking and Jonas (*30*) showed that the efficiency for differential settling induced collisions is a weak function of the interparticle separation at which coalescence is assumed to occur. Thus, the collision efficiencies for hard spheres can be used.

The open structure of the aggregate indicates that flow streamlines will cross the aggregate. Small particles moving on these streamlines are likely to be captured by purely hydrodynamic effects. Adler (*31*) computes the streamlines around a porous sphere of radius r and permeability p. A reasonable approximation is that, when the two approaching particles are very different in size, the flow field is determined solely by the presence of the larger one. For such particle encounters Adler's (*31*) drainage cross section, i.e., the cross section at infinity for streamlines which cross the aggregate, is equivalent to the collision cross section of the particles.

By use of the argument advanced by Pearson et al. (*19*), Adler's tabulated numerical results for simple laminar shear are used here for turbulent-induced coagulation. Adler's results are approximated with

$$E_{sh}(r_i,r_j) = 1.1616 - 0.288\xi + 0.0112\xi^2 \quad r_i \gg r_j \tag{2.8}$$

where $\xi = r_i/p^{1/2}$.

For differential settling the collision efficiencies for particles with large difference in size are computed from (*31*)

$$E_{ds}(r_i r_j) = 1 - \frac{b}{\xi} - \frac{a}{\xi^3} \quad r_i \gg r_j \tag{2.9}$$

where $\zeta = 2\xi^2 + 3 - 3(\tanh \xi)/\xi$, $a = -(1/\zeta)[\xi^5 + 6\xi^3 - [(\tanh \xi)/\xi](3\xi^5 + 6\xi^3)]$, and $b = (1/\zeta)\, 3\xi^3[1 - (\tanh \xi)/\xi]$. For aggregates with high porosity the permeability p can be estimated from Brinkman's equation applicable to a cloud of spherical particles (*32*):

$$p = \frac{c^2}{18}\left[3 + \frac{4}{1-e} - 3\left(\frac{8}{1-e} - 3\right)^{1/2}\right] \tag{2.10}$$

where c is the radius of the primary particles (or denser regions) in the aggregate, assumed to be $^1/_{20}$th of its diameter, and e its porosity computed from

$$e = \frac{\rho_p - \rho_f}{\rho_p - \rho_w} \tag{2.11}$$

where ρ_p is the density of the primary particles (or denser formations) which compose the aggregate.

The efficiencies given by eq 2.8 and 2.9 have been used for particle encounters with relative size less than 0.1 and when the larger particle possesses a relative density lower than 2.65; that is, it is considered a floc. To the knowledge of the authors, collision efficiencies for two porous spheres of comparable size do not exist. Since such particles will interact hydrodynamically as they approach each other, it is assumed that the collision efficiencies for hard spheres (with the 20% increased coalescence radius assumption) can be used.

In summary the following hypotheses are used here with regard to particle dynamics: Particles smaller than 3.5 μm in diameter are assumed to behave as solid spheres. Larger particles are considered flocs with reduced density and an amorphous shape which increases the collision radius of the equivalent in mass sphere by 20%. The increased chances of collisions between a porous aggregate and a floc or a solid particle are taken into account only for encounters between particles with relative size less than 0.1.

For this simulation the collision mechanisms are assumed additive, although this may not be strictly true (*33*), and only binary particle encounters are assumed to occur. It is also assumed that the ionic strength of the suspension is large enough that double-layer electrostatic forces do not influence the coagulation rate.

(c) Particle Size Distribution. The size distribution function $n(d)$ of a population of coagulating particles is defined by

$$\Delta N = n(d)\Delta d$$

where ΔN is the number of particles with a diameter in the size interval Δd, per unit volume of fluid. Atmospheric aerosols (*34*) and hydrosols (*35*) are found to exhibit the power law

$$n(d) = (\Delta N/\Delta d) = Cd^{-\alpha}$$

where the exponent α is a constant and the constant C depends on the total particle mass per unit volume of fluid. The surface ΔS, volume ΔV, and mass ΔQ of particles in the size range Δd, per unit volume of fluid, are then expressed as

$$\Delta S = C\frac{\pi}{4}d^{-\alpha+2}\Delta d$$

$$\Delta V = C\frac{\pi}{6}d^{-\alpha+2}\Delta d \qquad (2.12)$$

$$\Delta Q = C\frac{\pi}{6}\rho(d)d^{-\alpha+3}\Delta d$$

where the particle density $\rho(d)$ is in general a function of particle size.

In hydrosols α ranges from 2.5 to 5.6 (*21*) and depends on one or more physical mechanisms which induce particle collisions. Lawler et al. (*8*) stressed the significance of α for the water quality: some pollutants are expressed as mass concentrations (suspended solids), some concentrate on surfaces (trace metals), and for others the total number is important (pathogenic organisms).

(d) Resuspension. Strong fluid shear near the bottom of the tank results in resuspension of material previously deposited. Work on entrainment of sediments has focused on the determination of the critical conditions for the initiation of motion of the deposits (for an extended review, see ref 36). Individual particles resist resuspension by their weight while fine, cohesive sediments (incorporating fractions of silt or clay, for example) offer additional resistance to entrainment due to cohesive forces. It is widely accepted that the critical shear stress for the initiation of motion of noncohesive sediments can be obtained from Shields' curve. The critical velocity near the bottom is, in general, an increasing function of the grain size.

Knowledge of the resuspension of cohesive sediments is primitive. Experimental data for the critical conditions for the entrainment of cohesive sediments is not consistent, mainly because the cohesive forces depend on factors such as shear strength, mineral content, plasticity, and electrochemical condition of the deposits. Results of several experimental studies suggest that cohesive sediments exhibit increasing resistance to erosion with decreasing grain size (*36*).

For the simulation model the resuspension flux of the deposits is needed. To the knowledge of the authors, published information on the amount of entrained material from cohesive or noncohesive sediments does not exist. For the purpose of testing the sensitivity of results to scouring, a reduced deposition mass flux per unit volume of fluid is defined:

$$\text{deposition mass flux} = -w_p(1 - s)Q_p \qquad (2.13)$$

where s is a scouring parameter and Q_p the mass concentration of the suspended solids. For $s = 0$ only deposition takes place; for $0 < s < 1$ partial scouring occurs; $s = 1$ implies that deposition is balanced by scouring; $s > 1$ implies that scouring dominates. For a typical simulation run a value of $s = 0.15$ was chosen; this value of s agrees well with the experimental results of Takamatsu et al. (*37*) in a model settling tank. In addition, simulation runs with $s = 0$, $s = 0.4$, and $s = 0.8$ were performed.

Floc Breakup. Strong local fluid shear may cause the aggregates to break up. The effect is more important in the flocculation basin which often precedes the settling tank but can be significant in regions of the clarifier where turbulence levels are high.

Two floc breakup mechanisms are distinguished (*38*): Inorganic flocs tend to disintegrate due to surface erosion; in organic flocs the polymer bridge holding primary particles on the floc surface breaks when the shear strength of the polymer bridge is exceeded (filament fracture). Parker et al. (*38*) obtained experimental relationships between the maximum size of the aggregate and the local shear. For inorganic flocs they found

$$\text{ferric floc: } r_{max} = \frac{3.6 \times 10^5}{G^2}$$
$$100\ \mu\text{m} < r_{max} < 15\,000\ \mu\text{m}$$
$$\text{alum floc: } r_{max} = \frac{6 \times 10^3}{G} \qquad (2.14)$$
$$15\ \mu\text{m} < r_{max} < 250\ \mu\text{m}$$

and for conventional activated sludge flocs

$$r_{max} = \frac{2250}{G^{0.35}} \qquad 400\ \mu\text{m} < r_{max} < 1000\ \mu\text{m} \qquad (2.15)$$

where $G = (\epsilon/\nu)^{1/2}$ and r_{max} is in micrometers.

3. Computer Model

The settling tank is segmented into k equal rectangular cells with length a and height b (Figure 1). The flow field and the size distribution of the particles are uniform across the width of the tank, and the suspension is spatially homogeneous within each cell. The continuous particle size (radius) spectrum is divided into q logarithmically equal spaced sections within which all particles have the same mass (*39*). This procedure reduces the number of conservation equations to be integrated and renders the problem tractable for computer solution.

The discrete conservation equation for the development of the particle size distribution in any cell $k = (m, n)$ at time t is

$$\frac{dQ_{l,m,n}}{dt} = \left[\frac{1}{2}\sum_{i=1}^{l-1}\sum_{j=1}^{l-1}({}^{1a}\bar{\beta}_{i,j,l}Q_jQ_i + {}^{1b}\bar{\beta}_{i,j,l}Q_iQ_j) - \sum_{i=1}^{l-1}({}^{2a}\bar{\beta}_{i,l}Q_iQ_l - {}^{2b}\bar{\beta}_{i,l}Q_lQ_i) - \frac{1}{2}{}^{3}\bar{\beta}_{l,l}Q_lQ_l - Q_l\sum_{i=l+1}^{q}{}^{4}\bar{\beta}_{i,l}Q_i\right]_{m,n} + \frac{\bar{S}_l}{b}Q_{l,m,n+1} - \frac{\bar{S}_l}{b}Q_{l,m,n} + \frac{u_{m-1,n}Q_{l,m-1,n}}{a} - \frac{u_{m,n}Q_{l,m,n}}{a} + \hat{E}_{n,n+1}\frac{Q_{l,m,n+1} - Q_{l,m,n}}{b^2} + \hat{E}_{n-1,n}\frac{Q_{l,m,n-1} - Q_{l,m,n}}{b^2} \qquad (3.1)$$

where m and n denote, repectively, the horizontal and vertical index of the cell and are subscripts to all variables in the square brackets. $Q_{l,m,n}$ is the concentration of the suspension in section l in cell (m, n). The coagulation coefficients ${}^{1a}\bar{\beta}_{i,j,l}$, ${}^{1b}\bar{\beta}_{i,j,l}$, ${}^{2a}\bar{\beta}_{i,l}$, ${}^{2b}\bar{\beta}_{i,l}$, and ${}^{3}\bar{\beta}_{l,l}$, and ${}^{4}\bar{\beta}_{i,l}$ and settling coefficients $\bar{S}_l$ are weighted averages of the collision functions (Table I) over the size ranges in each interval and are listed in Table III. $\hat{E}_{n,n+1}$ is the vertical turbulent mixing coefficient for the exchange of momentum and mass between cells (m, n) and $(m, n+1)$ and is computed on the line separating the two cells. $u_{m,n}$ is the horizontal velocity assigned to the cell (m, n), calculated at its center.

Term 1 represents the flux of mass into section l by coagulation of particles from lower sections (i.e., particles of smaller size). Term 2 accounts for the loss of mass from section l when a particle in section l coagulates with a particle from lower sections. Term 3 represents the loss of mass from section l due to intrasectional coagulation and term 4 the loss of mass from section l when a particle from section l coagulates with a particle from a higher section. Terms 5 and 6 represent respectively gain and loss

Table III.[a] **Sectional Coagulation Coefficients with Geometric Constraint ($v_{i+1} \geq 2v_i$, $i = 0, 1, 2, \ldots q-1$)**

symbol	remarks	coefficient[b]
${}^{1a}\bar{\beta}_{i,j,l} = {}^{1b}\bar{\beta}_{i,j,l}$	$i < l-1, j < l-1$	0
${}^{1a}\bar{\beta}_{i,l-1,l} = {}^{1b}\bar{\beta}_{l-1,i,l}$	$1 < l \leq q,\ i < l-1$	$\int_{x_{i-1}}^{x_i}\int_{f(v_{l-1}-v)}^{x_{l-1}} \frac{u\beta(u,v)}{uv(x_i - x_{i-1})(x_{l-1} - x_{l-2})}\,dy\,dx$
	$1 < l \leq q,\ i = l-1$	$\int_{x_{i-1}}^{f(v_i-v_{i-1})}\int_{f(v_{l-1}-v)}^{x_{l-1}} \frac{u\beta(u,v)}{uv(x_{l-1} - x_{l-2})^2}\,dy\,dx + \int_{f(v_i-v_{i-1})}^{x_i}\int_{x_{l-2}}^{x_{l-1}} \frac{u\beta(u,v)}{uv(x_{l-1} - x_{l-2})^2}\,dy\,dx$
${}^{1b}\bar{\beta}_{i,l-1,l} = {}^{1a}\bar{\beta}_{l-1,i,l}$	$1 < l \leq q,\ i < l-1$	$\int_{x_{i-1}}^{x_i}\int_{f(v_{l-1}-v)}^{x_{l-1}} \frac{v\beta(u,v)}{uv(x_i - x_{i-1})(x_{l-1} - x_{l-2})}\,dy\,dx$
${}^{2a}\bar{\beta}_{i,l} = {}^{1a}\bar{\beta}_{i,l,l+1}$	$1 < l \leq q,\ 1 \leq i < l$	$\int_{x_{i-1}}^{x_i}\int_{f(v_l-v)}^{x_i} \frac{u\beta(u,v)}{uv(x_i - x_{i-1})(x_l - x_{l-1})}\,dy\,dx$
${}^{2b}\bar{\beta}_{i,l}$	$1 < l \leq q,\ 1 \leq i < l$	$\int_{x_{i-1}}^{x_i}\int_{x_{l-1}}^{f(v_l-v)} \frac{v\beta(u,v)}{uv(x_i - x_{i-1})(x_l - x_{l-1})}\,dy\,dx$
${}^{3}\bar{\beta}_{l,l} = {}^{1a}\bar{\beta}_{l,l,l+1}$	$1 \leq l \leq q$	$\int_{x_{i-1}}^{f(v_l-v_{l-1})}\int_{f(v_l-v)}^{x_l} \frac{(u+v)\beta(u,v)}{uv(x_l - x_{l-1})^2}\,dy\,dx + \int_{f(v_l-v_{l-1})}^{x_l}\int_{x_{l-1}}^{x_l} \frac{(u+v)\beta(u,v)}{uv(x_l - x_{l-1})^2}\,dy\,dx$
${}^{4}\bar{\beta}_{i,l}$	$1 \leq l < q,\ l < i \leq q$	$\int_{x_{i-1}}^{x_i}\int_{x_{l-1}}^{x_l} \frac{u\beta(u,v)}{uv(x_i - x_{i-1})(x_l - x_{l-1})}\,dy\,dx$
$\bar{S}_l$	$1 \leq l < q$	$\int_{x_{l-1}}^{x_l} \frac{w(v)}{(x_l - x_{l-1})}\,dx$

[a] Adapted from ref 39. [b] Where $x_i = \log v_i = f(v_i)$, $u = \exp(y)$, $v = \exp(x)$, and u,v denote particle mass, the mass v_i is the upper limit of section i, $\beta(u,v)$ is the collision function obtained from Table I, and $w(v)$ is Stokes' settling velocity of particles with mass v.

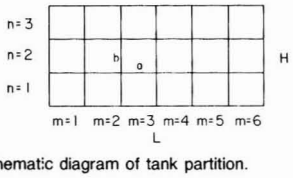

Figure 1. Schematic diagram of tank partition.

of mass for the cell (m, n) resulting from particles sedimenting at their Stokes' settling velocity $w = {}^2/_9 g[(\rho_f - \rho_w)/\mu]r^2$. Term 7 corresponds to the advective transfer of mass and term 8 to the turbulent transport of mass from cell to cell.

The accumulation of particle mass at the bottom of the tank is obtained from

$$\frac{dQ^0_{l,m,1}}{dt} = \frac{(1-s)}{b} Q_{l,m,1}\bar{S}_l \qquad (3.2)$$

where $Q^0_{l,m,1}$ is the deposited mass is section l from cell $(m,1)$. Thus, the computer model predicts the particle size distribution in the deposits and the thickness of the sludge blanket along the length of the tank. For simplicity it is assumed that the tank volume does not change due to sludge accumulation throughout the calculations.

Due to coagulation particles may exceed the maximum size allowed by the local shear (as suggested by eq 2.15). Their mass is then distributed equally among the smaller size fractions.

Incoming particles of a given size distribution can be introduced selectively at any height. Particles reaching the end of the tank are removed in the effluent from one or more cells.

The core of the computer program is the MAEROS code developed by Gelbard (*40*) at Sandia National Laboratories. This code simulates the evolution of the size distribution of a multicomponent aerosol in a completely mixed air chamber. The code is adapted here to water suspensions and modified to incorporate the spatial inhomogeneity of the tank and the exchange of particle mass and fluid volume between the cells.

For k cells and q sections a system of $k \cdot q$ first-order ordinary differential equations results. The Runge–Kutta–Fehlberg integration routine that MAEROS uses proved to be inefficient, because the introduction of advective and turbulent mass fluxes renders the system of equation stiff. Instead, Gear's (*41*) modification of Adams's multistep variable order predictor–corrector method is used. Gear's method uses information from previous steps to predict the derivative functions and extrapolate them into the next interval, therefore allowing a larger step size.

The geometric constraint $v_{i+1} > 2v_i$ $(i = 0, 1, \ldots q-1)$, where the mass v_i is the upper limit of section i, is imposed in the code on the sectionalization of particle mass, thus minimizing the number of sectional coefficients to be computed (*39*). The latter depend on the section boundaries, the collision function $\beta(r_i,r_j)$, and the physical dimensions of the cells. Normally 15 sections are used covering the particle size diameter range from 10^{-7} to 10^{-3} m. The higher size range contains insignificant mass throughout the calculations, so the particle mass is conserved.

From the three coagulation mechanisms listed in Table I only shear induced particle collisions are influenced by the flow. For the cells where turbulent shear induced collisions are comparatively unimportant, the same sectional coefficients are used, thus reducing the computational work.

The ability of the computer model to reproduce the actual operating characteristics of a settling basin depends on the mesh size used, both in the physical space and in the particle size-space. A finite cell size introduces an artificial mixing in the tank. Increased vertical mixing and reduced longitudinal mixing enhance the settling rate. The selection of the number of cells and particle size sections represents a comprise between accuracy and computational cost. Eighteen cells (3 rows and 6 columns) and 15 particle size sections are used; thus, a total of 270 ordinary dif-

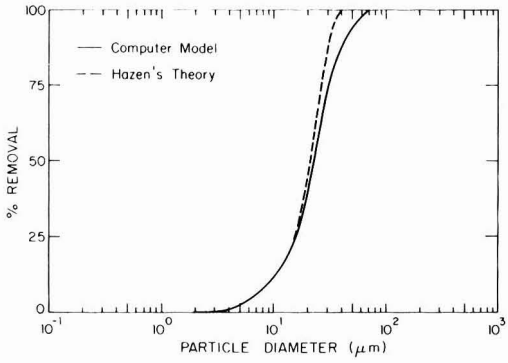

Figure 2. Numerical diffusion. The removal efficiencies for a noncoagulating suspension are compared with the predictions of Hazen's theory.

ferential equations are integrated simultaneously requiring about 12 min of central processor unit (CPU) time on an IBM 370/3032 computer for 5 h of settling. The numerical diffusion is evaluated by passage of a noncoagulating suspension through the basin. Particles enter the tank uniformly distributed with height and are subjected to a uniform velocity field. The removal efficiencies obtained are compared in Figure 2 with the predictions of Hazen's (*10*) theory. Since the mixing coefficients in sedimentation tanks are far from well-known, the additional mixing caused by the numerical diffusion is not considered to influence significantly the results.

4. *Conclusions*

The basic aim of this study has been to develop a numerical model simulating the operating of a rectangular sedimentation basin. The model includes all of the basic dynamics of particle collision and coagulation processes, including Brownian motion, turbulent shear, and differential sedimentation. Also included are estimates for the modification to particle collision efficiencies by van der Waals' forces and hydrodynamic interactions of particles. Specific attention is directed to transport processes such as particle advection, turbulent diffusion, and particle resuspension. The influence of the particle size–density relationship and floc deaggregation by turbulent shearing is also modeled. Of necessity, modeling of some of these processes has been somewhat empirical since the physical and biochemical nature of the flocs produced are often unique to a particular suspension. Nevertheless, the model developed is capable of predicting the evolution of an influent particle size distribution in flow through a sedimentation tank under both steady and unsteady operating conditions, and within reasonable computation time. Refinement of specific features of the model will only come from its application to actual operating systems coupled with further careful experimental work.

In the following paper (*42*) we apply the model to the operation of a specific sedimentation tank design and explore some of the possibilities for its use and further improvement.

Literature Cited

(1) EPA "Process Design Manual for Suspended Solids Removal"; Environmental Protection Agency: 1975.
(2) Alarie, R. L.; McBean, E. A.; Farquhar, G. J. *J. Environ. Eng. Div. (Am. Soc. Civ. Eng.)* **1980**, *106*, (EE2), 293–309.
(3) Tebbutt, T. H.; Christoulas, D. G. *Water Res.* **1975**, *9*, 347–356.
(4) Kawamura, S. *J.*—Am. *Water Works Assoc.* **1981**, *73*, 372–379.
(5) El-Baroudi, H. M. *J. Sanit. Eng. Div. Am. Soc. Civ. Eng.* **1969**, *95* (SA3), 527–544.
(6) Humphreys, H. W. *J.—Am. Water Works Assoc.* **1975**, *67*, 367–372.
(7) Shiba, S; Inoue, Y. *J. Environ. Eng. Div. (Am. Soc. Civ. Eng.)* **1975**, *101* (EE5), 741–757.
(8) Lawler, D. F.; O'Melia, C. R.; Tobiason, J. E. In "Particulates in Water: Characterization, Fate, Effects and Removal"; American Chemical Society: Washington, DC, 1980; Adv. Chem. *Ser.* No. 189.
(9) Dick, R. I. *J. Environ.* Eng. Div. (*Am. Soc. Civ. Eng.*) **1982**, *108* (EE2), 430–432.
(10) Hazen, A. Trans. *Am. Soc. Civ. Eng.* **1904**, *53* (980), 45–88.
(11) Camp, T. R. Trans. *Am. Soc. Civ. Eng.* **1945**, *111* (146), 895–936.
(12) Vanoni, V. A.; Brooks, N. H. Sedimentation Laboratory, California Institute of Technology, Pasadena, CA, 1957, Report E-68.
(13) Fischer, H. B.; List, E. J.; Koh, R. C. Y; Imberger, J.; Brooks, N. H. "Mixing in Inland and Coastal Waters"; Academic Press: New York, NY, 1979; Chapter 4.
(14) Blackadar, A. K. *J. Geophys. Res.* **1962**, *67* (8), 3095–3102.
(15) Tennekes, H.; Lumley, J. L. "A First Course in Turbulence"; The MIT Press: Cambridge, MA, 1972.
(16) Rudolfs, W.; Balmat, J. L. *Ind. Wastes* **1952**, *24* (3), 247–256.
(17) Valioulis, I. A.; List, E. J. *Adv. Colloid Interface Sci.*, in press.
(18) Smoluchowski, M. *Phys. Z.* **1916**, *17*, 557–585.
(19) Pearson, H. J.; Valioulis, I. A.; List, E. J. *J. Fluid Mech.*, in press.
(20) Findheisen, W. *Meteorol. Z.* **1939**, *56*, 365–368.
(21) Hunt, J. R. *J. Fluid Mech.* **1983**, *122*, 169–185.
(22) Adler, P. M. *J. Colloid Interface Sci.* **1981**, *83*, 106–115.
(23) Neiburger, M.; Lee, I. Y.; Lobl, E.; Rodriguez, L., Jr. Conference on Cloud Physics of the American Meterological Society, Tucson, AZ, 1974; pp 73–78.
(24) Davis, M. H. *J. Atmos. Sci.* **1972**, *29*, 911–913.
(25) Tambo, N.; Watanabe, Y. *Water Res.* **1979**, *13*, 409–419.
(26) Vold, J. M. *J. Colloid Sci.* **1963**, *18*, 684–695.
(27) Sutherland, D. N.; Goodarz-Nia, I. *Chem. Eng. Sci.* **1971**, *26*, 2071–2085.
(28) Sutherland, D. N. *J. Colloid Interface Sci.* **1967**, *25*, 373–380.
(29) Thiele, H.; Levern, H. S. *J. Colloid Sci.* **1965**, *20*, 679–694.
(30) Hocking, L. M.; Jonas, P. R. *Q. J. Metereol. Soc.* **1970**, *96*, 722–729.
(31) Adler, P. M. *J. Colloid Interface Sci.* **1981**, *81*, 531–535.
(32) Sutherland, D. N.; Tan, C. T. *Chem. Eng. Sci.* **1970**, *25*, 1948–1950.
(33) van de Ven, T. G. M.; Mason, S. G. *Colloid Polym. Sci.* **1977**, *255*, 794–804.
(34) Friedlander, S. K. *J. Meteorol.* **1960**, *17*, 373–374.
(35) Faisst, W. K. California Institute of Technology, Pasadena, CA, 1976, EQL Report 13.
(36) Vanoni, V. A. In "Sedimentation Engineering"; Vanoni, V. A., Ed.; ASCE; New York, NY, 1977.
(37) Takamatsu, T.; Naito, M.; Shiba, S. *Trans. Jpn. Soc. Civ. Eng.* **1970**, *2* (2), 389–293.
(38) Parker, D. S.; Kaufman, W. J.; Jenkins, D. *J. Sanit. Eng. Div., Am. Soc. Civ. Eng.* **1970**, *98* (SA1), 79–99.
(39) Gelbard, F.; Seinfeld, J. *J. Colloid Interface Sci.* **1980**, *78*, 485–501.
(40) Gelbard, F., Chevron Oil Field Research, La Habra, CA, personal communication, 1982.
(41) Gear, C. W. "Numerical Initial Value Problems in Ordinary Differential Equations"; Prentice-Hall: Englewood Cliffs, NJ, 1971.
(42) Valioulis, I. A.; List, E. J. *Environ. Sci. Technol.*, following paper in this issue.

Received for review January 14, 1983. Accepted August 22, 1983. Financial support for this work was provided by NOAA/Sea Grant NA80AA-D-00120, NOAA Grant NA80RA-DO-0084, and a Mellon Foundation Grant to the Environmental Quality Laboratory at Caltech.

Environ. Sci. Technol. 1984, 18, 248–253

Numerical Simulation of a Sedimentation Basin. 2. Design Application

Iraklis A. Valioulis and E. John List*

W. M. Keck Laboratory of Hydraulics and Water Resources, Division of Engineering and Applied Science, California Institute of Technology, Pasadena, California 91125

■ A numerical model of a rectangular settling tank is used to study the importance of selective variables on the settling process while demonstrating the capabilities of the computer simulation. The computer model follows the spatial and temporal development of the influent particle size distribution toward the outlet of the tank based on the fundamental mechanisms which govern particle motion and growth. It is shown that both the removal efficiency of a flocculating suspension and the effluent particle size distribution are influenced strongly by the mass concentration in the inflow, the influent particle size distribution, the floc size–density relationship, and the collision efficiencies of the particles. It is suggested that future experimental work should focus on obtaining information on the size–density relationship, the reentrainment of the deposits, and the collision efficiencies of flocs.

1. Introduction

Current design of settling tanks is empirical, based mainly on experience obtained from operating basins. Cost analyses cannot be performed, and frequently sedimentation basins fail to accomplish the goal they have been designed for. In part 1 of this work (*1*) we developed and described in detail a numerical simulation of a rectangular settling tank based on the fundamental mechanisms that govern particle motion and growth. The numerical model follows the spatial and temporal development of the influent particle size distribution through the tank, predicts the overall performance of the system, and gives detailed information on the particle size distribution at any location in the tank.

In this paper the simulation is applied to an actual system and reveals the importance of properties of the suspension and design parameters on the tank performance while demonstrating the capabilities of the simulation model.

2. Sensitivity Analysis

A standard wastewater treatment plant with parameters representative of treatment practice (Table I) is selected to illustrate the capabilities of the model. A logarithmic velocity profile is assumed. The influent particle mass flux is proportional to the influent fluid flux. Particles are removed as deposits when they reach the bottom of the tank or as effluent from all three cells at the end of the basin. Suspended solids, as traditionally defined, include all particles with diameters larger than 1 μm; colloidal particles range in size from 0.1 to 1 μm.

It is common practice to evaluate the performance of a settling tank by the fraction R_{SS} of suspended solids removed. This is only one measure of tank efficiency since the effectiveness of the settling process depends on how the mass is distributed in size space. R_{SS} is reported here for all cases examined together with the total solids removal efficiency R_{TS}. The relative magnitude of R_{SS} and R_{TS} indicates the importance of flocculation in transferring particle mass from the colloidal particle size range (<1 μm) to the suspended size range (>1 μm).

Sensitivity analysis is performed to determine the influence of selective variables on the steady-state plant performance. For the standard plant steady-state operation is reached after about 5 h of constant inflow. Under section 4 the dynamic response of the sedimentation basin to a temporally variable flow rate or concentration of inflow is examined.

Table I

Standard Plant	
depth	4 m
length	40 m
detention time	2 h
overflow rate	48 m^3/(m^2 day)

Influent Suspensions

raw water	total solid concn, mg/L	slope parameter α[a]	density
suspension A	400	4	variable[b]
suspension B	400	4	constant[c]
suspension C	200	4	variable
suspension D	400	3	variable

[a] The size distribution function $n(d)$ of the influent suspension follows the power law $n(d) = (\Delta N/\Delta d) = Cd^{-\alpha}$, where ΔN is the number of particles with a diameter in the size range Δd, per unit volume of fluid, the exponent α is a constant, and the constant C depends on the influent mass concentration. [b] For $r = 1.75$ μm, the relationship proposed by Tambo and Watanabe (*2*) is used (see ref 1):

$$\rho_f - \rho_w = 1.3/(200r)^{0.9}$$

where ρ_f and ρ_w are the densities (kg/m^3) of the floc and the water, respectively, and r is the particle radius (μm). For smaller particles, $\rho_f - \rho_w = 1650$ kg/m^3. [c] $\rho_f - \rho_w = 1000$ kg/m^3.

3. Steady-State Operation

(a) Constant/Variable Particle Density. The effluent particle size distributions of two suspensions, one following the size–density relationship of Tambo and Watanabe (*2*) (suspension A, standard case) and one with a constant particle density of 2000 kg/m^3 for all particles sizes (suspension B), are compared in Figures 1 and 2; Q is the mass concentration, and d is the particle diameter. The curves are best-fit approximations to the results of the simulation. For both suspensions the efficiencies for collisions between flocs are used. The influent size distribution has a slope parameter of $\alpha = 4$ which gives the same influent number size distribution but different influent mass distributions. The solid removal efficiencies are $R_{TS} = 61\%$ and $R_{SS} = 44\%$ for the variable density suspension and $R_{TS} = 53\%$ and $R_{SS} = 45\%$ for the constant density suspension. Large particles (larger than 20 μm) are removed less effectively in the case of the variable density suspension because of their reduced density. Their presence, however, increases the coagulation rate and the transfer of mass toward larger size sections. As a result, the number of particles in the size fraction 0.5–20 μm remaining in the effluent is lower for the variable density suspension, and the overall mass removal efficiency is higher. However, note that suspended solids analysis would, contrary to this result, indicate a similar tank performance in the treatment of the two suspensions.

 0013-936X/84/0918-0248$01.50/0

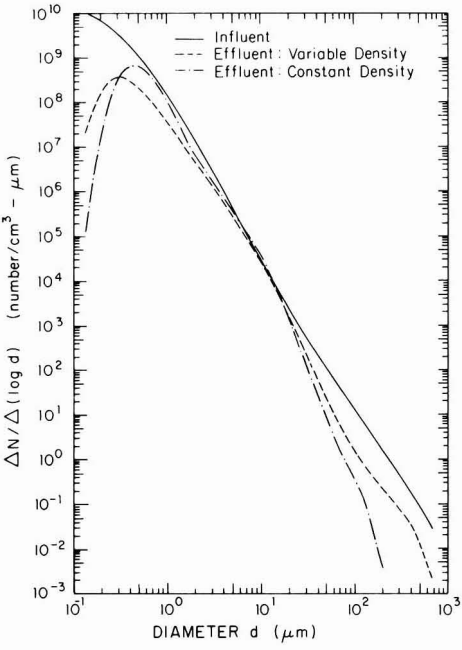

Figure 1. Comparison of variable density suspension A with constant density suspension B. Number distribution function.

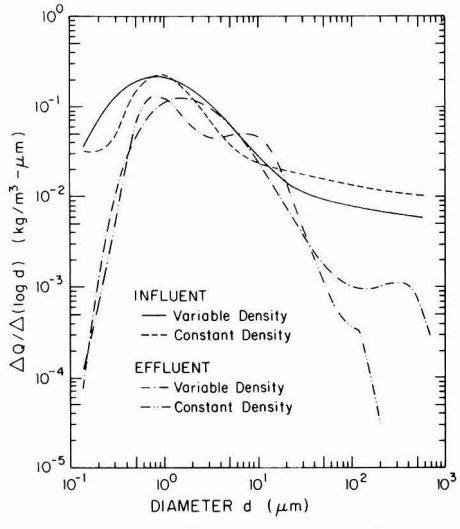

Figure 2. Comparison of variable density suspension A with constant density suspension B. Mass distribution function.

The development of the mass size distribution of suspensions A and B along the tank, averaged over its cross section, is shown in Figure 3. Two distinctive peaks in both mass size distributions develop near the particle sizes 0.5 and 10 μm. The constant density suspension loses all particles larger than 10 μm by the time it reaches the midpoint of the tank, but coagulation recreates such particles near the end of the basin. This is further illustrated in Figure 4 where the total mass (per unit width) deposited along the tank during the 2-h detention time under steady-state conditions is shown. For both suspensions most of the removal takes place in the first quarter of the tank length. Depletion of the large particles in suspension reduces the deposition rate of the constant

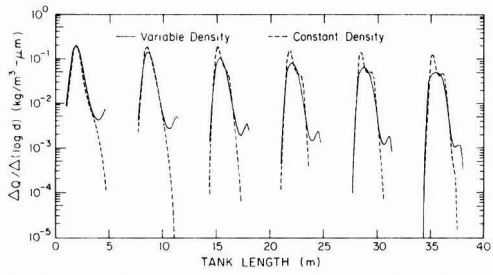

Figure 3. Evolution of the mass distribution functions of variable density suspension A and constant density suspension B through the tank.

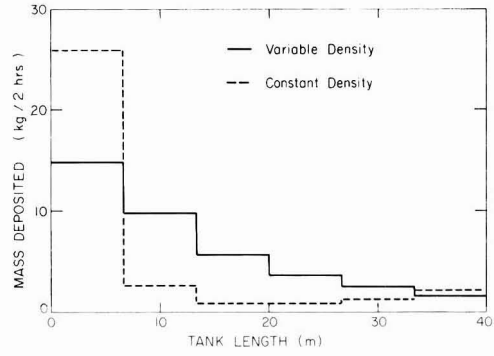

Figure 4. Mass accumulated at the bottom of the tank when variable density suspension A and constant density suspension B are treated under steady-state conditions.

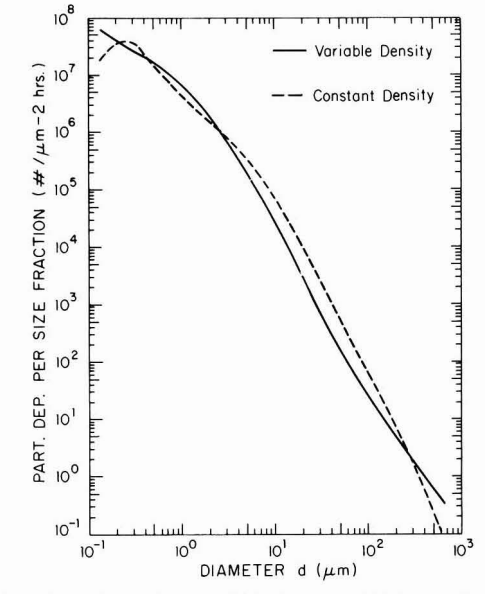

Figure 5. Number distribution in the deposits when variable density suspension A and constant density suspension B are treated under steady-state conditions.

density suspension near the middle of the tank and some time is required before settleable particles are created and settled. In contrast, a sludge blanket of decreasing thickness accumulates when the variable density suspension is treated.

The average particle number distribution in the deposits is depicted in Figure 5. Clearly this is not the particle size

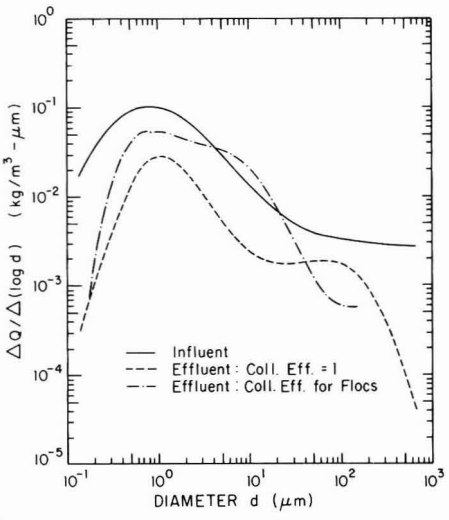

Figure 6. Effect of the collision efficiency on the effluent mass distribution function of variable density suspension C.

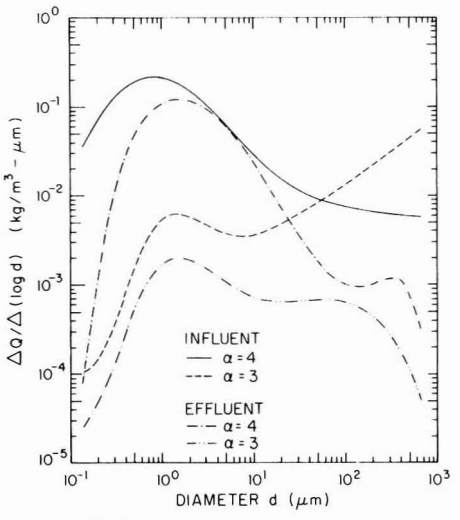

Figure 7. Comparison of the effluent mass distribution functions of suspension A with slope parameter $\alpha = 3$ and suspension D with slope parameter $\alpha = 4$.

distribution expected in the sludge since hindered motion and compression settling in the high density zone near the bottom of the tank will alter the sludge size distribution. It provides the input parameters, however, for the modeling of these settling processes. Information on the quantity and quality of the sludge blanket is useful in designing the sludge removal facilities of the tank.

(b) Hydrodynamic Efficiencies. In modeling particle coagulation in hydrosols the collision efficiencies are commonly either assumed unity or constant, independent of the absolute and relative sizes of the interacting particles. A variable density suspension (suspension C) with half the total solid concentration of the standard case is used to evaluate the importance of employing the proper collision efficiencies. Two cases are compared in Figure 6, one using the rectilinear coagulation functions (efficiency unity) and one the collision efficiencies for flocs (see section 2b in ref 1). The effluent particle size distributions are completely different in shape, and the reduction in the removal efficiency of the tank is dramatic. When the collision efficiencies for flocs are used, only 16% of the suspended and 39% of the total solids are removed, compared with 87% and 82%, respectively, for the hydrodynamically noninteracting suspension.

It is interesting to compare the removal efficiencies of the tank with suspensions A and C (where in both cases the collision efficiencies for flocs are used). Suspension A has a total solid concentration of 400 mg/L of which 250 mg/L is defined as suspended solids. For this influent 61% of the total solids are removed in the tank and 44% of the influent solids larger than 1 μm (the suspended solids), i.e., $R_{SS} = 44\%$. For influent suspension C with 200 mg/L total solids and 125 mg/L suspended solids, 39% of the total solids are removed and 16% of the suspended solids ($R_{SS} = 16\%$). Thus, halving the initial solid concentration reduced the effluent concentration by a factor of 1.28 for total solids and 1.33 for suspended solids. The low figure (16%) for the suspended solid removal for suspension C is indicative of the production of suspended solids by the coagulation process. A noncoagulating suspension gives removal efficiencies $R_{TS} = 20\%$ and $R_{SS} = 33\%$. Coagulation transfers mass through the particle size spectrum toward settleable particle sizes so that the total solid removal efficiency is increased but the suspended solids removal efficiency is reduced. Coagulation is responsible for this paradox. For the hydraulic conditions and the size–density relationship used here only particles larger than about 20 μm are removed by settling. Coagulation accumulates particle mass in the size range 1–40 μm, and this is characteristic of all simulations presented above. The rate of mass transfer to particle sizes larger than 40 μm is slow since the number of large particles which will extract mass from the immediately smaller size fractions is reduced because of settling, hence the remarkable reduction in suspended solid removal efficiency for the coagulating suspensions.

(c) Influent Particle Size Distribution. Suspension D has a total solid concentration of 400 mg/L, as for suspension A, but a flatter particle size distribution with $\alpha = 3$. This value of α implies a uniform surface area concentration distribution and increasing volume and mass concentrations with increasing particle size (see eq 2.12 in ref 1). Both coagulation and settling are enhanced, and so 98% of the solids are removed when suspension D is treated under the standard hydraulic conditions. Figure 7 illustrates the change in the mass distribution when suspensions A and D pass through the tank.

The volume average diameter is defined as

$$d_a = \frac{\sum_{i=1}^{q} \Delta N_i g_i}{\sum_{i=1}^{q} \Delta N_i}$$

where ΔN_i and g_i are respectively the number and the geometric mean diameter of the particles in section i. The development of d_a along the length of the tank for suspensions A and D is shown in Figure 8. The volume average diameter increases continuously in the case of suspension A, indicating that coagulation transfers mass through the size spectrum toward large particle size sections at a faster rate than sedimentation removes suspended mass. The situation is reversed for suspension D which has relatively more mass at large particle sizes.

(d) Longer Tank. For the same detention time a longer but more shallow tank with reduced overflow rate can be used. Longitudinal dispersion is enhanced and vertical

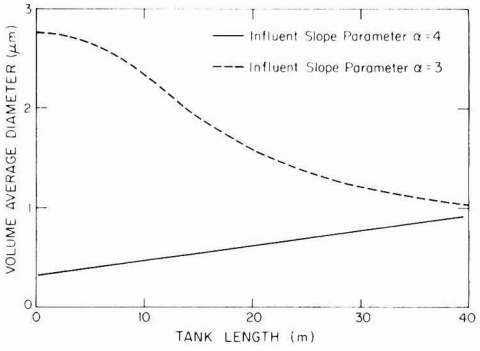

Figure 8. Evolution of the volume average diameter of variable density suspensions A (α = 3) and D (α = 4).

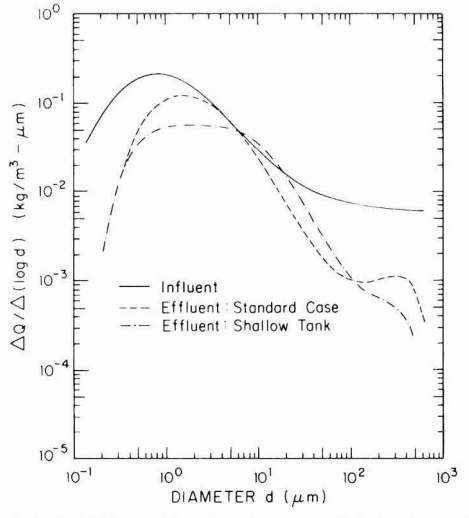

Figure 9. Comparison of the effluent mass distribution functions for the standard and the shallow tank both treating variable density suspension A.

turbulent mixing reduced. Large particles spend less time suspended, collecting fewer particles as they fall.

Suspension B was treated in a settling basin 64 m long and 2.5 m deep. The solid removal efficiencies were R_{TS} = 50% and R_{SS} = 27%, indicating a reduction in the removal efficiency of the basin. Figure 9 compares the effluent characteristics for the standard basin and the longer one, both treating suspension A. The stronger shearing in the shallow tank promoted coagulation of particles in the size range 0.5–10 μm, but larger particles, whose coagulation rate depends largely on differential settling induced collisions, tend to remain in suspension.

(e) Recirculation. The logarithmic velocity distribution is not realistic near the inlet and outlet of the basin and has been used above only to provide a convenient flow regime in order to examine other parameters of interest. Published data on the flow fields in settling tanks do not satisfy continuity of fluid mass. Thus, a flow field is assumed, including a circulation current, as shown in Figure 10. This is obviously one of an infinite number of possible flow patterns that can develop in a sedimentation tank and assumes that the inflow has a jetlike behavior. A variable mesh size is used in the vertical direction, and it is assumed, first, that one-fourth of the inflow moves horizontally along the upper row of cells and, second, that all

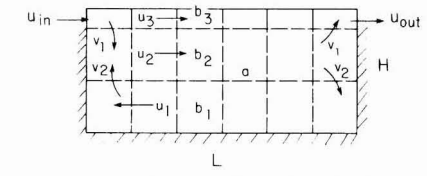

Figure 10. Schematic diagram of the recirculating flow pattern.

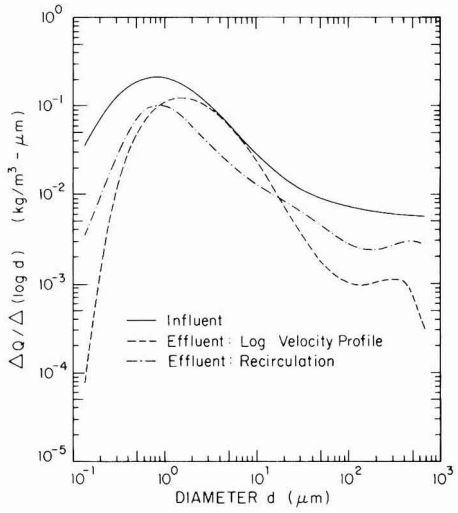

Figure 11. Effect of the flow field on the effluent mass distribution function of variable density suspension A.

vertical velocities in the tank are equal. This crude flow pattern enhances the mixing and the turbulence intensity at the lower section of the tank. The vertical mixing coefficient is estimated by using the mixing-length argument from

$$\hat{E} = (b_n + b_{n+1})(u_n + u_{n+1}) \qquad n = 1, 2$$

where b_n and u_n are, respectively, the depth and the horizontal velocity in the cells in row n. The turbulent energy dissipation rate, per unit mass of fluid, is estimated by using eq 2.3 in part 1 of this work (*1*). The intense local shearing enhances the coagulation rate but also breaks up any flocs which, according to eq 2.15 in ref 1, grow larger than about 1000 μm in diameter.

Figure 11 compares the tank effluent when suspension A is subjected to the recirculating flow field with the effluent of the standard case. The increased mixing in the tank, induced by the circulating current, causes more large particles to be carried over the effluent weir. Enhanced coagulation rates and the breakup of flocs exceeding 1000 μm in diameter—their mass is equally distributed among the other sections—result in smoother number and mass distributions in the effluent. The total solid removal efficiency remains 61%, but the suspended solid removal efficiency is increased to 54%, as compared with the standard case.

(f) Scouring. The sensitivity of the tank performance to scouring was investigated by performing simulation runs at various values of the resuspension parameter s (see eq 2.13 in ref 1), all other parameters remaining the same. The removal efficiencies obtained when suspension A was treated are listed in Table II. Included in the same table are the results for a noncoagulating suspension with the same characteristics as suspension A. In the case of the noncoagulating suspension the tank performance deteri-

Table II. Sensitivity of the Tank Performance to Scouring

	resuspension parameter, s^a	% total solids removed, R_{TS}	% suspended solids removed, R_{SS}
coagulating suspension	0	60.1	42.8
	0.15	60.6	43.6
	0.4	60.8	44.1
	0.8	55.7	38.2
noncoagulating suspension	0	21.6	33.9
	0.15	20.0	33.0
	0.4	18.8	29.7
	0.8	13.8	21.3

[a] See eq 2.13 in ref 1.

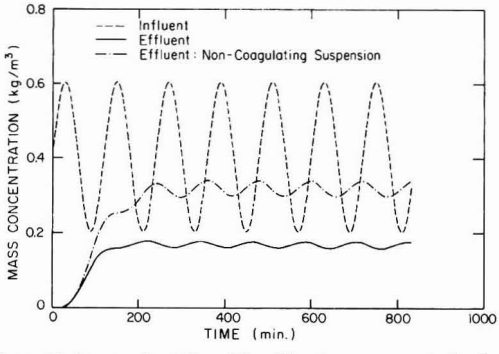

Figure 12. Temporal variation of the effluent mass concentration for a sinusoidally varying concentration in the inflow. The frequency of the sinusoidal input is equal to the inverse of the detention time (2 h), and its amplitude is equal to half the steady-state influent concentration.

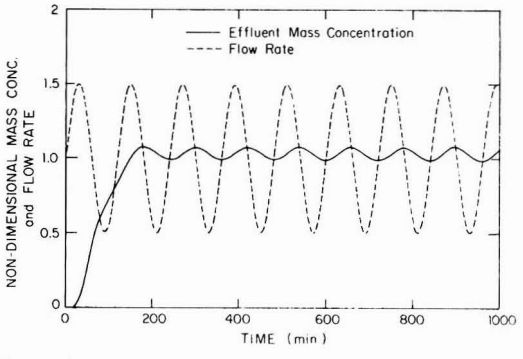

Figure 13. Nondimensional flow rate and effluent mass concentration. The flow rate is nondimensionalized with its time-averaged value, and the concentration with the steady-state effluent concentration is obtained when the flow rate is steady and equal to the time-averaged flow rate. The frequency of the sinusoidal input is equal to the inverse of the detention time (2 h), and its amplitude is equal to half the steady-state flow rate.

orates as the rate of resuspension increases. The sensitivity of the solid removal efficiency to s is in accordance with the results of Takamatsu et al. (*3*) for a nonflocculating suspension. On the contrary, when a suspension that undergoes coagulation is treated, resuspension of the deposits improves slightly the tank performance for small values of the resuspension parameter s; for large s the tank performance deteriorates.

Coagulation in the high mass concentration regions near the bottom of the tank, resulting from resuspension of previously deposited material, transfers mass toward larger particle size sections with a subsequent improvement in the tank performance. As the resuspension flux increases, however, a critical situation is reached, where coagulation cannot compensate for the reduced settling rates and so the solid removal efficiency of the basin is reduced.

4. *Unsteady Response*

In actual wastewater treatment plants the flow rate and the concentration in the inflow may vary considerably with time. The computer simulation is capable of predicting the dynamic response of the settling tank to a temporally variable input. For the purpose of demonstrating the capabilities of the computer model the effluent characteristics are investigated when a periodic variation in the influent concentration or the flow rate occurs.

The variable density suspension A is used to investigate the response of the tank to a sinusoidal variation in the influent concentration or the flow rate. The frequency of the sinusoidal input is equal to the inverse of the residence time of the suspension in the tank (2 h) and its amplitude equal to half the steady-state input.

Figure 12 shows the temporal variation in the effluent concentration when the mass concentration in the inflow varies sinusoidally with time. The tank acts as a filter and smooths the variations in the influent concentration. The effluent characteristics of a noncoagulating suspension, plotted in the same figure, indicate that numerical diffusion and turbulent dispersion and mixing are mainly responsible for the filtering action of the tank, while coagulation reduces significantly the time-averaged effluent concentration. Coagulation also reduces the time between the effluent and influent peak concentrations (modal time) from 90 min for the noncoagulating suspension to about 60 min. In both cases the modal time is smaller than the theoretical detention time; observed dispersion curves in model settling tanks show the same trend (*4*, *5*).

Figure 13 illustrates the effluent response to a sinusoidally varying flow rate. In this figure the flow rate, nondimensionalized with its time-averaged value, and the effluent mass concentration, nondimensionalized with the steady-state effluent concentration obtained when the flow rate is steady and equal to the time-averaged flow rate, are plotted against time. Note the very short modal time, about 30 min, and that the time-averaged effluent concentration is slightly higher than the one obtained when the flow rate is steady.

Figure 14 shows the mass distribution at the maximum and minimum effluent concentrations for the two time variable input simulations performed. The variation in the mass concentration function is larger when the flow rate varies with time.

5. *Conclusions*

A numerical model has been developed capable of simulating all of the essential features of the operation of a sedimentation tank. The model is based on a computer solution of an extended general dynamic equation describing the collisions and coagulation of particles in

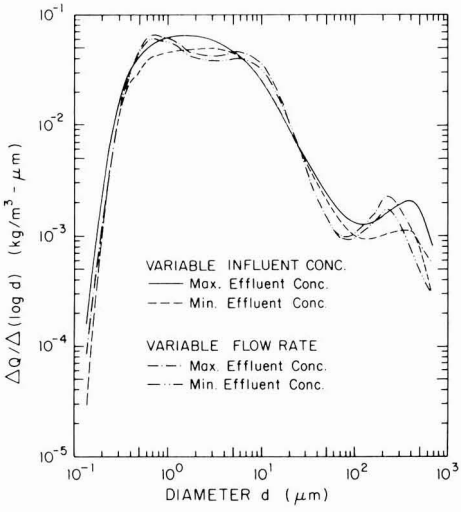

Figure 14. Effluent mass distribution functions for sinusoidally varying influent concentration and flow rate.

suspension. In this paper the model has been applied to a specific sedimentation tank design for the purpose of elucidating features of the model.

From the limited number of simulations presented here it is evident that particle collision efficiencies, the particle size–density relationship, and the shape of the influent particle size distribution affect dramatically both the characteristics of the effluent size distribution and the overall tank performance. The collision efficiencies between particles and the particle size–density relationship were modeled, of necessity somewhat arbitrarily, since, to the knowledge of the authors, no related published results exist; both depend on the physical and biochemical nature of the flocs and will be unique for a particular suspension, so their determination requires experimental work.

Scouring was modeled empirically, so conclusions cannot be drawn. Experimental and theoretical work on resuspension of cohesive sediments is in progress (*6*), and the results can be easily incorporated in the simulation.

The simulations of tank operation under un-steady-state inflow conditions suggest that moderate variations in influent concentration and flow rate do not significantly affect the quality of the effluent.

In summary, the model appears to give realistic simulations of the operation of a specific sedimentation tank. Clearly, further modifications, improvements, and trials will be necessary before it can be used with confidence in the design of new facilities. At this juncture, it appears that more experimental work on the nature of the particle size–density relationship, the resuspension of deposits, and the particle collision efficiencies is the crucial next step in improving the realism of the model.

Literature Cited

(1) Valioulis, I. A.; List, E. J. *Environ. Sci. Technol.*, preceding paper in this issue.
(2) Tambo, N.; Watanabe, Y. *Water Res.* **1979**, *13*, 409–419.
(3) Takamatsu, T.; Naito, M.; Shiba, S. *Trans. Jpn. Soc. Civ. Eng.* **1970**, *2* (2), 289–293.
(4) El-Baroudi, H. M. *J. Sanit. Eng. Div., Am. Soc. Civ. Eng.* **1969**, *95* (SA3), 527–544.
(5) Kawamura, S. *J.—Am. Water Works Assoc.* **1981**, *73*, 372–379.
(6) NOAA "Proceedings of a Pollutant Transfer by Particulates Workshop"; National Oceanic and Atmospheric Administration: Seattle, WA, 1982; pp 191–223.

Received for review January 14, 1983. Accepted August 22, 1983. Financial support for this work was provided by NOAA/Sea Grant NA80AA-D-00120, NOAA Grant NA80RA-DO-0084, and a Mellon Foundation Grant to the Environmental Quality Laboratory at Caltech.

Analysis for Trace Elements in Magnetohydrodynamic (MHD) Pilot Power Plant Effluents

Tom E. Clevenger,* Edward J. Hinderberger, Jr., Dennis A. Yates,† and W. Dennis James‡

Environmental Trace Substances Research Center, Columbia, Missouri 65201

■ Instrumental neutron activation analysis and inductively coupled argon plasma emission were evaluated as to their applicability for the multielement analysis of coal, slag, and fly ash from the University of Tennessee Space Institute's Magnetohydrodynamic pilot plant. Both techniques were successfully used in the analysis of these samples. The agreement between results from the instrumental neutron activation analysis and inductively coupled argon plasma emission methods was excellent, as was their agreement with NBS standard reference material values. The solubilization procedure developed for the ICAP analysis was capable of dissolving totally any of the MHD coal, slag, and fly ash samples. There is still a problem with the loss of the volatile elements and silicon when this technique is used.

Introduction

Magnetohydrodynamics (MHD) (*1*) is an energy alternative in which electricity is generated directly from thermal energy. This is accomplished by passing an electrically conductive fluid through a magnetic field, thereby inducing a voltage drop across the fluid stream. Electrodes convey the electricity to an inverter where the direct current power, naturally produced by the system, is transformed into alternating current, which can be transmitted directly into an electric power grid. MHD eliminates the energy loss due to the conversion of thermal to mechanical energy. When used in combination with a conventional steam plant, the efficiency is predicted to be about 50% or greater, as compared to 33–40% for the conventional power plant.

Initial development of MHD began during the late 1950s. Programs exist both in this country and abroad, notably in Japan and the U.S.S.R. The basic distinction between the U.S. and foreign programs is the emphasis on the type of fuel. The U.S.S.R. is currently using natural gas, while Japan is using fuel oil. In the U.S., emphasis is on coal as the primary fuel due to its abundance.

The range of pollutants from a MHD system is expected

†Present address: Perkin-Elmer Corp., Norwalk, CT 06856.
‡Present address: Department of Chemistry, Texas A&M University, College Station, TX 77840.

to be similar to that associated with direct combustion processes. However, due to the extremely high temperatures required in the MHD process as compared to the relatively low-temperature direct combustion technology, different amounts and species of various contaminants may be produced. In order to analyze these new waste products, new analytical methods may need to be developed.

The objective of this work was to evaluate the applicability of the analytical multielemental techniques of instrumental neutron activation analysis (INAA) and inductively coupled argon plasma emission spectroscopy (ICAP) for the analysis of the waste products produced from MHD power plants. The following elements were capable of being determined when these methods were used: (a) *trace elements*, lead, cadmium, nickel, beryllium, mercury, arsenic, antimony, tin, chromium, manganese, cobalt, copper, zinc, selenium, molybdenum, boron, and vanadium; (b) *major constitutents*, silicon, aluminum, iron, calcium, sodium, titanium, potassium, and magnesium.

The types of samples analyzed during this study included coal, slags, and fly ash from the University of Tennessee Space Institute's MHD pilot plant as well as several standard reference materials.

Experimental Section

Instrumental Neutron Activation Analysis. The samples underwent two separate procedures. One was the short pneumatic transfer tube irradiation and the second involved a long irradiation.

(1) **Short Procedure.** A total of 20–40 mg of each sample was weighed and sealed into a precleaned polyethylene irradiation vial. Standards were prepared by evaporation of the liquid primary standards onto filters, which were then sealed in vials. Each sample, standard, etc., was irradiated for 10 s in a pneumatic transfer position in the reactor's reflector at a thermal flux of 10^{14} neutrons/(cm^2·s) and counted for 250 s after a 10-min delay.

(2) Long Procedure. A total of 20–40 mg of each sample was weighed and sealed into a Suprasil quartz irradiation vial. For standards, a metal solution was evaporated onto either purified Al_2O_3 or SiO_2 by using very low heat. Low heat had to be used since it was found that Se was lost when exposed to high heat. Samples, standards, etc., were placed in an aluminum can, which was positioned for 20 h at a thermal flux of 10^{14} neutrons/(cm^2·s). After the samples were returned to the laboratory, the quartz vials were cleaned with aqua regia. After 2–3 weeks, they were counted to obtain information on intermediate half-lived nuclides. They were counted again after 2 months for measurement of longer lived nuclides.

All radioactive counting was done on a Nuclear Data 600 pulse height analyzer system, on Ortec lithium-drifted germanium detector, and associated electronics. All samples were counted with a system dead time of less than 10% and normalized to a pulser. Data reduction was performed by transferring the raw spectral data via magnetic tape to the University of Missouri's IBM system 370/168 computer. The GAM ANAL computer program was used for the data reduction. The isotopes used for the analyses are listed in Table I along with other pertinent information.

Inductively Coupled Argon Plasma Emission Analysis. The sample preparation procedure consisted of grinding the sample and running it through a 400-mesh screen. For coal 1-g sample was placed in a platinum crucible and dry ashed at 500 °C overnight. The dry ashed coal (or 0.2 g of fly ash) was transferred to a 100-mL Teflon beaker. The sample was wetted with 5 mL of deionized water. Two milliliters of $HClO_4$ (70%) and 12 mL of HF (40%) were added, and the mixture was heated to near dryness. An additional 8 mL of HF was added and heated to dryness to drive off excess $HClO_4$. A total of 2 mL of $HClO_4$ and several milliliters of water were added and evaporated to dryness. The residue was dissolved in 8 mL of 1:1 HCl and approximately 10 mL of water. It was then diluted to 25 mL with deionized water and analyzed on a Jarrell-Ash Model 975 32-channel Atom-comp ICAP emission spectrometer.

Table I. Information on Isotopes Used for Instrumental Neutron Activation Analysis

	isotope counted	γ energy counted, keV	half-life
		Short Irradiation	
Cu	^{66}Cu	1039	5.10 min
Na	^{24}Na	1368	15.0 h
V	^{52}V	1434	3.75 min
K	^{42}K	1524	12.4 h
Al	^{28}Al	1779	2.27 min
Mn	^{56}Mn	1811	2.28 h
Ca	^{49}Ca	3083	8.7 min
		Long Irradiation	
Se	^{75}Se	265	120 days
Cr	^{51}Cr	320	27.7 days
Fe	^{59}Fe	1099 and 1292	44.6 days
Co	^{60}Co	1173 and 1332	5.27 years
Sb	^{124}Sb	1693	60.2 days

Results and Discussion

Inductively Coupled Argon Plasma Emission Analysis. Because this technique requires the sample to be in solution, the sample preparation method is a critical step. Several methods were reviewed. Lithium metaborate and lithium tetraborate fusions were reported to be successful for dissolving some siliceous coal ash and related materials (*2–5*). Many different types of simple acid digestions were reported to have varying degrees of success. These included combinations of H_2SO_4, $HClO_4$, and HF (*6–8*), the use of H_2SO_4 and H_2O_2 (*9,10*), $HClO_4$–HIO_4 (*11*), HCl–HNO_3 (*12*), HNO_3–K_2ClO_4 (*13, 14*), and HNO_3–$HClO_4$ (*15*). An acid digestion bomb (*16–19*) was suggested as having the most potential of being the "universal" dissolution method, since elements such as As, Se, and Cr which can volatize when heated are retained in the bomb.

Several preparation procedures were tested, including various acid digestions, bomb digestions, and base fusions. To be acceptable, the preparation method would have to completely dissolve any type of MHD coal waste products such as coal, slag, or fly ash without interfering with the ICAP analysis. The basic fusions were successful in dissolving all types of samples but produced a final solution extremely high in salt content. Solutions with high dissolved solids will clog the nebulizer on the ICAP. In order to use the solutions from a fusion preparation, they would have to be diluted. In making such a dilution, several trace elements which are low will be rendered undetectable. This was found unsatisfactory. The fusion method was the only one that did allow for the successful analysis of silicon. However, because of the intense heat involved, any element easily volatilized would be lost.

The bomb digestion method offered the potential of a preparation method that would not lose the volatile elements. This method gave incomplete dissolution for the fly ash and slag samples. The company selling the product stated that a larger surface area would result in complete dissolution. The samples were ground to a finer mesh size, but incomplete dissolution still resulted.

The method chosen for this study, multiacid digestion,

Table II. Analysis Results Found for NBS SRM 1633 Fly Ash by Inductively Coupled Argon Plasma

	concentrations, μg/g		
element	current study	NBS value	Ondov et al. (39)
Ag	< 10		
Al	11900		12700
B	<40		
Ba	2540		2700
Be	15	(12)	
Ca	48100		47000
Cd	<2	1.45 ± 0.06	
Co	54	(38)	
Cr	110	131 ± 2	
Cu	132	128 ± 5	
Fe	64600		62000
Li	186		
Mg	13400		
Mn	465	493 ± 7	
Mo	<5		
Na	3230		3200
Ni	100	98 ± 3	
Pb	<100	70 ± 4	
Sn	<5		
Sr	1380	(1380)	
Ti	8140		7400
V	236		
Zn	206	214 ± 8	
K	15600	210 ± 20	16100

gave complete dissolution of all sample types. At first the "seeded" samples (large amount of potassium added to provide better ionization for MHD) produced some undissolved material after preparation. It was determined that this was $KClO_4$ and that its solubility product had been exceeded. This was easily corrected by decreasing the sample size (0.2 g). The resulting solution was compatible for ICAP analysis. It did have limitations. The volatile elements were lost as well as silicon. Except for these elements, this sample preparation in conjunction with ICAP was very successful. As can be seen in Table II, the results obtained by ICAP for the National Bureau of Standards standard reference fly ash sample were excellent.

Only two elements exceed 10% deviation from the accepted value, Co (42%) and Cr (16%). It is suspected that Cr may be volatilized during preparation and that there may be a spectral interference for Co.

Instrumental Neutron Activation Analysis. A thorough literature review was conducted in order to determine which were the optimum isotopes to count, potential irradiation times, and a preparation method for irradiation standards. Several researchers have reported using neutron activation for coal analysis (*20–30*). Much of this work was for coals only; slag and fly ash samples have a much higher level of many elements. These higher levels can create new problems. Rocks are known to be high in many of the same elements, and the activation analysis procedures used for rocks may be suitable for slag and fly ash. Several papers reporting the use of neutron activation for the analysis of rock samples (*31–38*) outlined excellent procedures.

A new and more effective means of preparing standards for irradiation and comparison of unknown samples was particularly desired. The main objectives for improving standard preparation included the following: minimizing standard vaporization of the standard solutions during evaporations; providing a matrix for the standard which would allow for postirradiation transfer, thus eliminating irradiation container background and blank problems; optimization of standards with respect to quantity of each element necessary in our experimental configuration; preparation of compatible multielement standards to expedite standard preparation.

Maximization of the surface area on which standard solutions evaporate reduces the need for elevation of temperature. To accomplish this and to provide a solid matrix capable of being transferred after irradiation, liquid standards were evaporated onto solid matrices. The feasibility of adsorption of elemental standards onto several types of material was tested. These materials included high purity powders such as Al_2O_3, SiO_2, sucrose, and V_2O_5 and the commercial filter papers Whatman 541 and Millipore HA. It was possible to obtain usable analytical standards by using all of these materials except sucrose and V_2O_5, which were found to be unsuitable.

Table III. Results for Standard Reference Materials Analyzed by Instrumental Neutron Activation Analysis

	NBS SRM 1632 coal		NBS SRM 1632a coal		NBS SRM 1635 coal	
	present study	NBS value	present study	NBS value	present study	NBS value
V	34	36 ± 3	44	44 ± 3	4.1	5.2 ± 0.5
Al	18000	18500 ± 1300	31000	30700	2600	3200
Mn	39	43 ± 4	23	28 ± 2	19	21.4 ± 1.5
Ca	3600	2600	2600	*a*	4800	*a*
Na	400	1000	1000	*a*	2320	*a*
Se	3.7	3.1	3.1	2.6 ± 0.7	1.0	0.9 ± 0.3
Cr	20	35	35	34.4 ± 1.5	1.9	2.5 ± 0.3
Fe	7900	10000	10000	11100 ± 200	1900	2400 ± 100
Co	6.6	7.5	7.5	6.8	0.64	0.65
Sb	3.8	0.6	0.6	0.58	0.13	0.14
	USGS W-1 rock		USGS BCR-1 rock		NBS SRM 1633 fly ash	
	present study	NBS value	present study	NBS value	present study	NBS value
V	305	264	410	400	*b*	
Al	81000	78600	74000	72300	*b*	
Mn	1300	*a*	1340	*a*	*b*	
Ca	81600	78300	49100	49700	*b*	
Na	17000	15900	*b*		*b*	
Se	*b*		*b*		13.3	10.2 ± 1.4
Cr	124	114	*b*		135	127 ± 6.4
Fe	72000	77600	87000	93700	58	62 ± 3
Co	56	0.47	45	38	48	41.5 ± 1.2
Sb	*b*		0.7	0.69	7.9	6.9 ± 0.6

[a] No value available. [b] Not determined.

Table IV. Sample Results

element, μg/g	Illinois no. 6 coal		slag no. 2		slag no. 3a		slag no. 3b		fly ash
	INAA	ICAP[a]	INAA	ICAP[a]	INAA	ICAP[a]	INAA	ICAP[a]	INAA
Al	10000	13100	43800	35700	47700	45200	34700	32600	5780
Be		2.2		6.3		8.3		8.4	
Ca		3100	8500	7800		10100		7700	<4400
Cd		<0.5		<0.5		0.5		<0.5	
Co	4.6	6.3	17	18	18	20	17	20	16
Cr	12		1300		2000		1500		1500
Cu		17		400		410		370	
Fe	18000	23000	61000	59000	66000	70000	57000	57000	56000
Hg		0.12		0.08		<0.01		0.07	
K		3000	300000	324000	300000	281000	340000	335000	360000
Mg		800		2400		3200		2500	
Mn	27	35	250	240	250	260	210	280	200
Mo		<2		<2		<2		<2	
Na		220		2000	2700	2200		3300	2000
Ni		15		87		95		89	
Pb		<100		<100		<100		<100	
Sb	0.9	<25	0.4	<25	<0.4	<25	0.5	<25	0.4
Se			4.8		5.6		<5		15
Sn		<5		<5		<5		<5	
V	20.6	26	55.7	62	63.3	78	55.8	72	58.7
Zn		94		249		196		278	

[a] Preparation method used would result in loss of As, B, Cr, Se, and Si.

Table V. Variation between Instrumental Neutron Activation Analysis and Inductively Coupled Argon Plasma

sample	% deviation from mean of the two methods							
	Al	Ca	Co	Fe	K	Mn	Na	V
Illinois no. 6 coal	13		16	12		13		12
slag no. 2	10	4	3	2	4	2		5
slag no. 3a	3		5	3	3	2	10	10
slag no. 3b	3		8	0	1	14		13

A clear advantage of the use of INAA was that sample preparation requiring dissolution with heat was not required. Therefore, elements which are easily volatilized will not be lost. With less sample preparation and handling, the possibility of contamination will also be reduced. Table III shows the excellent accuracy of the method. Six different standard reference materials were analyzed, and as can be seen, all of the results are within 25% of the accepted value except that for Se in the fly ash.

MHD Samples. In Table IV the results for samples of Illinois no. 6 coal, slag, and a fly ash from a MHD pilot plant at the University of Tennessee Space Institute are given.

Comparison of Methods. The agreement between the two analytical methods are excellent. Table V lists the percent variation between the two methods when aliquots of the same sample are analyzed. The average percent deviation is 6.9% with a range of 0–16%.

Conclusions

Two multielement analytical techniques for the analysis of trace elements in samples from a MHD power-generating pilot plant have been compared and validated. The agreement between results from the instrumental neutron activation analysis and inductively coupled argon plasma emission methods was excellent, as was their agreement with NBS standard reference material values.

The solubilization procedure developed for the ICAP analysis is capable of dissolving totally any of the MHD coal, slag, and fly ash samples. There is still a problem with the loss of the volatile elements and silicon when this technique is used. Other solubilization procedures will need to be used for these elements. Research needs to be continued to develop a method which will be suitable for all of the elements.

Literature Cited

(1) Anderson, R. N.; Horiuchi, G. K.; Jayarajan, A. *Ind. Res./Dev.* **1978**, *20*, 131–133.
(2) Medlin, J. H.; Suhr, N. H.; Bodkin, J. B. *At. Absorpt. Newsl.* **1969**, *8* (2), 95–97.
(3) Owens, J. W.; Gladney, E. S. *At. Absorpt. Newsl.* **1976**, *15* (4), 95–97.
(4) Muter, R. B.; Cockrell, C. F. *Appl. Spectrosc.* **1969**, *23* (5), 493–496.
(5) Boar, P. L.; Ingram, L. K. *Analyst (London)* **1970**, *95*, 124–130.
(6) Prasad, N. K. *Chem. Ind.* **1970**, 432–433.
(7) Prasad, N. K. *Chem. Ind.* **1972**.
(8) Burman, *ICP Inf. Newsl.* **1977**, *3* (2), 33–36.
(9) Murphy, J. *At. Absorpt. Newsl.* **1975**, *14* (6), 151–152.
(10) Coleman, W. M.; Szabo, P.; Wooton, D. L.; Dorn, H. C.; Taylor, L. T. *Fuel* **1977**, *56*, 195–198.
(11) Spielholtz, G. I.; Harvey, D. *Talanta* **1966**, *13*, 991–1002.
(12) Gladfelter, W. L.; Dickerhoof, D. W. *Fuel* **1976**, *55*, 360–361.
(13) Asthana, S. S. *Chem. Ind.* **1967**, 190.
(14) Asthana, S. S. *Chem. Ind.* **1967**, 1521.
(15) Prasad, N. K. *Chem. Ind.* **1968**, 444–445.
(16) Hartstein, A. M.; Freedman, R. W.; Platter, D. W. *Anal. Chem.* **1973**, *45* (3), 611–614.
(17) Block, C. *Anal. Chim. Acta* **1975**, *80*, 369–373.
(18) Gluskoter, H. J.; Lindahl, P. C. *Science (Washington, D.C.)* **1973**, *181*, 264–266.
(19) Davison, R. L.; Natusch, D. F. S.; Wallace, J. R.; Evans, C. A., Jr. *Environ. Sci. Technol.* **1974**, *8*, 1107–1113.
(20) Rowe, J. J.; Steinnes, E. *J. Radioanal. Chem.* **1977**, *37*, 849–856.
(21) Steinnes, E.; Rowe, J. J. *Anal. Chim. Acta* **1976**, *87*, 451–462.
(22) Block, C.; Chantal, R.; Dams, R. *Environ. Sci. Technol.* **1975**, *9*, 146–150.
(23) Nadkarni, R. A. *Radiochem. Radioanal. Lett.* **1975**, *21* (304), 161–176.
(24) Block, C.; Dams, R. *Anal. Chim. Acta* **1973**, *68*, 11–24.
(25) Ruch, R. R.; Cahill, R. A.; Frost, J. K.; Camp, L. R.; Gluskoter, H. J. *J. Radioanal. Chem.* **1977**, *38*, 415–424.
(26) Kucera, E. T.; Heinrich, R. R. *J. Radioanal. Chem.* **1976**, *32*, 137–150.
(27) Perricos, D. C.; Belkas, E. P. *Talanta* **1969**, *16*, 745–748.
(28) Weaver, J. N. *Anal. Chem.* **1973**, *45*, 1950–1952.

(29) Klein, H.; Andren, A. W.; Carter, J. A.; Emery, J. F.; Feldman, C.; Fulkerson, W.; Lyon, W. S.; Ogle, J. C.; Talmi, Y.; VanHook, R. I.; Bolton, N. *Environ. Sci. Technol.* **1975**, *9*, 973-979.
(30) Filby, R. H.; Shah, K. R.; Sautter, C. A. *J. Radioanal. Chem.* **1977**, *37*, 693-704.
(31) Filby, R. H.; Haller, W. A.; Shah, K. R. *J. Radioanal. Chem.* **1970**, *5*, 277-290.
(32) Jacobs, J. W.; Korotev, R. L.; Blanchard, D. P.; Haskin, L. A. *J. Radioanal. Chem.* **1977**, *40*, 93-114.
(33) Baedecker, P. A.; Rowe, J. J.; Steinnes, E. *J. Radioanal. Chem.* **1977**, *40*, 115-146.
(34) Watterson, J. I. W.; Sellschop, J. P. F. *J. Radioanal. Chem.* **1977**, *38*, 301-313.
(35) Van derKlugt, N.; Poelstra, P.; Zwemmer, E. *J. Radioanal. Chem.* **1977**, *35*, 109-114.
(36) Wanke, H.; Kruse, H.; Palme, H.; Spettel, B. *J. Radioanal. Chem.* **1977**, *38*, 363-377.
(37) Vasconcellos, M. B. A.; Lima, F. W. *J. Radioanal. Chem.* **1978**, *44*, 55-81.
(38) Ohde, S.; Ohta, N.; Tomura, K. *J. Radioanal. Chem.* **1978**, *42*, 159-167.
(39) Ondov, J. M.; Zoller, W. H.; Olmez, L.; Aras, N. K.; Gordon, G. E.; Rancitelli, L. A.; Abel, K. H.; Filby, R. H.; Shah, K. R.; Ragaini, R. C. *Anal. Chem.* **1975**, *47*, 1102-1109.

Received for review January 17, 1983. Accepted October 28, 1983.

Dynamics of a Fertilizer Contaminant Plume in Groundwater

Michael J. Barcelona* and Thomas G. Naymik

Water Survey Division-Illinois Department of Energy and Natural Resources, Champaign, Illinois 61820

■ A 2-year investigation has been conducted on the effects of a massive inorganic nitrogen fertilizer contamination of a sand and gravel aquifer in western Illinois. Groundwater monitoring in the early period of the project during near steady-state conditions disclosed that dissolved ammonium and nitrate levels exceeded 2000 and 1300 mg·L^{-1}, respectively. A numerical solute transport model was applied to the system which predicted that approximately 420 days would be necessary after source removal to permit recovery of the aquifer water to near background levels within the study site. Subsequent monitoring results generally supported the model prediction and demonstrated its usefulness for predicting transport and transformations of inorganic forms of nitrogen. The chemistry and microbiology of the impact groundwater showed significant changes attendant to pollutant removal which indicate that microbially mediated processes occurred in the aquifer.

Introduction

Incidents of groundwater contamination have been discovered with increasing frequency in the past decade. Early reports of polluted groundwater identified the impacts of leaking gasoline pipelines or storage tanks (*1*). It was further recognized that organic groundwater contaminants from landfills or industrial sources interact significantly with inorganic chemical constituents and that remediation efforts must be chosen carefully with a clear understanding of subsurface chemistry and biology (*2*). Recent groundwater studies have become more sophisticated and involved in response to the seemingly endless varieties of pollutant mixtures and differing subsurface conditions (*3*). It is now clear that contaminant migration and fate in groundwater systems generally conform to fundamental hydrologic and chemical principles (*4*). However, there are few case studies that treat the fate and transport of reactive chemical species under the influence of known hydrologic, chemical, and biological constraints.

In a previous report, the discovery of a massive ammonium and nitrate contaminated 5-ha area over a sand and gravel aquifer near Meredosia in Morgan County, IL, was detailed while the source was still in place (*5*). The extent of the contamination was treated under steady-state conditions, and a numerical solute transport model (*6*) was applied to predict the time necessary after source removal for the aquifer in a study area to return to background conditions. Expanded investigations in the period after source removal have disclosed the general applicability of such models to the dynamics of shallow aquifer systems with interesting implications for improving our understanding of the response of the subsurface to localized contamination.

Methods

A large uncovered stockpile of salvaged ammonium and nitrate salts had been weathered at the surface of an alluvial sand and gravel aquifer for at least 3 years. The source was not on the property of the cooperating industry but was located on an adjacent tract. The extent of groundwater contamination was discovered when drinking and process water on the property showed elevated ammonium levels and severe pump binding problems. A network of shallow (8.6 m) sandpoints and deep (28 m) production wells completed just above bedrock were used for monitoring. Dissolved oxygen (azide modification of the Winkler method), alkalinity, pH, and temperature were measured on site. Ammonium and total organic carbon (TOC) samples were preserved in the field. NH_4^+, NO_2^-, NO_3^-, and Fe(II) subsamples were refrigerated and determined immediately on return to the laboratory, usually within 4-6 h after sampling. Major ionic constituents, total Fe, and Mn were determined by using Standard Methods (*7*).

Redox potentials were calculated via the Nernst equation from the REDEQL2 (*8*) output of equilibrium chemical speciation. Mass and charge balances generally agreed to within ±15% of the total dissolved solids (TDS) (corrected for NH_4^+ loss on drying) except for samples which exceeded 2500 mg·L^{-1} TDS. Most probable number enumerations (MPN) of nitrifying bacteria were performed by a five-tube replicate method (*9*) determining both nitrite and nitrate positives by spot test reactions.

Average linear groundwater flow velocities between a well designated as the source location, well SP1, and various wells within the network were calculated from measured hydraulic head differences, hydraulic conductivities in the area ($\sim 1.4 \times 10^{-3}$ m·s^{-1}), and an effective porosity of 0.1. These velocities were used in calculating apparent contaminant removal rates after dilution corrections were made on the observed concentration at each monitoring well and at the source. For removal rate calculations during the post-steady-state period, the average

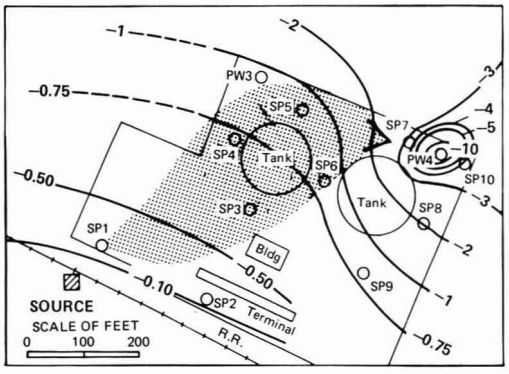

Figure 1. Map of site with diagram of sampling well network and generalized flow path of contaminant plume.

Table I. Composition of the Solid Fertilizer

insoluble fraction (rocks, wood, charcoal, paper), %	52.3
soluble fraction, % gravimetric composition	
CO_3^{2-}	27.7
SO_4^{2-}	27.7
Ca^{2+}	14.9
NH_4^+	13.8
K^+	6.89
PO_4^{3-}	5.89
Cl^-	1.29
NO_3^-	1.18
Na^+, Mg^{2+}	0.64

time of travel between each downgradient well and the source was calculated. Then the interpolated source (SP1) concentration of NH_4^+ or NO_3^- at the time the average parcel of water left the source was used to calculate apparent removal of each species.

Results and Discussion

Overview of the Contamination Situation. A schematic diagram of the study site, including well locations and a generalized flow path of the steady-state plume, are shown in Figure 1. SP denotes sandpoint wells, while PW denotes the two high-capacity production wells. SP1 was chosen as the measure of source strength since it was located as near as practical to the fertilizer bins on the adjacent property.

The salvaged fertilizer was sampled at several locations in the storage area and composited. An analysis of the composite sample is shown in Table I. The solid material was made up of a large amount of solid debris, since it originated from fire-damaged fertilizer production facilities. The soluble fraction was primarily composed of carbonates, sulfates, and the nutrients NH_4^+, K^+, PO_4^{3-}, and NO_3^-. Since chloride made up a portion of the soluble matter, it was chosen as a conservative tracer for plume definition and calibration of the solute transport model. The choice was based on the success of previous applications (*10*) and the fact that chloride provided a more conservative indicator of contaminant dilution effects than did potassium ion. The chloride to fertilizer-associated ion ratios in groundwater samples showed a high degree of homogeneity throughout the study, despite the fact that the fertilizer bins were emptied in June 1980. These results suggest that a large reserve of leached materials was present in the unsaturated zone, near SP1. For this reason, SP1 was considered a reliable indicator of "source" conditions. It is from this point that the investigation proceeded.

Application of the Solute Transport Model. Sampling of the shallow well network on six occasions during 1980 disclosed that ammonium concentrations at SP1 averaged 2020 $mg \cdot L^{-1}$ with a 4% relative standard deviation (coefficient of variation). Water levels and chemical analyses of groundwater samples from all wells were performed during April 1980. Additional data were obtained from tracer experiments run between SP4 and PW3 and SP10 and PW4. With these and other hydrologic data a numerical solute transport model was designed. Particulars of the application of the random-walk solute transport code have been described in detail (*6*). The model for the site was calibrated separately with both chloride and total ammonia concentration distributions. This was done under steady-state flow conditions, since the hydraulic gradient remained stable between late 1979 and June 1980 and there were no significant changes in the concentration distributions of the principal contaminants at the source during this period.

Transport model simulations were made to predict the decay of the contaminant plume once the source was removed in order to plan appropriate remedial action. Simulations predicted that 420 days would be required for system flushing after source removal. The observed concentrations in the reference source, SP1, are compared as a function of time with the predictions from the solute transport model (STM) in parts a (ammonia) and b (nitrate) of Figure 2. The predictions were made on the basis of total source removal in June 1980. In general, both the chloride and ammonia solute transport models show good agreement with the observed concentrations of ammonia and nitrate at SP1 during the initial 6–8-month period following removal of the fertilizer from the surface bins. As time progressed, observed ammonia removal was somewhat greater, and nitrate removal was less than predicted. The chloride calibrated model showed better agreement in the later period (March 1981 on) after source removal but did not account for the peak concentrations which accompanied later spring and early summer recharge events.

Between April and August 1981 the plume boundaries stayed rather constant, water levels rose 6–8 ft over the winter levels, and average linear velocities increased to 0.48 $\pm$ 0.08 $m \cdot day^{-1}$. The spring recharge in 1981 was accompanied by an increase of approximately 70% in both NH_4^+ and NO_3^- levels between March and August. These peaks are presumed to be due to the leaching of contaminant held in the unsaturated zone near the designated source well. Increases in observed ammonia and nitrate concentrations during the summer of 1981 showed the influence of recharge events and the consequent rise in regional water levels. Detailed transient flow conditions would have been necessary to incorporate these events into the model. Our prediction (*5*) of the time necessary to reduce source concentrations of the major contaminants within the study area to near background levels was based on a steady rate of flushing. It was accurate within $\pm$120 days as revealed by observations in the post-source removal period.

The solute transport model appears to be a powerful means of predicting long-term source strength decay to about 20% of the steady-state concentration maxima. This was true over most of the study period despite the fact that recharge events and regional increases in water levels caused the release of additional contaminants held in the unsaturated zone. Several researchers have observed high variability of NO_3^- in shallow groundwater systems receiving large inputs of fertilizer or feedlot runoff (*11*). The variability has been attributed, at least in part, to appli-

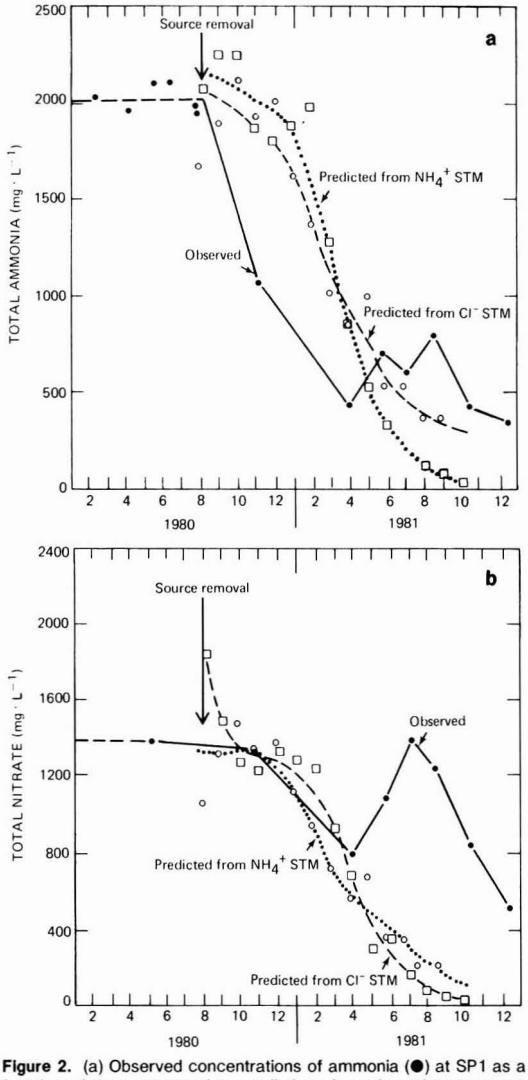

Figure 2. (a) Observed concentrations of ammonia (●) at SP1 as a function of time compared to predictions from the solute transport model (STM). Predicted ammonia concentrations are shown for both the chloride-calibrated STM (O) and the ammonia-calibrated STM (□). (b) Observed concentrations of nitrate (●) at SP1 as a function of time compared to predictions from the solute transport model (STM). Predicted nitrate concentrations are shown for both the chloride-calibrated STM (O) and the ammonia-calibrated STM (□).

cation rates and recharge events. The influences of regional effects and microbial transformations cannot be ignored in data interpretation (*12*). The relative magnitudes of these processes are discussed below in further examination of the chemical data.

Chemical Changes in Groundwater Composition. Detailed analytical results for the steady-state period and for two (of five) dates following source removal are shown in Table II. The table includes the designated source well (SP1), a shallow well (SP4), and a deep well (PW3) along the general path of the plume. (All analytical results for the project are available (see paragraph at end of paper regarding supplementary material)). The largest net changes in water chemistry from either background or steady-state conditions occurred at the source well where total dissolved solids dropped to about 13% of the

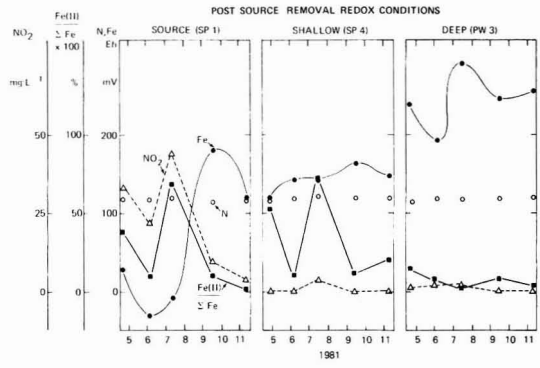

Figure 3. Redox conditions after removal of the pollution source. The concentrations of reduced species NO_2^- (Δ) and Fe(II) (■) are plotted vs. the calculated equilibrium redox potentials (mV) from the Fe(III)/Fe(II) couple (●) and the average from the NO_3^-/NH_4^+ and NO_2^-/NH_4^+ (O) couples.

steady-state value over 20 months. Similarly, ammonia and nitrate decreased to 16 and 37% of their respective levels in 1980.

High variability in nitrate, ammonia, TDS, and pH was observed in the shallow groundwater during the late spring and summer of 1981 in response to recharge events and the consequent regional increase in water levels through Sept 1981. Dissolved oxygen, nitrite, chemical oxygen demand (Cl^- corrected, COD), ferrous iron, and most probably number values of nitrifying bacteria showed considerable overall variability which is evidence of their sensitivity to recharge events, pH, and redox potential changes, as well as presumed chemical and biochemical reactions.

Nitrite ion showed the highest overall variability in the shallow portion of the aquifer, reaching a maximum in the source well of 39.8 $mg \cdot L^{-1}$. The coincidence of high nitrite and dissolved oxygen levels is a contradiction of known redox stability. This may be attributed to a positive interference on the Winkler oxygen determination caused by nitric oxide (*13*). Nitric oxide is an intermediate in the microbial transformation of inorganic nitrogen species which normally accumulates in closed systems at low pH (*14*). The magnitude and nature of this contamination situation may make these observations unique in the literature. Nonetheless, these results cast serious doubt on the reliability of Winkler dissolved oxygen measurements in closed culture systems or in groundwater when oxygen is observed in confined situations distant from the recharge areas (*15*).

Efforts to measure Eh in the field with a modified flow-through device (*16*) failed to yield reliable results. This was principally due to large quantities of gases which exsolved from the groundwater as it was pumped from the well bore. Attempts to make a reliable estimate of its composition by chromatographic methods were unsuccessful due to the large amounts of nitrogen present.

In order to provide a qualitative indication of oxidation–reduction conditions in the system, equilibrium redox potentials were calculated via the Nernst equation from equilibrium speciation calculations on the basis of the Fe(III)/Fe(II), NO_3^-/NH_4^+, and NO_2^-/NH_4^+ couples. Despite the need to make the guarded assumption of equilibrium and reversibility of electrochemical behavior required by this procedure (*17*), it is possible to obtain precise estimates of the redox condition which aid in the interpretation of groundwater chemistry (*18*). The averaged results of the redox calculations for the post source

Table II. Chemical Characteristics of Groundwater at the Site

(A) Source Well (SP1)[a]

	background[b]	steady-state 1980	10 months after source removal, 4/22/81	17 months after source removal, 11/17/81
pH, pH units	7.80	8.91	8.63	8.60
TDS	380	7710	3054	990
Ca^{2+}	66	2.8	11.1	4.60
Mg^{2+}	28	3.9	43.5	14.7
Na^{+}	10	8.0	10.0	7.90
K^{+}	1.5	60	46.0	24.2
Cl^{-}	22	188	140	62
SO_4^{2-}	50	196	98	110
alkalinity, mequiv·L^{-1}	4.8	62.5	22.4	11.2
dissolved oxygen[e]	ND[d]	ND	15.9	5.0
NH_4^{+}[c]	0.06	2114	747	359
NO_3^{-}	14	1380	1087	514
NO_2^{-}	ND	ND	29.2	3.20
Si	13	ND	3.6	30.3
Fe(total)	0.74	0.60	0.35	0.22
Fe(II)	ND	ND	0.050	0.028
Mn	0.18	ND	0.03	0.01
COD	ND	ND	26.8	10.9
TOC	ND	ND	4.91	3.21
MPN, nitrifiers $L^{-1} \times 10^{-2}$	ND	ND	7000	230

(B) Downgradient Wells (SP4 and PW3)[a]

	shallow (SP4)			deep (PW3)		
	1980	4/22/81	11/17/81	1980	4/22/81	11/17/81
pH, pH units	7.40	7.82	7.50	7.31	7.22	7.15
TDS	1906	1147	1252	2013	1033	1108
Ca^{2+}	68	34.4	84.5	108	81.3	85.5
Mg^{2+}	34	20.2	30.0	150	26.2	27.4
Na^{+}	10	8.50	8.30	16	8.50	8.50
K^{+}	62	82.3	32.4	25	18.6	19.3
Cl^{-}	47	30	48	13	34	30
SO_4^{2-}	112	83.6	105	90.0	136	101
alkalinity, equiv·L^{-1}	11.8	9.24	7.1	17.2	8.19	8.7
dissolved oxygen[e]	ND[d]	0.64	0.97	ND	3.2	8.2
NH_4^{+}[c]	282	176	124	137	150	134
NO_3^{-}	570	233	365	440	246	157
NO_2^{-}	ND	0.021	0.013	ND	0.100	0.018
Si	ND	9.41	31.4	ND	4.58	14.1
Fe(total)	0.20	0.12	0.13	<0.02	0.13	0.22
Fe(II)	ND	0.065	0.081	ND	0.020	0.012
Mn	ND	0.02	0.02	ND	0.78	0.51
COD	ND	7.32	4.9	ND	6.00	2.6
TOC	ND	2.10	2.51	ND	2.43	2.91
MPN, nitrifier $L^{-1} \times 10^{-2}$	ND	7900	230	ND	54000	230

[a] All tabulated values are in milligrams per liter unless otherwise specified. [b] SWS and IEPA files for Meredosia Municipal Supply upgradient from site. [c] Represents total ammonia. [d] ND, not determined. [e] A systematic error makes these values questionable; see Results and Discussion.

removal period are plotted in Figure 3, together with the observed NO_2^- and Fe(II) levels expressed as a percentage of the total iron in the samples. The Eh values suggest that the shallow groundwater system was poised between −34 and +180 mV during this period. The redox potentials for the inorganic nitrogen couples were uniformly +115 ± 10 mV. These values were insensitive to chemical changes in the system caused by recharge and the rise in water levels through the summer of 1981 with the exception of slight effects of dilution. Eh values for the ferric–ferrous couple significantly increased in the shallow groundwater (SP1 and SP4) during this period. This was also reflected in decreased NO_2^- and Fe(II) concentrations and COD levels observed on the 9/15 and 11/17 sampling dates.

Most probable number (MPN) values for the aerobic nitrifiers also peaked as the water levels rose in the region. Estimates of NO_2^- relative to NO_3^- positive samples ranging from 2×10^2 to 5×10^6 nitrifiers·L^{-1} were roughly equivalent in samples during the post source removal period with the exception of the 7/14 sampling date. On 7/14/81, peak NO_2^-, Fe(II), and MPN levels were observed. The MPN levels were not correlated significantly with redox potential values or the apparent rates of ammonia removal calculated after dilution correction. These rates, which varied from 7 to 74 μmol·L^{-1}·day^{-1}, were based on average groundwater travel times between the designated source (SP1) and the other shallow wells. Approximately 30% of the apparent ammonia removal was supported by both alkalinity reduction and an increase in nitrate as would be required by microbial nitrification processes. Nonetheless, it was clear that microbial processes played an observable role in ammonia removal in the shallow aquifer. The MPN procedure is a semiquantitative indicator of the presence of microorganisms. One must be aware that the determination is based on probability relationships and it is prone to a high margin of error. Also, systematic errors may be large in water sampling, since populations of attached microoganisms may be much

greater than "planktonic" numbers (*19*).

Due to the systematic error in the dissolved oxygen determinations and the physical and legal constraints on our investigation imposed by site conditions, a more detailed interpretation of the chemical data would be purely speculative.

The study of groundwater pollution situations demands close consideration of hydrogeologic, chemical, and biochemical processes. Further, the exhaustive characterization of system variables may be necessary to identify major sinks or removal processes in these situations.

Conclusions

Solute transport models are powerful tools to predict the characteristics of groundwater contaminant plumes. This is particularly true in regions of high groundwater flow where dilution is a major flushing mechanism. The present model yielded good predictions for the time necessary for levels of major contaminants in the grossly polluted area to drop to about 20% of their concentration maxima.

Subsurface microorganisms play an observable role in the transformation and fate of inorganic nitrogen species. Their activity is limited by oxygen supply, substrate availability, and various physical factors. In less permeable subsurface environments with lower rates of groundwater flow, the relative contribution of chemical or biochemical removal processes to net contaminant removal could be judged more accurately.

Observations of free dissolved oxygen, especially in contaminated groundwater systems, should be corroborated by redox potential measurements and the analytical determination of redox-sensitive chemical species. Microbial-catalyzed reversibilty of the redox couples NO_3^-/NH_4^+ and NO_2^-/NH_4^+ is questionable in highly contaminated groundwater systems despite the fact that these chemical species dominate solution chemistry.

Acknowledgments

We acknowledge the support of various field and laboratory staff of the Water Survey, including Ed Garske, Mike O'Hearn, Kenni James, and Pam Beavers. The review and comments of Bruce Rittmann, John T. Wilson, and two anonymous reviewers were very much appreciated.

Supplementary Material Available

Table I containing analytical results of the groundwater monitoring in this study (4 pages) will appear following these pages in the microfilm edition of this volume of the journal. Photocopies of the supplementary material from this paper or microfiche (105 × 148 mm, 24X reduction, negatives) may be obtained from Distribution Office, Books and Journals Division, American Chemical Society, 1155 16th St., N.W., Washington, DC 20036. Full bibliographic citation (journal, title of article, author, page number) and prepayment, check or money order for $7.50 for photocopy ($9.50 foreign) or $6.00 for microfiche ($7.00 foreign), are required.

Registry No. NH_4^+, 14798-03-9.

Literature Cited

(1) Committee on Enviromental Affairs, American Petroleum Institute, Washington, DC, 1972, Publication No. 4149, pp 1–36.
(2) Todd, D. K.; McNulty, D. E. O. "Polluted Groundwater"; Water Information Center, Inc.: Port Washington, NY, 1974; pp 1–179.
(3) Shuckrow, A. J.; Pajak, A. P.; Touhill, C. J. Contract Report 68-03-2766 to Solid and Hazardous Waste Research Division, USEPA-MERL, Cincinnati, OH, 1980, NTIS PB-81-189359.
(4) Roberts, J. R.; Cherry, J. A.; Schwartz, F. W. *Water Resour. Res.* **1982**, *18*, 525–534.
(5) Naymik, T. G.; Barcelona, M. J.; *Ground Water* **1981**, *19*, 517–526.
(6) Prickett, T. A.; Naymik, T. G.; Lonnquist, C. G. Illinois State Water Survey, 1981, Bulletin 65, pp 1–103.
(7) American Public Health Association "Standard Methods for the Examination of Water and Wastewater", 14th ed.; American Public Health Association, American Water Works Association, and Water Pollution Control Federation, Joint Publication: Washington, DC, 1975.
(8) McDuff, R. E.; Morel, F. M. Keck Laboratories, California Institute of Technology, Pasadena, CA, REDEQL 2 Computer Program, T. R. EQ-73-02.
(9) Environment Canada "Methods for Microbiological Analysis of Waters, Waters, Wastewaters and Sediments"; Applied Research Division, Canada Centre for Inland Waters, Fisheries and Environment: Burlington, Ontario, Canada, 1978, pp 5–7.
(10) Kimmel, G. E.; Braids, O. C. *Geol. Surv. Prof. Pap. (U.S.)* **1980**, *No. 1085*, 1–38.
(11) Exner, M. E.; Spalding, R. F.; *Water Resour. Res.* **1979**, *15*, 139–147.
(12) Taylor, R. G.; Russell, T. W.; Foster, M. New Mexico Water Resources Research Institute, New Mexico State University, Las Cruces, NM, 1979, Water Research Report 114, pp 1–20.
(13) Barcelona, M. J.; Garske, E. E. *Anal. Chem.* **1983**, *55*, 965–967.
(14) Painter, H. A. *Water Res.* **1970**, *4*, 393–450.
(15) Winograd, I. J.; Robertson, F. N. *Science (Washington, D.C.)* **1982**, *216*, 1227–1230.
(16) Garvis, D. G.; Stuermer, D. H.; *Water Res.* **1980**, *14*, 1525–1527.
(17) Stumm, W.; Morgan, J. J. "Aquatic Chemistry"; 2nd ed.; Wiley: New York, 1981; pp 1–780.
(18) Champ. D. R.; Gulens, J.; Jackson, R. E. Can. *J. Earth Sci.* **1979**, *16*, 12–23.
(19) Marxsen, J. *Verh.—Int. Ver. Theor. Angew. Limnol.* **1981**, *21*, 1371–1375.

Received for review February 17, 1983. Revised manuscript received June 30, 1983. Accepted October 3, 1983. The work was partially supported by the Illinois Department of Energy and Natural Resources and the Research Board of the University of Illinois at Urbana–Champaign with the cooperation of the W. R. Grace Chemical Co.

Environ. Sci. Technol. 1984, 18, 262–264

Photochemical Separation of Xenon and Krypton

Christine E. Geosling* and Terence Donohue*

Laser Physics Branch, Naval Research Laboratory, Washington, DC 20375

■ A technique is described for the separation of xenon from krypton using photolytically produced fluorine atoms as the reactive species. Stable XeF_2 is produced when a mixture of xenon, krypton, and fluorine gases is irradiated with near-ultraviolet light. KrF_2 is not stable at the near room temperature conditions of the experiment. Separation factors (enrichments) greater than 1000 for Xe/Kr are reported for yields of less than 98%. Even higher yields (resulting from longer photolyses) are possible, but then separation factors become slightly smaller.

Introduction

There is increasing interest in new methods for noble gas separation for reasons of both cost and safety. The prevalent separation method for xenon and krypton is cryogenic distillation (*1*) generally as a byproduct from the manufacture of liquid air. This process, while well developed and reliable, is relatively energy intensive. Another source for these noble gases may become available in the future, as the products from nuclear fission, found as offgases from either nuclear reactors or reprocessing plants (*2–5*). A number of novel rare gas separation methods have been recently developed (*6*) to both take advantage of this new source and also reduce or eliminate the radioactive hazards found with these offgases.

The separation costs arise primarily from the thermodynamically inefficient production of low temperatures required for separation, near liquid nitrogen temperatures (−196 °C). While the amount of rare gases separated constitute only a very small fraction of the volume processed by a commercial liquid air plant, noble gas purity requirements involve extensive amounts of distillation. Elimination of this feature, as found in the room temperature process described here, would reduce processing costs. Furthermore, a safety hazard is found when the cryogenic process is used with the gaseous products from spent nuclear fuel. Radiolysis of the air and water always present produces ozone (*6*), which becomes explosive when condensed as a liquid at temperatures below about −120 °C. The incentives for developing a noncryogenic separation technique is clear in this situation.

Of the isotopes of Xe and Kr produced by nuclear fission, only one, ^{85}Kr, has a significant half-life (of ~10 years). Furthermore, krypton constitutes only 6.5% of the total rare gases, so that a simple elemental separation process is sufficient to produce xenon free of any radioactive isotopes (*2*). Further photochemical enrichment of this isotope is possible but not necessary for most applications. We have, in fact, investigated such a molecular laser isotope separation scheme (*7*).

The discovery of the first noble gas compounds was soon followed by the first reports that some of these compounds could be synthesized photochemically (*8*). XeF_2, XeF_4, and XeF_6 can be made thermally from Xe and F_2; however, temperatures of ~250 °C are necessary for establishment of equilibrium on a reasonable time scale. It is relatively straightforward to make XeF_2 photochemically, but photochemical production of KrF_2 requires quite severe conditions such as in the cryogenic liquid or solid states (*9, 10*). This difference in stabilities between the two difluorides is the basis for the separation technique presented here.

Xenon difluoride is produced when a mixture of xenon and fluorine is irradiated in the ultraviolet (UV), into the absorption band of the fluorine molecule. This band is relatively weak (ϵ of ~3.0 $L \cdot mol^{-1} \cdot cm^{-1}$) and broad, peaking at 285 nm, and photolysis in this region results in the production of fluorine atoms (*11*). Any photolytic source can be used as long as the wavelength is appropriate, from about 250 to 350 nm. It is not necessary that the mechanism resulting in XeF_2 production be totally understood. Indeed, some of the details have yet to be fully explained (*12*). The significant feature is that a photochemical process involving the rare gases can be made selective for xenon, where the products are molecular and can be readily separated from reagents.

Experimental Section

The xenon and krypton used in these experiments were 99.995% pure from Air Products. The fluorine was 98% from Matheson and the nitric oxide 99.0% from Matheson.

The gases were handled in an all-metal vacuum line passivated with fluorine. Removable traps were used to transfer samples to the mass spectrometer for analysis. Two photolysis cells were used. A quartz cell with fused quartz windows was employed in the initial experiments, but production of SiF_4 by action of fluorine on the cell walls was found to interfere with the mass spectral product analysis. For most of the experiments, a stainless steel cell with CaF_2 UV quality windows was used. This cell was also passivated with fluorine before use.

In a typical experiment about 150 torr of krypton and 150 torr of xenon were admitted to a holding trap and an analysis trap. The analysis trap was then closed and taken to the mass spectrometer (Finnigan Model 3100) for a reference spectrum to allow exact determination of the Xe/Kr ratio. The remainder of the rare gas mixture was then condensed into the photolysis cell by lowering the temperature to −196 °C using liquid nitrogen. About 250 torr of fluorine was then added to the photolysis cell which was then sealed and removed for photolysis. The pressures of reagents were calculated to give a small excess of fluorine over that required for complete conversion to XeF_2.

The photolysis cell was maintained at room temperature with its cold finger immersed in a dry ice/2-propanol slush at −78 °C and irradiated with either a 150-W xenon lamp (Oriel), a 500-W medium-pressure mercury lamp (Oriel), or a XeF laser (351 nm; Lumonics Model 261, operated at an average power of 2 W). As irradiation proceeded, fine crystals of XeF_2 were observed to condense on the inside of the cell near the mouth of the cold finger. No observable or measureable amounts of KrF_2 were ever isolated in any experiment, not surprising considering the poor stability of this compound. In other experiments, XeF_2 was found to condense at temperatures as warm as 10 °C, but −78 °C was used to ensure maximum product yields.

After photolysis, the cell was reattached to the vacuum line and the unreacted fluorine pumped off at −196 °C. A dry ice/2-propanol slush was then placed on the cell, and the unreacted Xe and Kr were condensed into another trap at −196 °C to allow mass spectral analysis of the product yield. Cryogenic temperatures were used here for ease of product analyses and complete material recovery in a single

stage "proof of principle" set of experiments. The product XeF_2 crystals were then subjected to three freeze/pump/thaw cycles between −78 and 25 °C, then transferred to the analysis trap, and finally gently heated to decompose the compound into Xe, and Kr and F_2 for mass spectral analysis. This trap contained clean copper wool to remove the fluorine produced during this process.

Analysis

The separation factor, β, was calculated from the mass spectral peak heights of several of the Xe and Kr isotopes according to the equation

$$\beta = \frac{\text{Xe/Kr(products)}}{\text{Xe/Kr(reactants)}} \quad (1)$$

where Xe/Kr(products) is the ratio of xenon and krypton obtained from decomposed product crystals after all volatiles have been removed (see below). Xe/Kr(reactants) is simply the initial ratio of reactant gases. The ^{84}Kr peak was used exclusively in the calculations, since it was found to be least affected by impurity peaks in the mass spectrum. However, there was always enough background interferences to preclude exact measurement of the Kr peak intensities; thus, all measurements were lower bound estimates. However, there were no background interferences whatsoever in the region where Xe peaks were found, and the measured xenon isotope peak intensities always reflected the natural abundance isotope ratio. Calculations using any of the xenon peaks gave essentially similar separation factors, but the ^{129}Xe peak, among the most intense, was generally used in the calculations.

The yield was calculated from the amounts of unreacted xenon and krypton remaining after photolysis according to

$$\text{yield} = \left(1 - \frac{\text{Xe/Kr(unreacted)}}{\text{Xe/Kr(reactants)}}\right)100\% \quad (2)$$

where Xe/Kr(unreacted) is the ratio of xenon and krypton remaining volatile over product crystals after irradiation (see below). Xe/Kr(reactants) is as previously defined. It was possible to obtain yields near 100% with long irradiation times, but at the expense of small drops in β. This is most likely due to inclusion of Kr (or, less likely, KrF_2) in the product XeF_2 during crystallization.

Results and Discussion

The separation factors and yields for photochemical separation of xenon and krypton are given in Table I. The yield rises linearly with photolysis time and then levels off as 100% reaction is approached. The separation factors, however, do not give such a monotonic trend, except possibly that larger extents of photolysis tend to give poorer separations. This could possibly be due to the relative difficulty of degasing the larger amount of material deposited in the longer photolysis experiments. In most cases, the magnitude of the separation factor obtained was dependent upon the ability to distinguish and measure very small product Kr peaks among mass spectral background and impurities near the limit of sensitivity of the mass spectrometer. These factors varied from experiment to experiment. Thus, actual separations are always larger than those listed in Table I.

Runs 14 and 15 were carried out with added impurity gases, air and NO, respectively, since these are the most likely impurities encountered in nuclear reactor offgases. Added air had essentially no effect on the yield or β. Added NO, however, increased the separation factor greatly while decreasing the yield. There were no new peaks in the product mass spectrum of the sample with air; however, the product spectra of the sample with NO contained significant peaks corresponding to both N_2O and NO_2. These results show that the photochemical separation method can be successfully employed without the need for preliminary separation steps to eliminate nonnoble gas constituents (*3*, *4*).

Table I. Separation Factors and Yields for Xe/Kr Separations

irrad time, h	run no.	source	β	yield, %
1.0	11	Hg lamp	1100	34
1.5	12	Hg lamp	1300	50
1.5	7	Hg lamp	1700	*e*
2.0	10	Hg lamp	350	74
4.0	9	Hg lamp	100	98.7
6.0	13	Hg lamp	500	99.8
1.25[a]	2	Hg lamp	300	*e*
3.0[a]	1	Xe lamp	7	*e*
4.0[b]	14	Hg lamp	1000	98
4.0[c]	15	Hg lamp	7000	64
1.0	8	XeF laser[d]	300	7

[a] Quartz photolysis cell. [b] 50 torr of room air added. [c] 50 torr of NO added. [d] 351 nm. [e] The yield was not measured in these experiments.

In conclusion, we have demonstrated a technique for separating xenon from krypton by a selective reaction with photolytically produced fluorine atoms near room temperature and atmospheric pressure conditions. Separation factors greater than 1000 have been achieved, and product yields greater than 99% are possible, with some reduction in product purities. The conditions used here, however, are not optimum for a full-scale separation process. Even though Kr is only 0.02% by volume of a reprocessing offgas stream and Xe constitutes 2.1%, recovery of F_2, use of several cascaded stages and a continuously flowing system can improve efficiencies markedly (*8*,*13*). Larger mercury lamps can be made to operate more efficiently than those used in the present system. In fact, a single 10-kW Hg lamp would be an adequate photolytic source for processing the entire offgases from a typical nuclear reprocessing plant. The costs involved in cooling are small, since XeF_2 can be condensed at near room temperature. The process can be operated at or near atmospheric pressure, which can give large throughputs while avoiding the risks of operating at higher pressures. Possibly the largest barrier to a practical application of this concept will be solving the problem of handling fluorine in these environments.

Registry No. Krypton, 7439-90-9; xenon, 7440-63-3; fluorine, 7782-41-4.

Literature Cited

(1) Handley, G. G. In "Noble Gases"; Stanley, R. E.; Moghissi, A. A., Eds.; ERDA TIC CONF-730915 (avail. NTIS): Springfield, VA, 1973; p 90.
(2) Rohrmann, C. A. *Isot. Radiat. Technol.* **1971**, *8*, 253.
(3) Mastera, S. G.; Laser, M.; Merz, E. *Environ. Sci. Technol.* **1978**, *12*, 85.
(4) Bohnenstingl, J.; Heidendael, M.; Laser, M.; Mastera, S.; Merz, E. In "Management of Radioactive Wastes from the Nuclear Fuel Cycle"; International Atomic Energy Agency: Vienna, 1976; p 129.
(5) Stein, L. In "Noble Gases"; Stanley, R. E.; Moghissi, A. A., Eds.; ERDA TIC CONF-730915 (avail. NTIS): Springfield, VA, 1973; p 376.
(6) Bendixsen, C. L.; Buckham, J. A. In "Noble Gases"; Stanley, R. E.; Moghissi, A. A., Eds.; ERDA TIC CONF-730915

(avail. NTIS): Springfield, VA, 1973; p 290.
(7) Donohue, T., U. S. Naval Research Laboratory, unpublished data, 1981.
(8) Weeks, J. L.; Chernick, C. L.; Matheson, M. S. *J. Am. Chem. Soc.* **1962**, *84*, 4612.
(9) Streng, L. V.; Streng, A. G. *Inorg. Chem.* **1966**, *5*, 329.
(10) Turner, J. J.; Pimentel, G. C. *Science (Washington, D.C.)* **1963**, *140*, 974.
(11) Calvert, J. G.; Pitts, J. N. "Photochemistry"; Wiley: New York, 1966; p 184.
(12) Messing, I.; Smith, A. L. *J. Phys. Chem.* **1982**, *86*, 927.
(13) Weeks, J. L.; Matheson, M. S. In "Noble Gas Compounds"; Hyman, H. H., Ed.; University of Chicago Press: Chicago, IL, 1963; p 89.

Received for review April 1, 1983. Revised manuscript received August 23, 1983. Accepted September 19, 1983. This work was partially supported by the Office of Basic Energy Sciences of the Department of Energy.

Aggregation and Colloidal Stability of Fine-Particle Coal Suspensions

Paul R. Schroeder* and Alan J. Rubin

Water Resources Center, The Ohio State University, Columbus, Ohio 43210

■ The aggregation and colloidal stability of colloidal coal suspensions in the presence of varying concentrations of hydrogen ions, neutral salts, and aluminum sulfate were investigated. Critical concentration and critical pH values for coagulation and stabilization were determined from turbidity changes during settling following aggregation. Two colloidal suspensions of a bituminous coal representing stability extremes due to oxidation were compared. In the absence of other coagulants, vigorous oxidation lowered the isoelectric point of the coal sol from pH 5.1 to pH 1.1 and the pH for stabilization from 7.5 to 2.6. The coagulation of the suspensions followed the Schulze–Hardy rule as hydrophobic sols although the oxidized coal sol was slightly less sensitive to neutral salts. The entire log aluminum sulfate concentration–pH stability limit diagram for the oxidized coal sol was established. The boundaries of settling of the coal in the presence of aluminum sulfate were similar to other hydrophobic sols except for small differences in alkaline solutions. Regions of ionic coagulation, rapid coagulation due to enmeshment in aluminum hydroxide precipitate, and restabilization were also observed and delineated.

Introduction

Billions of gallons of fine-particle coal suspensions are generated annually by wet cleaning and sizing methods in the coal industry (*1*). These black wash waters are usually treated by plain settling and then discharged to our nation's stream carrying large quantities of fine coal particles (*2, 3*). Chemical clarification should be employed to promote the settling of colloidal particles in order to meet the suspended solids' effluent discharge limit of 0.07 g/L imposed on the industry (*4*). Therefore, the aggregation and colloidal stability of fine-particle coal suspensions are of practical importance as well as of theoretical interest.

In ordinary treatment practice, clarification is usually accomplished upon aggregation of the colloidal particles using iron or aluminum salts. These metal salts hydrolyze to form complex species or precipitate depending upon solution pH. Generally, the salts are used as aggregating agents at or near neutrality where the insoluble hydroxide is the predominate form. Under these conditions, it is apparent that mechanisms of aggregation occur other than simple ionic coagulation as predicted by the Schulze–Hardy rule. With hydrophobic colloids these mechanisms are controlled primarily by solution pH and metal salt concentration and are less dependent on the properties of the sol itself (*5, 6*). The effects of a specific sol, however, must be determined experimentally.

As with many other sols the colloidal stability of coal is dependent on particle size and the presence of surface ionizable groups. Oxidation of coal surfaces occurs rapidly in nature by weathering and exposure to the atmosphere (*7*). Marinov (*8*) and Czuchajowski (*9*) in studies with air and other oxidants have shown that the quantity of hydroxyl and ionizable carboxyl surface groups increases with the extent of oxidation. In this study aqueous colloidal suspensions of a bitmuinous coal representing extremes in stability were compared. One group of suspensions was freshly ground, with minimum oxidation resulting only from exposure to air, while others were vigorously oxidized with hydrogen peroxide.

The fine-particle coal suspensions were characterized by experimental techniques used in past studies in this laboratory (e.g., *10–12*). Reductions in turbidity during quiescent settling following addition of coagulants were used to indicate aggregation. The first series of experiments with these sols involved the determination of their isoelectric points (pH_i) by microelectrophoresis and their critical pH for stabilization (pH_s) in the absence of aggregants except hydrogen ion. Next, neutral salts were employed as coagulants at constant pH and the sols were compared by using Težak's formulation of the Schulze–Hardy rule (*13, 14*). The final study was run to establish the entire aluminum(III) concentration–pH stability limit diagram ("domain") for oxidized colloidal coal. These diagrams delineate the regions or zones of aggregation and stabilization of a sol as determined by the hydrolysis products of the aluminum(III) salt (*15, 16*). The Al(III) concentration range in this study was varied from 10^{-7} to 10^{-1} M over the pH range 2–13.

Experimental Section

Solutions and Suspensions. Carbonate-free distilled water was used in the preparation of the solutions and suspensions. All chemicals were reagent grade. Stock solutions of $NaNO_3$ and $ErCl_3 \cdot 6H_2O$ (Ventron Alfa Chemicals) were prepared directly from the dried salts and not standardized. The stock solutions of $BaCl_2 \cdot 2H_2O$, $Ca(NO_3)_2 \cdot 4H_2O$, $Al_2(SO_4)_3 \cdot 18H_2O$, and $Al(NO_3)_3 \cdot 9H_2O$ were standardized by titration with ethylenediaminetetraacetic acid (EDTA) using Eriochrome Black T as the indicator (*17*). Solutions of NaOH and HNO_3, which were stand-

* Address correspondence to this author at the U.S. Army Engineer Waterways Experiment Station, WESEE, Vicksburg, MS 39180.

 0013-936X/84/0918-0264$01.50/0

ardized potentiometrically vs. potassium hydrogen phthalate and tris(hydroxymethyl)aminomethane, respectively, were used for pH adjustment. To eliminate aging effects, diluted aluminum solutions were prepared from the stock solutions just prior to each set of experiments.

The coal suspensions were prepared for a highly volatile, low sulfur, low ash bituminous coal from the Elkhorn seam in Kentucky. The coal was finely ground, ball milled, and passed through a 400-mesh standard U.S. Series sieve. Five grams of −400-mesh coal was mixed with 1L of 3×10^{-4} M NaOH in a blender until thoroughly wetted and dispersed to form the stable "unoxidized" coal suspensions. Oxidized coal was prepared in 2-g batches of −400-mesh coal with 10 mL of 30% hydrogen peroxide and 200 mL of distilled water in a shaker bath at 80 °C for 4 h. These coal slurries were then filtered, washed, filtered again, and resuspended in distilled water (*18*). Oxidation produced a coal of greater wettability and dispersibility. Any suspension having an unusually low pH was discarded. Typically, the pH ranged between 5.5 and 6.0 for oxidized coal sols and between 9.5 and 10.0 for unoxidized coal. All suspensions were allowed to settle and age to form sols of the most stable particles. The stability of the coal suspensions improved with age since after 2 weeks their turbidities remained nearly constant. The effects of oxidation with hydrogen peroxide on the properties of coal have been discussed previously by Rubin and Kramer (*18*).

The surface areas of the coal particles were measured with a Quantasorb analyzer manufactured by Quantachrome Corp. by using the multipoint BET adsorption method with nitrogen gas. The ground, sieved coal had a surface area of 7.2 m^2/g prior to oxidation and 9.3 m^2/g afterward.

Procedures. The aggregation experiments were performed directly in 19 × 105 mm round cuvettes with 10-mL test samples without the aid of slow mixing. Five-milliliter aliquots of a coal suspension were added to a series of cuvettes with NaOH solution when needed for pH adjustment. A second series of solutions, consisting of coagulating salt and/or HNO_3, were prepared in small glass vials. Each test sample was formed by transferring the contents of a single vial to a cuvette containing the coal. Both acid and base were never present in a test sample. The cuvette was stoppered, shaken for 10 s, and then allowed to settle. The "initial turbidity" of the sample was measured within 1 min following its preparation. Subsequent readings were estimated by absorbance measurements at 400 nm with a Coleman Model 14 spectrophotometer or by light scattering measurements taken with a Coleman Model 9 nephelometer. Sample turbidities followed Beer's law; an absorbance of 0.6 was equivalent to 28 mg/L coal.

Two types of experimental approaches were used to study aggregation. In one, the series of test samples were prepared at constant pH while the concentration of either aluminum or one of the neutral salts was systematically varied. The turbidities of the samples were plotted as a function of the logarithm of the coagulant concentration of the sample to determine graphically the critical concentrations for coagulation and for stabilization. The critical coagulation concentration (c.c.c.) is defined as the limiting or lowest concentration that just initiates aggregation. The critical stabilization concentration (c.s.c.) is the lowest concentration at which stabilization is just completed. The other type of aggregation experiments involved holding the aluminum concentration constant in a series of samples while the pH was systematically varied.

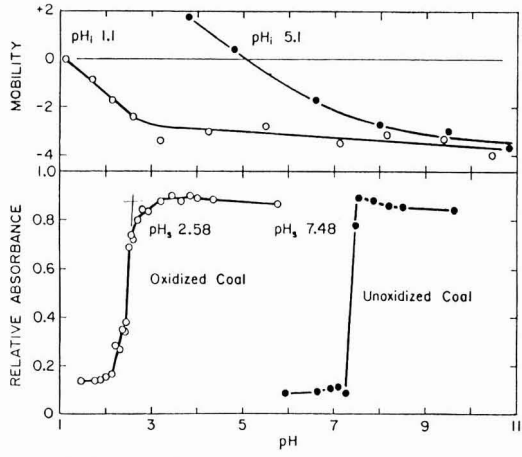

Figure 1. Effect of pH on the stability and electrophoretic mobility of colloidal coals. The 24-h settling data shown.

From these results the critical pH values for coagulation and for stabilization were obtained graphically from the plots of the resultant turbidities as a function of sample pH. The definitions of the critical pH for coagulation (pH_c) and for stabilization (pH_s) are analogous to those of the corresponding critical concentrations in that a given sol is stable in the pH region greater than or equal to a pH_s and lower than a pH_c. Similar experiments were performed to determine the effects of pH on colloidal stability in the absence of other coagulants.

The pH of all samples was measured with a Sargent-Welch Model NX pH meter equipped with a combination electrode. Electrophoretic mobility data were obtained with a device manufactured by Zeta-Meter, Inc., to determine the isoelectric points of the coal suspensions.

Results and Discussion

Effects of pH. The isoelectric point and the pH for stabilization were determined to examine the effect of hydrogen ion on suspension stability in the absence of other coagulants. Electrophoretic mobility and turbidity data for oxidized and unoxidized coal suspensions are shown as a function of pH in Figure 1. The mobility data have units of $\mu m \cdot cm/(v \cdot s)$. Particles of the unoxidized coal were positively charged at low pH and negatively charged elsewhere, and its isoelectric point (pH_i) occurred at pH 5.1. Between pH 4 and pH 8 its mobility decreased sharply and approached a constant value above pH 8.5 where ionization of the coal surface was essentially complete. Following vigorous oxidation with hydrogen peroxide the coal was negatively charged throughout the pH range of observation as the pH_i decreased to approximately 1.1. Oxidized coal particles had greater negative mobility than unoxidized coal at all pH values, indicating greater electrostatic repulsion and, therefore, stability. Above pH 3.5 the mobility remained nearly constant at $-3.8\ \mu m \cdot cm/(v \cdot s)$, approximately the same value for the unoxidized coal. Apparently, vigorous oxidation produced more easily ionizable surface groups on the coal, predominantely carboxyl groups, which lower the pH_i from 5.1 to 1.1.

The stability of many sols is dependent on pH since many colloids preferentially adsorb hydrogen or hydroxide ions (*19*). These ions promote instability by charge neutralization and adsorptive coagulation. Furthermore, hydrogen ions are potential determining in that they reduce the surface potential of negatively charged particles.

Table I. Summary of log Critical Coagulation Concentrations for Ionic Coagulation Studies

sol	coagulant $NaNO_3$	$Ca(NO_3)_2$	$BaCl_2$	$ErCl_3$	$Al_8(OH)_{20}^{4+}$
		Oxidized Coal			
aged 22 days, pH 6.0	−1.19		−3.01		−6.45[a]
aged 38 days					
pH 5.1	−1.36	−3.04		−5.00	−6.35[b]
pH 6.5	−1.13	−3.07	−3.24	−5.01	
pH 9.0	−1.09	−3.04	−3.09	−5.00	
aged 100 days					
pH 5.3	−1.31	−3.22		−4.91	−6.15[a]
pH 6.2	−1.11		−3.24	−5.40	−6.60[a]
average results	−1.20	−3.09	−3.14	−5.06	−6.39
		Unoxidized Coal			
aged 7 days, pH 9.0	−2.32	−3.60	−3.60	−5.40	
aged 14 days, pH 8.0	−1.99	−3.56		−5.30	
aged 14 days, pH 8.0	−2.35		−3.65	−5.40	
average results	−2.22	−3.58	−3.62	−5.37	

[a] Aluminum sulfate. [b] Aluminum nitrate.

Consequently, coagulation occurs at much lower concentrations of hydrogen ions than of indifferent cations with a 1+ charge.

The turbidity data shown in Figure 1 for oxidized and unoxidized coal sols aged 22 and 8 days, respectively, show the effects of pH on stability. The pH_s of each sol was determined from the intersection obtained by extrapolating the steepest portion of the settling curves between the settling and stability regions to the turbidity value of the stable sol. Suspensions of oxidized and unoxidized coal were stable above pH 2.58 and 7.48, respectively. Oxidation lowered the pH_s in the same manner and for analogous reasons as it decreased the pH_i. For both suspensions the pH_s occurred at nearly the same electrophoretic mobility value, which is representative of the minimum potential required for colloidal coal to remain stable by electrostatic repulsion.

Ionic Coagulation Studies. The coal suspensions were coagulated with aluminum(III) and neutral salts to examine the applicability of the Schulze–Hardy rule and the influence of oxidation, suspension age, and pH on their colloidal stability. In these experiments the pH was maintained above the pH_s where the suspensions were stable in the absence of coagulants. The ionic coagulants used in the studies were Na^+, Ca^{2+}, Ba^{2+}, Er^{3+}, Al^{3+}, and, presumably, the $Al_8(OH)_{20}^{4+}$ ion. Due to hydrolysis the aluminum species present are dependent on both pH and the applied Al(III) concentration. Below pH 4 and 1×10^{-3} M Al(III), Al^{3+} is the main species (*15*). Between pH 5 and pH 7 and below 1×10^{-5} M Al(III), $Al_8(OH)_{20}^{4+}$ is believed to be the dominant species present along with $AlOH^{2+}$ and $Al(OH)_3$ precipitate (*20*). Erbium chloride, though not commonly used, was an excellent salt to examine ionic coagulation with a 3+ ion. The salt is soluble in water and does not precipitate with sulfate, nitrate, and carbonate. Erbium has only a single oxidation state, +3, and does not hydrolyze below pH 12. All of the other salts in this study were commonly employed simple electrolytes.

Oxidized coal suspensions aged 38 days were coagulated at pH 5.1, 6.5, and 9.0 by $NaNO_3$, $Ca(NO_3)_2$, and $ErCl_3$ to determine if suspension pH has a significant effect on ionic coagulation. Turbidity data from experiments at pH 6.5 are shown in Figure 2. The filled circles, open squares, and open circles represent the absorbances of the samples measured after 1, 12, and 40 h of settling, respectively. Data from three time periods are shown only for coagulation by calcium ions, but similar results were obtained with the other salts. The c.c.c. was determined by extrapolating the steepest portion of the settling curve to intersect with the turbidity value of the stable suspension as shown in lines with the 40-h data for calcium ion. The log molar concentration of the intersection point was −3.07, corresponding to a c.c.c. of 8.5×10^{-4} M Ca^{2+}. Note that similar results could be obtained with the 1- and 12-h data, and consequently, the c.c.c. was judged to be independent of time. The oxidized coal settled effectively at concentrations just greater than the c.c.c. with 90% removals occurring within 40 h. The removals obtained at concentrations below the c.c.c. were slight. Similar results were also observed with sodium nitrate and erbium chloride; the concentrations required for coagulation were 7.4×10^{-2} M for Na^+ and 9.8×10^{-6} M for Er^{3+}. As shown in Table I, the critical coagulaton concentrations at other pH values were not significantly different. The c.c.c. values at pH 5.1 were only about 0.2 log molar concentration unit lower than at pH 9.0. This difference was probably caused by the decrease in ionization and surface potential of the coal at lower pH as evident from the electrophoretic mobility data. Kratohvil et al. (*21*, *22*) have shown that a decrease in either surface charge density or solvation generally lowers the electrolyte concentration required to induce coagulation.

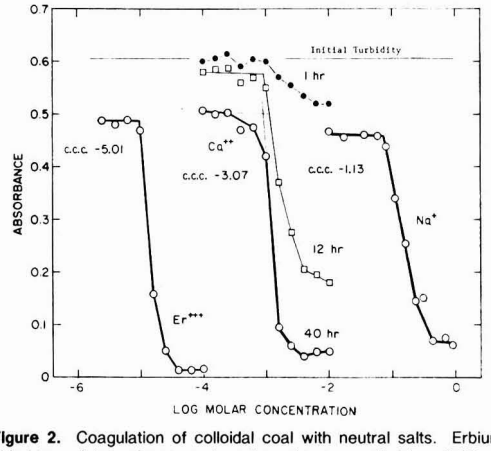

Figure 2. Coagulation of colloidal coal with neutral salts. Erbium chloride, calcium nitrate, and sodium nitrate at pH 6.5. Oxidized −400-mesh coal aged 38 days.

Experiments were also performed to examine the influence of aging on the stability of oxidized coal suspen-

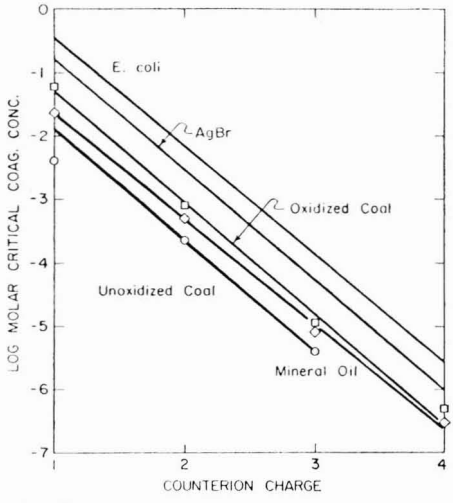

Figure 3. Težak plot of the Schulze–Hardy rule for various hydrosols.

sions in the presence of aluminum(III) and neutral salts. Aging the coal sols increased their stability in the absence of coagulants as evident by their turbidity which remained nearly constant after aging for 14 days. The tests were performed near pH 6 on sols aged 22, 38, and 100 days. The c.c.c. values, given Table I, for the different aged suspensions with each coagulant were not significantly different. On the other hand, the settling curves for older suspensions had sharper breaks between the stability and settling regions.

Unoxidized coal suspensions aged 7 days at pH 9 and 14 days at pH 8 were also coagulated with $NaNO_3$, $Ca(NO_3)_2$, $BaCl_2$, and $ErCl_3$. The settling curves were very similar to those for oxidized coal, but the respective c.c.c. values with each coagulant, except $NaNO_3$, were 0.5 log unit lower or one-third as high as the c.c.c. values for oxidized coal. Unexpectedly, coagulation of the unoxidized coal sol with sodium ion was achieved with a concentration one-tenth as high as the c.c.c. for oxidized coal. This may have occurred because the suspensions were aged in 5×10^{-4} M NaOH to maintain stability. These lower c.c.c. values for unoxidized coal were due possibly to its lower surface ionization as evident from the electrophoretic mobility data shown in Figure 1, but these c.c.c. values were also lower than the c.c.c. values for oxidized coal sols of similar electrophoretic mobility values. Consequently, the increase in the c.c.c. values resulting from oxidation may be partially due to increases in the electrostatic forces, but much of the difference was because oxidized coal sols were more hydrophilic. Matijević (*23*) has demonstrated that increases in surface charge density and hydrophilicity would increase the concentrations of neutral salts required for coagulation.

The c.c.c. values for the coal suspensions are compared conveniently by using Težak's formulation of the Schulze–Hardy rule as shown in Figure 2. Težak (*13*, *14*) has shown with hydrophobic sols that the logarithms of the critical coagulation concentrations when plotted as a function of counterion charge typically form a straight line. The slope of the line, which depicts the influence that the coagulant charge has on coagulation, has been demonstrated to be very similar for different hydrophobic sols, but the intercepts vary considerably (*6*, *23*). Sols stabilized predominantly by electrostatic forces presumably should have the same slope since destabilization proceeds by the same

Table II. Summary of Težak Plot Characteristics for Various Suspensions

suspension	slope	intercept	ref
oxidized coal	−1.73	0.53	
unoxidized coal	−1.77	−0.06	
TiO_2	−1.67	−0.33	10
montmorillonite	−1.60	0.20	6
AgBr	−1.75	1.01	24
E. coli	−1.72	1.30	11
mineral oil	−1.65	0.01	

Table III. Summary of Critical pH Data for Studies with Aluminum(III)

Al(III) concentration				
M	log M	pH_s	pH_c	pH_s
28 mg/L Oxidized Coal–Aluminum Sulfate				
0				2.58
6.3×10^{-6}	−5.2			6.8
1.0×10^{-5}	−5.0	5.25	6.15	6.52
1.6×10^{-5}	−4.8	5.2	6.25	6.91
3.0×10^{-5}	−4.5	5.05	6.6	7.6
5.0×10^{-5}	−4.3		6.5	7.9
8.0×10^{-5}	−4.1	4.81	6.45	
1.0×10^{-4}	−4.0	4.80	5.7	8.65
1.3×10^{-4}	−3.9	4.55	4.95	8.5
2.5×10^{-4}	−3.6		4.65	9.0
4.0×10^{-4}	−3.4		4.45	9.05
5.0×10^{-4}	−3.3		4.40	9.15
1.0×10^{-3}	−3.0		4.35	9.88
3.0×10^{-3}	−2.5		4.1	10.7
1.0×10^{-2}	−2.0		4.0	11.75
2.0×10^{-2}	−1.7		3.68	12.08
1.0×10^{-1}	−1.0		3.70	12.62
28 mg/L Oxidized Coal–Aluminum Nitrate				
2.0×10^{-5}	−4.7		6.94	7.24
3.1×10^{-4}	−3.5			9.46
1.0×10^{-2}	−2.0			11.73
2.3 mg/L Oxidized Coal–Aluminum Sulfate				
1.3×10^{-4}	−3.9		4.63	8.05
1.0×10^{-3}	−2.75		4.13	10.66
38 mg/L Unoxidized Coal–Aluminum Sulfate				
0				7.48
2.0×10^{-4}	−3.7	4.58	4.70	9.34
1.0×10^{-2}	−2.0			11.65

mechanism. The intercept of the Težak plot is dependent on colloidal properties of the sols including their hydrophilicity, surface charge density, and size (*23*).

The Težak plot for colloidal coal suspensions (Figure 3) shows that the slopes for both oxidized and unoxidized coals were typical of hydrophobic sols although the c.c.c. of Na^+ for unoxidized coal was clearly lower than anticipated. For comparison, the slope and intercept for several other sols are also listed in Table II. As expected, oxidized coal had a higher intercept than unoxidized coal since oxidized coal, being more hydrophilic, is more stable in the presence of salts. The slopes for both coals fell within the range observed for other sols and the intercept for unoxidized coal was lower or as low as that of any sol previously studied in this laboratory (*6*).

Aggregation with Aluminum Salts. Oxidized coal suspensions aged 22 days were aggregated with Al(III) salts, principally aluminum sulfate, by using two experimental approaches to determine the critical concentrations and pH values for coagulation and for stabilization. The critical pH and concentration values are listed in Tables III and IV, respectively. Typical results from experiments to determine critical pH values in the presence of Al(III) are presented in Figures 4 and 5. In Figure 4 the 15-min

Table IV. Summary of Critical Concentration Data for Studies on 28 mg/L Oxidized Coal with Aluminum Sulfate

	-log Al(III) molar concentration		
pH	c.c.c.	c.s.c.	c.c.c.
2.50	6.50		
3.00	5.80		
3.50	5.54		
3.95	5.55		
4.25	5.54		
4.60	5.55		
5.0	5.55	4.60	3.90
5.5	5.55	4.91	3.95
6.0	5.55	4.94	4.05

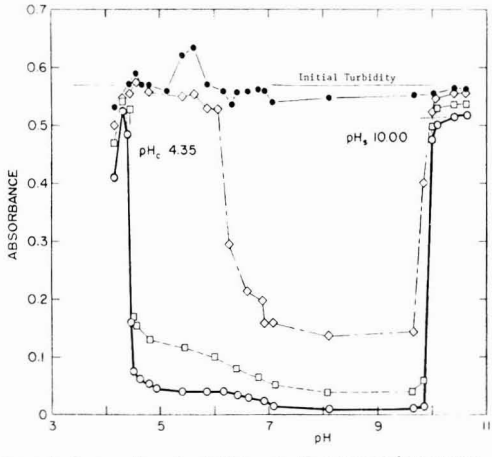

Figure 4. Aggregation of colloidal coal with 1.0×10^{-3} M $Al(SO_4)_{3/2}$ as a function of pH. (●) 15-min, (◊) 1-h, (□) 3-h, and (O) 12-h settling data.

and 1-, 3-, and 12-h settling curves for aggregation by 1.0×10^{-3} M $Al(SO_4)_{3/2}$ are shown by plots of the turbidities of the test samples as a function of pH. Virtually no settling occurred in 15 min although $Al(OH)_3$ precipitate was present. The coal settled most rapidly above pH 6 as evident from the 1-h turbidity data. Within 3 h, the limits of the "sweep zone" of rapid aggregation were established and remained unchanged. Complete clarification was achieved in this zone within the 12-h period of observation. At low pH the coal was aggregated slowly by ionic coagulation with Al^{3+}. A narrow region of stability, centered at pH 4.3 (possibly because of the formation of $AlOHSO_4$), separated the ionic or "slow" cogulation region from the sweep zone. Rapid aggregation by enmeshment in flocs of $Al(OH)_3$ precipitate, the sweep zone, extended from the pH_c at 4.35 to the pH_s at 10.0. The coal sol remained stable above the latter pH value.

Data from similar experiments using 3×10^{-5} M $Al(SO_4)_{3/2}$ are shown in Figure 5 where the 3-, 10-, and 24-h turbidity values are presented as a function of pH. The coal was aggregated more slowly at this concentration, 10 mg/L alum as $Al_2(SO_4)_3 \cdot 18H_2O$, which is but 3% of the dose used in the previous experiments. Twenty-four hours of settling was required to achieve complete clarification and to fully establish the boundaries of the sweep zone. Ionic coagulation occurred very slowly below pH 5.05. The coal retained stability across the broad pH range from 5.05 and 6.65 due to restabilization by charge reversal from adsorption of highly charged aluminum complexes such as $Al_8(OH)_{20}^{4+}$ (*10*, *20*). The sweep zone was much narrower at this Al(III) concentration, extending only from

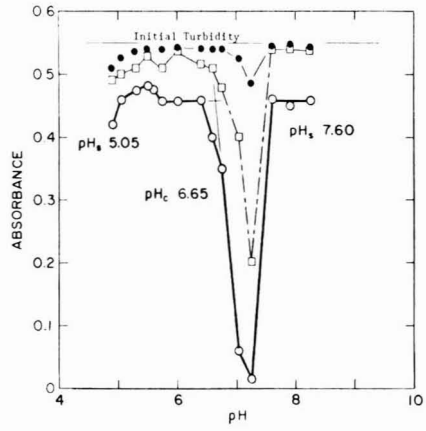

Figure 5. Aggregation of colloidal coal with 3.0×10^5 M $Al(SO_4)_{3/2}$ as a function of pH. (●) 3-h, (□) 10-h, and (O) 24-h settling data.

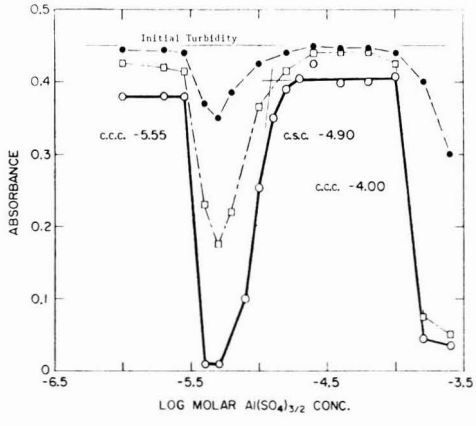

Figure 6. Aggregation of colloidal coal with aluminum sulfate at pH 6.0. (●) 3-h, (□) 10-h, and (O) 20-h settling data.

the pH_c at 6.65 to the pH_s at 7.60.

Typical results of experiments performed to determine critical concentrations are shown in Figure 6. In this case, the 3-, 10-, and 20-h turbidity data for the samples at pH 6.0 were plotted as a function of Al(III) concentration, and the critical concentrations were determined by essentially the same procedures as used in the ionic coagulation studies. During the first 3 h of the tests the turbidities decreased only slightly in the coagulation regions. In 10 h the concentration limits of the settling regions were established. The clarification rate was greater in the settling region at higher concentrations of aggregant since 85% removals were attained near 2×10^{-4} M $Al(SO_4)_{3/2}$ while only 50% removals occurred near 5×10^{-6} M Al(III). Within 24 h the coal sol was completely clarified in both ranges. The rate of clarification in both concentration ranges was similar to the removal rate which occurred in the sweep zone in Figures 7 and 5. The lower c.c.c., at 2.8 $\times 10^{-6}$ M $Al(SO_4)_{3/2}$, represents the minimum Al(III) concentration which can induce aggregation. Restabilization occurred at Al(III) concentrations higher than the c.s.c. at 1.3×10^{-5} M Al(III) and lower than the c.c.c. at 1.0×10^{-4} M $Al(SO_4)_{3/2}$. The c.s.c., which is the minimum concentration of aggregant to stabilize the sol, was determined graphically in the same manner as c.c.c. values. Above 1.0×10^{-4} M $Al(SO_4)_{3/2}$ the positively charged restabilized coal was coagulated by sulfate ion and en-

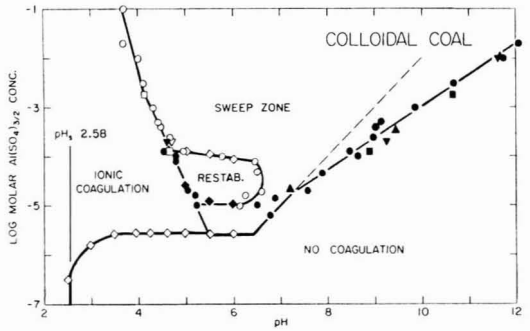

Figure 7. Aluminum sulfate concentration–pH stability limit diagram for colloidal coal. Oxidized −400-mesh coal aged 25 days. Filled symbols are stabilization values, and open symbols are coagulation values. Diamonds are turbidity–concentration data. All other symbols are turbidity–pH data.

meshed in flocs of $Al(OH)_3$ precipitate.

The results observed from the data shown in Figures 4–6 were representative of aggregation at other aluminum(III) concentrations. In summary, two distinct rates of aggregation, corresponding to two regions and mechanisms of aggregation, were observed across the pH range investigated at each alum concentration. At low pH the settling proceeded more slowly than at neutral pH. The difference was very pronounced at concentrations above 1×10^{-4} M Al(III). Throughout the region of low pH coal was coagulated by either ionic aluminum species or hydrogen ion. In the neutral pH range aluminum hydroxide precipitated and settled rapidly, thereby enmeshing the colloidal coal and completely clarifying the suspension. The boundaries or limits of this zone of sweep aggregation were nearly independent of time. Increasing the concentration of aluminum(III) broadened the pH range of the sweep zone and increased the rate of clarification in aggregation regions at both low and neutral pH. Restabilization was observed in the pH range between 5.0 and 6.5 at Al(III) concentrations between 1.1×10^{-5} and 1.0×10^{-4} M. Coagulation by aluminum(III) was not observed at concentrations below 2.8×10^{-6} $Al(SO_4)_{3/2}$ or in the alkaline pH range above the sweep zone.

The results of the experiments on aggregation with aluminum salts can be examined in its entirety by using a plot of the critical coagulation and stabilization values. These values and their associated pH or Al(III) concentration values from Table III and IV were plotted as shown in Figure 7 by using the logarithm of the applied $Al(SO_4)_{3/2}$ concentration as the ordinate and the solution pH as the abscissa. Figure 7 is the aluminum sulfate "stability limit diagram" (SLD) or "stability domain" for oxidized colloidal coal. Each point in the SLD is along a boundary separating distinct domains of settling and stability. The open symbols are critical coagulation values, and the filled symbols are critical stabilization values. The critical $Al(SO_4)_{3/2}$ concentrations are represented by diamonds whereas all other symbols are critical pH values. The squares represent values for a dilute oxidized coal suspension (2.3 mg/L), and the dels are critical pH values for an unoxidized coal sol. The triangles are for experiments on oxidized coal with $Al(NO_3)_3$ instead of $Al(SO_4)_{3/2}$.

The stability limit diagram has four distinct zones. The main zone of clarification by aluminum is the central region labeled as the sweep zone. This zone lies between the boundaries formed by the pH_c values on the acid side and the pH_s values on the alkaline side and above the lowest $Al(SO_4)_{3/2}$ c.c.c. values. In this region aluminum hydroxide precipitates and enmeshes the oxidized coal. The resulting flocs settle very rapidly and sweep the coal out of suspension. Aggregation due to ionic coagulation also occurred in the zone to the left of the sweep zone. This is a region of relatively slow coagulation caused by electrostatic destabilization induced by ionic aluminum species and hydrogen ions. Below pH 2.58 the coal suspensions would be destabilized even in the absence of aluminum sulfate due to coagulation by hydrogen ions.

The oxidized coal suspensions remained stable in two regions. The principal region of stability, labeled "no coagulation", was located to the right of the sweep zone and below the horizontal c.c.c. line for the ionic coagulation. To the right of the sweep zone coal remained stable because at high pH aluminum hydroxide hydrolyzes to form aluminate ion, $Al(OH)_4^-$, which was incapable of coagulating the negatively charged coal particles. Below the horizontal c.c.c. line the Al(III) concentration was too low to induce coagulation. The other stability region was the zone of restabilization where highly charged aluminum ions, presumably the $Al_8(OH)_{20}^{4+}$ ion, was adsorbed sufficiently by the coal and aluminum hydroxide precipitate to reverse their charges (*10*, *15*, *25*). Charge reversal had the effect of restabilizing the sol, thereby preventing coagulation by cations. The minimum aluminum(III) concentration required to reverse the charge, the c.s.c., formed the lower boundary of the restabilization zone. At high aggregant concentrations the restabilized sol was coagulated by the negatively charged sulfate ion added with aluminum(III). The c.c.c. values for this coagulation by sulfate ion delineated the top boundary of the zone. The right side of the restabilization zone was governed in part by aluminum hydroxide precipitation as the left side was controlled by the formation of $AlOH^{2+}$ and Al^{3+} at pH values below the sweep zone instead of $Al_8(OH)_{20}^{4+}$. The relative size and location of the zone are also controlled by properties of the sol, especially its specific surface area and particle concentration (*10*).

The location and shape of the right and left boundaries of the sweep zone are controlled by the hydrolysis of aluminum and interactions between the sol and specific aluminum species. Typically, significant interactions do not occur with hydrophobic sols, and therefore, the right boundary is determined by the hydrolysis equilibrium between aluminum hydroxide and aluminate:

$$Al(OH)_3(s) + H_2O \rightleftharpoons Al(OH)_4^- + H^+$$

This relationship predicts a slope of +1.00 with an intercept of log K_4 on the stability limit diagram as follows:

$$K_4 = [Al(OH)_4^-][H^+]$$

$$\log K_4 = \log [Al(OH)_4^-] + \log [H^+]$$

$$\log [Al(OH)_4^-] = pH + \log K_4$$

At the point where only an infinitesimal amount of $Al(OH)_3$ remains in equilibrium with $Al(OH)_4^-$, which is at the boundary

$$\log [Al(OH)_4^-] \simeq \log [Al(III)]$$

where [Al(III)] is the applied concentration of aluminum(III) as plotted on the SLD. Therefore

$$\log [Al(III)] = pH + \log K_4$$

The right boundary of the SLD for oxidized coal, as determined by linear regression, had a slope of 0.64 and an intercept of −9.35 with a correlation coefficient of 0.991.

Table V. Summary of Sweep Zone Boundary Data for Various Colloids with Aluminum Sulfate

	left boundary		right boundary		
suspension	slope	intercept	slope	intercept	ref
oxidized coal	−3.25	10.94	0.64	−9.35	
TiO_2	−3.53	12.1	0.96	−12.0	10
montmorillonite	−3.67	13.3	0.91	−11.2	6
illite	−3.2		0.98	−12.2	6
E. coli	−3.46		0.88	−11.0	12
$Al(OH)_3$ precipitate	−3.41	11.35	0.92	−12.55	20

These results are clearly different from the boundaries for other sols (see Table V) previously examined in this laboratory (*6*, *10*, *12*, *20*). The right boundary determined for TiO_2 is shown as a dashed line in Figure 7 to illustrate the significance of the change. This suggests that some specific interaction occurred at high pH between aluminum and coal, presumably, with its hydroxyl and carboxyl surface groups. Mangravite et al. (*26*) obtained similar results for a 5 mg/L humic acid sol with aluminum sulfate. His data produced a slope of 0.67 and an intercept of −9.60. At higher humic acid concentrations, the slope was even smaller, and the intercept was higher. Humic acid and oxidized coal, especially at high pH, possess similar ionic functional groups (*8*, *9*).

Several sets of experiments were conducted to identify the cause of the differences in the slope and intercept of the right boundary. Aggregation was examined at three concentrations of aluminum nitrate (instead of aluminum sulfate) to determine if the effect was caused by interactions between sulfate ion and coal. The resulting critical pH values, plotted as triangles in the SLD, were not significantly different than the values for aluminum sulfate. Experiments were also performed at two concentrations of aluminum sulfate on a dilute oxidized coal sol (2.3 mg/L) and on an unoxidized (minimally oxidized) coal suspension. The results for unoxidized coal, plotted as dels in the SLD, also were not different than those obtained previously, indicating that the change was not caused by vigorous oxidation; possibly, superficial oxidation was sufficient to cause the effect. The critical pH values for the dilute oxidized coal suspensions, presented as squares in the SLD, similarly produced essentially the same slope. The intercept was about 0.2 log unit lower, but this difference appears to be insignificant. This effect on the right boundary of the SLD, which must be caused by a property of the coal sol, is as yet not understood.

The left boundary of the sweep zone was very similar to boundaries obtained with aluminum sulfate for aggregation of other sols and precipitation of $Al(OH)_3$ in the absence of sols (see Table V). Its slope and intercept were −3.25 and 10.94, respectively. Analysis of this boundary cannot be performed simply since at least two hydrolyzed species, $AlOH^{2+}$ and $Al_8(OH)_{20}^{4+}$, coexist with $Al(OH)_3(s)$. This prevents use of the stepwise transition analysis employed on the alkaline boundary; however, boundary comparisons indicated that the left boundary was controlled by aluminum hydrolysis. Therefore, coal behaved like other hydrophobic sols and did not influence aluminum hydrolysis above 1×10^{-4} M Al(III) in the acidic pH range.

The final observation to be made from the SLD is that the horizontal line formed by c.c.c. values in the ionic coagulation region apparently meets the horizontal c.c.c. boundary of the sweep zone. This is of interest for two reasons. First, on the basis of the past interpretations of the Težak plot and SLD, the c.c.c. values forming the bottom of the SLD are presumed to be caused by the $Al_8(OH)_{20}^{4+}$ species whereas the c.c.c. values in the ionic coagulation region are a result of the Al^{3+} species. On the basis of the results shown in the Težak plot (Figure 3), the c.c.c. values for 3+ ions should be about 1.7 log units higher than for 4+ ions. Therefore, since the applied Al(III) concentration is stoichiometrically 8 times (0.9 log unit higher than) the $Al_8(OH)_{20}^{4+}$ concentration, the c.c.c. values for the ionic coagulation region with Al(III) should be typically about 0.8 log unit (1.7–0.9) higher than for the sweep zone and not equal as apparent from the SLD. Second, on the basis of the Težak plot and the c.c.c. for Er^{3+}, the Al^{3+} c.c.c. observed in the ionic coagulation region was much lower than expected. A possible explanation, which would account for both discrepancies from that expected for hydrophobic sols, follows from the results of studies with aluminum sulfate on the aggregation of coal and humic acid sols. Humic acid reacts with aluminum(III) between pH 3 and pH 5 to form an aluminum humate precipitate (*26*). Therefore, in a similar manner aluminum(III) may adsorptively coagulate or precipitate the coal since both sols possess similar chemical characteristics. Presumably, this mechanism would operate uniformly throughout both aggregation regions at low concentrations of aluminum(III) to produce the same horizontal c.c.c. line in the ionic coagulation region and sweep zone.

Conclusions

The stability of colloidal coal in the presence of neutral salts was examined as a function of the solution pH and the extent of aging and oxidation of the coal sols. Both oxidized and unoxidized coals behaved as hydrophobic colloids and were coagulated in accordance with the Schulze–Hardy rule. Oxidation greatly enhanced the stability of coal by increasing the surface ionization. The oxidized coal had greater electrophoretic mobility and was more hydrophilic than unoxidized coal. Aging did not significantly affect the stability of the coal sols toward electrolytes. The stability of the suspensions was very sensitive to pH. Unoxidized coal was unstable below pH 7.5 while highly oxidized coal was stable above pH 3. Above the pH_s of the sols, ionic coagulation was only slightly affected by pH.

The aggregation of oxidized coal by aluminum sulfate was systematically investigated, and its entire log $Al(SO_4)_{3/2}$ concentration–pH stability limit diagram was established. The boundary in the acid region of the diagram was similar to that of other hydrophobic sols in its slope and intercept. In the alkaline region the boundary was not typical, in that its slope of 0.64 was much smaller than the predicted slope of 1.0 for the $Al(OH)_3$ precipitation boundary. The intercept was also much higher than expected, indicating that there was probably a specific interaction between aluminum and humic (hydroxycarboxylic) groups on the coal. Restabilization, typical of hydrophobic sols, occurred near pH 6 due to charge reversal by adsorption of highly charged soluble aluminum complexes on the coal. Aggregation was controlled primarily by the hydrolysis and precipitation of aluminum hydroxide.

Registry No. $NaNO_3$, 7631-99-4; $Ca(NO_3)_2$, 10124-37-5; $BaCl_2$, 10361-37-2; $ErCl_3$, 10138-41-7; $Al_2(SO_4)_3$, 10043-01-3; $Al(NO_3)_3$, 13473-90-0.

Literature Cited

(1) "Mineral Yearbook 1970"; U.S. Bureau of Mines: Washington, DC, 1972; Vol. I.

(2) Lucas, J. R.; Maneval, D. R.; Foreman, W. E. In "Coal Preparation", 3rd ed.; Leonard, J. W.; Mitchell, D. R., Eds.;

American Institute of Ming and Metallurgical Engineers: New York, 1968.
(3) Aplan, F. F. In A. M. Gaudin Memorial International Flotation Symposium; Fuerstenau, M. S., Ed.; American Institute of Mining and Metallurgical Engineers: New York, 1976.
(4) *Fed. Resist.* **1977**, *80*, 21380.
(5) Packham, R. F. *J. Colloid Sci.* **1965**, *20*, 81–92.
(6) Rubin, A. J.; Blocksidge, H. *J.—Am. Water Works Assoc.* **1979**, *71*, 102–110.
(7) Sun, S.-C. *Min. Eng. (Littleton, Colo.)* **1954**, *6*, 396–401.
(8) Marinov, V. N. *Fuel* **1977**, *56*, 165–170.
(9) Czuchajowski, L. *Fuel* **1960**, *39*, 377–385.
(10) Rubin, A. J.; Kovac, T. W. In "Chemistry of Water Supply, Treatment, and Distribution"; Rubin, A. J., Ed.; Ann Arbor Science: Ann Arbor, MI, 1974; Chapter 8.
(11) Rubin, A. J.; Hayden, P. L.; Hanna, C. P. *Water Res.* **1969**, *3*, 843–852.
(12) Rubin, A. J.; Hanna, G. P. *Environ. Sci. Technol.* **1968**, *2*, 358–362.
(13) Težak, B. *J. Phys. Chem.* **1953**, *57*, 301–307.
(14) Matijević, E.; Schulz, K. F.; Težak, B. *Croat. Chem. Acta* **1956**, *28*, 81–91.
(15) Matijević, E.; Janauer, G. E.; Kerker, M. *J. Colloid Sci.* **1964**, *19*, 333–346.
(16) Matijević, E.; Mathai, K. G.; Ottewill, R. W.; Kerker, M. *J. Phys. Chem.* **1961**, *65*, 826–830.
(17) Vogel, A. I. "Quantitative Inorganic Analysis"; Wiley: New York, 1961.
(18) Rubin, A. J.; Kramer, R. J. *Sep. Sci. Technol.* **1982**, *17*, 535–560.
(19) Van Olphen, H. "Clay Colloid Chemistry"; Wiley: New York, 1963.
(20) Hayden, P. L.; Rubin, A. J. In "Aqueous-Environmental Chemistry of Metals"; Rubin, A. J., Ed.; Ann Arbor Science: Ann Arbor, MI, 1974; Chapter 9.
(21) Kratohvil, S.; Janauer, G. E.; Matijević, E. *J. Colloid Interface Sci.* **1969**, *29*, 187–194.
(22) Kratohvil, S.; Matijević, E. *J. Colloid Interface Sci.* **1976**, *57*, 104–114.
(23) Matijević, E. *J. Colloid Interface Sci.* **1973**, *43*, 217–245.
(24) Matijević, E.; Broadhurst, D.; Kerker, M. *J. Phys. Chem.* **1959**, *63*, 1552–1557.
(25) Matijević, E., Stryker, L. J. *J. Colloid Interface Sci.* **1966**, *22*, 68–77.
(26) Mangravite, F. J., Jr.; Buzzell, T. D.; Casell, E. A.; Matijević, E.; Saxton, G. B. *J.—Am. Water Works Assoc.* **1975**, *67*, 88–94.

Received for review April 28, 1983. Accepted September 20, 1983.

Characterization of Surface Species on Coal Combustion Particles by X-ray Photoelectron Spectroscopy in Concert with Ion Sputtering and Thermal Desorption

George E. Cabaniss and Richard W. Linton*

Department of Chemistry, The University of North Carolina, Chapel Hill, North Carolina 27514

■ The surface chemical composition of ash particles collected in the electrostatic precipitator of a power plant burning high sulfur coal was determined by using X-ray photoelectron spectroscopy (XPS). A bulk particle sample was separated into magnetic and nonmagnetic fractions for comparison to the unfractionated sample. After XPS characterization, the samples were subjected to rare gas ion (Ar^+) sputtering to remove surface material. The XPS technique then was used to detect any sputter-induced composition changes. These results were compared with data obtained by heating similar samples under high vacuum and recording XPS data as a function of temperature (20–200 °C). Effects of sample temperature on the extent of differential charging phenomena influencing XPS photopeaks and chemical state information also were documented.

Introduction

Recent trends in global political stability, energy costs, and public perception of the health risks of energy production byproducts have influenced the United States in adopting a short-term energy policy more dependent on domestic coal supplies. Aerosol formation during the combustion of coal is particularly significant in that smaller particles (<1 μm) are not as efficiently trapped by emission control devices and may subsequently travel great distances before deposition (*1*). These microscopic particles may be preferentially and irreversibly trapped in alveolar regions of the lung (*2*, *3*) where they are in intimate contact with body fluids and tissue. Aerosol toxicity probably is due in part to trace elements present on the surface of the particles (*4*, *5*) as well as sorbed organics such as polynuclear aromatic hydrocarbons and their chemical derivatives (*6*). Recent reports also have suggested a correlation between the combustion of fossil fuels and acid precipitation and deposition (*7–10*).

The composition of materials sorbed on the various types of particles (i.e., soot, aluminosilicates, iron oxides, etc.) that make up coal fly ash is of primary importance. These sorbates are exposed to atmospheric gases and solar radiation as well as being susceptible to aqueous leaching before or after deposition. In this report, the surface composition of ash derived from a midwestern coal is determined by X-ray photoelectron spectroscopy (XPS). In order to estimate the relative amount of surface-specific species that is also volatile, the sample was heated from ambient temperature to 200 °C while the residual gas composition of the ultrahigh vacuum analysis chamber was monitored by electron impact mass spectroscopy. After sample heating, surface composition was again determined by XPS. These results were compared to surface compositions determined before and after inert ion (Ar^+) etching used to remove both involatile and volatile surface species.

Materials and Methods

Ash collected at 200 °C from the electrostatic precipitator of a midwestern coal-fired electrical generation plant was separated into magnetic and nonmagnetic fractions (operationally defined) by using a standard Teflon-coated stir bar enclosed in a polypropylene test tube. In order to reduce entrapment of nonmagnetic particles in the magnetic fraction, magnetic particles were subjected to three magnetic transfers. The ash was found to be approximately 30% by weight magnetic particles. These particles are thought to originate largely from pyrite (FeS_2)

0013-936X/84/0918-0271$01.50/0

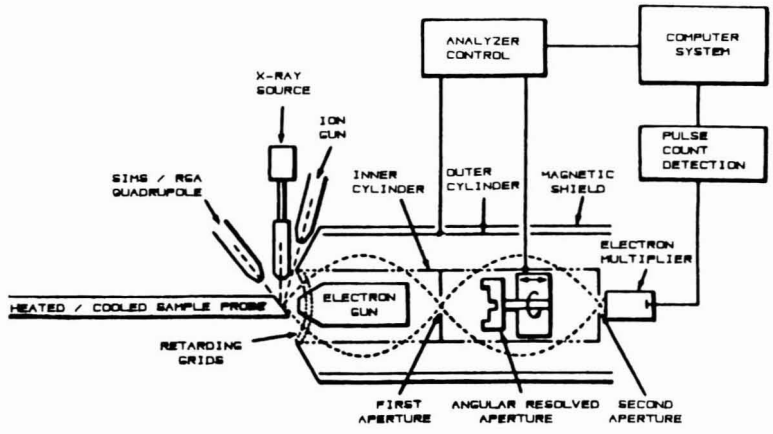

Figure 1. Schematic of Physical Electronics Model 548 photoelectron spectrometer.

framboids in coal which may be converted into magnetite (Fe_3O_4) during combustion (*11*). The magnetic and nonmagnetic fractions were analyzed separately to determine if adsorption characteristics or surface composition varied significantly with particle matrix type. Before XPS analysis, the magnetic particles were degaussed by using a standard audio tape head demagnetizer. Ash samples were then pressed into lead foil (mp 327.5 °C; Alfa Products, 00179) with a standard pellet press. Lead foil was used as the support material, rather than the more commonly employed indium foil, because of lead's higher melting point. X-ray photoelectron spectroscopy was performed on a Physical Electronics Model 548 XPS/Auger electron spectrometer (Figure 1) equipped with a heated sample probe (Model 02-120) and heater control (Model 20-028). All XPS data were collected at analysis chamber pressures less than 8.0×10^{-9} torr. Low-resolution spectra used in quantitative analysis were acquired with the photoelectron pass energy at 100 eV while high-resolution spectra used for chemical state determinations were acquired with a pass energy of 25 eV. Analyzer control, data acquisition, Mg $K\alpha_{3,4}$ satellite removal, and other data manipulation were performed on a dedicated microcomputer system (*12*). Quantitative elemental concentration values were calculated by using normalized photoelectron peak areas and empirical atomic sensitivity factors (*13*). Speciation information was obtained by charge referencing all photoelectron binding energies to the Si ($2p_{3/2}$) photoelectron peak which was assigned a value of 102.6 eV binding energy. This is the literature value (*14*) of various silicates which have been shown to be the dominant forms of silicon in coal ash by X-ray powder diffraction (*15*).

Surface species were further classified as volatile or involatile by observing their behavior upon sample heating or inert ion (Ar^+) etching. During heating, the residual gas composition of the analysis chamber was monitored (0–250 amu) on a spectrEL quadrupole mass spectrometer (Extranuclear Laboratories) equipped with an electron impact ion source. Mass spectral measurements were obtained before sample introduction into the analysis chamber, just after sample introduction, during sample heating from ambient temperature to 100 °C, and during heating from 100 to 200 °C. Concurrently, surface composition was determined by XPS at room temperature and 100 and 200 °C. Data were then compared with results obtained from similar samples in which argon ion etching (Kratos Minibeam I ion gun, 20 min, 4.5 keV kinetic energy, 15 mA emission current, and partial pressure of 4.2×10^{-5} torr of argon) was used to remove approximately 20 nm of the particle surfaces. After sputtering, XPS analysis was repeated. Bulk elemental analysis was performed on an AEI MS-7 spark source mass spectrometer (SSMS). The experimental detail and results of the SSMS determination have been reported previously as well as surface analyses using Auger electron spectroscopy and ion microprobe mass spectrometry (*4*).

Table I. XPS Surface Composition (Percent Atomic)[a]

element	magnetic	unfractionated	nonmagnetic
Na (1s)	0.5 (12)	0.5 (16)	0.4 (64)
Fe (2p)	2.4 (16)	1.6 (8)	1.1 (4)
O (1s)	54.6 (3)	45.9 (5)	42.0 (5)
Ca (2p)	1.0 (15)	0.8 (9)	0.7 (10)
C (1s)	23.6 (9)	36.2 (8)	43.5 (5)
S (2p)	5.4 (8)	4.2 (6)	3.7 (7)
N (1s)	0.4 (6)	trace	trace
Si (2p)	5.1 (14)	4.1 (5)	3.6 (3)
Al (2p)	3.1 (11)	2.5 (2)	2.4 (8)
As (3d)	0.6 (11)	0.6 (44)	0.6 (15)
P (2s)	3.5 (26)	3.2 (10)	2.0 (6)

[a] Values listed are the mean of three determinations (different samples). The values in parentheses are the percent relative deviations from the mean value. Detectable elements are normalized to 100% atomic concentration.

Results and Discussion

The surface composition of magnetic ash, nonmagnetic ash, and unfractionated ash as determined by XPS appears in Table I. Since carbon appears to be the predominant element in the nonmagnetic particles, that fraction apparently is composed mostly of carbonaceous soot. The high oxygen content of both fractions is expected since X-ray powder diffraction has shown (*15*) that the crystalline components of the matrix (bulk) of similar ash material is composed primarily of refractory oxides such as α-quartz, hematite, magnetite, calcium oxide, and mullite ($3Al_2O_3 \cdot 2SiO_2$). Also, surface-sorbed species such as carbonates (*16*), sulfates, nitrates, water, and carbon dioxide are likely to contribute to XPS-detected oxygen. The high concentration of sulfur on the ash surface is related in part to the use of a high sulfur (>1%) coal.

If XPS only provided surface qualitative elemental analysis, previous studies using Auger spectroscopy and ion microprobe spectroscopy data would be sufficient to

Table II. Surface Speciation

element	magnetic fraction E_b (eV)	magnetic fraction species[c]	nonmagnetic fraction E_b (eV)	nonmagnetic fraction species[c]
Fe ($2p_{3/2}$)	711.1	Fe_3O_4	710.0	Fe_2O_3
O (1s)	complex		complex	
Ca ($2p_{3/2}$)[a]	347.9	Ca^{2+}	347.9	Ca^{2+}
C (1s)	complex		complex	
S (2p)	168.9	SO_4^{2-}	169.3	SO_4^{2-}
N (1s)	low S/N		low S/N	
Si (2p)[b]	102.6	silicate	102.6	silicate
Al (2p)[a]	74.6	aluminate	74.7	aluminate
As (3d)	low S/N		low S/N	
P (2s)	191.8	?	190.4	?

[a] "Low-resolution" XPS used to determine the value (100 eV pass energy); all other values determined by using 25 eV pass energy. [b] Si 2p used as charge reference (E_b = 102.6 eV). [c] Species assignment based on E_b from ref 14.

characterize the surface of this ash (*4*). However, XPS offers the advantage of providing additional chemical speciation information as well as facile semiquantitative analysis for elements greater than about 1% atomic concentration in the surface region.

Table II shows the binding energy and predominant chemical form of the most abundant elements in both magnetic and nonmagnetic fractions. The principal form of iron in the magnetic fraction apparently is magnetite (Fe_3O_4), while the binding energy of iron in the nonmagnetic fraction is consistent with hematite (Fe_2O_3). Calcium is in the divalent state in both fractions, while the predominant form of sulfur appears to sulfate. The absence of photopeak intensity at a binding energy corresponding to SO_2 suggests that any sorbed SO_2 is either desorbed under the high vacuum analysis conditions or surface oxidized to sulfate. Because of the many possible cations and mixtures of cations that can bind to sulfate (H^+, NH_4^+, Na^+, K^+, Ca^{2+}, Mg^{2+}, Fe^{2+}, Fe^{3+}), it is not possible to assign specific cations to sulfate as detected by XPS. The sulfur concentration present as SO_4^{2-}, however, is slightly more than sufficient to charge balance the total detectable amounts of Na, Ca, Fe, and N present in each sample (Table I), assuming Na^+, Ca^{2+}, Fe^{2+}, and NH_4^+. These cations, and combinations thereof, would be likely candidates for sulfate counterions. Indeed, discrete crystallites of $CaSO_4$ have been observed on fly ash surfaces using electron microprobe/diffraction techniques, and alkali–alkaline earth–iron sulfates are principal constituents of corrosive deposits in coal-burning power plants (*4*).

The binding energies of silicon and aluminum (Table II) indicate +4 and +3 oxidation states, respectively, and are consistent with quartz and aluminosilicate X-ray powder diffraction structural assignments (*15*). Oxygen and carbon photoelectron line shapes are quite complex. This result is expected due to the complex mixed oxide matrix of fly ash as well as the many different chemical forms of surface carbon likely to be present (i.e., elemental carbon, polynuclear aromatic hydrocarbons including oxygen- and nitrogen-containing derivatives, carbon dioxide, carbonates, etc.). Further discussion of XPS oxygen and carbon data will be presented later.

An interesting result is that phosphorus appears to exist in different, albeit unknown, chemical forms in the magnetic and nonmagnetic fractions. Since the photoelectron peak observed is less sensitive than the more commonly observed P ($2p_{3/2}$) photoelectron, explicit literature values are not available for more definitive structural assignment. The P ($2p_{3/2}$) photoelectron peak was not analytically useful under experimental conditions due to an interference from lead (4f) in the lead backing material.

Table III. XPS of Magnetic Fraction after Thermal Desorption or Sputtering

element	normalized area ratios: 100 °C/ room temp	200 °C/ room temp	after Ar^+ sputtering/ before Ar^+ sputtering
Matrix (Bulk) Elements			
Al (2p)	1.0	1.1	2.3
Ca (2p)	1.0	1.0	2.2
Fe (2p)	1.2	1.7	2.8
O (1s)	1.0	1.1	1.0
P (2s)	1.0	1.1	1.0
Si (2p)	1.0	1.0	1.1
Surface-Enriched Elements			
As (3d)	0.8	0.9	NA[b]
C (1s)	1.0	0.8	0.5
N (1s)	trace	ND[a]	NA[b]
S (2p)	1.0	1.1	0.5

[a] Not detected. [b] Not available.

Table IV. XPS of Nonmagnetic Fraction after Thermal Desorption or Sputtering

element	normalized area ratios: 100 °C/ room temp	200 °C/ room temp	after Ar^+ sputtering/ before Ar^+ sputtering
Matrix (Bulk) Elements			
Al (2p)	1.0	0.9	2.0
Ca (2p)	1.0	1.0	2.1
Fe (2p)	1.1	1.6	4.4
O (1s)	1.0	1.0	1.0
Si (2p)	1.1	1.0	1.2
Surface-Enriched Elements			
As (3d)	0.7	0.4	NA[a]
C (1s)	1.0	1.0	0.8
N (1s)	ND[b]	trace	NA
P (2s)	1.2	1.3	ND
S (2p)	1.1	1.1	0.5

[a] Not available. [b] Not detected.

Tables III and IV show changes in relative surface composition in magnetic and nonmagnetic fractions, respectively, as a function of sample heating and argon ion etching (approximately 20 nm of surface removed by etching). Elements having approximately the same or higher normalized areas after heating or ion etching are denoted as matrix elements (constituents of the particle bulk). Elements that exhibit a reduction in normalized areas after heating or sputtering have been classified as surface enriched elements; elements that exhibit lower normalized area upon heating obviously exist in a volatile surface chemical form. Sulfur clearly exists as an involatile sulfate, while classification of oxygen as a matrix element (Tables III and IV) is somewhat misleading since it is also an important constituent of various adsorbates. According to residual gas mass spectrometric analysis, oxygen in the form of water is the most significant volatile absorbed species on both magnetic and nonmagnetic fractions.

Carbon-containing compounds are important adsorbates on the magnetic particles. Approximately 20% of the surface carbon can removed by heating to 200 °C, and a 50% reduction in surface carbon results from ion sputtering (Table III). A vast number of sorbed organic compounds including various polynuclear aromatic species (*6*), CO_2, and carbonate are among the many possible carbon-containing adsorbates. Although Natusch et al. (*16*) have suggested that most carbonates are stable beyond 200

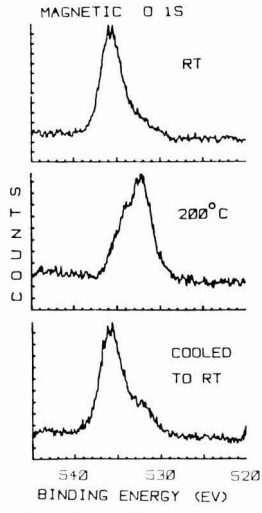

Figure 2. Oxygen 1s photopeak (25 eV pass energy) for the magnetic ash fraction as a function of temperature. Binding energies are not charge corrected. RT = room temperature spectrum; 200 °C = spectrum acquired at 200 °C; cooled to RT = spectrum acquired after cooling to room temperature from 200 °C.

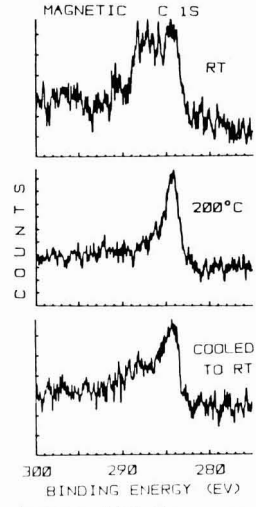

Figure 3. Carbon 1s photopeak (25 eV pass energy) for the magnetic ash fraction as a function of temperature. Binding energies are not charge corrected. Temperature designations are as in Figure 2.

°C on ash surfaces, this XPS study suggests volatile surface carbonates are present. A minor carbon 1s component in the magnetic fraction at about 290 eV (uncorrected binding energy) largely disappears following a 200 °C heating cycle. The binding energy is appropriate for surface carbonates, but the assignment is complicated by differential charging effects to be discussed. Vacuum chamber residual gas analysis using a quadrupole mass spectrometer did not show significant increases in the intensities of carbon-containing ions upon sample heating. However, sensitivity was limited by spectrometer positioning of ≥5 cm from the sample surface. Carbon also appears to be much less efficiently removed by heating or ion sputtering for the nonmagnetic particles (Table IV). The much higher bulk carbon (e.g. soot) content of the nonmagnetic fraction (Table I) minimizes the possibility of substantial decreases in the total carbon 1s signal intensity following the removal of carbon-containing adsorbates.

Phosphorus again exhibits variations in line shape and surface enrichments between fractions. The magnetic fraction phosphorus is apparently part of the bulk of this ash material. However, nonmagnetic fraction phosphorus seems to be primarily a surface species since it is removable by ion etching. This evidence along with differences in charge-corrected phosphorus photoelectron binding energies in the magnetic and nonmagnetic fractions indicate that phosphorus exists in different forms on the different types of ash.

It is important to note that the utility of the XPS-derived chemical state information is limited by sample charging phenomena and their temperature dependence. Sample charging is frequently compensated for via subtraction of a constant energy correction to all experimental binding energies. The correction factor is obtained by comparison of the experimental binding energy of an element of known chemical state to that of literature values. However, this approach is not totally valid unless all parts of the sample charge uniformly. For a heterogeneous particulate sample such as coal fly ash, it is apparent that some individual particles may be highly electrically conductive (e.g., graphitic soot) while others may be much more nonconducting (e.g., aluminosilicates), leading to nonuniform or differential charging of the sample.

Typical high-resolution XPS results for oxygen 1s appear in Figure 2 for the magnetic fraction as a function of temperature. The binding energy (E_b) scale has not been corrected for sample charging. The elevated temperature (200 °C) shifts the uncorrected E_b to lower values apparently reflecting the temperature dependence of electrical conductivity. The peak shape and uncorrected binding energy return to very nearly the original values upon cooling to room temperature, indicating that the 200 °C spectrum is not substantially altered by desorption of oxygen-containing surface species. If the E_b of each oxygen spectrum (Figure 2) is corrected by using the silicon $2p_{3/2}$ peak (E_b = 102.6 eV for silicates), the oxygen E_b corresponding to maximum intensity occurs at the same location (531.7 eV) for all temperatures.

Some differential charging also is observed in that the low E_b tails of the oxygen 1s peaks will occur below the range of known values if charge corrected to the silicon $2p_{3/2}$ energy for silicates. Thus, the oxygen peak shape reflects both variable chemical state and electrical conductivity effects. For example, oxygen-containing species sorbed to graphite soot may exhibit minimal electrical charging relative to surface-associated or bulk oxygen-containing compounds in the various nonconducting metal oxides which comprise the majority of the magnetic fraction particles.

Photoelectron peaks of other elements show similar behavior upon heating of either magnetic or nonmagnetic fractions. The carbon 1s peak (Figure 3), however, exhibits somewhat different characteristics in that the majority of it does not charge to the same degree as the oxygen 1s or silicon $2p_{3/2}$ photopeaks. In fact, much of the carbon shows virtually no charging consistent with the presence of a graphitic soot component (literature value for graphitic carbon 1s E_b is 284.3 eV). The original spectrum also shows higher E_b carbon components which may reflect both more oxidized forms of surface carbon or differential charging. For example, deposition of hydrocarbons on nonconducting metal oxide particles would shift the apparent carbon E_b several electron volts higher relative to the same species sorbed to a conductive sootlike particle.

Alternatively, oxidized carbon such as CO_3^{2-} would be shifted about 4 eV higher in E_b relative to adsorbed hydrocarbons on the same particle substrate (*14*).

The carbon 1s behavior also differs from the oxygen 1s in that the original carbon line shape is not exactly restored following a heating/cooling cycle. Upon cooling from 200 °C to room temperature, the higher binding energy components appear attenuated relative to the original carbon spectrum. This is the likely result of the substantial desorption of both volatile hydrocarbons and oxidized forms of surface carbon such as carbonate upon heating.

Conclusion

The utility of XPS surface analysis in concert with ion sputtering and thermal desorption has been illustrated. Iron, oxygen, calcium, silicon, and aluminum are elemental constituents of the bulk of magnetic and nonmagnetic fractions of coal fly ash particles. Binding energies of these elements in the surface region yield speciation information consistent with bulk structures suggested by X-ray powder diffraction. Other elements such as carbon, oxygen, sulfur, and nitrogen are associated at least in part with surface deposits on ash particles in the form of volatile and involatile compounds. Such species are potential environmental hazards in part because they are surface enriched and constitute a direct interface with the natural environment. For example, sulfate-rich surface layers on in-stack coal fly ash are highly soluble in aqueous media (*4*). If particles that escape from emission control devices have similar properties, they would be implicated as potential contributors to acid rain formation and deposition.

Literature Cited

(1) Björseth, A.; Lunde, G.; Lindskog, A. *Atmos. Environ.* **1979**, *13*, 45–53.
(2) Nagelschimit, G.; Nelson, E. S.; King, E. J.; Attygalle, D.; Yoganathan, M. *AMA Arch. Ind. Health* **1957**, *16*, 188–202.
(3) Morrow, P. E. *J. Ind. Hyg. Assoc.* **1965**, *25*, 213.
(4) Linton, R. W.; Williams, P.; Evans, C. A., Jr.; Natusch, D. F. S. *Anal. Chem.* **1977**, *49*, 1514–1521.
(5) Keyser, T. R.; Natusch, D. F. S.; Evans, C. A., Jr.; Linton, R. W. *Environ. Sci. Technol.* **1978**, *12*, 768–773.
(6) Crisp, C. E.; Fisher, G. L.; Lammert, J. E. *Science (Washington, D.C.)* **1978**, *199*, 73–75.
(7) Cowling, E. G. *Environ. Sci. Technol.* **1982**, *16*, 110A–123A.
(8) Glass, N. R.; Arnold, D. E.; Galloway, J. N.; Hendrey, G. R.; Lee, J. J.; McFee, W. W.; Norton, S. A.; Powers, C. F.; Rambo, D. L.; Schofield, C. L. *Environ. Sci. Technol.* **1982**, *16*, 162A–169A.
(9) Hileman, B. *Environ. Sci. Technol.* **1982**, *16*, 323A–327A.
(10) Munger, J. W.; Eisenreich, S. J. *Environ. Sci. Technol.* **1983**, *17*, 32A–42A.
(11) Lauf, R. J.; Harris, L. A. Rawlston, S. S. *Environ. Sci. Technol.* **1982**, *16*, 218–220.
(12) Woodard, F. W.; Woodward, W. S.; Reilley, C. N. *Anal. Chem.* **1981**, *53*, 1251A–1266A.
(13) Wagner, C. D.; Davis, L. E.; Zeller, M. V.; Taylor, J. A.; Raymond, R. H.; Gale, L. H. *SIA, Surf. Interface Anal.* **1981**, *3*, 211–225.
(14) Wagner, C. D.; Riggs, W. M.; Davis, L. E.; Moulder, J. F.; Muilenburg, G. E., Eds. "Handbook of X-Ray Photoelectron Spectroscopy"; Perkin-Elmer Corp., Physical Electronics Division: Eden Prairie, MN, 1978.
(15) Miguel, A. H. Ph.D. Thesis, University of Illinois, Urbana, IL, 1976, pp 45–46.
(16) Bauer, C. F.; Natusch, D. F. S. *Environ. Sci. Technol.* **1981**, *15*, 783–788.

Received for review May 18, 1983. Accepted November 4, 1983. This research was supported by EPA Grant R807560. The XPS facility was funded in part by the National Science Foundation (Chemical Instrumentation) and the North Carolina Board of Science and Technology.

Octachlorostyrene in Lake Ontario: Sources and Fates

Ray Kaminsky and Ronald A. Hites*

School of Public and Environmental Affairs and Department of Chemistry, Indiana University, Bloomington, Indiana 47405

■ The concentration of octachlorostyrene (OCS) was measured in dated segments of 11 sediment cores taken from Lake Ontario in order to establish the depositional history of this compound in the lake. Using this information, we have deduced that OCS (as well as other chlorinated styrenes and chlorinated polycyclic aromatic hydrocarbons) originates primarily from the waste product of electrolytic chlorine production. This waste, called "taffy", resulted from the chlorination of the tar or pitch used to bind graphite electrodes; its improper disposal led to the introduction of chlorinated aromatic compounds into the environment. OCS is present in all major sediment depositional areas of Lake Ontario and may be subject to biomagnification. Although OCS exhibited no toxicity or mutagenicity in a bacterial bioassay, the long-term environmental impact of chlorinated styrenes is still unknown.

Introduction

In 1972, octachlorostyrene (OCS) was found in the tissues of terns, ducks, and cormorants from the Rhine River and The Netherlands (*1*, *2*). In 1976, fish from Friefjordan, Norway, were found to contain hexa- and heptachlorostyrenes as well as octachlorostyrene (*3*, *4*). In that same year, OCS was discovered in fish from Saginaw Bay, Lake Huron, the Detroit River, and Lake Ontario (*5*). Since then, chlorinated styrenes have been found in fish from Lake St. Clair and Lake Erie (*6*) as well as from the Ashtabula River, OH (*7*). The presence of OCS in these samples has been particularly puzzling since this compound has never been a commercial product. OCS may have been considered as a component of polystyrene and as a PCB replacement, but OCS was never anything but an experimental oddity. Thus, the widespread occurrence of OCS in the lower Great Lakes was not explicable.

In 1982, we found chlorinated styrenes in a few surficial sediments from Lake Ontario (*8*). We proposed but did not prove that these compounds, as well as various chlorinated polycyclic aromatic hydrocarbons, were associated with the wastes from the electrolytic production of chlorine. Until recently, this process employed anodes made from graphite, and it was the chlorination of the coal tar pitch binder used in these anodes that produced much of the chlorinated organic waste related to these processes (*9*, *10*). Since coal tar pitch is highly aromatic, its chlorination products would be a likely source of chlorinated aromatics. This hypothesis linked the findings of chlorinated styrenes in Norway (where a magnesium manufacturer was the only source of contamination) with those

0013-936X/84/0918-0275$01.50/0

Figure 1. Locations and station numbers of sediment cores taken from Lake Ontario.

of the Great Lakes (where the production of chlorine predominates) because both these processes used graphite anodes in the electrolytic decomposition of a chloride brine (*11*). This paper will confirm the above hypothesis and determine the distribution and the sources of OCS in Lake Ontario by an analysis of 11 sediment core samples.

Experimental Section

Sediment Core Sampling. Although fish appear to readily accumulate OCS and are sensitive indicators of its presence, they are usually too migratory to provide information about geographic distribution or possible sources. Sediment cores, however, provide depositional histories at specific locations. After the concentration of OCS in dated core segments from various locations is determined, it might be possible to trace these compounds back to their sources. Sediment cores were collected from Lake Ontario by the Canada Centre for Inland Waters in July 1981 and Sept 1982 from the locations shown in Figure 1. The samples were obtained by subcoring Shipek box-core samples in such a way as to maintain the chronological integrity of the sediment. The cores were frozen prior to shipment to our laboratory to prevent mixing and were kept frozen until analyzed.

Extraction. Solvents used in all phases of the analysis were glass distilled. Acid-washed glassware and core-sectioning implements were solvent rinsed. Each core was thawed in a horizontal position and then sectioned at 2-cm intervals. The thawed interstitial core water was drained from several cores prior to sectioning and extracted with methylene chloride. Since gas chromatographic electron capture analysis revealed no chlorinated compounds in these extracts, the interstitial water was discarded for the rest of the analyses. Each segment was individually loaded into a glasswool-packed, glass, extraction thimble and extracted in a Soxhlet apparatus for 24 h with isopropyl alcohol followed by methylene chloride for 24 h. The extracts were desulfured on a copper column and fractionated on silica gel according to a procedure described elsewhere (*8*).

Analysis. Each fraction was analyzed by gas chromatographic methane negative chemical ionization mass spectrometry using a Hewlett-Packard 5840A gas chromatograph directly linked to an HP 5985B mass spectrometer (*12*). The samples were chromatographed on a J & W DB-5 narrow bore, fused silica capillary column held at 30 °C for 4 min, then programmed to 280 °C at 4 °C/min, and held at 280 °C for 30 min. The carrier gas was helium flowing at a velocity of 40 cm/sec. The mass spectrometer was scanned from 35 to 700 amu at 266 amu/s. The injector and interface temperatures were both 285 °C, and the source and analyzer temperatures were 250 °C. Identification of the chlorinated styrenes was based on comparison of retention times and mass spectra with those of authentic standards. OCS was quantified by ratioing the area of the base peak (m/e 308) to that of external standards of authentic OCS. These figures were then corrected to account for the 80% recovery found for OCS by the extraction and workup of spiked, preextracted sediments. The relative standard deviation of these measurements was estimated to be less than ±30%.

Sedimentation Rate. The sedimentation rate at each location was determined by measuring the ^{137}Cs activity of each core segment. Following extraction, each segment was oven-dried at 100 °C and weighed. Portions of dried sediment were carefully weighed into zip-loc bags or scintillation vials and then counted for 24 h each on a Li/Ge detector coupled to a 4096-channel multichannel analyzer. Detector response was calibrated by using a standard ^{137}Cs solution, and background levels were determined every 24 h. Sedimentation rates were calculated as the length of sediment accumulated between the time of peak atmospheric ^{137}Cs input (1963) and its onset in 1952 (*13*).

Results and Discussion

Source of OCS. Octachlorostyrene was detected in 8 of the 11 cores, and its concentration is plotted as a function of year of deposition in Figure 2. A Gaussian curve has been fitted to these data as an aid to visualization; these curves are a guide for the eye and do not imply a model of depositional history.

Whenever OCS concentration exceeded about 5 ng/g, we found nearly equivalent amounts of three isomers of heptachlorostyrene. Relatively small amounts of hexachlorostyrene were also observed whenever OCS levels were 20 ng/g or higher. Several chlorinated naphthalenes, phenanthrenes, and pyrenes were also associated with these higher levels.

To aid in the interpretation of these results, a few historical details pertaining to the production of chlorine are in order. Chlorine is produced by the electrolysis of an aqueous NaCl or KCl solution. NaOH or KOH forms at the cathode, and Cl_2 (gas) forms at the anode. The anodes were commonly made from powdered graphite with coal tar pitch as a binder. The chlorine formed at the anode tended to react with the binder and produced a mixture of chlorinated organics which were later removed as waste called "gunk" or "taffy" (*10*, *14*, *15*). It is this taffy which we believe to be the source of OCS.

Most electrolytic systems gave chlorine which was 99.6–99.8% pure (*14*, *15*). While this was adequate for most early uses, in 1924, these impurities were discovered to foul the valves of newly developed water treatment equipment designed to use liquid chlorine (*9*). The clog was composed of the more nonvolatile components of taffy condensed on a matrix of ferric chloride and was known as "taffy tar". Efforts on the part of chlorine manufacturers to purify their product did not achieve widespread success until the current technique of countercurrent washing was developed in 1937 (*15*). Thus, if our hypothesis is correct, OCS should not occur in Lake Ontario sediment earlier than 1937. Examination of Figure 2 reveals that Lake Ontario first began receiving OCS about 1940, shortly after the production of taffy began.

Following the onset of taffy production (and presumably its disposal) the chlorine industry in the Great Lakes area experienced an annual average growth of 6–7% (*16*). This trend prevailed until about 1970 when production suffered a decline which persisted for the next 10 years (see solid line in Figure 3). The core data (see Figure 2) show that OCS levels in Lake Ontario sediment coincide with the rise and fall of chlorine production. However, chlorine pro-

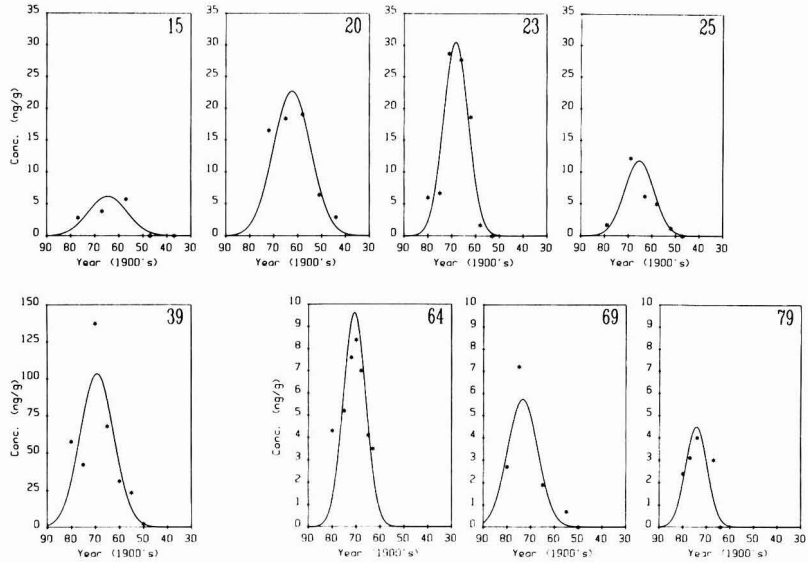

Figure 2. Concentration (ng/g dry weight) of octachlorostyrene vs. year of deposition at the eight Lake Ontario sites where OCS was found. Note, there are three different concentration scales. The Gaussian curves are aids to visualization.

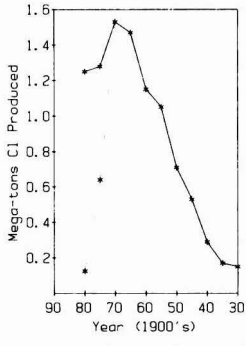

Figure 3. Chlorine production in the Great Lakes states as a function of year. Solid line, total production (*16*); dotted line, estimated graphite electrode production in 1975 and 1980.

duction did not cease, as the OCS data might imply. The explanation for this precipitous decline in OCS levels lies with the replacement of graphite anodes with metal anodes beginning in the early 1970s. So rapid and widespread was this conversion, that the metal anodes dominated nearly half the industry by the middle of the decade (*11*) and most of the remainder by 1982 (see dotted line in Figure 3). Of course, these metal electrodes do not produce chlorinated organic waste (i.e., taffy) (*10*). Consequently, their rapid adoption by the industry resulted in a correspondingly rapid decline in OCS. The core data (see Figure 2) record just such a trend and reinforce the link between OCS, taffy, and the chlorine industry.

Because chlorine production and magnesium production share similar technologies, some of the OCS in the Great Lakes may have originated from the magnesium industry. However, the levels of magnesium production have generally been several thousand times less than those of chlorine (*17*, *18*). In addition, there is only one major magnesium producer in the Great Lakes area while the shores of the Niagara River alone have four major chlorine manufacturers. The contribution of OCS to Lake Ontario by the magnesium industry, therefore, must be minor compared to that of the chlorine industry.

The composition of the pitch binder used in the few remaining graphite anodes has changed since the mid-1970s. The industry has apparently switched from an aromatic coal-based to an aliphatic petroleum-based pitch. We would, therefore, expect the chlorinated waste associated with this new pitch to be composed of a lower proportion of aromatic constituents compared to the pitch commonly in use prior to 1970. This situation, together with the nearly total abandonment of graphite anodes discussed above, is rather unfortunate from an analtyical point of view because it virtually eliminates the possibility of obtaining a sample of taffy representative of that produced prior to 1970. We were, however, able to obtain a modern sample of taffy for analysis, and our sample contained 200 ppb of OCS. As we might expect, none of the more highly aromatic chlorinated compounds could be detected. However, these results do serve to strengthen our assertion that chlorinated styrenes were associated with taffy prior to 1970.

A final line of evidence in support of our taffy hypothesis is the correlation between the geographic occurrence of OCS in sediment and fish and the location of chlorine production sites. OCS has been identified in sediments or fish from nine locations in the United States. In each case, chlorine producers who used graphite anodes prior to 1970 were located close by (see Table I). At the same time, adjacent areas not receiving the effluent of a chlorine plant do not contain OCS. For example, fish from the Ashtabula River, OH, contain high concentrations of OCS whereas fish from the nearby Conneaut River contain no chlorinated styrenes (*19*). Chlorine producers are located along the Great Lakes from Midland, MI, to Lake Ontario. Similarly, fish collected from Saginaw Bay to Lake Ontario have been found to contain OCS while those from Lake Superior, Lake Michigan, and upper Lake Huron do not contain chlorinated styrenes (*6*).

Taking all our evidence into consideration, we feel confident that the primary source of chlorinated styrenes (as well as chlorinated polycyclic aromatic hydrocarbons) in the Great Lakes, particularly Lake Ontario, is taffy from chlorine production.

Fate of OCS. OCS was probably introduced into the

Table I. Geographic Association between OCS and Chlorine Producers

location at which OCS was found	concn, ng/g	medium	ref	chlorine producer
Commencement Bay, WA	0-20	sediment	27	Hooker Chem. and Pennwalt Corp., Tacoma, WA
White Lake, MI	trace	sediment	28	Hooker Chem., Montague, MI
Saginaw Bay, Lake Huron	2-110	fish	5	Dow Chemical, Midland, MI
Lake St. Clair	230	fish	5	Dow Chemical, Sarnia, Ontario
Ashtabula River, OH	140-400	fish	7	Int'l Minerals and Chem. Corp. and RMI Co., Ashtabula, OH
Lake Erie	34	fish	6	Pennwalt Corp., Wyandotte, MI
Lake Ontario	35-280	fish	5, 8	Hooker Chem., Olin Corp., and du Pont & Co., Niagara Falls, NY
Calcasieu Lake, LA	50-360	sediment	this work	PPG Industries, Lake Charles, LA

Figure 4. Concentration isopleths of octachlorostyrene in Lake Ontario. Open circles indicate data from grab samples; closed circles indicate data from sediment cores.

western portion of Lake Ontario (Figure 2, sites 15, 20, 23, and 25) from chlorine plants along the shores of the Niagara River. The distribution of OCS in the western portion of the lake appears to coincide with the known sedimentation rates for this end of the lake (*20*, *21*). This pattern is more readily discerned by mapping the OCS data as concentration contours (see Figure 4). The amounts of OCS in each core were summed and divided by the sediment dry weight to obtain the average concentration. Supplementary data from grab samples (*8*) were used to increase resolution.

OCS seems to be associated with the offshore, fine grain particles rather than the nearshore sands, and thus the region of highest concentration (sites 20 and 23) is localized in the area of fine grain sedimentation nearest to the Niagara River outlet. From here, OCS seems to spread westward. A similar distribution was observed for mercury (*22*) and PCB's (*23*), the sources of which were also determined to be the Niagara River. Transport is probably also occurring in an easterly direction along the south shore of Lake Ontario. The assumption that this transport continues along the south shore toward midlake is reasonable in light of the occurrence of OCS at site 39 and the absence of any known source in this area. This also agrees with the distribution of other sediment-entrained compounds which enter the lake through the Niagara River (*22–24*).

The high (>100 ng/g) concentration at site 39 (midlike) is surprising. We expect OCS to accumulate here because the area possesses a high sedimentation rate. It is surprising, however, that the levels at site 39 and in a grab sample taken 1 year earlier at this site (*8*) are the highest measured in the lake. It is interesting to note that unusually high concentrations of mercury were observed just offshore of the Genessee River outlet (*22*). Although techniques of chlorine production which would lead to the release of both mercury and OCS wastes (e.g., electrolytic chlorine production using mercury as the cathode) are employed in the Great Lakes basin, no record of chlorine production of any sort exists for the Genessee River basin (*16*). Thus, their abundance at this location remains a mystery.

OCS was detected in the eastern end of Lake Ontario (sites 64 and 69) at concentrations similar to those at sites 15 and 25 from the western end and are thus higher than we might expect if due simply to transport from the Niagara region. The eastern portion of the lake, however, may have recevied some OCS from Syracuse, NY, through the Oswego River. Chlorine production using mercury cells has been in operation there since the turn of the century, and Thomas et al. (*22*) have reported high concentrations of mercury in sediment at the mouth of the Oswego River. The shape and size of the contour of this region shown in Figure 4 are those of the sedimentation rate isopleth which is half the value of the rates at sites 64 and 69 and thus serves only as an estimate of the area actually containing OCS.

The concentration measured at the inlet to the Saint Lawrence River (site 79) was quite low. Because there is no known industrial source of OCS in this region, the source of OCS is most likely the transport of sediment from the southeastern end of the lake. The existence of a northerly current which connects these two regions (*25*) supports this supposition.

Toxicity of OCS. Although many studies document the occurrence of OCS (and occasionally other chlorinated styrenes) in various species of fish and birds, no toxicological data have been reported. As part of our investigation, OCS was found to be neither toxic nor mutagenic to *Salmonella typhimurium* strain TM677 when a forward mutagenesis bioassay with and without metabolic activation was used at OCS concentrations up to 250 $\mu g/\mu L$ (Howard Lieber, personal communication). Although apparently not harmful to bacteria, the possibility remains that OCS could be accumulated in higher organisms.

Conclusion

By examining the historical record preserved in sediment cores, we are able to propose a scenario for the introduction and fate of OCS in Lake Ontario. Chlorine produced by graphite electrodes contained a waste product known as taffy which consisted of highly chlorinated compounds including OCS. The bulk of OCS appears to have been introduced at the western end of the lake probably through the Niagara River from chlorine plants along its banks. Accumulation in sediments at the western end of the lake began shortly after taffy was first produced in the late 1930s. Its increasing concentration in the sediments up until 1970 reflected the growth of the chlorine industry up to that point. With the adoption of techniques which

eliminated taffy during the 1970s came the rapid decline of OCS in the sediments. The synchronization of taffy production (as traced through chlorine production) and the concentration of OCS is so precise that it can best be explained only with the assumption that taffy (a liquid) was never permanently disposed of and perhaps may have been dumped into the Niagara River. During the 40 years of its input, OCS accumulated in all of the major depositional zones of Lake Ontario.

We suspect the above scenario is applicable to other regions of the Great Lakes adjacent to sites of chlorine production and that it would explain reports of OCS in fish from these areas. Whether bottom feeders such as carp absorb it from sediment through their gut or from consumption of benthos, OCS becomes biomagnified through the food chain (*6*). The chain continues to aquatic birds such as great blue herons (*26*) and cormorants and even to seals (*2*). Now that the concentration of OCS is descreasing in the surficial sediments, and thus becoming less available to the biota, we expect its concentration in fish and their predators will begin to decrease. Unfortunately, we still lack the detailed toxicological knowledge necessary to predict the long-term impact of chlorinated styrenes on the environment.

Acknowledgments

We are indebted to R. Allan, R. A. Bourbonniere, K. L. E. Kaiser, and B. Oliver of the Canada Centre for Inland Waters for providing Lake Ontario Sediment samples, to D. N. Edgington of the Center for Great Lakes Studies, University of Wisconsin–Milwaukee, and T. Ward of the Indiana University Cyclotron Facility for radioisotope dating, to H. Lieber of the Massachusetts Institute of Technology for bacterial bioassays, and to S. Sikes for assistance in the preparation of the manuscript.

Registry No. Cl_2, 7782-50-5; OCS, 29082-74-4.

Literature Cited

(1) Koeman, J. H.; ten Noever de Branw, M. C.; de Vos. R. H. *Nature (London)* **1969**, *221*, 1126–1128.
(2) ten Noever de Branw, M. C.; Koeman, J. H. *Sci. Total Environ.* **1972**, *1*, 427–432.
(3) Lunde, G.; Ofstad, E. B. *Fresenius' Z. Anal. Chem.* **1976**, *282*, 395–399.
(4) Ofstad, E. B.; Lunde, G.; Martinsen, K.; Rygg, B. *Sci. Total Environ.* **1978**, *10*, 219–230.
(5) Kuehl, D. W.; Kopperman, H. L.; Veith, G. D.; Glass, G. E. *Bull. Environ. Contam. Toxicol.* **1976**, *16*, 127–132.
(6) Kuehl, D. W.; Johnson, K. L.; Butterworth, B. C.; Leonard, E. N.; Veith, G. D. *J. Great Lake Res.* **1981**, *7*, 330–335.
(7) Kuehl, D. W.; Leonard, E. N.; Welch, K. J.; Veith, G. D. *J. Assoc. Off. Anal. Chem.* **1980**, *63*, 1238–1244.
(8) Kaminsky, R.; Kaiser, K. L. E.; Hites, R. A. *J. Great Lakes Res.* **1983**, *9*, 183–189.
(9) White, G. C. "Handbook of Chlorination"; Van Nostrand Reinhold: New York, 1972.
(10) "Alkali and Chlorine Products". In "Kirk-Othmer Encyclopedia of Chemical Technology"; Wiley: New York, 1980.
(11) Handie, D. W. F. "Electrolytic Manufacture of Chemicals from Salt"; The Chlorine Institute Inc.: New York, 1975.
(12) Jensen, T. E.; Kaminsky, R.; McVeety, B. D.; Wozniak, T. J.; Hites, R. A. *Anal. Chem.* **1982**, *54*, 2388–2390.
(13) Robbins, J. A.; Edgington, D. N. *Geochim. Cosmochim. Acta* **1973**, *39*, 285–296.
(14) Laubusch, E. J. *J.—Am. Water Works Assoc.* **1959**, *51*, 742–748.
(15) Penfield, W.; Cushing, R. E. *Ind. Eng. Chem.* **1939**, 377–381.
(16) Chlorine Institute Pamphlet 10 "North American Chlor-Alkali Industry Plants and Production Data Book"; The Chlorine Institute Inc.: New York, 1982.
(17) Gross, W. H. "The Story of Magnesium"; American Society for Metals: Cleveland, OH, 1949.
(18) International Magnesium Association "Magnesium Production by World Zone"; International Magnesium Association: Dayton, OH, 1983.
(19) Veith, G. D.; Kuehl, D. W.; Leonard, E. N.; Welch, K.; Pratt, G. *Pestic. Monit. J.* **1981**, *15*, 1–8.
(20) Thomas, R. L.; Kemp, A. L. W.; Lewis, C. F. M. *J. Sediment. Petrol.* **1972**, *42*, 66–84.
(21) Kemp, A. L. W.; Harper, N. S. *J. Great Lakes Res.* **1976**, *2*, 324–340.
(22) Thomas, R. L. *Can. J. Earth Sci.* **1972**, *9*, 636–651.
(23) Frank, R.; Thomas, R. L.; Holdrinet, M.; Kemp, A. L. M.; Braun, H. E. *J. Great Lakes Res.* **1979**, *5*, 18–27.
(24) Holdrinet, M.; Frank, R.; Thomas, R. L.; Hetling, L. J. *J. Great Lakes Res.* **1978**, *4*, 69–74.
(25) Robertson, A.; Jenkins, C. F. *Ambio* **1978**, *7*, 106–112.
(26) Reichel, W. L.; Prouty, R. M.; Gay, M. *J. Assoc. Off. Anal. Chem.* **1977**, *60*, 60–62.
(27) Burrows, D. G.; MacLeod, W. D.; Ramos, S. L.; Brown, D. W., presented at the 29th Annual Conference on Mass Spectrometry and Allied Topics, Minneapolis, MN, 1981.
(28) McVeety, B. D., Indiana University, personal communication, 1982.

Received for review June 9, 1983. Accepted October 13, 1983. This research was supported by U.S. Environmental Protection Agency Grant 808961.

Environ. Sci. Technol. 1984, 18, 280–287

Analysis of the Characteristics of Complex Chemical Reaction Mechanisms: Application to Photochemical Smog Chemistry

Joseph A. Leone and John H. Seinfeld*

Department of Chemical Engineering, California Institute of Technology, Pasadena, California 91125

■ To elucidate the features of complex chemical reaction mechanisms, we develop an analysis based on the use of so-called "counter species", fictitious products added to the reactions in the mechanism that allow one to determine the relative contributions of individual reactions to the overall behavior of the mechanism. The method is developed by considering a mechanism for the atmospheric photooxidation of the three simplest aldehydes and is then applied, in a full-scale simulation, to analyze the behavior of a complex chemical reaction mechanism for photochemical smog. The method is shown capable of providing answers to previously inaccessible questions such as the relative contributions of individual hydrocarbons to photochemical ozone formation. Application of the counter species concept to analyze complex environmental reaction mechanisms is straightforward and can be readily implemented in the standard routines in widespread use for solving sets of chemical reaction rate equations.

Introduction

A number of important systems in environmental chemistry are characterized by lengthy and complex chemical reaction mechanisms. In such complex mechanisms it is not generally possible to determine the relative contributions of individual reactions or of certain reaction subnetworks to the overall behavior of the mechanism. Sensitivity analysis, in which the responses of the concentrations to perturbations in parameters (such as rate constants) are computed, is one technique to ascertain the relative importance of individual reactions on predicted behavior (*1–3*).

As a means of elucidating the features of a chemical reaction mechanism, we introduce here a simple technique based on the use of species, which we term counter species. The counter species do not represent actual chemical entities; rather they are purely mathematical quantities that allow us to track flows in a mechanism. In the past, counter species have been used to keep track of the integrated reaction rate for a given chemical reaction (*12–14*). In this paper, we greatly expand the use of this idea as a part of an analysis technique that allows one to examine the inner workings of complex mechanisms, answering questions that were previously inaccessible. The technique is very simple to use and can be implemented readily in the standard computer routines used for solving sets of chemical rate equations.

Because the counter species idea is a simple one, we devote most of this paper to illustrations of its use. In particular, mechanisms describing the chemistry of photochemical smog are notably complex (*4–8*), and consequently, we will develop the counter species method through its application to two reaction mechanisms arising in the description of photochemical smog.

Concept of Counter Species

In this section we introduce the counter species concept using an abbreviated mechanism for photochemical smog.

Photooxidation of the Three Simplest Aldehydes. Let us consider one of the simplest atmospheric reaction mechanisms—the photooxidation of the three aldehydes, formaldehyde, acetaldehyde, and propionaldehyde, in the presence of NO and NO_2. For the purpose of illustrating the technique, assume that we wish to limit the number of species appearing in our mechanism by lumping propionaldehyde together with acetaldehyde. A typical reaction mechanism for this situation might contain the following reactions:

$$NO_2 + h\nu \xrightarrow[O_2]{} NO + O_3 \quad (1)$$

$$NO + O_3 \rightarrow NO_2 + O_2 \quad (2)$$

$$HO_2\cdot + NO \rightarrow NO_2 + OH\cdot \quad (3)$$

$$HCHO + h\nu \xrightarrow[2O_2]{} 2HO_2\cdot + CO \quad (4)$$

$$HCHO + h\nu \rightarrow H_2 + CO \quad (5)$$

$$HCHO + OH\cdot \xrightarrow[O_2]{} HO_2\cdot + CO + H_2O \quad (6)$$

$$CH_3CHO + h\nu \xrightarrow[2O_2]{} CH_3O_2\cdot + HO_2\cdot + CO \quad (7)$$

$$CH_3CHO + OH\cdot \xrightarrow[O_2]{} CH_3C(O)O_2\cdot + H_2O \quad (8)$$

$$CH_3C(O)O_2\cdot + NO \xrightarrow[O_2]{} NO_2 + CH_3O_2\cdot + CO_2 \quad (9)$$

$$CH_3C(O)O_2\cdot + NO_2 \rightarrow CH_3C(O)O_2NO_2(PAN) \quad (10)$$

$$PAN \rightarrow CH_3C(O)O_2\cdot + NO_2 \quad (11)$$

$$CH_3O_2\cdot + NO \rightarrow CH_3O\cdot + NO_2 \quad (12)$$

$$CH_3O\cdot + O_2 \rightarrow HCHO + HO_2\cdot \quad (13)$$

$$NO_2 + OH\cdot \rightarrow HNO_3 \quad (14)$$

In the atmosphere these aldehydes react to produce HO_2, CH_3O_2, and $CH_3C(O)O_2$ radicals that can convert NO to NO_2 and thus cause $[NO_2]/[NO]$, and consequently O_3, to increase. Ozone formation will continue as long as aldehydes and NO_x are both present. NO_x is consumed via reactions 10 and 14, so ultimate O_3 yields are limited by NO_x availability as well as by how fast the aldehydes lead to O_3 formation through the conversion of NO to NO_2.

In analyzing mechanisms for photochemical smog, the key features which need to be examined concern (1) the relative importance of the various radical initiation and termination steps and (2) the conversion of NO to NO_2, which ultimately leads to the accumulation of O_3. For example, in the reaction mechanism shown above, NO to NO_2 conversions occur via reactions 3, 9, and 12. We seek to know the number of these NO to NO_2 conversions attributable to formaldehyde, acetaldehyde, and propionaldehyde and, within each of these, the number due to

 0013-936X/84/0918-0280$01.50/0

Table I. Initial Conditions and Photolysis Rates for the Three Aldehyde/NO_x Simulation[a]

initial reactant concn, ppb	photolysis rates, $(min)^{-1}$
$[NO]_0$, 600	$k_1 = 0.35$
$[NO_2]_0$, 80	$k_3 = 8.2 \times 10^{-4}$
$[HCHO]_0$, 100	$k_5 = 8.2 \times 10^{-4}$
$[CH_3CHO]_0$, 50	$k_7 = 1.3 \times 10^{-4}$
$[CH_3CH_2CHO]_0$, 7	

[a] Temperature = 298 K; pressure = 1 atm.

photolysis and OH reaction. In order to obtain this information, we first rewrite the mechanism as the following:

$$NO_2 + h\nu \xrightarrow[O_2]{} NO + O_3 \quad (1)$$

$$NO + O_3 \rightarrow NO_2 + O_2 \quad (2)$$

$$HO_2\cdot + NO \rightarrow NO_2 + OH\cdot + C3 \quad (3)$$

$$HCHO + h\nu \xrightarrow[2O_2]{} 2HO_2\cdot + CO + C4 \quad (4)$$

$$HCHO + h\nu \rightarrow H_2 + CO \quad (5)$$

$$HCHO + OH\cdot \xrightarrow[O_2]{} HO_2\cdot + CO + H_2O + C6 \quad (6)$$

$$CH_3CHO(a) + h\nu \xrightarrow[2O_2]{} CH_3O_2\cdot + HO_2\cdot + CO + C7 \quad (7)$$

$$CH_3CHO(a) + OH\cdot \xrightarrow[O_2]{} CH_3C(O)O_2\cdot + H_2O + C8 \quad (8)$$

$$CH_3C(O)O_2\cdot + NO \xrightarrow[O_2]{} NO_2 + CH_3O_2\cdot + CO_2 + C9 \quad (9)$$

$$CH_3C(O)O_2\cdot + NO_2 \rightarrow CH_3C(O)O_2NO_2(PAN) \quad (10)$$

$$PAN \rightarrow CH_3C(O)O_2\cdot + NO_2 \quad (11)$$

$$CH_3O_2\cdot + NO \rightarrow CH_3O\cdot + NO_2 + C12 \quad (12)$$

$$CH_3O\cdot + O_2 \rightarrow HCHO + HO_2\cdot + C13 \quad (13)$$

$$NO_2 + OH\cdot \rightarrow HNO_3 + C14 \quad (14)$$

$$HCHI + h\nu \xrightarrow[2O_2]{} 2HO_2\cdot + CO + C15 \quad (15)$$

$$HCHI + h\nu \rightarrow H_2 + CO \quad (16)$$

$$HCHI + OH\cdot \xrightarrow[O_2]{} HO_2\cdot + CO + H_2O + C17 \quad (17)$$

$$CH_3CHO(b) + h\nu \xrightarrow[2O_2]{} CH_3O_2\cdot + HO_2\cdot + CO + C18 \quad (18)$$

$$CH_3CHO(b) + OH\cdot \xrightarrow[O_2]{} CH_3C(O)O_2\cdot + H_2O + C19 \quad (19)$$

Three changes have been made from the original mechanism. First, for reasons that will be made clear shortly, reactions 15, 16, and 17 have been added to the mechanism. For now, we note that whenever a species that is present initially is also formed as a product in the reaction mechanism, we represent this species by two separate species. Thus, we now have photolysis and OH reactions for both HCHO (formaldehyde formed as a product) and HCHI (initially present formaldehyde). If there were initially 30 ppb of formaldehyde present, we would specify 30 ppb as the initial concentration of HCHI.

The second change from the original mechanism is the addition of reactions 18 and 19. Because we wish to distinguish the NO to NO_2 conversions due to the initial acetaldehyde from those due to the initial propionaldehyde, we include reactions for both CH_3CHO(a) (acetaldehyde) and CH_3CHO(b) (propionaldehyde). If there were initially 20 ppb of acetaldehyde and 5 ppb of propionaldehyde, we would specify 20 ppb of CH_3CHO(a) and 5 ppb of CH_3CHO(b) as initial conditions.

The third change from the original mechanism is the addition of fictitious products, C*i*, to some of the reactions. These products are produced only in one reaction and are not consumed. For instance, one "molecule" of C9 is formed for each molecule of NO converted to NO_2 by reaction 9. Since C*i* counts the number of times reaction *i* has occurred, we call C*i* a counter species, and we term the analysis using the C*i* a counter species analysis.

The next step in the counter species analysis is to determine the fraction of the molecules of any product species S that has led to NO to NO_2 conversions up until any time *t*:

F_s = (number of NO/NO_2 conversions due to produced species S, up to time *t*)/(number of molecules of S formed up to time *t*)

Using this definition and the mechanism shown above, we find that

$$F_{HO_2} = \frac{C3}{2C4 + C6 + C7 + C13 + 2C15 + C17 + C18}$$

$$F_{HCHO} = \frac{F_{HO_2}(2C4 + C6)}{C13}$$

$$F_{CH_3O} = \frac{C13(F_{HO_2} + F_{HCHO})}{C12}$$

$$F_{CH_3O_2} = \frac{C12(1 + F_{CH_3O})}{C7 + C9 + C18}$$

$$F_{CH_3C(O)O_2} = \frac{C9(1 + F_{CH_3O_2})}{C8 + C19}$$

The reason for dividing formaldehyde into two species, HCHI (representing the initially present formaldehyde) and HCHO (representing formaldehyde produced by reaction 13), can now be explained fully. We need to form F_{HCHO}, which represents the fraction of all *produced* formaldehyde molecules that lead to NO to NO_2 conversions. By definition, this fraction does not involve any of the initially present HCHO. Thus, we must separate the two types of formaldehyde in order to properly calculate the relation F_{HCHO}. The desired quantities are then expressed in terms of the fractional relations:

number of NO to NO_2 conversions measured as a concentration due to

photolysis of initial formaldehyde = $2C15F_{HO_2}$

photolysis of initial acetaldehyde = $C7(F_{CH_3O_2} + F_{HO_2})$

photolysis of initial propionaldehyde = $C18(F_{CH_3O_2} + F_{HO_2})$

OH reaction of initial formaldehyde = $C17F_{HO_2}$

Table II. Counter Species Results Calculated after 6 h of Irradiation for the Three Aldehyde/NO_x Simulation

(A) Fractional Relation Results

species (S)	fractional value (F_S)
$HO_2\cdot$	1.00
HCHO	0.43
$CH_3O\cdot$	1.43
$CH_3O_2\cdot$	2.43
$CH_3C(O)O_2\cdot$	3.39

(B) Integrated Rates

reaction	amount of NO to NO_2 conversions attributable to each reaction, ppb	amount of radicals produced via each reaction, ppb	amount of radicals scavenged via each reaction, ppb	amount of NO_x sinks attributable to each reaction, ppbN
formaldehyde photolysis	38	44.7		
formaldehyde + OH	25			
acetaldehyde photolysis	6	3.3		
acetaldehyde + OH	71			
propionaldehyde photolysis	0.5	0.3		
propionaldehyde + OH	5.7			
PAN formation			0.3	0.3
HNO_3 formation			48	48

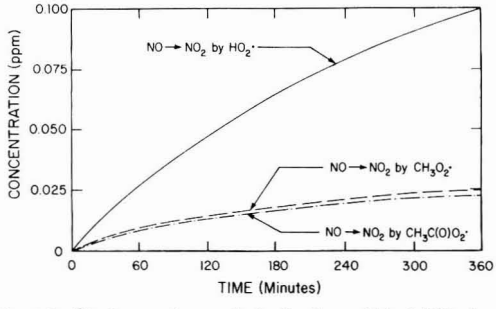

Figure 1. Counter species results for the three aldehyde/NO_x simulation. Number of NO to NO_2 conversions due to hydroperoxyl ($HO_2\cdot$), methylperoxy ($CH_3O_2\cdot$), and peroxyacetyl ($CH_3C(O)O_2\cdot$) radicals.

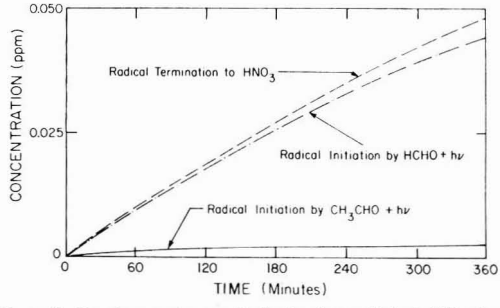

Figure 2. Counter species results for the three aldehyde/NO_x simulation. Number of radical initiation and radical termination steps for the most important radical-producing and radical-scavenging reactions.

OH reaction of initial acetaldehyde = $C8F_{CH_3C(O)O_2}$

OH reaction of initial propionaldehyde = $C19F_{CH_3C(O)O_2}$

If desired, we can gain additional information from the counter species analysis. For example

NO to NO_2 conversions due to

photolysis of produced HCHO = $2C4F_{HO_2}$

OH reaction of produced HCHO = $C6F_{HO_2}$

radical initiation due to the photolysis of

formaldehyde = 2C15 + 2C4

acetaldehyde = 2C7

propionaldehyde = 2C18

radical termination to

PAN = [PAN]

HNO_3 = [HNO_3]

It is of interest to calculate these quantities for a given

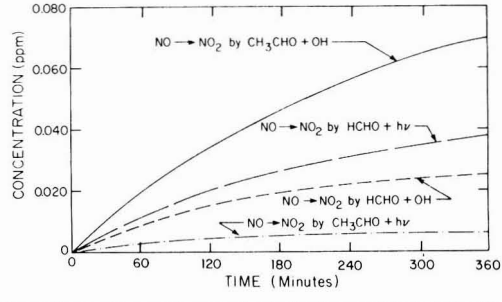

Figure 3. Counter species results for the three aldehyde/NO_x simulation. Number of NO to NO_2 conversions due to the photolysis and OH reactions of formaldehyde and acetaldehyde.

set of initial conditions and photolysis rates. These are shown in Table I. The initial NO_x and aldehyde concentrations are approximately twice the typical values found in early morning Los Angeles air. The counter species results are given in Table II and shown in Figures 1–3. We see that the CH_3CHO + OH reaction accounts for most of the NO to NO_2 conversion, while the photolysis of acetaldehyde and propionaldehyde give rise only to a small percentage of the NO oxidations. Figure 1 shows that most of the NO to NO_2 conversions involve the HO_2 radical via reaction 3. The results shown in Figure 2 in-

Table III. Initial Conditions for the Hydrocarbon/NO_x Simulation

species	initial concn, ppb	lumped classification in the Atkinson et al. mechanism (7)	initial condition, ppb
propane	17.0	propane	17.0 propane
acetone	35.2	acetone	35.2 acetone
isobutane	0.2	alkane	0.2 alkane
n-butane	166	alkane	166 alkane
2,3-dimethylbutane	97.6	alkane	97.6 alkane
ethene	43.2	ethene	43.2 ethene
propene	10.6	propene	10.6 propene
trans-2-butene	0.7	butene	0.7 butene
cis-2-butene	13.0	butene	13.0 butene
2-methyl-2-butene	14.8	butene	14.8 butene
benzene	1.6	benzene	1.6 benzene
toluene	16.8	toluene	16.8 toluene
ethylbenzene	6.4	toluene	6.4 toluene
m-xylene	42.4	xylene	42.4 xylene
isopropylbenzene	0.4	toluene	0.4 toluene
n-propylbenzene	0.1	toluene	0.1 toluene
m-ethyltoluene	1.0	xylene	1.0 xylene
1,2,3-trimethylbenzene	1.6	xylene	1.6 xylene
formaldehyde	38.0	formaldehyde	38.0 HCHO
acetaldehyde	20.0	acetaldehyde	20.0 CH_3CHO
propionaldehyde	3.2	RCHO	3.2 RCHO
NO	301.0		
NO_2	41.0		
HONO	12.0		
CO	7 450		
H_2O, ppm	15 500		
O_2, ppm	210 000		
M, ppm	1 000 000		
	Totals for the Lumped Classes		
propane	17.0		
alkane	263.8		
acetone	35.2		
ethene	43.2		
propene	10.6		
butene	28.5		
benzene	1.6		
toluene	23.7		
xylene	45.0		
HCHO	38.0		
CH_3CHO	20.0		
RCHO	3.2		

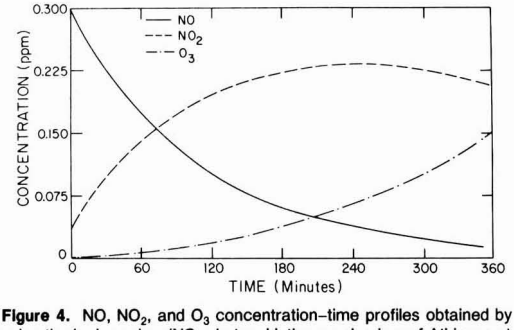

Figure 4. NO, NO_2, and O_3 concentration–time profiles obtained by using the hydrocarbon/NO_x photooxidation mechanism of Atkinson et al. with initial conditions shown in Table IV.

dicate that the only important radical initiation step is formaldehyde photolysis and that the only significant radical termination process and NO_x sink are nitric acid formation.

With simple mechanisms such as the three aldehyde mechanisms shown above, there is an alternate way of using counter species to obtain the desired information. By applying the pseudo-steady-state approximation to the HO_2, CH_3O_2, and CH_3O radicals, we can write a compact mechanism in which these fast-reacting species are eliminated. With these "condensed" mechanisms the number of NO to NO_2 conversions due to each reaction pathway is given by the counters themselves. No fractional relationships are needed.

Unfortunately, all of the useful chemical reaction mechanisms describing photochemical smog are much more complicated than the simple aldehyde mechanism presented above. With these mechanisms, it becomes extremely difficult to eliminate the fast-reacting species using the pseudo-steady-state approximation. Nevertheless, the counter species analysis provides an effective means to examine the properties of these complex mechanisms. Such an analysis is presented in the next section.

Application of Counter Species To Analyze a Complex Atmospheric Reaction Mechanism

A number of chemical reaction mechanisms have been proposed as suitable for inclusion in urban airshed simulation models (*7–10*). Each of these mechanisms uses some form of hydrocarbon "lumping" in order to reduce the number of species and reactions to a reasonable number. Typical of these is the mechanism proposed by Atkinson et al. (*7*), which we analyze in this section. This mechanism uses the lumped molecule approach, in which one or more reactants of similar structure and reactivity are grouped into a single class. For example, this mechanism represents

Table IV. Counter Species Relations and Results for the Number of NO to NO_2 Conversions Attributable to Various Radicals, Inorganic Compounds, and Organics Appearing in the Hydrocarbon/NO_x Photooxidation Mechanism of Atkinson et al. (7)

(A) NO Oxidation by Radical Species

species	NO to NO_2 conversions: counter species expressions[a]	ppb	%
$HO_2\cdot$	C7	279	58.9
$AO_2\cdot$	1.7C33	59.3	12.6
$CH_3O_2\cdot$	C29	35.6	7.5
hydroxyalkylperoxy radicals[b]	C44 + C45 + 0.9C46	34.1	7.2
$CH_3C(O)O_2\cdot$	C28	27.7	5.8
ADD	0.75C61	14.5	3.1
EL	3C65	11.3	2.4
$C_2H_5O_2\cdot$	C38	3.2	0.7
$CH_3\dot{C}HO\dot{O}$	C54	3.1	0.7
ADD2	0.75C71	1.6	0.3
$RCO_3\cdot$	C37	1.4	0.3
$PO_2\cdot$	C31	0.9	0.2
$XO_2\cdot$	C41	0.9	0.1
$\dot{C}H_2\dot{O}_2$	C50	0.6	0.1
$ARO_2\cdot$	0.75C74	0.5	0.1
$ARO_3\cdot$	C79	~0	0
$PHO_2\cdot$	C80	~0	0
total		473.7[d]	100

(B) NO Oxidation by Inorganic Compounds

species	counter species expression	NO to NO_2 conversions, ppb
O_3	C2	25070
NO_3	C14	220

(C) NO Oxidations by Different Reaction Pathways

reaction pathway[c]	NO to NO_2 conversions: counter species expression	ppb	%
HCHO + OH	$C23F_{HO_2\cdot}$	9.3	2.0
HCHO + $h\nu$	$2C21F_{HO_2\cdot}$	14.8	3.1
CH_3CHO + OH	$C25F_{CH_3C(O)O_2\cdot}$	17.8	3.8
CH_3CHO + $h\nu$	$C24(F_{HO_2\cdot} + F_{CH_3O_2\cdot})$	2.3	0.5
RCHO + OH	$C34F_{RCO_3\cdot}$	2.7	0.6
RCHO + $h\nu$	$C39(F_{HO_2\cdot} + F_{C_2H_5O_2\cdot})$	0.5	0.1
total aldehyde		47.4	10.1
propane + OH	$C30F_{PO_2\cdot}$	1.9	0.4
ALK + OH	$C32F_{AO_2\cdot}$	115.2	24.3
total alkanes		117.1	24.7
ethene + OH	$C44(1 + F_{HO_2\cdot} + 2F_{HCHO})$	30.5	6.4
propene + OH	$C45(1 + F_{HO_2\cdot} + F_{CH_3CHO} + F_{HCHO})$	18.6	3.9
butene + OH	$0.9C46(1 + F_{HO_2\cdot} + 2F_{CH_3CHO})$	59.8	12.7
total alkene + OH		108.9	23.0
ethene + O_3	$C47(0.12F_{HO_2\cdot} + 0.4F_{\dot{C}H_2\dot{O}_2} + F_{HCHO})$	1.9	0.4
propene + O_3	$C48[0.5(F_{HCHO} + F_{CH_3CHO}) + 0.2(F_{\dot{C}H_2\dot{O}_2} + F_{CH_3\dot{C}HO_2} + F_{HO_2} + F_{CH_3O_2\cdot})]$	3.2	0.7
butene + O_3	$C49(F_{CH_3CHO} + 0.4F_{CH_3\dot{C}HO_2} + 0.3F_{HO_2\cdot} + 0.45F_{CH_3O_2\cdot})$	25.4	5.3
total alkene + O_3		30.5	6.4
total alkene		139.4	29.4
benzene + OH	$0.25C58(F_{cresol} + F_{HO_2\cdot}3F_{ADD})$	0.9	0.2
toluene + OH abstraction	$0.75C74(1 + F_{HO_2\cdot}) + C79 + C80$	1.2	0.2
toluene + OH addition	$0.20C59(F_{cresol} + F_{HO_2\cdot} + 3.25F_{ADD})$	14.0	2.9
xylene + OH	$0.25C60(F_{cresol} + F_{HO_2\cdot} + 3F_{ADD})$	73.9	15.6
total aromatic		90.0	18.8
$CH_3C(O)CH_3$ + $h\nu$	$C43(F_{CH_3C(O)O_2\cdot} + F_{CH_3O_2\cdot})$	2.9	0.6
OH + CO	$C12F_{HO_2}$	80.6	17.0
		474.4[d]	100
miscellaneous			
toluene ring opening	$0.65C59F_{ADD}$	12.4	2.6
cresol ring opening	$C70F_{ADD2}$	5.2	1.1
conjugated γ-dicarbonyl (DIAL) reactions	$C62F_{EL}$	20.9	4.4
glyoxal ($(CHO)_2$) reactions	$C66F_{HO_2\cdot} + C67F_{HCHO}$	0.6	0.1

Table IV (*Continued*)

reaction pathway[c]	NO to NO_2 conversions: counter species expression	ppb	%
methylglyoxal ($CH_3C(O)CHO$) photolysis	$C69(F_{CH_3C(O)O_2\cdot} + F_{HO_2\cdot})$	27.8	5.9
methylglyoxal + OH	$C68F_{CH_3C(O)O_2\cdot}$	4.4	0.9
MEK + $h\nu$	$C42(F_{C_2H_5O_2\cdot} + F_{CH_3C(O)O_2\cdot})$	7.4	1.6
MEK + OH	$C40F_{XO_2}$	3.4	0.7

[a] The C*i* in these expressions are fictitious products added to each of the reactions in the Atkinson et al. (7) mechanism. For example, C7 is listed as a product in reaction 7. [b] These radicals are formed in the OH–alkene reactions (reactions 44–66). [c] In cases where a species is both present initially and formed as a product, the numbers and expressions shown above refer only to the initially present amount. For example, the 14.8 ppb of NO to NO_2 conversions shown under formaldehyde photolysis is due to the photolysis of initially present formaldehyde. [d] Obviously, the total amount of NO to NO_2 conversions shown in parts A and C of this table must agree if the counter species analysis has been performed correctly.

the alkenes in the following manner. Ethene is treated separately because it reacts with OH and O_3 at significantly slower rates than other alkenes. The terminal alkenes are lumped into one group whose chemistry is represented by that of propene. In the same fashion, the chemistry of *trans*-2-butene is used to represent that of all internally bonded alkenes. This type of approach is used with each of the hydrocarbon groups, resulting in a mechanism that contains 81 reactions and 52 species.

A detailed description and derivation of the Atkinson et al. mechanism can be found in the original paper (7) and is therefore not presented here. The only differences between the mechanism used in this study and that originally presented by Atkinson et al. (7) are (1) the three chamber-dependent reactions and the SO_2 reaction are not included here, (2) some photolysis rates have been changed to reflect experimental data that have been acquired since the original mechanism was published, and (3) counter species have been added to many of the reactions. The initial conditions chosen for this study correspond to those used in smog chamber experiment SUR-119J, performed at the University of California, Riverside (*11*), the detailed composition of which is shown in Table III, together with the corresponding initial conditions to be used with the Atkinson et al. (7) mechanism. The concentration–time profiles of NO, NO_2, and O_3, obtained by using this slightly modified Atkinson et al. mechanism, with the above-mentioned initial conditions, are given in Figure 4.

The counter species analysis of this mechanism proceeds in the same manner as was shown earlier with the simple aldehyde mechanism. We first formulate the F_s, which represents the fraction of species S that have led to NO to NO_2 conversions up until any specified time. Next, we formulate expressions for the number of NO to NO_2 conversions due to various species and reaction pathways. Table IV shows these relationships, together with their resulting values after 6 h of the simulation. Listed in section A of Table IV is the number of NO to NO_2 conversions attributable to the various radicals appearing in this system. We see that a majority of the NO oxidations are caused by HO_2 radicals and that most of the remaining NO to NO_2 conversions are due to alkylperoxy (AO_2), methylperoxy (CH_3O_2), hydroxyalkylperoxy (R-OH-O_2), and peroxyacetyl ($CH_3C(O)O_2$) radicals. For comparison, section B of Table IV shows the number of NO oxidations due to the inorganic reactions. Section C of Table IV presents the most useful counter species results, from which we can draw many conclusions. For example, we see that the di- and trialkylbenzenes, represented in this mechanism by xylene, account for 82% of the NO to NO_2 conversions due to the aromatic hydrocarbons. Of the 19% of the total NO oxidations that are due to the aromatics, 6% are due to methylglyoxal photolysis alone. We also conclude that alkene–OH reactions lead to significantly more NO to NO_2 conversions than alkene–O_3 reactions. In addition, notice that the percent of NO to NO_2 conversions due to the alkane plus OH reaction (24.7%) is about the same as the percent conversion due to alkene–OH reactions (23.0%). This is an interesting result since alkanes are generally viewed as less important than alkenes or aromatics. Also notice that the amount of NO converted to NO_2 due to the alkanes is completely dominated by the $n \geq 4$ alkanes (butane in the Atkinson et al. mechanism). This leads us to conclude that, for most urban applications, treating propane as unreactive will not cause any noticeable change in the predictive ability of lumped mechanisms. One last point which we note here is that the ketones and higher aldehydes ($n > 2$) lead to only a small number of NO to NO_2 conversions.

The second type of information that we desire, and which the counter species analysis provides, concerns radical initiation and termination and NO_x sinks. These results are presented in Table V. We see that for the test case considered here, formaldehyde photolysis is the most important radical source. The photolysis of O_3 and methylglyoxal is also important, as is the reaction of O_3 with the internally bonded alkenes (butene). The most important radical and NO_x sink are nitric acid formation via reaction 5. Peroxyacetyl nitrate (PAN) formation represents the only remaining NO_x and radical sink of any significance. The most important radical sources and sinks for the first 6 h of the simulation are shown in Figure 5.

Conclusions

The counter species analysis developed here enables one to assess quantitatively the importance of individual reactions and reaction subnetworks to the overall behavior of a complex chemical mechanism. The method is conceptually simple and is easy to implement with any mechanism. By applying the counter species analysis to a complex chemical mechanism describing photochemical smog, we are able to determine the relative importance of individual hydrocarbons and reaction steps to ozone formation, radical initiation and termination, and NO_x removal.

The counter species analysis has applications in any problem where complex chemical reaction mechanisms arise. Applications relevant to the field of atmospheric hydrocarbon chemistry include the following:

(1) The first application is evaluating the performance of "lumped" reaction mechanisms by applying the counter species analysis to both the lumped and explicit mechanisms. One could then quantitatively evaluate how well

Table V. Radical Source, Radical Sink, and NO_x Removal Results from the Counter Species Analysis of the Hydrocarbon/NO_x Photooxidation Simulation

reaction(s)	counter species expression	integrated rates: radical sources, ppb	integrated rates: radical sinks, ppb	integrated rates: NO_x sinks, ppb
HCHO + $h\nu$	2C21	33.5		
O_3 + $h\nu$	2C3	24.8		
$CH_3C(O)CHO$ + $h\nu$	2C69	18.0		
O_3 + butene	1.35C49	12.5		
HONO + $h\nu$	C6-C4	11.7		
CH_3CHO + $h\nu$	2C24	5.2		
cresol + NO_3	C72	4.1		
MEK + $h\nu$	2C42	3.0		
O_3 + propene	0.9C48	1.6		
$CH_3C(O)CH_3$ + $h\nu$	2C43	1.5		
O_3 + ethene	0.52C47	1.0		
RCHO + $h\nu$	2C39	0.5		
HNO_3 formation	C5		76.1	76.1
PAN formation			17.2	17.2
aromatic nitrate formation	0.25(C61 + C71)		5.4	5.4
nitrophenol formation	C73		4.1	4.1
$CH_3\dot{C}HO_2$ reactions	C54 + C55 + C57		4.0	
alkyl nitrate formation	0.1C33		3.5	3.5
LNO_2 formation			2.9	2.9
alkyl nitrate from OH + butene	0.1C46		1.9	1.9
$\dot{C}H_2\dot{O}_2$ reactions	C50 + C51 + C53		1.1	
PPN formation			0.8	0.8
benzyl nitrate formation	0.25C74		0.2	0.2
HO_2NO_2 formation			0.2	0.2
PBZN formation			~0	~0
H_2O_2 formation	C10		~0	~0
HNO_3 formation	C17 + C72			8.6
N_2O_5 formation				0.4
		117.4	117.4	121.3

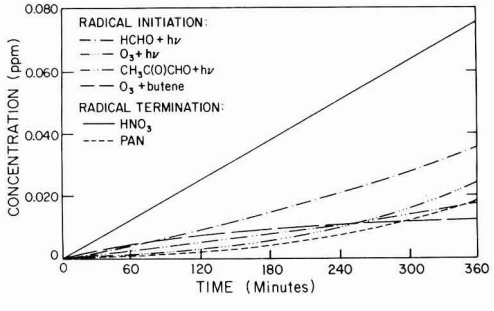

Figure 5. Counter species results for the hydrocarbon/NO_x simulation. Number of radical initiation and radical termination steps for the most important radical-producing and radical-scavenging reactions.

each reaction in the lumped mechanism represents the actual chemistry as depicted in the explicit mechanism.

(2) The second application is comparing two or more mechanisms that describe the same system. For example, different lumped reaction mechanisms can be compared to see exactly how the corresponding lumped classes in each mechanism compare with regard to O_3 formation, radical production, etc.

(3) The third application is obtaining a better understanding of how hydrocarbons should be grouped into classes in lumped mechanisms. In addition, the analysis will help one to choose which hydrocarbons, or lumped classes, can be eliminated without significantly affecting mechanism predictions.

(4) The fourth application is evaluating the importance of individual reaction steps and reaction pathways toward oxidant formation, radical initiation and termination, and NO_x sinks, as was illustrated for the Atkinson et al. (7) mechanism in this paper.

Registry No. O_3, 10028-15-6; HCHO, 50-00-0; CH_3CHO, 75-07-0; CH_3CH_2CHO, 123-38-6; NO, 10102-43-9; NO_2, 10102-44-0.

Literature Cited

(1) Falls, A. H.; McRae, G. J.; Seinfeld, J. H. *Int. J. Chem. Kinet.* **1979**, *11*, 1137–1162.
(2) McRae, G. J.; Tilden, J. W.; Seinfeld, J. H. *Comput. Chem. Eng.* **1982**, *6*, 15–25.
(3) Koda, M.; McRae, G. J.; Seinfeld, J. H. *Int. J. Chem. Kinet.* **1979**, *11*, 427–444.
(4) Atkinson, R.; Darnall, K. R.; Lloyd, A. C.; Winer, A. M.; Pitts, J. N., Jr. *Adv. Photochem.* **1979**, *11*, 375–487.
(5) Whitten, G. Z.; Killus, J. P.; Hogo, H. "Modeling of Simulated Photochemical Smog with Kinetic Mechanisms"; U.S. Environmental Protection Agency: 1980; EPA-600/3-80-028a, pp 1–348.
(6) Hendry, D. G.; Baldwin, A. C.; Golden, D. M. "Computer Modeling of Simulated Photochemical Smog"; U.S. Environmental Protection Agency: 1980; EPA-600/3-80-029, pp 1–207.
(7) Atkinson, R.; Lloyd, A. C.; Winges, L. *Atmos. Environ.* **1982**, *16*, 1341–1355.
(8) Killus, J. P.; Whitten, G. Z. "A New Carbon-Bond Mechanism for Air Quality Modeling", final report to the U.S. Environmental Protection Agency under Contract 68-02-3281, 1982, pp 1–107.
(9) Dodge, M. C. "Combined Use of Modeling Techniques and Smog Chamber Data to Derive Ozone-Precursor Relationships"; U.S. Environmental Protection Agency: 1977; EPA-600/3-77-001a, pp 881–889.
(10) Falls, A. H.; Seinfeld, J. H. *Environ. Sci. Technol.* **1978**, *12*, 1398–1406.

(11) Pitts, J. N.; Winer, A. M.; Darnall, K. R. "Chemical Consequences of Air Quality Standards and of Control Implementation Programs: Roles of Hydrocarbons, Oxides of Nitrogen, and Aged Smog in the Production of Photochemical Oxidant", final report to the California Air Resources Board under Contract 4-212, 1976, pp 1–444.
(12) Graedel, T. E. *J. Phys. Chem.* **1977**, *81*, 2372–2374.
(13) Jeffries, H. E., personal communication.
(14) Whitten, G. Z., personal communication.

Received for review May 2, 1983. Accepted October 3, 1983. This work was supported by the State of California Air Resources Board Agreement A2-042-32.

Summertime Variations in Polycyclic Aromatic Hydrocarbons at Four Sites in New Jersey

Ronald Harkov

Office of Science and Research, New Jersey Department of Environmental Protection, Trenton, New Jersey 08625

Arthur Greenberg and Faye Darack

Department of Chemical Engineering and Chemistry, New Jersey Institute of Technology, Newark, New Jersey 07102

Joan M. Daisey and Paul J. Lioy*

Institute of Environmental Medicine, New York University Medical Center, Tuxedo, New York 10987

■ Variations in the summertime concentrations of selected polycyclic aromatic hydrocarbons (PAH) collected by using inhalable particulate samplers (IPM-$D_{50} < 15$ μm) at four sites in New Jersey are presented and examined. The levels of PAH found in this study are consistent with other urban values reported in the literature. While day-to-day trends in PAH concentrations at the four sites were influenced by regional meteorology, it appears that local sources had the greatest influence on ambient levels. Comparison of selected PAH with IPM, EOM (extractable organic matter), and SO_4^{2-} values at each site showed weak correlations. However, intersite and intrasite Spearman rank correlations among PAH were significant and suggest a common type of source emitter at the urban locations during the summer. The intersite correlations also reflect the proximity of the four sites.

Introduction

Polycyclic aromatic hydrocarbons (PAH) are components of the organic aerosol which have both mutagenic and carcinogenic properties (*1*). These pollutants have been measured in ambient air for over 20 years, yet the majority of these studies have only focused on the potent animal carcinogen benzo[*a*]pyrene. Most recent studies of PAH have been concerned with the determination of average concentrations without regard to daily or seasonal variations in atmospheric levels (*2–5*). In addition, some limited research has been directed toward identifying PAH sources (*6–8*). The present study, however, is directed toward careful analysis of the daily and seasonal variations of PAH concentrations, meteorological influences, relative concentration of selected PAH (i.e., PAH profiles), and correlations with other pollutants as well as measures of biological activity. The latter point will be the subject of another paper on the Ames mutagenicity assay of these samples. The aim is to contribute to the understanding of the environmental significance of this class of compounds.

The PAH study detailed here is a part of the New Jersey Airborne Trace Element and Organic Substance (ATEOS) program which has been described elsewhere (*9–11*). In the present paper, results are reported from the summer of 1981 field campaign. The daily variability between and within sampling locales and relationships between documented meteorological events and source types are analyzed and discussed.

Experimental Section

Sampling. The sampling protocols and site descriptions for the ATEOS program have been described in detail elsewhere (*9–11*) and will only be briefly outlined. A General Metal Works size-selective inlet ($D_{50} < 15$ μm) high volume sampler (40 CFM) was used to collect ambient aerosol in preignited Gelman-AE fiberglass filters. IPM samples were collected simultaneously by a colocated size-selective inlet sampler which used Spectrograde filters, thus allowing for analysis of additional pollutants. Twenty-four hour sampling occurred from 10 a.m.–10 a.m. 7 days per week at three urban sites (Camden, Elizabeth, and Newark) and one rural background site (Ringwood) for the 6-week period from July 6, 1981, to August 14, 1981. The four sites are shown on a map of New Jersey (Figure 1).

The Newark site, in northeastern New Jersey, is at the interface of a highly industrialized area and a stable residential community; petrochemical, inorganic chemical, leather tanning, truck and auto painting, and precious metal recovery and refining facilities are located within 1 km of the site. Refineries and petrochemical and commercial areas are near the Elizabeth site which is about 8 km from the Newark site and within a residential community. The Camden site, in the southwest part of the state, is heavily influenced by a variety of industries located along the Delaware River to the west as well as by the Philadelphia airshed. Ringwood State Park is located in the extreme northeast of New Jersey, some 60 km from Newark.

Analysis. A complete description of the analytical procedure is found elsewhere (10) and can be outlined as follows. Airborne particulate matter collected on filters was subjected to sequential Soxhlet extraction with cyclohexane (CX), dichloromethane (DCM), and acetone (ACE), and each fraction was subjected to rotoevaporation and nitrogen gas blow down. The CX fraction was utilized for PAH analysis. (Very small amounts of PAH remain in the DCM fraction relative to the preceding CX fraction.)

0013-936X/84/0918-0287$01.50/0

Table I. Geometric Mean Concentrations (M_G) of Selected Polycyclic Aromatic Hydrocarbons (PAH) at Four Sites in New Jersey during the Summer of 1981 ATEOS Program

	Newark		Elizabeth		Camden		Ringwood	
	n[a]	M_G[b]	n	M_G	n	M_G	n	M_G
benzo[*a*]pyrene (BaP)	33	0.23	28	0.14	29	0.20	11	0.06
benzo[*e*]pyrene (BeP)	37	0.18	34	0.13	37	0.14	11	0.03
benzo[*j*]fluoranthene (BjF)	37	0.16	33	0.09	37	0.13	10	0.06
benzo[*k*]fluoranthene (BkF)	28	0.20	22	0.14	33	0.15	8	0.03
benzo[*b*]fluoranthene (BbF)	30	0.27	23	0.20	30	0.27	10	0.06
indeno[1,2,3-*cd*]pyrene (IcdP)	29	0.46	27	0.26	27	0.34	12	0.09
benzo[*ghi*]perylene (BghiP)	36	0.56	33	0.41	35	0.35	10	0.09
coronene (Cor)	36	0.47	33	0.35	35	0.29	9	0.08
perylene (Per)	27	0.10	22	0.04	23	0.06	9	0.03
dibenz[*ac*]anthracene (DBacA)	36	0.03	29	0.03	32	0.03	9	0.02

[a] Number of resolvable samples. [b] M_G = geometric mean concentration in ng/m^3. Values for 7/21-22 in Newark (ng/m^3): BaP, 8.74; BeP, 6.12; BjF, 6.50; BkF, 7.97; BbF, 11.16; IcdP, 16.36; BghiP, 9.52; Cor, not resolvable; Per, 3.29; DBacA, 0.88.

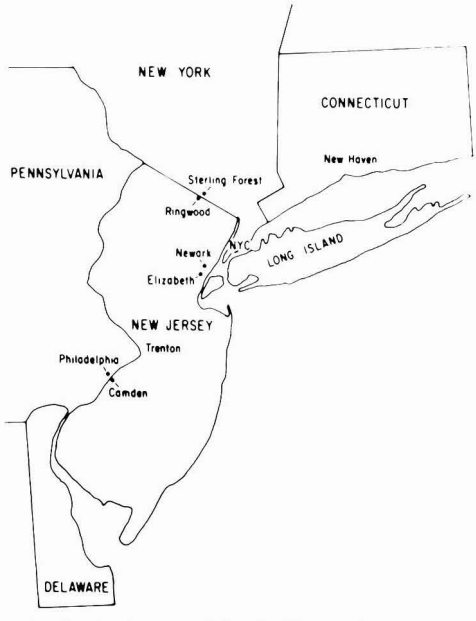

Figure 1. Site locations used in the ATEOS project and nearby reference urban areas.

These steps were followed by addition of an internal standard, 1-methyltrypticene, and separation of the PAH class from other CX-soluble organics using thin-layer chromatography (TLC) on silica gel G plates (fluorescent coated). The plates were developed with *n*-hexane–toluene, 1:1. Tetrahydrofuran washing of the scraped TLC adsorbent was followed by concentration under nitrogen to about 0.1 mL and injection of 10–20 μL into a high-performance liquid chromatography (HPLC) apparatus operated in the reverse-phase mode using Perkin-Elmer PAH/10 and Separations Group Vydac columns with elution by aqueous acetonitrile (*10*). Eluting compounds were monitored simultaneously by UV absorbances at 280 and 365 nm as well as fluorescence (360-nm excitation, >440-nm emission).

Data Assurance. All sampling and analyses in the ATEOS program are subject to a rigorous quality assurance and quality control (qa/qc) plan as described in a previous report (*10*). The qa/qc for PAH includes comparison with NBS standards, interlaboratory comparisons, internal standards, spikes, blanks, Beer's law plots, daily standardization of instruments, and comparison of 280/365 nm UV ratios and UV/fluorescence ratios of the samples to those of standards. In those instances in which the identity of a compound could not be confirmed by these ratios, the compounds's concentration was omitted from the data set.

Results

The 6-week geometric means for 10 PAH compounds measured during the summer of 1981 ATEOS campaign are shown in Table I. Due to the low concentrations of particulate organic matter found at the Ringwood site, this data set represents 3-day composites. Generally, Newark exhibited the highest PAH values, with Camden and Elizabeth being very similar and Ringwood having considerably lower values.

Figure 2 shows the daily variation in concentration for benzo[*a*]pyrene at all four sites during the campaign. Lioy et al. (*12*) have shown in a previous analysis that there were three episodes of regional photochemical smog, which were characterized by high IPM, SO_4^{2-}, ozone, and EOM (extractable organic matter) levels. Although the levels of six selected PAH [benzo[*a*]pyrene (BaP), benzo[*e*]pyrene (BeP), coronene (Cor), benzo[*ghi*]perylene (BghiP), indeno [1,2,3-*cd*]pyrene (IcdP), and benzo[*j*]fluoranthene (BjF)] were also higher during episode (EP) than in nonepisode (NEP) periods (Table II), no strong relationship was noted with the above pollutants (i.e., $R_{sp} < 0.6$, $p > 0.01$; R_{sp} = Spearman correlation coefficients). These six PAH compounds were chosen because they include the most complete data set during these time periods. Values of $R_{sp} > 0.7$ were only found for BaP and BjF vs. cyclohexane-soluble organics (CX) at the Newark site. It is clear that the selected PAH concentrations can vary significantly according to the influence of specific source emitters at each site. For example, the extremely high levels in Newark on July 21–22 were not found in Ringwood or Camden. Unfortunately, the Elizabeth sample for that date could not be resolved by HPLC analysis. However, less localized pollution patterns can also be discerned through statistical analysis. For example, when intersite comparisons were made between the Newark and Elizabeth sites (only 8 km apart), Spearman correlation coefficients for the six selected PAH were greater than 0.6 and highly significant ($p < 0.001$; Table III). In contrast,the correlations for PAH concentrations at these two northern New Jersey urban sites with those at the southern urban site, Camden, over 100 km distant, are much poorer (Table III). It is also noteworthy that while the geometric means for PAH were generally 50–80% higher for EP than NEP

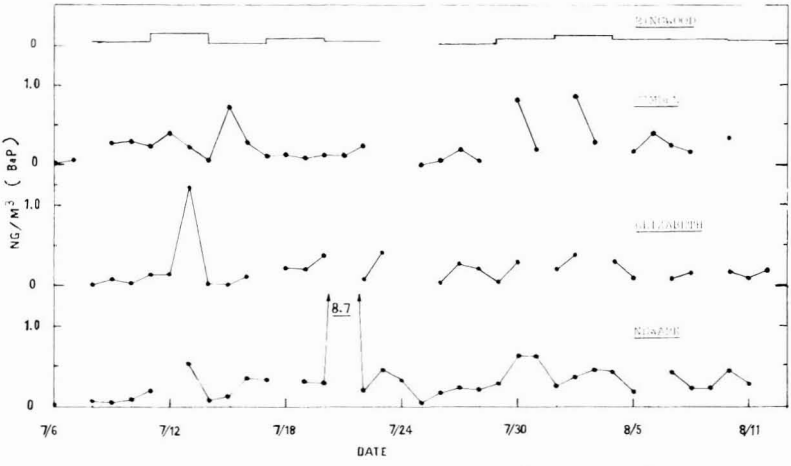

Figure 2. Daily concentrations of BaP measured at all ATEOS study sites during the 1981 summer study.

Table II. Geometric Mean Concentrations (M_G) of Six PAH at the Three Urban Sites in Nonepisode Periods (NEP) and Episode Periods (EP) during the Summer of 1981

	Newark				Elizabeth				Camden			
	NEP		EP		NEP		EP		NEP		EP	
	n[a]	M_G[b]	n	M_G	n	M_G	n	M_G	n	M_G	n	M_G
BaP	24	0.21	9	0.33	20	0.12	8	0.22	21	0.23	8	0.22
BeP	25	0.17	12	0.20	25	0.11	9	0.25	25	0.14	12	0.16
BjF	25	0.14	12	0.23	25	0.09	9	0.11	25	0.12	12	0.15
BghiP	26	0.48	10	0.81	23	0.39	10	0.52	23	0.32	12	0.43
IcdP	20	0.55	9	0.89	17	0.30	10	0.57	16	0.44	11	0.46
Cor	26[c]	0.20	10	0.43	24	0.18	9	0.30	34	0.17	11	0.19

[a] n = number of resolvable samples. [b] Concentrations are reported in ng/m³. [c] No data point for 7/21-22 day; see footnote *b* of Table I.

Table III. Intersite Spearman Rank Correlations (R_{sp}) for Six PAH and Cyclohexane-Soluble Organics (CX)

	BaP	BeP	BjF	IcdP	BhgiP	Cor	CX
Elizabeth/Newark	0.76[a]	0.63[a]	0.62[a]	0.84[a]	0.63[a]	0.75[a]	0.83[a]
Camden/Newark	0.29	0.52	0.26	0.51	0.37	0.52	0.39
Camden/Elizabeth	0.03	0.37	0.18	0.44	0.37	0.45	0.45

[a] Significant at $p < 0.001$.

at the Newark and Elizabeth sites, the corresponding increase at Camden is generally less than 25% (Table II). This parallels the findings for EP/NEP comparisons of EOM (10) at the urban sites in which Newark and Elizabeth levels increased by 70–100% at Newark and Elizabeth and only 40–60% at Camden. Spearman rank correlations for the selected PAH within each of the urban sites reveal $R_{sp} > 0.70$ that were significant at the $p < 0.001$ level, indicating that similar types of PAH sources were present near each site. The PAH compound distributions (or profiles), shown in Figure 3, were also similar.

Discussion

The levels of PAH reported here are similar to those found in other U.S. urban areas in the summer (*1*) and at a number of monitoring sites in New Jersey during 1979 (*13*). Sumertime PAH levels tend to be at a minimum, reflecting changes in prevailing meteorology and a lack of a major PAH source, residential fossil fuel combustion for heating (*1*). While one would also anticipate greater photochemical and chemical decomposition (e.g., with ozone) during the summer period, the similarities between relative proportions of different PAH (i.e., PAH profiles) when summer and winter samples are compared are strong (*13*). Clearly, more research is needed in this area in order to understand ambient PAH profiles in terms of sources and atmospheric decomposition pathways.

The major PAH source during the summer in New Jersey is most likely motor vehicle emissions, an area source, although specific point sources may have a disproportionately large impact on ambient concentrations on individual days at each of the urban sites. An analysis of the information from the summer of 1981 campaign indicates the importance of motor vehicle emission contributions to ambient PAH levels. The daily variations in concentration of the PAH are similar for the Newark and Elizabeth sites even though the point sources in these two areas differ (e.g., see BaP in Figure 2). Source commonality is supported by similarities in PAH profiles measured at each site (Figure 3). It should again be noted that site proximity for Newark and Elizabeth strengthens the observed correlation. It must also be noted that New Jersey has the highest motor vehicle density in the United States and that motor vehicles are major sources for a large number of organic air pollutants (*14–16*). A comparison of the ratios of five selected PAH (BeP, BjF, IcdP, BghiP,

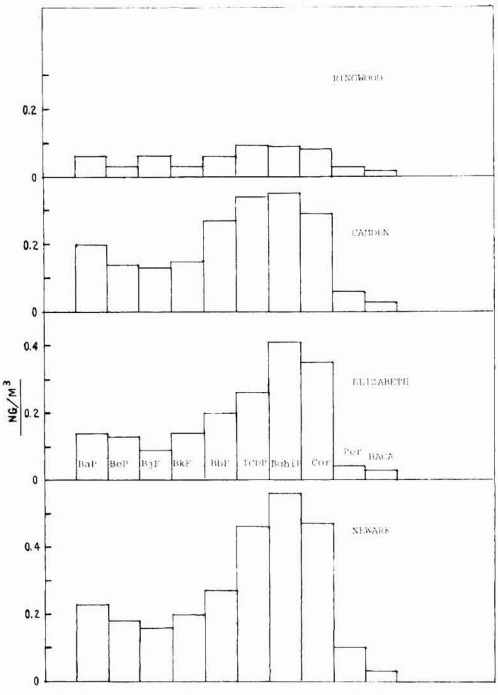

Figure 3. Histogram of arithmatic mean concentrations of selected PAH measured at all ATEOS study sites during the 1981 summer study.

and Cor) to BaP, to source emissions data from the literature (*4*, *14*, *17–19*), is appropriate for analyzing the impact of automotive emissions on New Jersey (Table IV). A number of observations can be made from this comparison. The PAH:BaP ratios change only slightly at the urban and rural sites for summertime episodic (EP) and nonepisodic (NEP) periods, with the greatest difference occurring at the Newark site. Since BghiP and Cor levels are indicative of motor vehicle contributions to ambient PAH levels, the ratios of these two compounds to BaP can be used as indicators of the relative contribution of this source to atmospheric PAH concentrations in New Jersey during the summer of 1981. Both tunnel and automobile exhaust studies (Table IV) have produced a number of different Cor:BaP and BghiP:BaP ratios. These ratios differ between studies due to differences in sampling and analytical methods, in sampling season, and, in the case of tunnels, in motor vehicle composition and exhaust circulation rates. For the purposes of this report, ratios of Cor:BaP = 2.5 and BghiP:BaP = 2.3 are adopted from recent studies in the Lincoln and Holland Tunnels (*18*) which connect New York City and northeastern New Jersey. Tunnel and exhaust condensate ratios are presented in Table IV for comparison. The ratios from the tunnel samples are more appropriate for comparison for two reasons: first, the analytical procedures are identical; second, the motor vehicle composition in the tunnels should be similar to the traffic composition at the urban New Jersey sites. On the basis of the ratios, it appears that the Elizabeth site is affected primarily by motor vehicle emissions during EP as well as NEP. In contrast, Newark seems to be influenced by motor vehicles during NEP, but additional sources are important during EP. These observations are not surprising considering that these two sites are only 8 km apart and contain a high density of motor vehicles. However, the presence of other PAH

Table IV. (A) Ratios of Selected PAH to BaP from Summer of 1981 ATEOS Campaign during Nonepisode Periods (NEP) and Episode Periods (EP) and (B) PAH:BaP Ratios Derived from Tunnel and Exhaust Data

(A) Ambient Studies

	Newark		Elizabeth		Camden		Ringwood	
	NEP	EP[a]	NEP	EP	NEP	EP	NEP	EP
BaP	1.0	1.0	1.0	1.0	1.0	1.0	1.0	1.0
BeP	0.9	0.6	0.8	1.0	0.7	0.7	3.6	0.5
BjF	0.7	0.7	0.6	0.7	0.6	0.7	0.8	0.7
IcdP	2.3	1.7	1.8	2.2	1.8	1.5	1.0	1.8
BghiP	3.0	2.2	2.8	2.4	1.7	1.7	1.2	1.2
Cor	2.4	1.8	2.4	2.3	1.6	1.3	0.8	1.8

(B) Tunnel and Exhaust Studies

	Cor:BaP	BghiP:BaP	sample type
Grimmer et al. (*17*)	1.6	2.3	tunnel
Kebbekus et al. (*18*)	2.5	2.3	tunnel
Handa et al. (*4*)		2.8	tunnel
Lee et al. (*19*)	1.6		exhaust
Grimmer (*14*)	2.5	4.0	exhaust

[a] Newark values do not include 7/21–22 data.

sources in the area of the Newark site can be deduced from selected PAH:BaP ratios observed on 7/21–7/22 (see Table I). On that day, the PAH levels were virtually as high as the sum of all the other campaign days. Specifically, the IcdP:BaP and BghiP:BaP ratios (1.3 and 1.1, respectively) were considerably lower than the NEP ratios (2.3 and 3.0, respectively).

The poor correlations of the selected PAH with IPM, SO_4^{2-}, and ozone found in this study are not surprising considering that PAH are primary pollutants and, during the summer season, SO_4^{2-} and ozone are secondary contaminants and will be a combination of some locally produced and transported material. Both SO_4^{2-} and acetone-soluble matter are the two components that have been determined to dominate daily IPM variability in New Jersey during the summer (*11*). Acetone-soluble matter and SO_4^{2-} make up nearly 50% of the IPM and together furnish the most likely explanation of the weak correlations between IPM and PAH. Only the CX fraction shows any significant correlation with PAH, and this correlation is strongest for the Newark site. Since the above arguments indicate that there are non-motor vehicle sources at the Newark site, one must anticipate the presence of industrial sources emitting both CX and PAH. A potential source–category for the PAH at the Newark site is secondary-nonferrous metal smelters. This point finds some support in the data analysis since the CX fraction was significantly correlated ($R_{sp} > 0.70$, $p\ g\ 0.001$) with Pb, Cu, Fe, Ni, and Zn. However, more summer samples and wind rose analyses will be necessary to evaluate the significance of this source type.

Conclusions

The daily levels of selected airborne particulate PAH in New Jersey during the summer of 1981 are presented. Spearman rank correlation coefficients were significant for six selected PAH for certain intersite as well as intrasite comparisons. These results, along with selected PAH:BaP ratios and correlations with Pb, indicate that motor vehicle traffic was the major PAH source during the summer. The influence of additional non-motor vehicle PAH sources is apparent at the Newark site, and their influence was particularly significant on July 21–22, when PAH levels were virtually equal to the other sampling days combined.

This serves to reemphasize the well-known limitations in occasional, as opposed to daily, sampling.

Acknowledgments

We thank all the those members of the ATEOS program who have run sites and completed sample analyses and data analysis. We also thank Thomas Burke, Director of Science and Research of the New Jersey Department of Environmental Protection, for his continuing encouragement on this project.

Literature Cited

(1) Santodonato, J.; Howard, P.; Basu, D. *J. Environ. Pathol. Toxicol.* **1981**, *3*, 1–364.
(2) Faoro, R. B.; Manning, J. A. *J. Air Pollut. Control Assoc.* **1981**, *31*, 62–64.
(3) Katz, M.; Chan, C. *Environ. Sci. Technol.* **1980**, *14*, 838–843.
(4) Handa, T.; Kato, Y.; Yanamura, T.; Ishii, T., *Environ. Sci. Technol.* **1980**, *14*, 416–422.
(5) Butler, J. D.; Crossby, P. *Sci. Total Environ.* **1979**, *11*, 53–58.
(6) Daisey, J. M.; Leyko, M. A.; Kneip, T. J. "Polycyclic Aromatic Hydrocarbons"; Jones, P. W.; Leber, P., Eds.; Ann Arbor Press: Ann Arbor, MI, 1979; pp 201–215.
(7) Daisey, J. M.; Lioy, P. J. *J. Air. Pollut. Control Assoc.* **1981**, *31*, 567–569.
(8) Greenberg, A.; Bozzelli, J. W.; Cannova, F.; Forstner, E.; Giorgio, P.; Stout, D.; Yokoyama, R. *Environ. Sci. Technol.* **1981**, *31*, 567–569.
(9) Harkov, R.; Fischer, R. *Proc. Annu. APCA Conf., 75th* **1982**, 1–20 (Paper 82-1.1).
(10) Lioy, P. J.; Daisey, J. M.; Greenberg, A.; Bozzelli, J.; Kebbekus, B.; McGarrity, G. "First Annual Report of the ATEOS Program"; New Jersey Department of Environmental Protection: Trenton, NJ, 1982; pp 1–270.
(11) Lioy, P. J.; Daisey, J. M.; Atherholt, T.; Bozzelli, J.; Darack, F.; Fischer, R.; Greenberg, A.; Harkov, R.; Kebbekus, B.; Kneip, T. J.; Louis, J.; McGarrity, G.; McGeorge, L.; Reiss, N. M. *J. Air Pollut. Control Assoc.* **1983**, *33*, 649–657.
(12) Lioy, P. J.; Daisey, J. M. Reiss, N. M.; Harkov, R. *Atmos. Environ.* **1983**, *17*, 2321–2330.
(13) Bozzelli, J. W.; Kebbekus, B. B.; Greenberg, A. "Analysis of Selected Toxic and Carcinogenic Substance in Ambient Air in New Jersey"; New Jersey Department of Environmental Protection: Trenton, NJ, 1980.
(14) Grimmer, G. "Analysis of Automobile Exhaust Condensates in Air Pollution and Cancer in Man", 1977, IARC Publication No. 16.
(15) Hampton, C. V.; Pierson, W. R.; Harvey, T. M.; Updegrave, W. S.; Marano, R. S. *Environ. Sci. Technol.* **1982**, *16*, 287–298.
(16) Hampton, C. V.; Pierson, W. R.; Schuetzle, D.; Harvey, T. M. submitted for publication in *Environ. Sci. Technol.*
(17) Grimmer, G.; Naujack, K. W.; Schneider, D. "Polynuclear Aromatic Hydrocarbons"; Bjorseth, A.; Dennis, A. J., Eds.; Battelle Press: Columbus, OH, 1980; pp 107–125.
(18) Kebbekus, B. B.; Greenberg, A.; Bozzelli, J. W.; Darack, F.; Eveleens, C.; Horgan, L.; Strangeland, L. *J. Air Pollut. Control Assoc.* **1983**, *33*, 328–330.
(19) Lee, F. S. C.; Prater, T. J.; Ferris, F. *Polynuclear Aromatic Hydrocarbons*, Jones, P. W.; Leber, P., Eds.; Ann Arbor Press: Ann Arbor, MI, 1979; pp 83–110.

Received for review July 21, 1983. Accepted October 3, 1983. This research is sponsored by the New Jersey Department of Environmental Protection, Trenton, NJ.

NOTES

Butyltin Compounds and Inorganic Tin in Sediments in Ontario

R. James Maguire

Environmental Contaminants Division, National Water Research Institute, Department of the Environment, Canada Centre for Inland Waters, Burlington, Ontario, Canada L7R 4A6

■ A method has been developed for the analysis of butyltin species and inorganic tin in sediments, and the presence of these compounds in sediments in Ontario is reported for the first time. Although inorganic tin occurred frequently in sediments collected around the province, butyltin species were found mainly in the sediments of harbors, reflecting earlier findings on their occurrence in water, with which these findings are compared. Tri-*n*-butyltin, the most toxic of the butyltin species to aquatic life, was present at 0.5 mg/kg (dry weight) in the top 2 cm of sediment in Toronto Harbour. In addition, tri-*n*-butylmethyltin and di-*n*-butyldimethyltin were found in the sediment of a few harbors, indicating that some butyltin species can be methylated in aquatic environments.

Introduction

Organotin compounds are used in three main ways, viz., as stabilizers for polyvinyl chloride, as catalysts, and as biocides (*1*). The increasing annual use of organotin compounds raises the possibility of environmental pollution. Organotin compounds are a class of compounds about which more information is sought under Canada's Environmental Contaminants Act (*2*) regarding toxicology and environmental fate. Recently we reported the occurrence of butyltin species and inorganic tin in water at 30 locations in Ontario (*3*); this article reports a method for the analysis of butyltin species and inorganic tin in sediments and the concentrations of these compounds in sediments collected at the same time as the aforementioned water samples.

Experimental Methods

Materials. Bis(tri-*n*-butyltin) oxide (97%), di-*n*-butyltin dichloride (96.5%), *n*-butyltin trichloride (95%), tin (99.9%), and 2 M *n*-pentylmagnesium bromide in diethyl ether were from Ventron (Danvers, MA) (three different lots of *n*-pentylmagnesium bromide purchased after this work was completed were found to contain unacceptably high concentrations of the four butylpentyltin compounds,

Table I. Recoveries of Butyltin Species and Inorganic Tin from "Spiked" Sediment[a]

	% recovery					
spiked concn, mg/kg	Bu_3Sn^+	Bu_2Sn^{2+}	$BuSn^{3+}$	Sn(IV)	Bu_3MeSn	Bu_2Me_2Sn
100	108 ± 11	97 ± 6	94 ± 9	96 ± 21	95 ± 8	71 ± 14
1	63 ± 35	180 ± 100	55 ± 26	105 ± 29	104 ± 6	55 ± 16
0.2	81 ± 31	119 ± 34	74 ± 29	101 ± 11	96 ± 5	48 ± 12
0.01	106 ± 12	98 ± 13	103 ± 7		94 ± 11	34 ± 11

[a] Average figures of triplicate determinations on both test sediments.

$Bu_nPe_{4-n}Sn$); 2-hydroxy-2,4,6-cycloheptatrien-1-one (tropolone) was from Aldrich (Milwaukee, WI); Florisil was from Fisher Scientific (Toronto, Ontario); sulfuric and hydrochloric acids were Aristar grade from BDH Chemicals (Toronto, Ontario); all organic solvents were pesticide grade from Caledon Laboratories (Georgetown, Ontario); water was distilled and passed through a "Milli-Q" system (Millipore Ltd., Mississauga, Ontario). Butylpentyltin ($Bu_nPe_{4-n}Sn$) standards were prepared and purified according to the method of Maguire and Huneault (*4*). Butylmethyltin ($Bu_nMe_{4-n}Sn$) standards were gifts, prepared according to the method of Chau et al. (5).

Extraction of "Spiked" Sediment. One gram of freeze-dried test sediment (from the middle of Lake Ontario), which had been ground with a mortar and pestle, was "spiked" with a hexane solution of bis(tri-*n*-butyltin) oxide, di-*n*-butyltin dichloride, and *n*-butyltin trichloride. The mixture was rotated on a rotary evaporator for 15 min, then the hexane was evaporated and 0.01 mL of Sn(IV) in 10% HCl was added to the sediment, and the sediment was tumbled for another 15 min on the rotary evaporator, but no attempt was made to evaporate the small quantity of water. The sediment was then refluxed for 2 h with 0.25 g of tropolone in 100 mL of benzene, a complexing agent–solvent system which had earlier been shown to be effective for the extraction of butyltin species and Sn(IV) from water (*4*). The mixture was filtered, and volatile butylpentyltin ($Bu_nPe_{4-n}Sn$) derivatives for gas chromatographic analysis were prepared by refluxing the filtrate with 10 mL of *n*-pentylmagnesium bromide for 1 h. Excess Grignard reagent was deactivated by adding 50 mL of 1 N H_2SO_4, and the organic layer was separated, dried, and reduced to ca. 1 mL of a deep red solution. This solution was applied to a 2 cm i.d. × 0.5 m column of activated Florisil and eluted with ca. 400 mL of hexane. The hexane solution was evaporated to 1.0 mL of a colorless or faintly yellow solution and analyzed by gas chromatography with a modified flame photometric detector (*4*). "Spiking" experiments were done in triplicate at 100, 1, 0.2, and 0.01 mg/kg (dry weight) of the butyltin species and Sn(IV), with two test sediments from the middle of Lake Ontario. Each solution to be analyzed was injected 3–5 times into the gas chromatograph. Appropriate reagent and sediment blanks were analyzed in a similar fashion. Chromatographic conditions were as described previously (*4*), with the exception that the 3% OV-225 column was held initially at 135 °C for 10 min, followed by a 50 C°/min rise to 230 °C, at which temperature it was held for 5 min. This high-temperature cycle was necessary to preserve the sensitivity of the detector.

Subsequent chromatographic analyses of the sediment extracts showed the presence of tri-*n*-butylmethyltin and di-*n*-butyldimethyltin in some samples; therefore, the efficiency of extraction of these two compounds under the conditions described above was also examined. For these two compounds, the OV-225 column was held at 70 °C for 2 min, followed by a 10 C°/min rise to 230 °C and a final "hold" at 230 °C for 5 min.

Sample Collection and Analyses. Sediment samples were collected with an Ekman dredge at various locations in Ontario in the summer of 1981. The top 2 cm was scraped off into glass jars. The sediment was air-dried, stones and pieces of wood were removed, and the sediment was ground with a mortar and pestle. Three 1-g samples of each sediment were extracted and analyzed as described above. Determination of concentrations was done by comparison of peak areas to those of known standards on the OV-225 column. Confirmation of identity was done by cochromatography with known standards on the OV-225 column and a 3% OV-1 column. For the butylpentyltin derivatives the temperature of the OV-1 column was held at 170 °C for 10 min, followed by a 50 C°/min rise to 230 °C and a 5-min hold at 230 °C. For the butylmethyltin derivatives, the temperature of the OV-1 column was held at 120 °C for 2 min, followed by a 10 C°/min rise to 230 °C and a 5-min hold at 230 °C. Each solution to be analyzed was injected 3–5 times into the gas chromatograph. Appropriate reagent blanks were analyzed in a similar fashion. A chromatographic peak was not accepted as real unless it was at least twice as large as any corresponding peak in the reagent blank. Particular attention was paid to the possibility of methylmagnesium bromide contamination of the *n*-pentylmagnesium bromide, but no contamination was evident.

For brevity, each of the *n*-butyltin species is referred to here as though it existed only in cationic form (e.g., Bu_3Sn^+, where Bu = *n*-butyl); this formalism is not meant to imply exact identities for these species in sediment.

Although Sn(IV) was the only inorganic tin species for which recoveries were determined, the inorganic tin present in the sediment samples is reported as total recoverable inorganic tin, since it has been shown that hydride derivatization of either Sn(IV) or Sn(II) yields SnH_4 (*6*), and thus, any Sn(II) that may be present in the sediments may similarly be pentylated to Pe_4Sn.

Results and Discussion

Table I shows that, in general, and at times within a fairly wide range of experimental error, the recoveries of Bu_3Sn^+, Bu_2Sn^{2+}, $BuSn^{3+}$, and Sn(IV) from sediment were quantitative, and so the recoveries reported below for the field samples were not corrected. Recovery experiments with Sn(IV) below 0.2 mg/kg could not be done because the two test sediments contained enough naturally occurring tin to dwarf the spike. The minimum detectable concentration in sediment of each butyltin species and inorganic tin was about 5 μg/kg (dry weight). After the presence of Bu_3MeSn and Bu_2Me_2Sn in the sediment extracts was discovered, their recoveries from sediment using the above method were determined and are also shown in Table I. Bu_3MeSn extraction was quantitative, but there were significant losses of Bu_2Me_2Sn, probably largely due to volatilization during rotary evaporation of solvent (*4*). Recoveries of these two compounds from the field samples reported below were also uncorrected, and the minimum

Table II. Concentrations (mg/kg Dry Weight) of Butyltin Species and Total Recoverable Inorganic Tin (TRIT) in Top 2 cm of Sediment[a]

location	$[Bu_3Sn^+]$	$[Bu_2Sn^{2+}]$	$[BuSn^{3+}]$	[TRIT]
Lake Superior (Thunder Bay)				$(4.39 \pm 0.20) \times 10^{-1}$
Lake Superior (Red Rock)				$(4.00 \pm 0.10) \times 10^{-1}$
Turkey Lake 2				1.00 ± 0.03
Turkey Lake 3				$(5.92 \pm 0.30) \times 10^{-1}$
Turkey Lake 4				$(7.23 \pm 0.20) \times 10^{-1}$
Turkey Lake 5				$(5.22 \pm 0.36) \times 10^{-1}$
Sault Ste. Marie Harbor				1.74 ± 0.04
Nepewassi Lake (Sudbury)				$(2.08 \pm 0.22) \times 10^{-1}$
Lake Nipissing (North Bay)				$(6.85 \pm 0.57) \times 10^{-1}$
Plastic Lake				1.12 ± 0.05
Owen Sound Harbor				$(7.70 \pm 0.44) \times 10^{-1}$
Lake St. Clair (marina)	$(1.25 \pm 0.47) \times 10^{-1}$	$(7.35 \pm 3.33) \times 10^{-2}$	$(2.32 \pm 0.51) \times 10^{-2}$	$(1.14 \pm 0.27) \times 10^{-1}$
Port Dover Harbor	$(1.29 \pm 0.30) \times 10^{-1}$	$(6.49 \pm 1.97) \times 10^{-2}$	$(9.38 \pm 1.86) \times 10^{-2}$	$(3.14 \pm 0.09) \times 10^{-1}$
Grand River (mouth)	$(3.09 \pm 0.62) \times 10^{-2}$	$(8.97 \pm 0.72) \times 10^{-3}$	$(1.41 \pm 0.04) \times 10^{-2}$	$(2.36 \pm 0.10) \times 10^{-1}$
Toronto Harbor	$(5.39 \pm 0.66) \times 10^{-1}$	$(3.48 \pm 1.91) \times 10^{-1}$	$(5.80 \pm 0.99) \times 10^{-1}$	5.13 ± 0.15
Whitby Harbor	$(1.10 \pm 0.20) \times 10^{-1}$	$(4.86 \pm 0.60) \times 10^{-2}$	$(1.38 \pm 0.17) \times 10^{-2}$	$(1.31 \pm 0.11) \times 10^{-1}$
Belleville Harbor				1.45 ± 0.04
Kingston Harbor	$(4.09 \pm 0.26) \times 10^{-1}$	$(1.52 \pm 1.02) \times 10^{-1}$		1.59 ± 0.05
St. Lawrence River 1				$(5.78 \pm 0.22) \times 10^{-1}$
St. Lawrence River 2				$(8.20 \pm 0.94) \times 10^{-2}$

[a] Precise sampling locations are available upon request.

detectable concentration of each compound was also about 5 μg/kg (dry weight).

Table II shows the concentrations of Bu_3Sn^+, Bu_2Sn^{2+}, $BuSn^{3+}$, and inorganic tin in sediment at various locations in the province. This table omits several locations at which water samples were collected (cf. ref 3) but at which (i) no butyltin species or inorganic tin was detected in the sediment (Turkey Lake 1 and Collingwood Harbour), (ii) sediment samples were not collected at the same time as the water samples (Hamilton Harbour), or (iii) sediment samples could not be obtained because of the nature of the lake or river bottom (Marathon, Ramsey Lake, St. Clair River 1, 2, and 3, Mitchell Bay, and Thames River). The results of Table II are in general greement with the observations of butyltin species and inorganic tin in the waters (*3*) overlying the sediments. Inorganic tin was widespread, and butyltin species were present in harbors, most likely because tributyltin compounds are used in some antifouling boat paints and paints for dock structures (*1*). These results are also consistent with those of Seidel et al. (7), who found Sn(IV) and $BuSn^{3+}$ in California coastal sediments in areas where there was extensive boating or shipping, at concentrations up to 11 and 0.01 mg/kg (dry weight), respectively. In this study, Toronto Harbour contained the highest concentration of Bu_3Sn^+ of any sediment collected, about 0.5 mg/kg (dry weight). Tri-*n*-butyltin is the most toxic of the butyltin species to aquatic biota, with an LD_{100}^{12d} value of 5 μg/L for rainbow trout yolk sac fry (*8*). The toxicological significance of high concentrations of Bu_3Sn^+ in sediment has yet to be established; however, it is worth noting that the Bu_3Sn^+ concentration in the subsurface water of Toronto Harbour was 0.84 μg/L (*3*).

The earlier observation of surface water microlayer concentrations of butyltin species 10^4 times greater than subsurface water concentrations at some locations (*3*) prompted an estimate of the relative amounts of butyltins in the two "compartments" and showed that at some locations the surface microlayer contained a significant amount of butyltin species compared to that contained in the whole depth of underlying water. The sediment results now allow the amounts of butyltin species in the surface microlayer to be put into better perspective.

An estimate of the amounts of butyltin species and inorganic tin in the surface microlayer, subsurface water, and top 2 cm of sediment was made by (i) considering a sample of water of length, width, and depth A, B, and C meters, respectively, upon which rests a microlayer D meters thick, and which itself rests upon a layer of sediment E meters thick, (ii) supposing that the concentration of the compound of interest is X micrograms per liter in the surface microlayer, Y micrograms per liter in the subsurface water, and Z milligrams per kilogram in the sediment, and (iii) assuming that X, Y, and Z are invariant with their respective depths or thicknesses. The amount (μg) of the compound of interest in each compartment is thus 10^3 $ABDX$ for the surface microlayer, 10^3 $ABCY$ for the subsurface water, and 10^6 $dfABEZ$ for the sediment, in which case d, the density (g of sediment wet weight/mL of sediment), is assumed to be 1.4 (*9*), and f (g of sediment dry weight/g of sediment wet weight) is 0.5, the average figure for the 20 locations in this study.

The amounts of the butyltin species and inorganic tin in each compartment were estimated with the earlier data (*3*), Table II above, and with $E = 0.02$ m and $A = B = 1$ m. The results are shown in Table III. The estimates were only made for those locations in which a particular species was present in every compartment, with the exception of Toronto Harbour; therefore, there are no estimates for $BuSn^{3+}$. The results show that in 16 of 20 cases the sediment contained more than 50% of the butyltin species or inorganic tin and that in the remaining 4 cases the subsurface water contained more than 50% of the butyltin species or inorganic tin. In Whitby Harbour, the surface microlayer contained 10% of the Bu_2Sn^{2+} present in all three compartments; however, in general, it can be concluded that although high concentrations of butyltin species in surface microlayers may pose a hazard to surface-dwelling biota, for purposes of calculating mass balance the carrying capacity of the surface microlayer for butyltin species is insignificant.

The biomethylation (*10–15*) and chemical methylation (*16*, *17*) of inorganic tin and methyltin species have received a good deal of attention lately, but there have heretofore been no reports of biological or abiotic methylation of organotin species other than methyltin compounds. Blair et al. (*13*) were unable to detect Bu_3MeSn in cultures of tributyltin-resistant bacteria which had been inoculated with Bu_3SnCl, and Guard et al. (*11*) asserted that biomethylation of Bu_3Sn^+ would not likely be more

Table III. Estimates of Amounts (μg) per m^2 of Butyltin Species and Total Recoverable Inorganic Tin (TRIT) in Surface Microlayer, Subsurface Water, and Top 2 cm of Sediment

location	amounts, μg/m^2 surface microlayer	subsurface water	sediment
	Bu_3Sn^+		
Lake St. Clair (marina)	3.05	5.82×10^3	1.75×10^3
Toronto Harbor		4.20×10^3	7.55×10^3
Whitby Harbor	8.40×10^{-2}	2.50×10^2	1.54×10^3
Kingston Harbor	2.88×10^{-1}	5.00×10^1	5.73×10^3
	Bu_2Sn^{2+}		
Lake St. Clair (marina)	6.42	1.46×10^4	1.03×10^3
Toronto Harbor	8.76×10^1	1.35×10^3	4.87×10^3
Whitby Harbor	1.35×10^2	4.50×10^2	6.80×10^2
Kingston Harbor	2.34	1.50×10^2	2.13×10^3
	TRIT		
Turkey Lake 2	2.54×10^1	6.36×10^3	1.40×10^4
Turkey Lake 4	2.53	2.40×10^2	1.01×10^4
Sault Ste. Marie Harbor	2.34	1.21×10^4	2.43×10^4
Owen Sound Harbor	1.25×10^1	1.28×10^3	1.08×10^4
Lake St. Clair (marina)	3.96×10^{-1}	1.20×10^4	1.60×10^3
Port Dover Harbor	1.50×10^{-1}	5.00×10^1	4.40×10^3
Toronto Harbor	3.43	5.20×10^3	7.18×10^4
Whitby Harbor	3.80×10^1	1.05×10^4	1.83×10^3
Belleville Harbor	4.80	2.65×10^3	2.03×10^4
Kingston Harbor	2.76	3.40×10^3	2.23×10^4
St. Lawrence River 1	8.40×10^{-2}	8.00×10^1	8.09×10^3
St. Lawrence River 2	4.80×10^{-2}	1.40×10^2	1.15×10^3

Table IV. Concentrations (μg/kg Dry Weight) of Methylated Butyltins in Top 2 cm of Sediment

location	$[Bu_3MeSn]$	$[Bu_2Me_2Sn]$
Port Dover Harbour	10.9 ± 3.6	12.3 ± 3.1
Grand River (mouth)		11.1 ± 6.0
Toronto Harbour	22.8 ± 7.7	
Kingston Harbour	15.0 ± 4.0	

than a minor process. Table IV shows that Bu_3MeSn and Bu_2Me_2Sn were found in the sediment of some harbors which also contained butyltin species. Since tetraalkyltin compounds do not have dispersive uses with regard to the environment but are mainly used as intermediates in the production of other organotin compounds (*18*), it is unlikely that the Bu_3MeSn and Bu_2Me_2Sn were of anthropogenic origin. Thus, it appears that not only (i) can Bu_3Sn^+ and Bu_2Sn^{2+} be methylated in aquatic environments but also (ii) methylation may be a significant pathway of transformation for the butyltin species since the concentrations of Bu_3MeSn and Bu_2Me_2Sn in sediment at the locations shown in Table IV vary between 4 and 8% and between 19 and 124%, respectively, of the concentrations of Bu_3Sn^+ and Bu_2Sn^{2+}. Research is in progress on the relative contributions of abiotic and biological pathways to the degradation or transformation of Bu_3Sn^+ in Toronto Harbour.

Acknowledgments

I thank G. A. Bengert, O. Keir, E. J. Hale, and H. Huneault for collecting the samples and G. A. Bengert for providing the butylmethyltin standards.

Registry No. Bu_3Sn^+, 36643-28-4; Bu_2Sn^{2+}, 14488-53-0; $BuSn^{3+}$, 78763-54-9; Bu_3MeSn, 1528-01-4; Bu_2Me_2Sn, 1528-00-3; Sn, 7440-31-5.

Literature Cited

(1) Zuckerman, J. J.; Reisdorf, R. P.; Ellis, H. V., III; Wilkinson, R. R. In "Organometals and Organometalloids, Occurrence and Fate in the Environment"; Brinckman, F. E.; Bellama, J. M., Eds.; American Chemical Society: Washington, DC, 1981; ACS Symp. Ser. No. 82, p 388–422.
(2) Canada Department of the Environment and Department of National Health and Welfare In "The Canada Gazette Part I"; Canadian Government Publishing Centre: Ottawa, Ontario, Canada, Dec 1, 1979; pp 7365–7370.
(3) Maguire, R. J.; Chau, Y. K.; Bengert, G. A.; Hale, E. J.; Wong, P. T. S.; Kramer, O. *Environ. Sci. Technol.* **1982**, *16*, 698–702.
(4) Maguire, R. J.; Huneault, H. *J. Chromatogr.* **1981**, *209*, 458–462.
(5) Chau, Y. K.; Wong, P. T. S.; Bengert, G. A. *Anal. Chem.* **1982**, *54*, 246–249.
(6) Brinckman, F. E.; Jackson, J. A.; Blair, W. R., Olson, G. J.; Iverson, W. P. In "Trace Metals in Sea Water"; Wong, C. S.; Boyle, E.; Bruland, K. W.; Burton, J. D.; Goldberg, E. D., Eds.; Plenum Press: New York, 1983; pp 39–72.
(7) Seidel, S. L.; Hodge, V. F.; Goldberg, E. D. *Thalassia Jugosl.* **1980**, *16*, 209–222.
(8) Seinen, W.; Helder, T.; Vernij, H.; Penninks, A.; Leeuwangh, P. *Sci. Total Environ.* **1981**, *19*, 155–166.
(9) Marshall, W. K.; Roberts, J. R. In "Proceedings of a Symposium on Fenitrothion: The Long-Term Effects of Its Use in Forest Ecosystems"; Roberts, J. R.; Greenhalgh, R.; Marshall, W. K., Eds.; National Research Council of Canada: Ottawa, Ontario, 1977; NRCC No. 16073, pp 253–278.
(10) Huey, C.; Brinckman, F. E.; Grim, S.; Iverson, W. P. *Proc. Int. Conf. Transp. Persistent Chem. Aquat. Ecosyst.* **1974**, 73–78.
(11) Guard, H. E.; Cobet, A. B.; Coleman, W. M., III *Science (Washington, D.C.)* **1981**, *213*, 770–771.
(12) Chau, Y. K.; Wong, P. T. S.; Kramar, O.; Bengert, G. A. *Heavy Met. Environ., Int. Conf., 3rd* **1981**, 641–644.
(13) Blair, W. P.; Jackson, J. A.; Olson, G. J.; Brinckman, F. E.; Iverson, W. P. *Heavy Met. Environ., Int. Conf., 3rd* **1981**, 235–242.
(14) Jackson, J. A.; Blair, W. R.; Brinckman, F. E.; Iverson, W. P. *Environ. Sci. Technol.* **1982**, *16*, 110–119.
(15) Hallas, L. E.; Means, J. C.; Cooney, J. J. *Science (Washington, D.C.)* **1982**, *215*, 1505–1507.
(16) Dizikes, L. J.; Ridley, W. P.; Wood, J. M. *J. Am. Chem. Soc.* **1978**, *100*, 1010–1012.
(17) Fanchiang, Y.-T.; Wood, J. M. *J. Am. Chem. Soc.* **1981**, *103*, 5100–5103.
(18) Van der Kerk, G. J. M. In "Organotin Compounds: New Chemistry and Applications"; Zuckerman, J. J., Ed.; American Chemical Society: Washington, DC 1976; Adv. Chem. Ser. No. 157, pp 1–25.

Received for review February 22, 1983. Accepted October 20, 1983.

Environ. Sci. Technol. 1984, 18, 295–297

CORRESPONDENCE

Comment on "Partition Equilibria of Nonionic Organic Compounds between Soil Organic Matter and Water"

SIR: The article of Chiou et al. (*1*) stated that sorption of nonionic organic compounds on soils from water solution occurs by equilibrium partitioning into a soil organic phase and that adsorption by minerals is relatively unimportant in wet soils. Evidence presented by Chiou does not prove a partitioning model of sorption to the exclusion of a physical adsorption model. The partitioning model apparently was chosen as a convenient explanation of the effect of soil organic matter on sorption of nonionic compounds and its relation to the sorbate octanol–water partition coefficient. Chiou et al. (*1*) have assumed without proof that a particular relation between organic content and sorption is valid for all soils. Although there is a correlation between organic content and sorption, considerable variation exists between soils (*2, 3*). Hamaker et al. (*4*) observed that K_{om} values for soils with high organic content are usually lower than K_{om} values for "normal" soils and that soils with very low organic content give high K_{om} values.

Shin et al. (*5*) found that adsorption of DDT on soil extracted with ether or alcohol was considerably enhanced over that for the unextracted soil. Solvent extraction removed selected organic species with little change in total organic content. This change in soil sorption with change in soil organic matter composition is a strong argument against a partitioning model.

Adsorption of nonionic organic compounds by soil minerals is not insignificant. MacIntyre et al. (*3*) and Pierce et al. (*6*) observed significant adsorption by natural and synthetic clay minerals. Natural sediments whose organic matter has been removed by H_2O_2 digestion show adsorption ranging from 25% to 150% of that for nondigested sediments (*3, 5–7*). Anomalously high K_{om} values calculated for soils with very low organic content may be explained by adsorption by mineral phases.

Application of the Flory–Huggins theory, or of a partitioning model, to soil organic matter requires several unproven assumptions and is not needed to explain the variation of the measured distribution coefficient with sorbate solubility. Chiou's relationship of K_{om} with sorbate solubility provides no information about K_{om} because only one soil of fixed organic content and composition was studied. The distribution constant–sorbate solubility relation is reflective of the degree of incompatibility of nonionic solutes with water. Compounds of low solubility are excluded from the water structure and associate with surfaces, producing higher distribution coefficients.

Chiou et al. (*1*) use the observed linearity of adsorption isotherms and absence of competitive effects as evidence for a partitioning mechanism. Such behavior is also consistent with a physical adsorption model in which each of the soil minerals and organic phases is considered as a separate adsorbent. Isotherms based on physical adsorption models can have a wide linear range. Isotherms are linear when there is considerable free substrate available to adsorb more sorbate molecules. The sparing water solubility of nonionic organics may limit maximum concentrations to values still within the linear portion of the adsorption isotherm. Noncompetitive sorption of 1,3-dichlorobenzene and 1,2,4-trichlorobenzene can be predicted by a physical adsorption model. MacIntyre et al. (*3*) observed similar noncompetitive sorption for components of hydrocarbon mixtures on clays and sediments. The clays contained little organic matter so partitioning into an organic phase was unlikely. The affinity for adsorption sites of sorbate molecules of such size and molecular structure must be similar since van der Waals forces predominate. Failure to observe competitive adsorption is therefore not surprising.

Literature Cited

(1) Chiou, C. T.; Porter, P. E.; Schmedding, D. W. *Environ. Sci. Technol.* **1983**, *17*, 227–231.
(2) Means, J. C.; Hassett, J. J.; Wood, S. G.; Banwart, W. L. In "Carcinogenis, Polynuclear Aromatic Hydrocarbons"; Jones, P. W.; Leber, P., Eds.; Ann Arbor Science: Ann Arbor, MI, 1979; Vol. 1, pp 327–340.
(3) MacIntyre, W. G.; Smith, C. L.; deFur, P. O.; Su, C. W. *Air Force Eng. Serv. Cent., Eng. Serv. Lab., [Tech. Rep.] ESL-TR (U.S.)* **1982**, *ESL-TR*-82-06, 1–53.
(4) Hamaker, J. W.; Thompson, J. M. In "Organic Chemicals in the Soil Environment"; Marcel Dekker: New York, 1972; Vol. 1, Chapter 2.
(5) Shin, Y. O.; Chodan, J. J.; Wolcott, A. R. *J. Agric. Food Chem.* **1970**, *18*, 1129.
(6) Pierce, R. H., Jr.; Olney, C. E.; Felbeck, G. T., Jr. *Geochim. Cosmochim. Acta* **1974**, *38*, 1061–1073.
(7) Meyers, P. A.; Quinn, J. G. *Nature (London)* **1973**, *244*, 23–24.

William G. MacIntyre,* Craig L. Smith

College of William and Mary
Virginia Institute of Marine Science
School of Marine Science
Gloucester Point, Virginia 23062

SIR: In their argument against the partitioning as the major process of soil sorption from water, MacIntyre and Smith (*1*) cited (i) the variation of K_{om} values among soils and (ii) the enhancement of soil sorption with (partial) removal of soil organic content. They thereby suggested that (iii) the adsorptive contribution by soil minerals in aqueous systems is important. They also questioned (iv) the significance of the log K_{om}–log S_w (water solubility) relationship derived by application of the Flory–Huggins theory for solutes in soil humic phase and (v) the criteria for partition equilibria based on isotherm linearity (or, more strongly, failure to observe nonlinearity) and absence of solute competition even at high relative concentrations in soil sorption. In a recent article, Mingelgrin and Gerstl (*2*) have made similar inquiries to the validity of the partition concept.

We have stated quite clearly in our paper (*3*) that the K_{om} values of a compound in different soils can vary to some extent since the composition of the humic components is not constant. Another important factor not illustrated before that affects the K_{om} value is the effect on the water solubility of relatively insoluble solutes by humic components that get dispersed from soil into water (either in dissolved state or in association with colloidal soil particulates) (*4, 5*), and which may not be effectively spun

down even at high gravity. The resulting effect on the apparent K_{om} can be rationalized as follows.

The concentration of the solute in humic-containing water (C_w^*) differs from that in pure water (C_w) by the relation

$$C_w^* = C_w + xKC_w \quad (1)$$

where x is the mass of the dispersed humic components per unit volume of water and K is the concentration ratio of the solute between the dispersed humic materials and water. The magnitude of x depends obviously on factors such as the organic content and composition of the soil and the water-to-soil ratio used in sorption experiments. K appears to have the same magnitude as K_{om} on the basis of the data of Carter and Suffet (*6*) and Wershaw et al. (*7*) for DDT in humic-containing water in comparison with the K_{om} value of DDT (*8*).

In practically all sorption studies, no distinction has been made between C_w^* and C_w, and C_w^* has been used as the abscissa scale in the isotherm plot of soil uptake vs. equilibrium concentration in water. The amount sorbed is normally calculated by difference based on C_w^*. When x is moderately low (say, <100 ppm), there will be hardly any change in the humic content of the bulk soil with usual soil–water ratios in sorption experiments. By eq 1, C_w^* will not be significantly different from C_w for relatively water-soluble solutes having $K_{om} < 1000$, for example. With K_{om} in the order of 10^5, as for DDT, C_w^* will, however, be many times greater than C_w. Carter and Suffet (*6*) show that C_w^* is about $4C_w$ for DDT with $x = 16$ ppm for a natural humic acid in water. Thus, when C_w^* is used to calculate K_{om}, the amount of the humic substances in water at the level cited could easily influence the apparent K_{om} value of DDT by a factor of 4 without even taking into account the effect of humic composition of the bulk soil phase. This effect is also evident in the studies of Means et al. (*9*, *10*) on the sorption of relatively insoluble aromatic compounds from water on soils/sediments, where, for instance, the highest equilibrium concentrations (C_w^*) of pyrene in the reported (linear) sorption isotherms are 5–20 times higher than the solubility of pyrene in pure water.

In the studies of Shin et al. (*11*) and Pierce et al. (*12*) with DDT, the pretreatment of the soils/sediments with organic solvents or with H_2O_2 apparently removes part of the soil organic content that may get dispersed from soil into water. The apparent K_{om} (or K_{oc}) values calculated for DDT would thus be higher for the treated soils than for the untreated soils by the reason stated above. For soils rich in organic content (such as peat and muck), there would likely be larger amounts of dispersed humus (as the solution is usually intensely colored), thus giving lower K_{om} values compared to those for "normal" soils with or without soil treatments. It should be noted that the commonly applied H_2O_2 digestion method does not remove "all" the organic content of the soil (*13*). Thus, the variation of K_{om} in different soils and the enhancement of K_{om} with solvent or reagent treatments of the soil cannot be taken as a rigorous basis for the significance of the adsorptive contribution by soil minerals from water, where the sorption isotherms show no obvious curvatures from low to high relative saturations (*8*, *14*, *15*).

In most reported studies on the uptake of organic solutes from water on clay minerals, it happens that trace amounts of the organic matter in clay have often been ignored in data analysis. A closer examination of the data reveals its significance. For instance, the uptake of lindane from water on Ca-Staten peaty muck (22% organic matter), Ca-Venado clay (6% O.M.), and Ca-bentonite clay (~0.3% O.M. by our analysis) in the study of Mills and Biggar (*16*) bears a close relationship to the respective organic contents. Karickhoff et al. (*17*) have vividly illustrated that the sorption of hydrocarbons on given sediment particle-size isolates (including clay fractions) is closely related to the particle organic carbon content. In our study on the uptake of lindane from water on Woodburn soil (1.9% O.M.) and Ca-bentonite, the isotherms are linear with capacities in close proportion to their organic contents. It thus appears that while one cannot rule out some linear adsorption of organics from water on soil minerals, this effect would be of lower magnitude than the uptake by the organic content in normal soils.

Our partition equation relating log K_{om} with log S_w was derived indeed with the basic assumptions contained in the Flory–Huggins theory. In spite of these assumptions, the Flory–Huggins theory has been widely accepted as a norm to the thermodynamic activity of small molecules in (amorphous) polymers. Our equation was formulated with the intent of expressing the effect of solute–water incompatibility (as given by log S_w) and the effect of solute–humic polymer incompatibility (on the basis of the Flory–Huggins theory) on log K_{om}. It is well-known that the swelling of amorphous polymers resulting from sorption of small molecules is basically a solubility phenomenon rather than an adsorption phenomenon (*18–21*). The application of the Flory–Huggins theory in our treatment is merely to comply with this criterion.

Interpretations given by MacIntyre and Smith (*1*) and by Mingelgrin and Gerstl (*2*) on the isotherm linearity and its implication on sorptive mechanisms are misleading. The linearity should be properly evaluated in terms of the relative saturation (the ratio of equilibrium concentration to solubility) rather than the absolute concentration of the solute in the medium from which it is sorbed. For solutes of sparing water solubility, high saturations are reached when equilibrium concentrations are close to solubility limits despite that the absolute concentrations are low. When the aqueous phase reaches saturation, the other phase (e.g., the soil phase) in equilibrium with it must simultaneously reach saturation. In the sorption of organic compounds from water on soil, the isotherms are practically linear to high relative concentrations and exhibit no obvious competition between the solutes. By contrast, the sorption isotherms of organic compounds from hexane and from vapor phase on dehydrated soils, where the sorption is controlled mainly by adsorption on soil minerals (*14*), exhibit distinctive curvatures and competitive effects even at very low relative concentrations. These data will be presented in our future publications.

To the extent that the soil uptake from aqueous solution can be effectively described by a linear partition model, the common use of the Langmuir adsorption model for interpreting the data from these systems (*2*) seems inappropriate. In the Langmuir model, the heat of adsorption per mole for similar compounds is approximately proportional to the molecular weight of the adsorbate. The slopes of the initial linear portions of the normalized Langmuir isotherms (capacity vs. relative saturation) on the same adsorbent should thus be steeper for adsorbates of higher molecular weights. The limiting adsorption capacity at saturation should again be greater for adsorbates of higher molecular weights. These expectations have not been observed in the sorption of nonionic organic compounds from water on soil. To the contrary, the sorption isotherms from water give no obvious curvatures at high relative saturations that are characteristic of the Langmuir adsorption, and the maximum capacities for different so-

lutes on the same soil appear to be in the same order of the solute solubility. This has been illustrated in our study (*3*) that the maximum capacity on Woodburn soil is much greater for benzene or chlorobenzene than for higher molecular weight 1,2,4-trichlorobenzene and PCBs, which is also consistent with the presumed partition of the solute into soil organic matter. Such a reversal has no parallel in the Langmuir theory. The insistence on the use of the Langmuir model appears to be based more on tradition than on objective analyses of the data.

Literature Cited

(1) MacIntyre, W. G.; Smith, C. L. *Environ. Sci. Technol.*, preceding paper in this issue.
(2) Mingelgrin, U.; Gerstl, Z. *J. Environ. Qual.* **1983**, *12*, 1.
(3) Chiou, C. T.; Porter, P. E.; Schmedding, D. W. *Environ. Sci. Technol.* **1983**, *17*, 227.
(4) Leenheer, J. A. In "Contaminants and Sediments"; Baker, R. A., Ed.; Ann Arbor Science Publishers, Inc.: Ann Arbor, MI, 1980; Vol. 2, pp 267–277.
(5) Leenheer, J. A.; Stuber, H. A. *Environ. Sci. Technol.* **1981**, *15*, 1467.
(6) Carter, C. W.; Suffet, I. H. *Environ. Sci. Technol.* **1982**, *16*, 735.
(7) Wershaw, R. L.; Burcar, P. J.; Goldberg, M. C. *Environ. Sci. Technol.* **1969**, *3*, 271.
(8) Chiou, C. T.; Peters, L. J.; Freed, V. H. *Science (Washington, D.C.)* **1979**, *206*, 831.
(9) Means, J. C.; Hassett, J. J.; Wood, S. G.; Banwart, W. L. In "Polynuclear Aromatic Hydrocarbons"; Jones, P. W.; Leber, P., Eds.; Ann Arbor Science Publishers, Inc.: Ann Arbor, MI, 1979; pp 327–340.
(10) Means, J. C.; Wood, S. G.; Hassett, J. J.; Banwart, W. L. *Environ. Sci. Technol.* **1982**, *16*, 93.
(11) Shin, Y. O.; Chodan, J. J.; Wolcott, A. R. *J. Agric. Food Chem.* **1970**, *18*, 1129.
(12) Pierce, R. H., Jr.; Olney, C. E.; Felbeck, G. T., Jr. *Geochim. Cosmochim. Acta* **1974**, *38*, 1061.
(13) Hance, R. J. *Weed Res.* **1965**, *5*, 98.
(14) Chiou, C. T.; Peters, L. J.; Freed, V. H. *Science (Washington, D.C.)* **1981**, *213*, 684.
(15) Chiou, C. T. In "Hazard Assessment of Chemicals: Current Developments"; Saxena, J., Fisher, F., Eds.; Academic Press: New York, 1981; Vol. I, pp 117–153.
(16) Mills, A. C.; Biggar, J. W. *Soil Sci. Soc. Am. Proc.* **1969**, *33*, 210.
(17) Karickhoff, S. W.; Brown, D. S.; Scott, T. A. *Water Res.* **1979**, *13*, 241.
(18) Flory, P. J. *J. Chem. Phys.* **1942**, *10*, 51.
(19) Flory, P. J. "Principles of Polymer Chemistry"; Cornell University Press: Ithaca, NY, 1953; pp 495–520.
(20) Huggins, M. L. *Ann. N.Y. Acad. Sci.* **1942**, *43*, 1.
(21) Hildebrand, J. H.; Prausnitz, J. M.; Scott, R. L. "Regular and Related Solutions"; Van Nostrand Reinhold: New York, 1970.

Cary T. Chiou*

U.S. Geological Survey
Denver Federal Center
Denver, Colorado 80225

Paul E. Porter

506 Bowen Avenue
Modesto, California 95350

Thomas D. Shoup

Agricultural Chemistry Department
Oregon State University
Corvallis, Oregon 97331

A New ACS Audio Course to help you understand and solve industrial and municipal waste-water problems . . . .

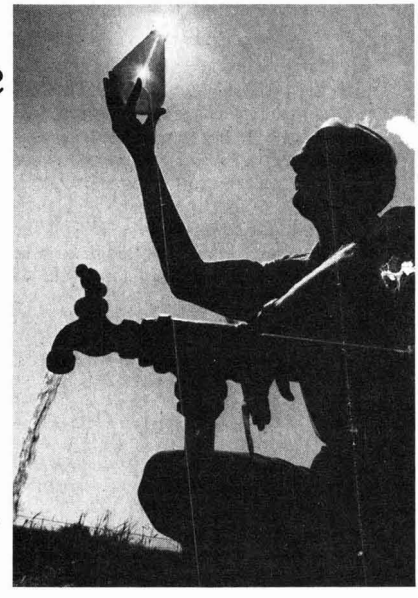

ACTIVATED SLUDGE:

Stoichiometry, Kinetics, and Mass Balances

Whether you're a chemist or chemical engineer, a biological scientist or civil engineer, if you need to understand aerobic, suspended growth, mixed culture systems, ACTIVATED SLUDGE will give you the most up-to-date information.

The bulk of the course focuses on the development of mass balance principles and their application to biological reactors. Using these principles, you'll learn how to apply stoichiometric and kinetic relationships to select appropriate system sizing, oxygen needs, nutrient levels and sludge-disposal methods.

In addition to treating common industrial waste problems, the author introduces advanced concepts and procedures required to analyze more complex problems.

To test your understanding, numerous problems are presented with detailed solutions.

INSTRUCTOR

Dr. Robert L. Irvine, Professor of Civil Engineering, University of Notre Dame, is a recognized expert on biological treatment in sequencing batch reactors.

COURSE MATERIALS

Five audiotape cassettes (6.2 hou playing time) and a 127-page manual, $275.00. Additional manuals for group use, 1 to 9 copies . . . $16.00 each; 10 or more copies . . . $12.80 each. (Catalog no. Z-57.)

NO-RISK GUARANTEE

Order now! If you're not completely satisfied, just return the course within ten days for a full refund or cancellation of invoice.

Please allow six weeks for delivery.

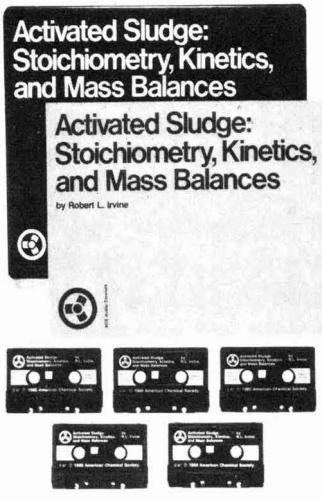

American Chemical Society
Education Department
1155 Sixteenth Street, N.W.
Washington, D.C., 20036
(202) 874-4588

Please send _____copy(ies) of
Activated Sludge: Stoichiometry, Kinetics, and Mass Balances at $275.00 each to:
Also send _____additional manuals for group study.

Name _____

Organization _____

Address _____

City/State/Zip _____

☐ Purchase order enclosed. ☐ Payment enclosed.

Charge my ☐ VISA ☐ MasterCard Expiration Date _____

Account No. _____

Interbank Code _____ (MasterCard Only)

Signature _____

☐ Please ship by air (billed at cost) ☐ Please send free catalog.

CHEMICAL RESEARCH FACULTIES: AN INTERNATIONAL DIRECTORY

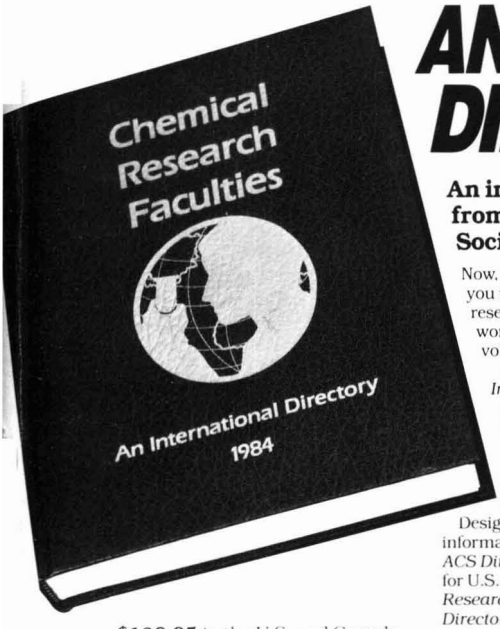

$129.95 in the U.S. and Canada
$155.95 in all other countries

An invaluable new resource from the American Chemical Society.

Now, for the first time, *all* the information you need about chemical research and researchers at universities around the world has been gathered into one volume.

Chemical Research Faculties: An International Directory contains a wealth of facts on more than 8,900 faculty members and 737 departments in 62 countries. And it's a book no academic institution or chemically oriented business can afford to be without.

Designed to provide the same type of information on an international scale that the *ACS Directory of Graduate Research* gives for U.S. and Canadian schools, *Chemical Research Faculties: An International Directory* includes listings for chemistry, chemical engineering, biochemistry, and pharmaceutical/medicinal chemistry.

It offers informative statistical tables on graduate programs worldwide. Organizes data on 63 chemical societies in 51 nations. And is cross-referenced three ways—by faculty, institution, and research subject—for easy use.

Indispensable for industry and academia alike.

If you're involved in chemical research, *Chemical Research Faculties: An International Directory* can keep you abreast of the latest developments in your area of specialization.

If you advise graduate students, it can help you steer them toward the programs they're seeking.

And if you're in a business even remotely related to chemical research, just one of the thousands of leads this book contains could pay for the purchase price many times over.

Why not fill out the order form right now? Or call 800/424-6747 and charge your VISA, MasterCard, or American Express.

And let *Chemical Research Faculties: An International Directory* open up a whole new world of professional possibilities.

ORDER FORM

☐ **YES! Please rush me my copy of the new international directory!**

	QTY.	U.S./ CANADA	EXPORT	TOTAL
Chemical Research Faculties: An International Directory	_____	**$129.95**	**$155.95**	_____
California residents, add 6% tax				_____
AMOUNT ENCLOSED				_____

☐ I have enclosed a check for $_____ payable to the American Chemical Society.
☐ Purchase Order # _____ enclosed.
Charge my ☐ VISA ☐ MasterCard ☐ American Express ☐ Barclaycard ☐ Access.

Name of cardholder _____

Account # _____

Expires _____ Interbank # _____ (MasterCard and Access)

Signature _____

Note: Please allow four to six weeks for delivery. Foreign payment must be made in U.S. currency by international money order, UNESCO coupons, or U.S. bank draft. Order through your local bookseller or directly from the American Chemical Society. Orders from individuals must be prepaid.

PLEASE SHIP BOOKS TO:

Name _____

Address _____

_____

_____

33

MAIL THIS ORDER FORM TO: American Chemical Society
Distribution Office, Department 33
1155 16th Street, N.W.
Washington, D.C. 20036

☐ **Please send me more information about the *ACS Directory of Graduate Research 1983*, which gives similar data for U.S. schools.**

Departmental Information
includes address and phone number, name of department head, advanced degrees offered, and principal areas of research.

Faculty Information
includes name, year of birth, title, degrees (with years and institutions), areas of specialization, current research, and recent publications.

Chemical Society Information
lists address, principal officer, publications, purpose, organizational structure, and number of members.

Guide to Chemical Research Institutions
lists all countries, universities, and departments in order of appearance, providing an overview of each section.

Four Organizational Sections
break down listings into chemistry, chemical engineering, biochemistry, and pharmaceutical/ medicinal chemistry.

Faculty Index
helps you keep up with colleagues' moves and learn more about others in your area of specialization.

Statistical Tables
provide for each country the number of master's and doctoral degrees conferred in 1981 and 1982—as well as the number of full-time faculty, post-doctoral appointments, and students enrolled in advanced degree programs.

Institutional Index
provides a merged alphabetical listing that lets you find institutions known by name but not location.

Index of Research Subjects
helps you locate universities, departments, and individuals doing research related to your own.

800-424-6747

Martek Means More Than Monitors

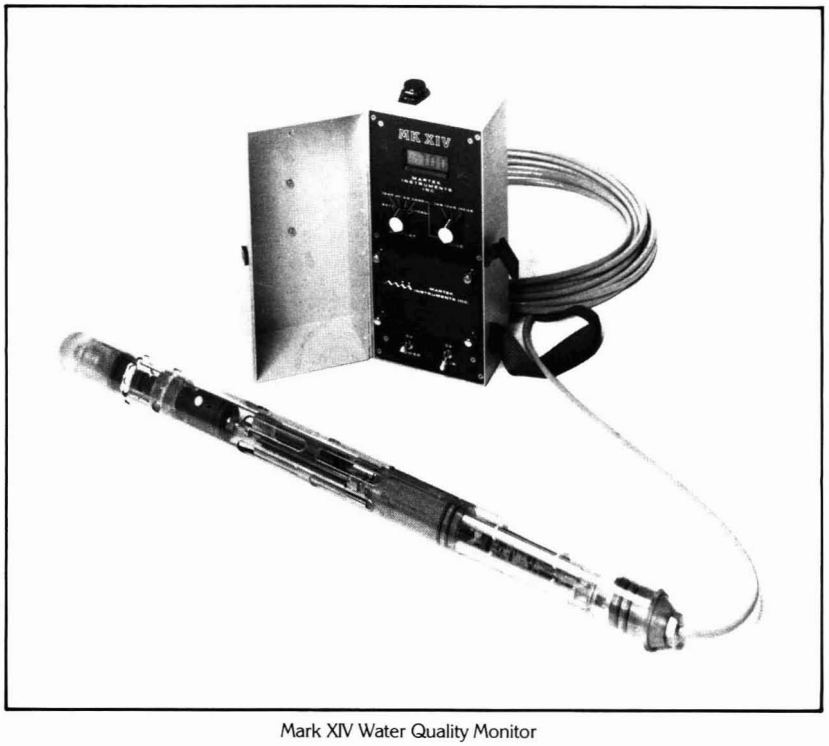

Mark XIV Water Quality Monitor

Naturally, we're proud of our state-of-the-art water quality monitoring systems. But we're equally proud of the personalized post-sale service we make available to users of our systems. Whether you have a hard-to-fit application or need factory service or consultation, our applications specialists and service engineers are only a phone call away. The service doesn't stop after the sale!

If you haven't measured with Martek as yet, we have an exciting new system which sets new standards for ground water monitoring—the low-cost Mark XIV Water Quality Monitor. This multiparameter system provides *in situ* measurement of pH, temperature-corrected conductivity, temperature and dissolved oxygen. It features a unique sensor housing, 26 inches long and less than two inches in diameter, making it ideal for critical borehole monitoring applications.

Perhaps you already know Martek through its other versatile monitoring systems, such as the Mark XV Water Quality Microprocessor which combines the sophistication of digital measurement with the simplicity of rugged field instruments. This system is designed for direct *in situ* measurement of seven parameters: temperature, salinity or temperature-corrected conductivity, depth, dissolved oxygen, pH, and specific ions.

The quality of Martek products is matched only by the quality of its service and post-sale technical support. You owe it to yourself to find out more about Martek.

MARTEK INSTRUMENTS, INC.

17302 Daimler St. • P.O. Box 16487 • Irvine, CA 92713 • (714) 540-4435 • Telex 692-317

CIRCLE 3 ON READER SERVICE CARD